ISTANBUL TECHNICAL UNIVERSITY ★ GRADUATE SCHOOL

DEVELOPMENT OF A SPATIAL MODEL ON NUCLEAR POWER PLANT ACCIDENTS BASED ON VULNERABILITY AND EVACUATION PLANS

Ph.D. THESIS

Maryna BATUR

Department of Geomatics Engineering

Geomatics Engineering Programme

JULY 2025

ISTANBUL TECHNICAL UNIVERSITY ★ GRADUATE SCHOOL

DEVELOPMENT OF A SPATIAL MODEL ON NUCLEAR POWER PLANT ACCIDENTS BASED ON VULNERABILITY AND EVACUATION PLANS

Ph.D. THESIS

Maryna BATUR
(501202609)

Department of Geomatics Engineering

Geomatics Engineering Programme

Thesis Advisor: Prof. Dr. Reha Metin ALKAN

JULY 2025

ISTANBUL TEKNİK ÜNİVERSİTESİ ★ LİSANSÜSTÜ EĞİTİM ENSTİTÜSÜ

KIRILGANLIK VE TAHLIYE PLANLARINA DAYALI NÜKLEER SANTRAL KAZALARI İÇİN MEKANSAL BİR MODELİN GELİŞTİRİLMESİ

DOKTORA TEZİ

Maryna BATUR
(501202609)

Geomatik Mühendisliği Anabilim Dalı

Geomatik Mühendisliği Programı

Tez Danışmanı: Prof. Dr. Reha Metin ALKAN

TEMMUZ 2025

Maryna BATUR, a Ph.D. student of İTU Graduate School student ID 501202609 successfully defended the thesis entitled "DEVELOPMENT OF A SPATIAL MODEL ON NUCLEAR POWER PLANT ACCIDENTS BASED ON VULNERABILITY AND EVACUATION PLANS", which she prepared after fulfilling the requirements specified in the associated legislations, before the jury whose signatures are below.

Thesis Advisor :	**Prof. Dr. Reha Metin ALKAN** İstanbul Technical University	.....
Jury Members :	**Prof. Dr. Himmet KARAMAN** Istanbul Technical University	.....
	Prof. Dr. Haluk ÖZENER Boğaziçi University	.....
	Prof. Dr. Serdar EROL Istanbul Technical University	.....
	Prof. Dr. Engin GÜLAL Atlas University	.....

Date of Submission : 29 May 2025
Date of Defense : 03 July 2025

To my twins, Batuhan and Melisa, and my little son, Kaan

FOREWORD

This thesis would not have been possible without the guidance, support, and encouragement of many remarkable individuals, to whom I am sincerely grateful.

First and foremost, I extend my deepest thanks to my advisor, Prof. Dr. Reha Metin ALKAN, whose invaluable insights, unwavering support, and constant encouragement have shaped and strengthened this research. I am truly honored to have been his student and to have benefited from his mentorship throughout this journey.

I also thank my thesis committee members, Prof. Dr. Himmet KARAMAN and Prof. Dr. Haluk ÖZENER. I am especially grateful to Prof. Dr. KARAMAN for his deep engagement with my topic and insightful feedback, and to Prof. Dr. ÖZENER for his ongoing support and trust in my work. I feel so lucky to have met you in my life.

To all who contributed to this study through surveys and data collection – I thank you for your cooperation.

Lastly, I am deeply thankful to my family. To my parents, for their endless love and encouragement; to my husband, Murat BATUR, for his patience and steadfast support; to my twins, Melisa and Batuhan, whose curiosity kept me motivated; and to my little son, Kaan, born during this journey and my greatest inspiration – your presence made even the hardest days meaningful.

May 2025

Maryna BATUR
(M.Sc. in Geodesy)

TABLE OF CONTENTS

Page

FOREWORD ..... **ix**
TABLE OF CONTENTS ..... **xi**
ABBREVIATIONS ..... **xv**
SYMBOLS ..... **xix**
LIST OF TABLES ..... **xxv**
LIST OF FIGURES ..... **xxvii**
SUMMARY ..... **xxxi**
ÖZET **xxxv**
1. INTRODUCTION **1**
1.1 General 1
1.2 Problem Statement 1
1.3 Aims and Objectives 2
1.4 Hypothesis 2
1.5 Expected Contribution 4
1.6 Organization of the Thesis 5
2. LITERATURE REVIEW **7**
2.1 Understanding Nuclear risks 7
2.1.1 The nuclear age and disaster risk: a historical overview 7
2.1.2 Typologies of nuclear accidents: from reactor meltdowns to radiological terrorism 9
2.1.2.1 Reactor accidents 9
2.1.2.2 Spent fuel accidents 11
2.1.2.3 Radiological dispersal devices (RDDs) 11
2.1.2.4 Nuclear weapons accidents 11
2.1.2.5 Critically accidents 12
2.1.2.6 Transport accidents 12
2.1.2.7 Sabotage and terrorism 12
2.1.3 Key vulnerabilities and cascading effects: impact on health, ecosystems, and economies 12
2.1.3.1 Health impacts 12
2.1.3.2 Ecosystem impacts 13
2.1.3.3 Economic impacts 13
2.2 Overview of Major Nuclear Accidents: Chernobyl and Fukushima 14
2.3 Bibliometric Analysis of Research on Major Nuclear Accidents 15
2.3.1 Research questions, objectives, and contribution of the study 15
2.3.2 Data collection and research methodology 17
2.3.3 Geographically weighted regression: methodological framework 18
2.3.4 Temporal data exploration 20
2.3.5 Statistics and trending topics 21
2.3.5.1 Top productive journals 21
2.3.5.2 Top productive documents 24
2.3.5.3 Keywords analysis 26

2.3.6 Geographical distribution of research 28
2.3.7 Geospatial analysis results 31
2.4 Lessons from Chernobyl and Fukushima 41
2.4.1 Emergency response 41
2.4.1.1 The Chernobyl disaster 41
2.4.1.2 The Fukushima disaster 45
2.4.2 Environmental consequences 49
2.4.2.1 Chernobyl accident 49
2.4.2.2 Fukushima accident 51
2.4.3 Health consequences 52
2.4.3.1 Chernobyl accident 52
2.4.3.2 Fukushima accident 55
2.4.4 Economic impact 58
2.4.4.1 Chernobyl accident 58
2.4.4.2 Fukushima accident 60
2.4.5 Lessons and future directions 63
2.5 Spatial Modelling and Vulnerability Assessment 64
2.5.1 Vulnerability and hazard mapping 64
2.5.1.1 Theoretical foundations of vulnerability and hazard mapping 64
2.5.1.2 Methodological approaches to social vulnerability and hazard mapping 66
2.5.2 Evacuation modelling 68
2.6 Discussions on Literature Review 69
3. METHODOLOGY 73
3.1 Social Vulnerability Assessment 73
3.1.1 Selection of criteria and data collection 74
3.1.2 Best-Worst method 80
3.1.3 Analytic Hierarchy Process 81
3.1.4 Statistical assessment 83
3.1.4.1 Statistical comparison of BWM and AHP 83
3.1.4.2 Sensitivity analysis in Multi-Criteria Decision-Making 84
3.1.4.3 Hot and Cold spot analysis 85
3.2 Hazard Mapping 87
3.2.1 Gaussian Plume Model theory 87
3.2.2 Identification of the worst-case scenario 89
3.2.3 Data assimilation techniques for hazard mapping 93
3.2.3.1 Data assimilation for nuclear emergency management 93
3.2.3.2 Improving atmospheric dispersion modelling 94
3.2.3.3 Model formulation and framework 95
3.3 Evacuation Priority Mapping 100
3.4 Discrete Event Simulation For Evacuation Time Estimates 101
3.4.1 Radius-based and priority-based evacuation strategies 101
3.4.2 Modelling evacuation process using discrete event simulation 102
3.5 Evaluation of Nuclear Emergency Shelters 105
3.5.1 Study framework: weighted sum method 105
3.5.2 Origin-Destination cost matrix 108
3.5.3 Statistical evaluation 109
3.6 Health and Environmental Impact Assessment 109
3.6.1 Health impact: Total effective dose equivalent and cancer risk estimation 109

3.6.2 Environmental consequences: Cs-137 deposition and decay modeling . 111
3.7 Economic Loss Assessment 113
3.7.1 Direct economic losses assessment 114
3.7.2 Indirect economic losses assessment 115
3.7.3 Economic loss assessment methodology 116
4. CASE STUDY 119
4.1 History of Nuclear Power in Turkiye 119
4.2 Akkuyu Nuclear Power Plant: an Overview 120
4.2.1 Geographical and demographic profile 120
4.2.2 Safety and Risk Mitigation 122
4.2.3 Environmental and Socio-Economic Impact 123
4.3 Review of Related Legislation Regarding Akkuyu-NPP 123
4.3.1 IAEA standards 123
4.3.2 National energy policies 124
4.3.3 National emergency plan and safety responsibilities 125
4.4 Study Area Description 126
4.4.1 Meteorological data 126
4.4.1.1 Climatic Conditions 126
4.4.1.2 Wind Patterns 127
4.4.1.3 Precipitation 131
4.4.1.4 Humidity 131
4.4.2 Land use and agricultural activities 132
4.4.2.1 Land Use and Land Cover features 133
4.4.2.2 Agricultural activities in Mersin 133
4.4.2.3 Economic and Environmental Impacts of Agricultural Land Use ... 134
5. RESULTS AND DISCUSSION 135
5.1 Social Vulnerability Index to Nuclear Accident 135
5.1.1 Research criteria 135
5.1.2 Expert survey 136
5.1.3 SVI obtained with BWM 138
5.1.4 SVI obtained with AHP 140
5.1.5 Statistical assessment 141
5.1.5.1 Results of Wilcoxon Signed-Rank test 141
5.1.5.2 Sensitivity analysis results 142
5.1.5.3 Hot and Cold spot analysis results 143
5.1.6 Discussions 144
5.1.6.1 Significance of the SVI in the context of nuclear disaster management 144
5.1.6.2 Assessment of social vulnerability to nuclear accidents 146
5.1.6.3 Key findings and policy implications 147
5.1.6.4 Comparison with existing literature 147
5.1.6.5 Methodological considerations: BWM vs. AHP 147
5.1.6.6 Limitations and future research directions 148
5.2 Hazard Mapping 148
5.2.1 Simulation of Cs-137 release using GPM 148
5.2.2 Simulation of Cs-137 release using particle filter integrated with terrain-modified GPM 153
5.2.3 Model assessment 157
5.3 Evacuation Priority Mapping 161
5.4 Evacuation Time Estimates Results 163

5.4.1 Comparison of radius-based and priority-based evacuation strategies ... 163
5.4.2 Decision matrix and sensitivity analysis for evaluating evacuation strategies ... 167
5.5 Shelter Suitability Analysis in Nuclear Emergency Scenario ... 169
5.5.1 Spatial data ... 169
5.5.2 Origin-destination analysis for evacuation route planning ... 171
5.5.3 Origin-destination analysis of supply-access routes ... 172
5.5.4 Optimization process results ... 174
5.5.5 Model evaluation ... 178
5.5.5.1 Sensitivity analysis ... 178
5.5.5.2 Robustness and generalization ... 179
5.5.6 Discussions: optimization results for shelter allocation ... 180
5.6 Health and Environmental Implications from Postulated NPP Accident ... 182
5.6.1 TEDE and cancer risk calculations ... 182
5.6.2 Results from modeling radioactive deposition and decay mechanisms ... 183
5.7 Results from Economic Loss Assessment ... 185
5.7.1 The emergency response cost estimation ... 185
5.7.2 The decontamination cost estimation ... 187
5.7.3 The health-related cost estimation ... 188
5.7.4 The radioactive waste-related cost estimation ... 189
5.7.5 The compensation-related cost estimation ... 190
5.7.6 The administration-related cost estimation ... 191
5.7.7 The total estimated economic loss assessment ... 192
6. CONCLUSIONS AND RECOMMENDATIONS ... 195
6.1 Major Findings ... 195
6.2 Limitations of Research ... 197
6.3 Policy Recommendations for Emergency Response in Turkiye ... 198
6.4 Recommendations for Future Studies ... 199
REFERENCES ... 201
CURRICULUM VITAE ... 235

ABBREVIATIONS

ABM : Agent-based model
AHP : Analytic Hierarchy Process
AIC : Akaike Information Criterion
ARS : Acute Radiation Syndrome
BWM : Best Worst Method
CDF : Cumulative distribution function
CRM : Cancer risk map
CTBT : Comprehensive Nuclear-Test-Ban Treaty
CV : Coefficient of variation
DA : Data assimilation
DEM : Digital elevation model
DEMA : Disaster and Emergency Management Authority
DES : Discrete event simulation
DNA : Deoxyribonucleic acid
DRI : Disaster risk index
ECDF : Empirical cumulative distribution function
EPA : Environmental Protection Agency
EPZs : Emergency planning zones
GPM : Gaussian Plume Model
GPS : Global Positioning System
GDP : Gross Domestic Product
GIS : Geographic Information Systems
GWR : Geographically Weighted Regression
GSM : Global System for Mobile Communication
HYSPLIT : Hybrid Single-Particle Lagrangian Integrated Trajectory
IAEA : International Atomic Energy Agency
ICRP : International Commission on Radiological Protection
INES : International Nuclear and Radiological Event Scale
IQR : Interquartile range
KF : Kalman Filter

KS : Kolmogorov-Smirnov
LLNL : Lawrence Livermore National Laboratory
LULC : Land use land cover
LWR : Lighthill-Whitham-Richards
MAD : Mutually assured destruction
MAE : Mean absolute error
MCDA : Multi-criteria decision analysis
MGWR : Multiscale Geographically Weighted Regression
MOO : Multi-objective optimization
N : North
NARAC : National Atmospheric Release Advisory Center
NE : Northeast
NEP : National Emergency Plan
NPP : Nuclear Power Plant
NSC : Nuclear Safety Commission
NTP : Nuclear non-proliferation treaty
NW : Northwest
OD : Origin destination
OLS : Ordinary Least Squares
PAZ : Precautionary action zone
PAR : Pressure and release
PF : Particle Filter
PTSD : Post-traumatic stress disorder
PWR : Pressurized water reactor
Q : Scopus Quartile
RDDs : Radiological Dispersal Devices
RMSE : Root mean square error
RODOS : Real-time Online Decision Support
RQ : Research question
S : South
SSW : South-southwest
SW : Southwest
START : Strategic Arms Reduction Treaty
SVI : Social Vulnerability Index
TAEA : Turkish Atomic Energy Authority

TEDE : Total Effective Dose Equivalent
TEPCO : Tokyo Electric Power Company
TM-GPM : Terrain-modified Gaussian Plume Model
UPZ : Urgent protective action planning zone
USD : United Stated Dollar
VIF : Variance Inflation Factor
VRIM : Vulnerability-resilience indicators model
VVER-1200 : Water-water energetic reactor
WANO : World Association of Nuclear Operators
WHO : World Health Organization
WSM : Weighted sum method

SYMBOLS

a	**:** Stability dependent first constant
Ap	**:** Pairwise comparison matrix
A	**:** Very stable stability class
$\boldsymbol{AVG}$	**:** Average compensation per person
$\boldsymbol{A_j}$	**:** Activity of radionuclide ingested or inhaled
$\boldsymbol{A(t)}$	**:** Activity at time
$\boldsymbol{A_0}$	**:** Initial activity
$\boldsymbol{a_{Bj}}$	**:** Relative value from pairwise comparisons (best)
$\boldsymbol{a_{jw}}$	**:** Relative value from pairwise comparisons (worst)
$\boldsymbol{\alpha}$	**:** Empirical scaling factor
b	**:** Stability dependent second constant
B	**:** Unstable stability class
$\boldsymbol{\beta(u_i, v_i)}$	**:** Local regression coefficients at location
$\boldsymbol{\beta_0(u_i, v_i)}$	**:** Intercept at location
$\boldsymbol{\beta_k(u_i, v_i)}$	**:** Coefficients for the independent variable at location
Bq	**:** Becquerel
Bq/h	**:** Becquerel per hour
Bq/m^2	**:** Becquerel per square meter
Bq/m^3	**:** Becquerel per cubic meter
Bq/s	**:** Becquerel per second
c	**:** Stability dependent third constant
C	**:** Slightly unstable stability class
Ci	**:** Curie
$\boldsymbol{C(i,j)}$	**:** Cost of travelling from origin to destination point
$\boldsymbol{C_f}$	**:** Activity concentration in plants
$\boldsymbol{C_S}$	**:** Activity concentration in soil
$\boldsymbol{C_{total}}$	**:** Total economic losses
$\boldsymbol{C_{admin}}$	**:** Administrative costs
$\boldsymbol{C_{compens}}$	**:** Compensations

C_{decont} : Costs of decontamination

C_{health} : Health costs

C_{int} : Time-integrated air concentration

$C_{response}$: Costs of response

C_{waste} : Cost of radiological waste management

C_{worst} : Worst-case concentration

$C(x, y, z)$: Pollutant concentration at any point

CI : Consistency index

CR : Consistency ration

c_{person} : Costs for person

Cs-137 : CS-137

d : Stability dependent fourth constant

D : Neutral stability class

D : Deposition density

$\mathbf{D_b}$: Set of evacuees in the batch

D_i : Absorbed dose from radiation

d_{ij} : Distance between different locations

d_k : Distance of road segment along the path

Δw_j : Incremental change applied to the weight

E : Stable stability class

$E(G_i^*)$: Expected value of Getis-Ord statistic

e_j : Dose coefficient for radionuclide

EPI_i^{GMM} : Evacuation priority index geometric mean method)

EPI_i^{MAZ} : Evacuation priority index (maximum value approach)

EPI_i^{WSM} : Evacuation priority index (weighted sum method)

exp : Exponential function

F : Very stable stability class

G : Staggered delay between consecutive batches

G_i^* : The Getis-Ord statistic

$\mathbf{g/m^3}$: Gram per cubic meter

h : Bandwidth

$h(x)$: Terrain height at location

H : Release height

$\mathbf{H_S}$: Stack height

$\eta_t \sim N(0, \sigma_p^2)$	: Gaussian process noise with zero mean and variance
I-131	: I-131
j	: Criterion
kBq	: Kilo Becquerel
km	: Kilometer
L_{avg}	: Average value of errors across folds
L_i	: Error for the fold
λ	: Decay constant
λ_{max}	: Maximum eigenvalue
m	: Meter
m/s	: Meter per second
m^3/hr	: Cubic meters per hour
MAE	: Mean absolute error
$max_{i \in D_b} T_{travel,i}$	: Maximum travel time for batch
mm	: Millimeter
mm/h	: Millimeters per hour
min	: Minutes
mSv	: Milisievert
M_W	: Moment magnitude
n	: Total number of locations in the study area
N_p	: Number of evacuees
N_v	: Number of vehicles on the road
^oC	: Degrees of Celsius
π	: Pi value
$p\left(Z_t \mid U_t^{(i)}\right)$	: Conditional probability of the observed wind speed
P_n	: Population of a particular neighborhood
Pu-239	: Plutonium-239
Q	: Release rate
r	: Pearson correlation
$RMSE$	: Root mean square error
R^2	: Square root of errors
S_i'	: Sensitivity
S_j	: Supply-access time for shelter
Sr-90	: Stronium-90

$StdDev(G_i^*)$: Standard deviation of Getis-Ord statistic

Sv : Sievert

$T_{1/2}$: Half-life of radioactive material

$T_{congestion}$: Congestion delay

T_{eff} : Effective half-life

T_{env} : Environmental half-life

$T_{evac,b}$: Total evacuation time for a particular batch

T_{load} : Loading time

T_{mob} : Mobilization delay

T_{total} : Total evacuation time

t_{ij} : Travel time from neighborhood to shelter

TF : Transfer factor

u : Wind speed

(u_i, v_i) : Spatial coordinated of location

$U_0^{(i)}$: Wind speed of the particle at time zero

U_{init} : Initial wind speed

$U_{mod}(x)$: Terrain-modified wind speed at location

$U_t^{(i)}$: Estimated state

U_t^{mean} : Mean estimates

v_d : Deposition velocity

v_{ij} : Performance value of alternative with respect to criterion

v_k : Speed limit

w : Eigenvector containing the weights

$w_0^{(i)}$: Weight assigned to the particle

w_1 : Weight for evacuation time component

w_2 : Weight for supply-access time component

w_3 : Weight for overcrowding component

w_B : Weight assigned to the best criteria

wo_{ij} : Weight for observation relative to location

w_{ij} : Spatial weight between locations

w_R : Radiation weighting factor

w_T : Tissue weighting factor

w_w : Weight assigned to the worst criteria

Wi : Diagonal matrix of weights for location

$\mathbf{X}$: Matrix of independent variables

$\boldsymbol{X}$: Actual value of the factor

$\boldsymbol{x_j}$: Social vulnerability index value at particular location

$\boldsymbol{X_{ij}}$: Normalized value of the vulnerability factor for region

$\boldsymbol{X_{max}}$: Maximum values of the factor

$\boldsymbol{X_{min}}$: Minimum values of the factor

$\boldsymbol{X_n}$: Normalized value of the factor

$(\boldsymbol{x_i}, \boldsymbol{y_i})$: Coordinates of the origin

$(\boldsymbol{x_j}, \boldsymbol{y_j})$: Coordinates of the destination

$\mathbf{y}$: Cross wind distance

$\mathbf{Y}$: Vector of dependent variable values

$\boldsymbol{y_i}$: Dependent variable at location

$\boldsymbol{y_i^p}$: Predicted values

$\boldsymbol{y_m^p}$: Mean of predicted values

$\boldsymbol{y^m}$: Mean of the observed values

$\mathbf{Z}$: Standardized test statistic

$\mathbf{z}$: Vertical distance from the ground

$\boldsymbol{Z_{evac}(i,j)}$: Evacuation time component

$\boldsymbol{Z(G_i^*)}$: Standardized Getis-Ord statistic using a z-score

$\boldsymbol{Z_{overc}(j)}$: Overcrowding component

$\boldsymbol{Z_{supply}(j)}$: Supply-access time component

$\boldsymbol{Z_t}$: Observed wind speed

$\boldsymbol{\epsilon_i}$: Error term

ξ : Maximum deviation in judgments

σ : Standard deviation

$\boldsymbol{\sigma_p^2}$: Variance

$\boldsymbol{\sigma_y}$: Horizontal dispersion parameter

$\boldsymbol{\sigma_z}$: Vertical dispersion parameter

$\Delta\mathbf{H}$: Plume rise

$\boldsymbol{Adjusted\ Cost_{Turkiye}}$: Adjusted cost for Turkiye

$\boldsymbol{CRM_i}$: Cancer risk for particular neighborhood

$\boldsymbol{Reference\ Cost_{Japan}}$: Reference cost corresponding to Japan

$\boldsymbol{SVI_i}$: Social Vulnerability Index for region

$\boldsymbol{C_{TM}(x,0,0)}$: Terrain-modified concentration at downwind distance

LIST OF TABLES

Page

Table 2.1 : The INES and historical example. **10**
Table 2.2 : Top journals on Chernobyl accident related study..... **22**
Table 2.3 : Top journals on Fukushima accident related study..... **23**
Table 2.4 : Top cited documents on Chernobyl accident related study. **24**
Table 2.5 : Top cited documents on Fukushima accident related study. **25**
Table 2.6 : Independent variables and their potential influence on scientific research related to nuclear accidents..... **32**
Table 2.7 : Summary statistics for Global Moran's I. **33**
Table 2.8 : Summary statistics for coefficients estimates and OLS regression model analysis. **34**
Table 2.9 : Summary statistics for coefficients estimates and MGWR model analysis. **38**
Table 2.10 : Timeline of evacuation orders related to the Chernobyl accident. **44**
Table 2.11 : Demographic data of towns and regions affected by the Chernobyl accident and located out of an exclusion zone..... **44**
Table 2.12 : Chronology of orders related to the response to the Fukushima Daiichi accident **46**
Table 2.13 : Demographic data of Fukushima prefecture before and after the accident and dates of lifting the evacuation orders..... **48**
Table 2.14 : Radiation doses and associated health impacts across affected groups after the Chernobyl disaster **54**
Table 2.15 : Estimated Radiation Doses and Associated Health Impacts Across Affected Groups After the Fukushima Disaster. **56**
Table 3.1 : Factors and their functional relationship with vulnerability. **77**
Table 3.2 : Stability-dependent constants used in GPM. **89**
Table 3.3 : Characteristics of stability classes..... **90**
Table 3.4 : Input data parameters to identify the worst-case scenario. **92**
Table 3.5 : Risk coefficients and health impact. **111**
Table 5.1 : Description of criteria which shown in Figure 1..... **138**
Table 5.2 : Wilcoxon Signed-Rank test results. **142**
Table 5.3 : Input parameters for HotSpot software. **149**
Table 5.4 : Country-specific guidelines on emergency response. **153**
Table 5.5 : Statistical results of model evaluation. **158**
Table 5.6 : Results of the KS test. **159**
Table 5.7 : Comparison of Collective Radiation Dose and Estimated Cancer Cases for Radius-Based and Priority-Based Evacuation Strategies..... **167**
Table 5.8 : Decision matrix for evaluating radius-based and priority-based evacuation strategies across key performance criteria..... **167**
Table 5.9 : Assigned weights for each criterion based on sensitivity analysis. **169**
Table 5.10 : Road description. **171**
Table 5.11 : Cs-137 ground deposition thresholds (kBq/m2). **184**
Table 5.12 : Decontamination intensity. **187**

Table 5.13 : Volume of radioactive waste..... **189**

LIST OF FIGURES

Page

Figure 2.1 : Timeline of nuclear development. **7**
Figure 2.2 : Research methodology. **17**
Figure 2.3 : Research trends: a) Chernobyl accident related documents, b) Fukushima accident related documents. **20**
Figure 2.4 : Core research areas: a) Chernobyl accident related keywords, b) Fukushima accident related keywords. **27**
Figure 2.5 : Spatial distribution of scientific documents: a) Chernobyl accident related documents, b) Fukushima accident related documents. **29**
Figure 2.6 : Global collaborative network between the most productive countries: a) Chernobyl accident related collaboration, b) Fukushima accident related collaboration. **30**
Figure 2.7 : Geospatial analysis: the framework of the research design..... **31**
Figure 2.8 : Spatial distribution of selected independent variables at the country level across the world: a) GDP, b) Electricity production from nuclear, c) Nuclear reactors, d) Electricity consumption from nuclear. **35**
Figure 2.9 : Compound impact of energy and economic indicators on the spatial distribution of global scientific production: a) MGWR model for GDP, b) MGWR model for electricity production from nuclear, c) MGWR model for active nuclear reactors, d) MGWR model for electricity consumption from nuclear. **36**
Figure 2.10 : Performance of the MGWR model: a) Spatial distribution of local R^2, b) Spatial distribution of standard residuals. **37**
Figure 2.11 : Evolution of nuclear accident research (red stars indicate Chernobyl 1986 and Fukushima 2011 accidents, respectively). **39**
Figure 2.12 : Chernobyl disaster: a) Chernobyl exclusion zone, b) Chernobyl's reactor after the explosion (both pictures are taken form Encyclopedia Britannica). **42**
Figure 2.13 : Percent distribution of people affected by the Chernobyl accident: a) Distribution of evacuated population in the period of 1986 – 1990, b) Distribution of resettled population in the period of 1991 – 2000, c) Distribution of liquidators in the period of 1986 – 1987, d) Distribution of liquidators in the period of 1987 – 1989 ..... **43**
Figure 2.14 : Fukushima-Daiichi disaster: a) Aerial image taken after the disaster, b) Fukushima exclusion zone..... **45**
Figure 2.15 : Environmental contamination due to Chernobyl disaster: Maps showing radioactive contamination of the Europe by Cs137 after the accident and radioactive contamination of the territory of Ukraine by Cs137 before and after the disaster (1985 year) **50**

Figure 2.16 : The spatial distribution of radiation after the Fukushima disaster: a) Contamination of Japan as of April 2011, b) as of November 2016 c) Contamination of the Pacific Ocean at years 1.5 and 3.5. ..... **53**
Figure 3.1 : Research framework for estimation and mapping of social vulnerability to nuclear accident. **74**
Figure 3.2 : The hierarchical structure of the nuclear accident vulnerability criteria used in the study. **75**
Figure 3.3 : A representation of a GPM. **87**
Figure 3.4 : Worst-case scenario results. **91**
Figure 3.5 : Workflow of the proposed model on integration PF with GPM. **96**
Figure 3.6 : Workflow of the proposed methodology. **106**
Figure 3.7 : Estimated duration of Fukushima evacuee monthly compensation by zone. **115**
Figure 4.1 : Geographical location of Akkuyu NPP. **120**
Figure 4.2 : Demographic profile of Mersin province. **121**
Figure 4.3 : Topographic features of study area. **122**
Figure 4.4 : Monthly temperatures and sunshine days. **126**
Figure 4.5 : Seasonal wind roses: a) Winter, b) Spring, c) Summer, d) Autumn. .. **127**
Figure 4.6 : Box plots of monthly wind speed data. **128**
Figure 4.7 : Recurrence of atmospheric data: a) Stability categories, b) Wind speed. **130**
Figure 4.8 : Monthly precipitations and rainy days. **131**
Figure 4.9 : Monthly humidity levels. **132**
Figure 4.10 : Land Use and Land Cover of study area. **133**
Figure 5.1 : Spatial representation of research criteria: a) Population, b) Gender, c) Marital status, d) Level of education, e) Building density, f) Agricultural areas, g) Services of preparedness and coping capacity, h) Emergency response capabilities. **136**
Figure 5.2 : Dispersion of weights for each criterion. **137**
Figure 5.3 : Social vulnerability coefficient maps obtained with BWM: a) Demography map, b) Building and environmental system map, c) Preparedness map, d) Emergency response map, e) Coping capacity map, f) Physical exposure map, g) Resistance map, h) SVI map. **139**
Figure 5.4 : Social vulnerability coefficient maps obtained with AHP: a) Demography map, b) Building and environmental system map, c) Preparedness map, d) Emergency response map, e) Coping capacity map, f) Physical exposure map, g) Resistance map, h) SVI map. **140**
Figure 5.5 : Tornado chart. **143**
Figure 5.6 : Hot and cold spots of social vulnerability: a) BWM, b) AHP. **144**
Figure 5.7 : Results of simulation: a) Air concentration, b) TEDE, c) Ground deposition. **151**
Figure 5.8 : Cs-137 ground-level log-transformed concentration values over time and distance (first scenario): a) no terrain and no rain, b) no terrain with rain, c) terrain and no rain, d) terrain with rain. **154**
Figure 5.9 : Cs-137 ground-level log-transformed concentration values over time and distance (second scenario): a) no terrain and no rain, b) no terrain with rain, c) terrain and no rain, d) terrain with rain. **155**
Figure 5.10 : Cs-137 ground-level log-transformed concentration values over time and distance (third scenario): a) no terrain and no rain, b) no terrain with rain, c) terrain and no rain, d) terrain with rain. **156**

Figure 5.11 : Cross-validation of wind prediction using PF: a) Plot of measured versus predicted values of wind speed, b) Correlation plot between measured and predicted wind speed values. **158**
Figure 5.12 : Results of KS test: a) Histogram of errors, b) QQ plot of errors..... **160**
Figure 5.13 : K-fold cross-validation performance metrics. **161**
Figure 5.14 : Evacuation priority map: a) WSM, b) Geometric mean method, c) Maximum value approach. **162**
Figure 5.15 : Evacuation time estimates for radius-based and priority-based evacuations. Black dashed lines represent the 50% and 100% of population, blue and red dashed lines show the evacuation time when 50% and 100% of population is evacuated corresponding to radius-based and priority-based evacuations, respectively. **164**
Figure 5.16 : Evacuation time estimates for radius-based and priority-based evacuations accounting for vulnerable population. Black dashed lines represent the 50% and 100% of population, blue and red dashed lines show the evacuation timeframe in three phases. **165**
Figure 5.17 : Average TEDE doses received per person for each evacuation batch. **166**
Figure 5.18 : Sensitivity results for evaluating evacuation strategies. **168**
Figure 5.19 : Study area: a) Population within the 30-km radius zone, b) Location of shelters, depots, and neighborhoods' centroids, as well as road network. **170**
Figure 5.20 : OD analysis of evacuation routes to emergency shelters: a), b), c) Evacuation routes for Region A – thresholds 76 min, 90 min, and 115 min, respectively, d), e), f) Evacuation routes for Region B – thresholds 76 min, 90 min, and 115 min, respectively, g), h), i) Evacuation routes for Region C – thresholds 76 min, 90 min, and 115 min, respectively. **172**
Figure 5.21 : OD analysis of supply-access routes to emergency shelters: a),(b), c) supply-access routes for Region A – thresholds 5 min, 15 min, and 20 min, respectively; d), e), f) supply-access routes for Region B – thresholds 5 min, 50 min, and 90 min, respectively; g), h), i) supply-access routes for Region C – thresholds 15 min, 50 min, and 90 min, respectively. **173**
Figure 5.22 : Neighborhoods to shelter assignment map with shelter ranking: a) Region A, b) Region B, c) Region C. **175**
Figure 5.23 : Population assignment and remaining capacity in shelters: a) Region A, b) Region B, c) Region C..... **177**
Figure 5.24 : Sensitivity analysis: total objective value vs. weights..... **178**
Figure 5.25 : Results of k-fold cross-validation: mean objective value with standard deviation. **179**
Figure 5.26 : Health consequences from hypothetical accident: a) TEDE, b) Cancer risk. **183**
Figure 5.27 : Decay timeline of Cs-137 deposition by protective action category. **185**
Figure 5.28 : The emergency response costs. **186**
Figure 5.29 : The decontamination costs. **188**
Figure 5.30 : The health-related costs **188**
Figure 5.31 : The radioactive waste-related costs. **190**
Figure 5.32 : The compensation-related costs. **191**
Figure 5.33 : The administration-related costs..... **192**
Figure 5.34 : The total estimated costs. **192**

DEVELOPMENT OF A SPATIAL MODEL ON NUCLEAR POWER PLANT ACCIDENTS BASED ON VULNERABILITY AND EVACUATION PLANS

SUMMARY

Nuclear power plants (NPPs) offer considerable benefits in terms of energy security and climate change mitigation due to their low greenhouse gas emissions. However, the catastrophic consequences of accidents such as those at Chernobyl and Fukushima have underscored the urgent need for advanced emergency preparedness strategies. Traditional emergency responses, often based on static radius-based evacuation zones, fall short of addressing the spatial and social complexities involved in nuclear emergencies. In light of these limitations, there is an urgent need for spatially explicit models that integrate social vulnerability and evacuation dynamics to guide risk mitigation, preparedness, and policy decisions more effectively.

This study develops a comprehensive spatial model aimed at improving preparedness and response planning for nuclear accidents, with a specific focus on vulnerability assessment, hazard mapping, evacuation efficiency, shelter optimization, and economic loss estimation. The analysis is conducted within the emergency planning zone surrounding the Akkuyu NPP in Turkiye, an area characterized by diverse socioeconomic conditions, infrastructure types, and population densities. The first stage of the study involved the development of a Social Vulnerability Index (SVI), designed to identify and spatially map populations at heightened risk during nuclear incidents. Two independent multi-criteria decision-making methods, particularly Analytic Hierarchy Process (AHP) and Best-Worst Method (BWM), were applied separately to ensure methodological robustness. These approaches considered multiple vulnerability dimensions, including demographic, environmental, infrastructural, preparedness, and coping capacity factors and produced comparable spatial patterns of vulnerability across the study area.

To model the hazardous radiation dispersion, an enhanced hazard mapping approach was implemented by combining a Particle Filter (PF) algorithm with a Gaussian Plume Model (GPM). Unlike traditional models that rely solely on static meteorological inputs, the PF was employed to dynamically predict wind speed based on real-time atmospheric data. These wind speed predictions were then fed into the GPM to simulate the dispersion of radioactive material. This innovative fusion allows for dynamic and adaptive hazard prediction, resulting in more realistic and responsive hazard maps suitable for real-time emergency planning.

Building upon the SVI and the dynamic hazard mapping, a priority-based evacuation map was generated, identifying the sequence and urgency with which neighborhoods should be evacuated during a nuclear emergency. This approach was directly compared to the conventional radius-based strategy, commonly used in prior events such as the Fukushima accident. Evacuation time for both methods was estimated using Discrete Event Simulation (DES), a powerful tool capable of modeling the sequential flow of evacuees across road networks under various constraints, including road capacity and population density. The comparison revealed that while the radius-

based approach was marginally more time-efficient in total evacuation duration, the priority-based strategy was significantly more effective in evacuating socially vulnerable populations earlier in the process, thereby reducing their exposure to radiation and related health risks.

Shelter analysis constituted the next phase of the study, where the usability and distribution of existing emergency shelters were evaluated using a multi-dimensional optimization method. The optimization process included three key criteria: travel time from origin neighborhoods to shelters, accessibility to essential supplies (such as food, water, and medicine), and shelter overcrowding potential. This approach enabled the identification of optimal shelter sites capable of minimizing evacuation and supply access time while avoiding population congestion, ensuring more equitable and efficient shelter allocation during emergencies.

Finally, the study assessed the potential for indirect economic losses in the aftermath of a nuclear accident using spatial economic analysis. The loss assessment integrated multiple cost components, including emergency response costs, decontamination operations, radioactive waste management, public health expenditures, and compensation for displaced populations. The results revealed significant spatial heterogeneity in projected economic losses, with neighborhoods exhibiting higher SVI scores and closer proximity to the NPP being disproportionately affected. These findings underscore the compounded risk borne by socioeconomically vulnerable communities, not only in terms of immediate exposure but also in their long-term economic recovery.

By integrating vulnerability analysis, dynamic hazard modeling, simulation-based evacuation assessment, shelter optimization, and economic loss estimation, this research contributes a novel, spatially-explicit framework for nuclear emergency planning. The model offers valuable insights for policymakers and emergency planners, enabling more targeted and equitable interventions that balance operational efficiency with ethical responsibility. Furthermore, the proposed methodology enhances our understanding of the spatial dimensions of nuclear risk and provides a replicable template for emergency preparedness in other regions with nuclear infrastructure.

The results substantiate all three hypotheses articulated in the study.

First, the research strongly supports the hypothesis that vulnerability is not solely determined by geographic proximity to the NPP or direct radiation exposure. Instead, socio-economic and infrastructural disadvantages such as limited access to emergency resources, weak healthcare systems, inadequate transportation infrastructure, and low levels of disaster preparedness emerge as critical factors elevating community risk. In fact, several neighborhoods situated farther from the NPP but with poor infrastructure and mobility experienced higher total effective dose equivalent (TEDE) values than some closer, better-equipped communities. These findings highlight the complex and multidimensional nature of vulnerability, reinforcing that effective disaster planning must go beyond spatial proximity and incorporate localized, socially-informed strategies. Targeted interventions including tailored public education, equitable resource distribution, and community-specific preparedness plans are essential for reducing vulnerability and enhancing resilience.

Second, the priority-based evacuation strategy, though slower in terms of total evacuation time (26.1 hours vs. 21.8 hours for the radius-based model), outperformed the traditional method in terms of ethical distribution and health outcomes. Vulnerable

populations were evacuated earlier in the process, leading to a 14% reduction in TEDE and a 20.61% decrease in estimated cancer risk relative to the radius-based model. This highlights a critical ethical and operational dilemma: while faster evacuation may seem preferable, it may inadvertently exacerbate harm for those least able to cope.

Third, the indirect economic loss assessment confirmed that higher socioeconomic vulnerability is strongly correlated with greater long-term economic impacts. Approximately 35% of the study area that is comprising mostly vulnerable inner-periphery and urban-fringe neighborhoods was classified as high or very high in terms of economic loss. These communities face compounded challenges due to reduced access to healthcare, lower income levels, and dependence on single economic sectors (e.g., agriculture). The findings highlight the urgency of targeted mitigation strategies, such as resilient infrastructure development, financial aid programs, and community-based preparedness initiatives.

This study provides a comprehensive and empirically grounded spatial modeling framework that bridges critical gaps in nuclear emergency planning. It demonstrates that incorporating social vulnerability, dynamic hazard forecasting, and realistic evacuation simulation leads to more equitable and effective emergency response strategies. The proposed model serves as a decision-support tool capable of guiding emergency planners and policymakers in identifying high-risk populations, optimizing shelter allocation, and minimizing long-term socioeconomic disruption. Furthermore, the methodology is adaptable and scalable, offering valuable insights for other high-risk facilities, such as chemical plants or industrial zones.

Beyond its national relevance to Turkiye's nuclear energy strategy and civil protection systems, the study contributes to the global discourse on disaster risk reduction by offering a replicable framework for integrating social justice into emergency response. It supports the international goals of resilient disaster preparedness and aligns with international best practices for nuclear safety. By demonstrating how advanced spatial modeling can improve both operational efficiency and ethical accountability in disaster response, this research marks a significant advancement in the science and practice of nuclear emergency management.

KIRILGANLIK VE TAHLİYE PLANLARINA DAYALI NÜKLEER SANTRAL KAZALARI İÇİN MEKANSAL BİR MODELİN GELİŞTİRİLMESİ

ÖZET

Nükleer Enerji Santralleri (NES'ler), düşük sera gazı emisyonları sayesinde enerji güvenliği sağlama ve iklim değişikliğiyle mücadele etme açısından önemli avantajlar sunmaktadır. Ancak, Çernobil ve Fukushima gibi felaket niteliğindeki kazalar, nükleer acil durumlara karşı gelişmiş hazırlık stratejilerine duyulan acil ihtiyacı açık bir şekilde ortaya koymuştur. Geleneksel acil durum müdahale yöntemleri, genellikle sabit yarıçaplı tahliye bölgelerine dayandığından, nükleer kazaların ortaya çıkardığı mekânsal ve toplumsal karmaşıklıkları yeterince yansıtamamaktadır. Bu tür yaklaşımlar, riskin farklı topluluklar üzerindeki etkisini dikkate almadığı gibi, tahliye süreçlerinin dinamik yapısını da göz ardı etmektedir. Bu sınırlamaların ışığında, sosyal kırılganlık unsurlarını ve tahliye dinamiklerini birlikte ele alan, mekânsal olarak ayrıntılı modellerin geliştirilmesine yönelik ihtiyaç her geçen gün daha da artmaktadır. Bu tür bütünleşik yaklaşımlar, yalnızca risk azaltma çabalarını güçlendirmekle kalmaz; aynı zamanda hazırlık planlaması ve politika geliştirme süreçlerine daha etkili ve adil bir temel oluşturur.

Bu çalışma, nükleer kazalara yönelik hazırlık ve müdahale planlamasını iyileştirmeyi amaçlayan kapsamlı bir mekânsal model geliştirmektedir. Model, özellikle kırılganlık analizi, tehlike haritalaması, tahliye verimliliği, sığınak optimizasyonu ve ekonomik kayıp tahmini gibi çok boyutlu bileşenleri bir arada ele alarak risk yönetimi süreçlerine bütüncül bir yaklaşım sunmaktadır. Analizler, Türkiye'de yer alan Akkuyu Nükleer Güç Santrali (NGS) çevresindeki acil durum planlama bölgesi sınırları içerisinde gerçekleştirilmiştir. Bu bölge, farklı sosyoekonomik koşullar, altyapı türleri ve nüfus yoğunluklarıyla dikkat çeken heterojen bir yapıya sahiptir.

Çalışmanın ilk aşamasında, nükleer bir olay sırasında risk altında olabilecek toplulukları belirlemek ve mekânsal olarak haritalamak amacıyla Sosyal Kırılganlık Endeksi (SKE) geliştirilmiştir. Bu bağlamda, metodolojik sağlamlığı artırmak için iki bağımsız çok kriterli karar verme yöntemi kullanılmıştır: Analitik Hiyerarşi Süreci (AHS) ve En İyi-En Kötü Yöntemi (EİEKY). Her iki yöntem de birbirinden bağımsız olarak uygulanmış ve elde edilen sonuçlar karşılaştırılarak yöntemlerin güvenilirliği pekiştirilmiştir.

Bu karar verme süreçleri kapsamında, demografik yapı, çevresel etmenler, altyapısal durum, toplulukların hazırlıklı olma düzeyi ve başa çıkma kapasitesi gibi çeşitli kırılganlık boyutları dikkate alınmıştır. Elde edilen analizler sonucunda, çalışma alanı genelinde sosyal kırılganlık düzeylerinin mekânsal dağılımını yansıtan benzer örüntüler ortaya konmuştur. Bu sonuçlar, acil durumlara yönelik planlamaların kırılgan grupları önceliklendirecek şekilde şekillendirilmesi açısından kritik öneme sahiptir.

Tehlikeli radyasyon yayılımını modellemek amacıyla, gelişmiş bir tehlike haritalama yaklaşımı uygulanmıştır. Bu kapsamda, Parçacık Filtresi (PF) algoritması ile Gauss Plume Modeli (GPM) birleştirilerek yenilikçi ve dinamik bir modelleme süreci geliştirilmiştir. Geleneksel modeller çoğunlukla sabit meteorolojik verilerle sınırlı kalırken, bu çalışmada PF algoritması, gerçek zamanlı atmosferik verileri kullanarak rüzgâr hızını öngörmek üzere entegre edilmiştir. PF algoritması sayesinde elde edilen dinamik rüzgâr hızı tahminleri, daha sonra GPM'ye veri olarak aktarılmış ve bu sayede radyoaktif materyalin atmosferdeki yayılımı detaylı şekilde simüle edilmiştir.

Bu yenilikçi birleşim, yalnızca statik ve varsayımsal senaryolara dayalı değerlendirmelerin ötesine geçerek, değişen meteorolojik koşullara uyum sağlayabilen ve gerçek zamanlı veriyle güncellenebilen tehlike tahminlerinin yapılmasına olanak tanımaktadır. Modelin dinamik yapısı sayesinde, radyasyonun yayılımına ilişkin daha gerçekçi, hassas ve zamanla değişen risk haritaları oluşturulabilmektedir. Böylelikle, acil durum planlamaları için çok daha uygun, hızlı tepki verebilen ve duruma özgü müdahale stratejilerinin geliştirilmesini destekleyen bir sistem ortaya konmuştur.

Sosyal Kırılganlık Endeksi (SKE) ve dinamik tehlike haritalama analizine dayanarak, nükleer bir acil durumda mahallelerin hangi sırayla ve hangi öncelikle tahliye edilmesi gerektiğini belirleyen öncelik temelli bir tahliye haritası oluşturulmuştur. Bu yaklaşım, daha önce Fukushima kazası gibi olaylarda yaygın olarak kullanılan geleneksel yarıçap temelli tahliye stratejisiyle doğrudan karşılaştırılmıştır. Her iki yönteme ait tahliye süreleri, yol ağı üzerindeki nüfus hareketini çeşitli kısıtlar (örneğin yol kapasitesi ve nüfus yoğunluğu) altında ardışık olarak modelleyebilen güçlü bir araç olan Ayrık Olay Simülasyonu (AOS) kullanılarak tahmin edilmiştir. Karşılaştırma sonuçları, yarıçap temelli yaklaşımın toplam tahliye süresi açısından biraz daha zaman tasarruflu olduğunu ortaya koyarken, öncelik temelli stratejinin sosyal açıdan kırılgan toplulukların daha erken tahliye edilmesinde belirgin şekilde daha etkili olduğunu göstermiştir. Bu da, söz konusu grupların radyasyona maruz kalma süresini ve buna bağlı sağlık risklerini azaltma açısından önemli bir avantaj sağlamaktadır.

Çalışmanın bir sonraki aşamasını ise sığınak analizleri oluşturmuştur. Bu kapsamda, mevcut acil durum sığınaklarının kullanılabilirliği ve mekânsal dağılımları, çok boyutlu bir optimizasyon yöntemi kullanılarak değerlendirilmiştir. Optimizasyon süreci üç temel kriter etrafında yapılandırılmıştır: mahalle merkezlerinden sığınaklara olan seyahat süresi, temel ihtiyaç malzemelerine (örneğin gıda, su ve ilaç) erişilebilirlik düzeyi ve sığınaklarda oluşabilecek aşırı kalabalık riski. Bu çok kriterli yaklaşım, yalnızca tahliye ve malzeme erişim süresini en aza indirmekle kalmamış, aynı zamanda sığınaklarda nüfus yoğunlaşmasını önleyerek acil durumlar sırasında daha dengeli, adil ve etkili bir yerleştirme stratejisinin belirlenmesini mümkün kılmıştır.

Bu analizler sayesinde, sadece fiziksel yakınlık değil, aynı zamanda erişim eşitliği ve kapasite verimliliği gibi kritik unsurlar da dikkate alınmış; bu da afet yönetimi açısından daha sürdürülebilir ve insan odaklı planlama yaklaşımlarının önünü açmıştır.

Son olarak, bu çalışmada nükleer bir kazanın ardından ortaya çıkabilecek dolaylı ekonomik kayıplar, mekânsal ekonomik analiz yöntemi kullanılarak değerlendirilmiştir. Kayıp değerlendirmesi; acil müdahale maliyetleri, dekontaminasyon çalışmaları, radyoaktif atık yönetimi, halk sağlığı harcamaları ve yerinden edilen nüfusa yönelik tazminatlar gibi birden fazla maliyet bileşenini kapsamlı bir şekilde içermiştir. Elde edilen sonuçlar, öngörülen ekonomik kayıplarda belirgin bir mekânsal farklılık olduğunu ortaya koymuştur. Özellikle, SKE puanları

yüksek olan ve NGS'ne daha yakın konumlanan mahallelerin orantısız şekilde daha fazla etkilendiği tespit edilmiştir.

Bu bulgular, sosyoekonomik açıdan kırılgan toplulukların sadece radyasyona doğrudan maruziyet açısından değil, aynı zamanda uzun vadeli ekonomik iyileşme süreçlerinde de orantısız riskler taşıdığını güçlü bir şekilde ortaya koymaktadır.

Kırılganlık analizi, dinamik tehlike modellemesi, simülasyona dayalı tahliye değerlendirmesi, sığınak optimizasyonu ve ekonomik kayıp tahminlerini bütünleştiren bu çalışma, nükleer acil durum planlaması için yenilikçi ve mekânsal olarak ayrıntılı bir çerçeve sunmaktadır. Geliştirilen model, karar vericiler ve acil durum planlayıcıları için değerli içgörüler sağlayarak, operasyonel verimlilik ile etik sorumluluk arasında denge kuran daha hedefli ve adil müdahalelerin gerçekleştirilmesine olanak tanımaktadır. Ayrıca, önerilen metodoloji nükleer riskin mekânsal boyutlarını anlamamıza katkı sağlamakta ve nükleer altyapıya sahip diğer bölgelerde de acil durum hazırlıkları için tekrarlanabilir bir şablon sunmaktadır.

Elde edilen sonuçlar, çalışmada ortaya konulan üç temel hipotezi de güçlü biçimde desteklemektedir. İlk olarak, kırılganlığın yalnızca NGS'ne olan coğrafi yakınlık ya da doğrudan radyasyona maruz kalma ile açıklanamayacağı yönündeki hipotez net bir şekilde doğrulanmıştır. Araştırma, sosyoekonomik eşitsizlikler ve altyapı yetersizliklerinin, örneğin acil durum kaynaklarına sınırlı erişim, zayıf sağlık hizmetleri, yetersiz ulaşım altyapısı ve düşük afet hazırlık düzeyi, toplulukların risk seviyesini belirlemede başat rol oynadığını ortaya koymuştur.

Nitekim, NGS'ye daha uzak konumda bulunan bazı mahallelerin, altyapısal zayıflıklar ve düşük hareket kabiliyeti nedeniyle, daha yakın ama daha donanımlı mahallelere kıyasla daha yüksek Toplam Etkin Doz Eşdeğeri (TEDE) değerlerine maruz kaldığı tespit edilmiştir. Bu durum, kırılganlığın karmaşık ve çok boyutlu doğasını vurgulamakta; etkili afet planlamasının yalnızca mekânsal yakınlığa odaklanmakla kalmayıp, yerel koşulları ve toplumsal özellikleri dikkate alan stratejilerle desteklenmesi gerektiğini ortaya koymaktadır.

Bu bağlamda, kırılganlığı azaltmak ve toplumsal dayanıklılığı artırmak adına şu tür hedefli müdahaleler hayati öneme sahiptir: topluluklara özgü bilinçlendirme ve afet eğitimi programları, adil kaynak dağılımı politikaları ve mahalle bazında uyarlanmış hazırlık planlarının geliştirilmesi. Bu bütüncül yaklaşım, yalnızca acil durumlara daha etkin yanıt verilmesini sağlamakla kalmayacak, aynı zamanda uzun vadeli sürdürülebilirlik ve sosyal adalet açısından da güçlü bir temel sunacaktır.

İkinci olarak, öncelik temelli tahliye stratejisi toplam tahliye süresi açısından geleneksel yarıçap temelli modele kıyasla daha yavaş olsa da (öncelik temelli modelde 26,1 saat, yarıçap temelli modelde 21,8 saat), etik açıdan daha adil bir dağılım sağlamış ve sağlık sonuçları bakımından daha başarılı performans göstermiştir. Bu model, özellikle sosyal açıdan kırılgan nüfus gruplarının tahliye sürecinde daha erken aşamalarda bölgeden çıkarılmasını mümkün kılarak, bu grupların maruz kaldığı TEDE'ni %14 oranında azaltmış ve buna bağlı olarak tahmini kanser riski %20,61 oranında düşürülmüştür.

Bu bulgular, afet yönetiminde sıklıkla karşılaşılan önemli bir etik ve operasyonel ikilemi gözler önüne sermektedir: daha hızlı bir tahliye süreci ilk bakışta daha avantajlı görünse de, bu yaklaşım afetlere karşı baş etme kapasitesi düşük olan savunmasız topluluklar için zararı artırabilecek, eşitsizlikleri derinleştirebilecektir. Dolayısıyla,

sadece süreye dayalı verimlilik değil, aynı zamanda müdahalenin adil, kapsayıcı ve insan odaklı olması da büyük önem taşımaktadır.

Bu çerçevede, afet planlamasında operasyonel hız ile etik sorumluluk arasındaki dengeyi kurabilen, önceliklendirmeye dayalı stratejilerin yaygınlaştırılması, daha adil ve sürdürülebilir müdahale modellerinin geliştirilmesi açısından kritik bir adımdır.

Üçüncü olarak, dolaylı ekonomik kayıp değerlendirmesi, yüksek sosyoekonomik kırılganlık ile uzun vadeli ekonomik etkiler arasında güçlü bir korelasyon olduğunu doğrulamıştır. Çalışma alanının yaklaşık %35'lik bir bölümü (çoğunlukla kırılgan iç çevre mahalleleri ve kentsel kenar kuşaklardan oluşan alanlar) ekonomik kayıp açısından yüksek veya çok yüksek risk grubunda sınıflandırılmıştır. Bu topluluklar; sağlık hizmetlerine sınırlı erişim, düşük gelir düzeyleri ve tek bir ekonomik sektöre (örneğin tarım) bağımlı olmaları nedeniyle çok katmanlı zorluklarla karşı karşıyadır.

Elde edilen bulgular, dayanıklı altyapı yatırımları, finansal destek programları ve topluluk temelli hazırlık girişimleri gibi hedefe yönelik zarar azaltma stratejilerinin geliştirilmesi gerektiğini güçlü bir şekilde ortaya koymaktadır. Bu tür stratejiler, yalnızca afet sonrası iyileşmeyi hızlandırmakla kalmayacak, aynı zamanda kırılgan toplulukların uzun vadeli direnç kapasitesini artırmada da kilit rol oynayacaktır.

Bu çalışma, nükleer acil durum planlamasında kritik boşlukları dolduran, kapsamlı ve deneysel verilere dayalı bir mekânsal modelleme çerçevesi sunmaktadır. Sosyal kırılganlığın, dinamik tehlike tahminlerinin ve gerçekçi tahliye simülasyonlarının modele entegre edilmesiyle, daha adil ve etkili acil durum müdahale stratejilerinin geliştirilebileceği açıkça gösterilmiştir. Önerilen model, acil durum planlayıcıları ve politika yapıcılar için yüksek risk taşıyan nüfus gruplarının belirlenmesi, sığınakların en uygun şekilde tahsisi ve uzun vadeli sosyoekonomik zararların en aza indirilmesi konularında rehberlik edecek bir karar destek aracı olarak işlev görmektedir.

Ayrıca, bu metodoloji esnek ve ölçeklenebilir yapısıyla farklı riskli tesisler için de uygulanabilir; örneğin kimya fabrikaları, sanayi bölgeleri veya diğer tehlikeli altyapılar için değerli çıkarımlar sunmaktadır. Bu yönüyle, sadece Türkiye'nin nükleer enerji stratejisi ve sivil koruma sistemleri açısından değil, aynı zamanda küresel düzeyde afet risklerinin azaltılması alanında da önemli katkılar sağlamaktadır.

Çalışma, sosyal adaletin acil durum müdahalelerine nasıl entegre edilebileceğine dair tekrarlanabilir ve uygulanabilir bir çerçeve sunarak uluslararası dayanıklı afet hazırlığı hedeflerine destek vermekte ve nükleer güvenlik alanındaki uluslararası en iyi uygulamalarla uyum göstermektedir. Gelişmiş mekânsal modellemenin, afet müdahalelerinde operasyonel verimliliği artırırken etik sorumluluğun da güçlendirilmesine nasıl katkı sağlayabileceğini ortaya koyması, nükleer acil durum yönetimi bilimi ve pratiğinde kayda değer bir ilerlemeyi temsil etmektedir.

Bu bağlamda, çalışma yalnızca teknik ve bilimsel açıdan değil, aynı zamanda sosyal ve politik boyutlarda da kapsamlı bir yenilik sunmakta; afetlere karşı hazırlık ve müdahale süreçlerinde hem etkinliği hem de adaleti artırmak için kritik bir araç görevi görmektedir.

1. INTRODUCTION

1.1 General

The growing dependence on nuclear power as a primary energy source highlights the urgent need to ensure the safety and resilience of nuclear power plants (NPPs) (Xu et al., 2021). Nuclear energy is lauded for its efficiency and low greenhouse gas emissions, making it a pivotal component of the global energy strategy (Addo et al., 2023). However, it also presents substantial risks. Catastrophic accidents, such as those in Chernobyl (1986) and Fukushima (2011), have demonstrated the severe consequences of nuclear incidents, affecting human life, ecosystems, and infrastructure worldwide (Steinhauser et al., 2014). These disasters underscore the importance of comprehensive risk management, continuous safety improvements, and public engagement to enhance awareness and preparedness. One crucial aspect is the effective use of spatial modeling to understand and mitigate vulnerabilities, optimize evacuation plans, and minimize harm during nuclear emergencies. Additionally, fostering international cooperation and sharing best practices can help fortify the global nuclear safety framework, ensuring a safer and more sustainable future.

1.2 Problem Statement

NPP accidents, although rare, have catastrophic consequences that transcend geographical and temporal boundaries. The complexity of these events arises from the interplay of multiple factors, including the nature of the radioactive release, meteorological conditions, population density, and the effectiveness of emergency response mechanisms (Ayoub et al., 2024). Existing models often fall short in integrating spatial dynamics with vulnerability assessments and evacuation logistics. This gap creates a critical need for a comprehensive spatial model that can: (1) Accurately assess the vulnerability of areas surrounding NPPs; (2) Optimize evacuation plans based on real-time and simulated scenarios; and (3) Inform policymakers and emergency planners to enhance resilience against nuclear accidents.

1.3 Aims and Objectives

The primary aim of this research is to develop a spatial model that integrates vulnerability assessments and evacuation planning to enhance preparedness and response during NPP accidents. The specific objectives are:

1. To assess vulnerability: identify and analyze spatial patterns of vulnerability based on factors such as population density, infrastructure, socioeconomic conditions, and resistance to disaster.
2. To model evacuation scenarios: develop a dynamic evacuation model that accounts for factors such as road network capacity, population movement, and real-time meteorological data.
3. To integrate spatial and temporal data: combine geospatial technologies, simulation tools, and real-world data to create a comprehensive model.
4. To provide policy recommendations: offer actionable insights to policymakers for improving nuclear emergency management.

1.4 Hypothesis

The study is guided by the three hypotheses.

Hypothesis 1: Areas with higher Social Vulnerability Index (SVI) scores exhibit increased susceptibility to adverse outcomes during nuclear accidents, including prolonged evacuation times, greater exposure to radiation, and higher rates of post-incident socio-economic disruption, due to limited access to resources, infrastructure challenges, and pre-existing vulnerabilities.

This hypothesis can be explained in the way that communities with higher SVI scores often lack adequate transportation infrastructure and resources, resulting in longer evacuation times during emergencies (Brian 2011). Pre-existing vulnerabilities, such as lower vehicle ownership rates and limited public transportation options, exacerbate these delays. Also, higher SVI areas may have insufficient access to protective equipment, timely information, and medical care, leading to increased radiation exposure. Additionally, compromised infrastructure can delay response times and

hinder effective sheltering-in-place measures. These communities often face heightened socio-economic challenges due to pre-existing conditions such as high poverty rates, limited access to education, and fragile local economies. In post-incident, these factors contribute to prolonged recovery periods and greater overall disruption (Dolan and Messen, 2012). Factors such as health disparities and lower levels of preparedness contribute to the increased susceptibility of high SVI communities. These pre-existing vulnerabilities make it more difficult for these areas to cope with and recover from nuclear incidents.

Hypothesis 2: The priority-based evacuation method, which integrates SVI data with hazard maps, leads to more effective and timely evacuation outcomes compared to the traditional radius-based evacuation approach by prioritizing high-risk and vulnerable populations, optimizing resource allocation, and reducing overall evacuation time.

By using SVI data, emergency planners can identify and prioritize areas with the highest vulnerability, ensuring that populations at greater risk are evacuated first (Flanagan et al., 2011). This targeted approach helps protect those who are most susceptible to adverse outcomes during a nuclear accident. A priority-based evacuation method enables a more efficient use of resources, such as transportation and emergency services. By focusing efforts on high-risk areas first, resources can be allocated where they are needed most, ensuring a more effective evacuation process (Chiu and Zheng, 2007). Traditional radius-based evacuations may lead to unnecessary congestion and delays, as they do not differentiate between areas with varying levels of risk (Hsu and Peeta, 2014). By integrating SVI data and hazard maps, emergency planners can design evacuation routes and strategies that minimize bottlenecks and reduce the overall time required to evacuate affected populations.

Hypothesis 3: In the context of a nuclear accident, regions with higher socioeconomic vulnerability experience greater indirect economic losses, highlighting the need for targeted mitigation strategies to reduce long-term financial and social burdens.

Nuclear accidents often result in both immediate and long-term economic consequences. Direct losses, such as damage to infrastructure, evacuation expenses, and cleanup operations, are typically visible and quantifiable. However, indirect losses, which include long-term health care costs, economic disruptions, unemployment, declines in property values, and losses in agricultural productivity, often have far-reaching effects that are harder to measure but equally significant

(Eeckhoudt et al., 2000; Huhtala and Remes, 2017). This proposed hypothesis highlights that socioeconomic vulnerability plays a critical role in shaping the scale and distribution of these indirect losses. Vulnerable regions, characterized by lower income levels, limited access to healthcare, weaker infrastructure, and less diversified economies, are less equipped to absorb the shocks of a nuclear accident. For instance, populations with fewer financial resources may struggle to relocate, access medical treatment, or recover from economic displacement. Furthermore, the economic ripple effects, such as reduced consumer spending and diminished labor force participation, may exacerbate the challenges faced by these communities.

1.5 Expected Contribution

This research will make significant contributions to the field of nuclear safety and emergency management by:

1. Developing an innovative spatial model that bridges the gap between vulnerability assessment and evacuation planning, offering a nuanced understanding of potential impacts.
2. Providing a robust decision-support tool for emergency planners to optimize response strategies during nuclear accidents, ensuring swift and effective action to protect public safety.
3. Enhancing the understanding of spatial dynamics in nuclear emergencies, not only advancing academic literature but also offering practical applications for emergency response teams and policymakers.
4. Informing and shaping policies to improve the resilience of communities near NPPs, thereby reducing potential loss of life and property, and fostering safety and preparedness.
5. Facilitating international collaboration by sharing insights and data, thereby contributing to global efforts to enhance nuclear safety standards and response mechanisms.

1.6 Organization of the Thesis

This thesis is organized into six chapters, each of which systematically contributes to understanding and modeling nuclear emergency preparedness with a focus on vulnerability, evacuation efficiency, and economic impact.

The first chapter introduces the research topic, beginning with the problem statement, which highlights the significance of enhancing emergency preparedness in the vicinity of NPPs. It then outlines the research aim and objectives, and states the hypotheses that guide the analysis. Additionally, the chapter discusses the expected contributions of the research.

The second chapter presents a comprehensive review of existing literature relevant to the study. It begins with a brief history of nuclear engineering and the evolution of the nuclear age in the context of disaster risk. It examines the causes of nuclear accidents, with detailed overviews of the Chernobyl and Fukushima disasters. A bibliometric analysis of scientific research on these major accidents is conducted to identify trends and gaps. The lessons learned from Chernobyl and Fukushima are discussed, focusing on environmental and health impacts and economic consequences. Finally, the chapter reviews existing models on vulnerability assessment and evacuation modeling, providing the foundation for the methodology adopted in this research.

The third chapter describes the methodological framework of the study. It begins with the development of the SVI, followed by hazard mapping, which integrates a data assimilation (DA) technique for more accurate meteorological representation. The chapter then introduces evacuation priority mapping, identifying zones that require urgent response. This is followed by the methodology for estimating evacuation time, and the evaluation of existing shelters in terms of location, accessibility, and capacity. The final part of the chapter presents the methodology for assessing potential economic losses using spatial and socioeconomic data.

The fourth chapter provides detailed information about the study area, including key meteorological and climatic data, and land use land cover (LULC) characteristics. Furthermore, it discusses the national energy strategies, emergency preparedness plans, and institutional responsibilities for nuclear safety and disaster response, contextualizing the study within Türkiye's regulatory and strategic frameworks.

The fifth chapter presents the results of the study. The findings of the SVI, hazard mapping, and evacuation time estimations are discussed in detail. It also includes the results of the shelter evaluation analysis, identifying spatial and capacity-related issues. The outcomes of the economic loss assessment are presented using spatial analysis tools, providing insights into potential regional economic impacts following a nuclear incident.

The final chapter summarizes the key findings of the research and discusses its limitations. Based on the findings, it offers recommendations for future research directions, emphasizing methodological improvements and data requirements. Finally, the chapter proposes policy recommendations to support national-level disaster risk reduction and nuclear emergency planning, aiming to enhance resilience and public safety.

2. LITERATURE REVIEW

2.1 Understanding Nuclear risks

2.1.1 The nuclear age and disaster risk: a historical overview

The discovery of nuclear fission in the late 1930s marked the beginning of a new era that we now call the nuclear age (Eidemuller, 2021). From the very start, nuclear technology has been a double-edged sword. On the one hand, it brought major advances in energy production and medicine. On the other, it introduced serious risks, from nuclear accidents to long-term environmental damage. In this section, it is underlined how nuclear technology developed over time, the disaster risks it introduced, and how the world has responded to those risks. Figure 2.1 outlines the history of nuclear development.

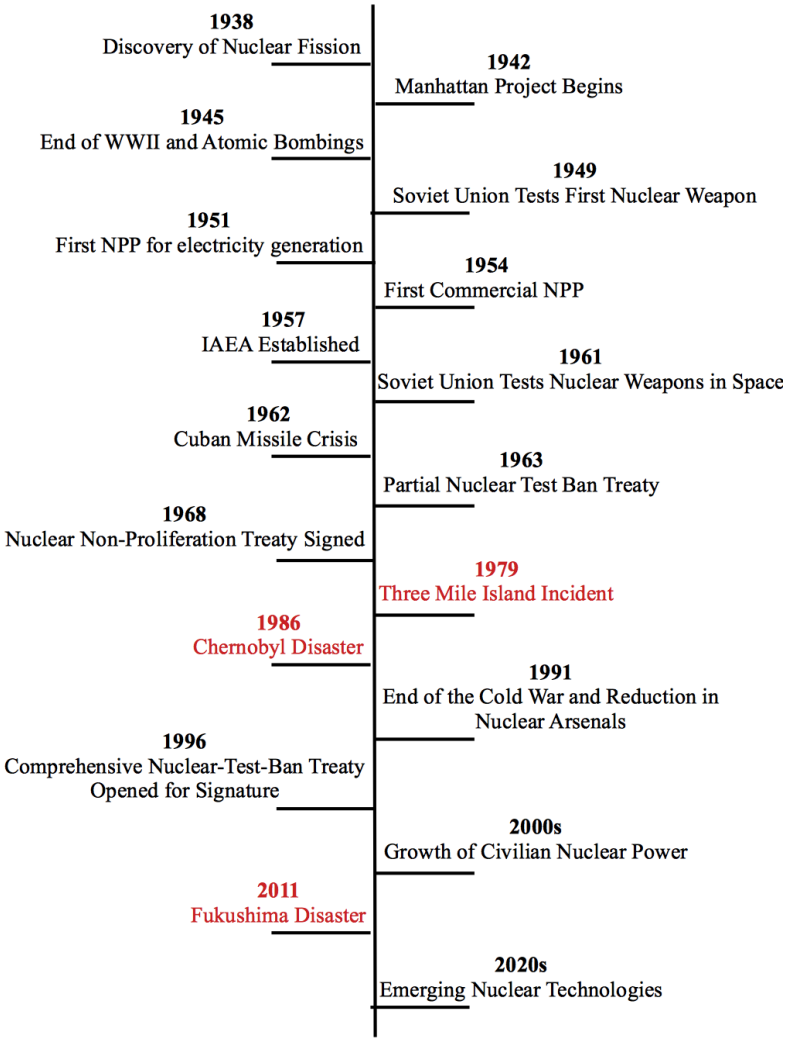

Figure 2.1 : Timeline of nuclear development.

The nuclear age began with the work of Otto Hahn and Fritz Strassmann in 1938, who discovered nuclear fission. Soon after, Lise Meitner and Otto Frisch explained how it worked from a theoretical perspective (Sime, 2012). Their discovery quickly gained attention during World War II. The U.S. government launched the Manhattan Project, a top-secret program that led to the development of the first atomic bombs. The bombings of Hiroshima and Nagasaki in August 1945 showed just how destructive nuclear energy could be, changing warfare and global politics forever (Reed, 2014). After the war, many countries began building up their nuclear arsenals, especially the United States and the Soviet Union. This arms race led to the creation of thousands of nuclear weapons and the development of doctrines like "mutually assured destruction" (MAD), which aimed to prevent war by making the cost of conflict too high for anyone to risk (Straub 2019). But having more weapons also meant more chances for things to go wrong. The Cuban Missile Crisis in 1962, for example, brought the world dangerously close to nuclear war. It became clear that some form of international control was needed. This led to agreements like the Nuclear Non-Proliferation Treaty (NPT) in 1968, designed to prevent the spread of nuclear weapons (Siracusa and Warren, 2018). At the same time, countries also started using nuclear energy for peaceful purposes. The 1950s and 60s saw the rise of civilian nuclear power, seen as a clean and abundant energy source (Sadekin et al., 2019). But over time, accidents exposed the risks. The partial meltdown at Three Mile Island (1979), the explosion at Chernobyl (1986), and the Fukushima disaster (2011) each showed how vulnerable nuclear power can be to system failures, human error, and natural disasters (Ohba et al., 2021). These events had serious consequences. Chernobyl contaminated large areas, and millions of people were exposed to radiation (Saenko et al., 2011. Fukushima, triggered by an earthquake and tsunami, raised concerns about building nuclear plants in unstable regions (Srinivasan and Rethinaraj, 2013). The environmental and health impacts of these disasters are long-lasting. Another major challenge is what to do with nuclear waste. Some types of waste stay dangerous for thousands of years, requiring secure storage and long-term planning. Many countries still don't have permanent solutions, which has fueled public opposition and slowed the expansion of nuclear power (Ramana 2018).

In response, governments and international bodies have taken steps to improve nuclear safety. The International Atomic Energy Agency (IAEA), created in 1957, promotes

the safe and peaceful use of nuclear energy. Other key agreements like the Comprehensive Nuclear-Test-Ban Treaty (CTBT) and the Strategic Arms Reduction Treaty (START) are also aimed to limit and reduce nuclear weapons (Lyman et al., 2017). There have also been advances in reactor design. Modern technologies, like Generation IV reactors, are being developed with safety, efficiency, and sustainability in mind (Locatelli et al., 2013).

As we face global issues like climate change and energy security, nuclear power is once again part of the conversation. It offers a low-carbon energy option, but it also comes with risks that society can't ignore (Mathew 2022). Balancing these pros and cons requires careful consideration, historical awareness, and a long-term commitment to both safety and sustainability. And looking back at history, the nuclear age has taught us some important lessons. First, nuclear risks don't respect borders, so transparency and international cooperation are crucial. Second, strong regulations and constant innovation are needed to prevent accidents. And third, public trust matters. Listening to societal concerns and involving people in decision-making can make nuclear technologies more acceptable and safer to use.

2.1.2 Typologies of nuclear accidents: from reactor meltdowns to radiological terrorism

Nuclear accidents encompass a broad spectrum of events, each varying in severity, causation, and impact. Understanding these issues is critical for developing robust emergency response plans, mitigation strategies, and regulatory frameworks. This section categorizes nuclear accidents into types, providing an in-depth analysis of their characteristics, triggers, and implications.

2.1.2.1 Reactor accidents

Reactor accidents are the most recognized type of nuclear accident due to their catastrophic potential and historical prominence (Gu 2018). These incidents occur within NPPs and are primarily associated with the failure of reactor core systems. The severity of reactor accidents is often classified using the International Nuclear and Radiological Event Scale (INES) (Mohammed Saeed et al., 2020). Table 2.1 lists a brief explanation of INES.

Table 2.1 : The INES and historical example.

Level	Description	Impact	Example
Level 0	No safety significance	An event with no safety relevance, often a minor operational issue	A small radiation leak at a research facility with no public impact
Level 1	Anomaly	A minor issue with safety systems, but no actual consequences; may involve a small radiation release within regulatory limits	Overexposure of a worker to radiation at Sellafield, UK (2009), with no environmental impact
Level 2	Incident	Significant failure in safety provisions but with no actual consequences; may involve worker overexposure or minor public exposure	The 1999 Tokaimura nuclear accident in Japan, where workers were exposed to radiation due to a criticality event, but the public was largely unaffected
Level 3	Serious incident	Very small release of radioactive material, likely causing limited public exposure; severe contamination within a facility	The 1987 Goiania accident in Brazil, which led to localized contamination
Level 4	Accident with local consequences	Minor release of radioactive material, possibly requiring protective measures; significant damage to the facility or severe health effects for workers	The 1957 Windscale fire in the UK, where a reactor fire released radioactive material, causing negligible local contamination
Level 5	Accident with wider consequences	Limited release of radioactive material, requiring some protective actions (e.g., evacuation); severe damage to the reactor core	The 1979 Three Mile Island accident in the USA, where a partial meltdown occurred, leading to a small radioactive release and local evacuations
Level 6	Serious accident	Significant release of radioactive material, requiring extensive countermeasures; widespread health and environmental effects	The 1957 Kyshtym disaster in the Soviet Union, where a waste tank explosion at the Mayak facility released radiation, contaminating a large area
Level 7	Major accident	Major release of radioactive material with widespread health and environmental effects, requiring long-term countermeasures	The 1986 Chernobyl disaster in Ukraine, where a reactor explosion released massive amounts of radiation, affecting large parts of Europe

A core meltdown of nuclear reactor happens when the fuel inside a nuclear reactor overheats and melts. Chernobyl (1986) and Fukushima Daiichi (2011) are two major examples of full meltdowns, where the reactor cores were severely damaged, leading to large releases of radiation. In contrast, the Three Mile Island accident (1979) was a partial meltdown, meaning only part of the core melted, and the damage was more limited and mostly contained (He and Guan, 2022).

2.1.2.2 Spent fuel accidents

Spent fuel and used nuclear reactor fuel remains both highly radioactive and very hot for a long time after it's removed from the reactor. It's usually stored in special pools to keep it cool and contained. Accidents can happen if the cooling water is lost, which can cause the fuel to overheat and possibly catch fire. Other risks include structural problems like leaks or even the pool collapsing, as well as external threats such as natural disasters. While these types of accidents don't get much attention, they can be extremely dangerous because spent fuel contains a large amount of radioactive material (Saegusa et al., 2010).

2.1.2.3 Radiological dispersal devices (RDDs)

Radiological Dispersal Devices, or RDDs as also often called "dirty bombs" are weapons that mix regular explosives with radioactive materials. The main goal of an RDD isn't to cause mass casualties like a nuclear bomb, but to spread radioactive contamination, create panic, and disrupt everyday life. These devices usually use radioactive materials from medical or industrial sources, like Cesium-137 (Cs-137). They're most dangerous when used in crowded places, like cities, where they can cause the most fear and disruption. While the immediate physical damage might not be severe, the cleanup process and the psychological effects on people can be very serious and long-lasting (Ledford 2009).

2.1.2.4 Nuclear weapons accidents

Nuclear weapons accidents, also known as "Broken Arrow" incidents, happen when there is an accidental detonation, loss, or theft of nuclear weapons. These events are especially dangerous because they involve both explosions and radiation. Two well-

known examples of such accidents are the Palomares incident in 1966 and the Thule Air Base crash in 1968 (Kahle 2022).

2.1.2.5 Critically accidents

Criticality accidents happen when fissile material accidentally starts a self-sustaining chain reaction. These incidents typically occur in research labs, enrichment plants, or while handling nuclear materials. Two notable examples are: (1) The Los Alamos accident in 1958, where mishandling of plutonium caused deadly radiation exposure and (2) The Tokaimura accident in 1999 in Japan, which was caused by unsafe practices during uranium handling (Bhanot 2000; Kanda et al., 2002).

2.1.2.6 Transport accidents

The transportation of nuclear materials including reactor fuel, waste, and isotopes poses risks due to potential accidents during transit. Scenarios include collisions, spills, or theft. Transport accidents are often mitigated by stringent packaging and monitoring protocols (Fentiman 2009).

2.1.2.7 Sabotage and terrorism

Intentional attacks on nuclear facilities or materials represent an emerging threat in the nuclear security landscape. Such events could involve cyberattacks on NPP systems to disrupt operations or safety measures and also physical attacks targeting critical infrastructure (Lee et al., 2021).

2.1.3 Key vulnerabilities and cascading effects: impact on health, ecosystems, and economies

2.1.3.1 Health impacts

Nuclear accidents pose serious risks to public health due to the release of radioactive materials, and these effects can be divided into immediate, short-term, and long-term consequences.

In the immediate aftermath, one of the most severe health issues is Acute Radiation Syndrome (ARS), which happens when people are exposed to high doses of radiation in a short time. Symptoms include nausea, vomiting, fatigue, and, in extreme cases,

death. Additionally, thermal burns and injuries from explosions or fires can worsen the situation, leading to more people needing urgent medical care (Belyi et al., 2013).

In the short term, psychological stress and anxiety are common among people living in areas affected by nuclear accidents. The uncertainty and fear that follow such events can lead to higher rates of depression, and substance abuse. Radiation can also contaminate food and water supplies, with radionuclides like Iodine-131 (I-131) and Cs-137 getting into the environment. This contamination increases the risk of thyroid cancer and other health problems due to internal radiation exposure (Orui et al., 2021).

Looking at the long-term effects, chronic exposure to low levels of radiation can raise the risk of cancers, especially leukemia, breast cancer, and thyroid cancer. Genetic mutations and hereditary issues may also appear in future generations, which can add to the ongoing health problems. Furthermore, the displacement of communities affected by the accident often leads to disruptions in healthcare access, worsening existing health disparities (Moller and Mousseau, 2011).

2.1.3.2 Ecosystem impacts

On land, radioactive fallout contaminates the soil, making it less fertile and hurting agricultural productivity. Plants and animals absorb radionuclides, which then enter the food chain, causing bioaccumulation. Forest ecosystems are also hit hard, with trees dying and biodiversity decreasing in affected areas. For example, in the Chernobyl Exclusion Zone, a phenomenon known as the “red forest” occurred, where pine trees turned reddish-brown and died shortly after the disaster (Yoschenko et al., 2018).

In aquatic environments, contamination of rivers, lakes, and oceans has a major impact on aquatic life. Radioisotopes like Stronium-90 (St-90) and Cs-137 linger in water bodies, causing long-term disruption to ecosystems. Fisheries face huge losses because radionuclides accumulate in fish and other aquatic organisms, making them unsafe for human consumption (Hirose 2016).

2.1.3.3 Economic impacts

The economic impact of nuclear accidents is massive, affecting both immediate costs and long-term financial burdens, along with indirect losses. In the immediate aftermath, emergency response efforts such as evacuation, first medical care, and containment of the accident demand huge financial resources. Local economies, especially in rural and coastal areas, also suffer from the loss of agricultural produce, livestock, and fisheries, which directly affects people's livelihoods. Long-term costs are also significant. Decontamination and remediation efforts, which can take decades, require extensive spending. For example, the Fukushima disaster involved huge costs for soil removal, water treatment, and rebuilding infrastructure (Hardie and McKinlet, 2014). Additionally, compensating affected populations for health care, relocation, and loss of income places a heavy financial strain on both governments and nuclear plant operators. The indirect losses are just as damaging. Property values and land usability in contaminated areas drop, reducing economic productivity. Public trust in nuclear energy also decreases, leading to less investment and higher costs for alternative energy sources. Tourism in affected areas usually declines as the stigma of nuclear contamination keeps visitors away. Finally, nuclear accidents can have global economic ripple effects. Disruptions in energy supply, especially if the affected plant is a major energy provider, can lead to higher energy prices and overall economic instability. Trade restrictions on food and goods from contaminated regions further amplify economic losses and disrupt international markets.

2.2 Overview of Major Nuclear Accidents: Chernobyl and Fukushima

Two of the biggest nuclear disasters in history are the Chernobyl accident in 1986 and the Fukushima Daiichi accident in 2011. The Chernobyl disaster happened on April 26, 1986, at the Chernobyl NPP near the town of Pripyat in Ukraine, which was part of the Soviet Union at the time (Steinhauser et al., 2014). The Fukushima accident occurred on March 11, 2011, in Japan's Fukushima Prefecture (Steinhauser et al., 2014). Even though the causes were different, both events had major consequences. At Chernobyl, the accident happened because the reactor had a bad design and the workers made mistakes during a safety test at night. This led to a huge explosion that released a lot of radioactive material (about 5.2 exabecquerels (EBq)) into the air. It spread over 200,000 square kilometers across Europe (Steinhauser et al., 2014). The Fukushima disaster started with a massive 9.0 earthquake followed by a tsunami. The

waves flooded the power plant and knocked out the backup generators, which caused the reactors to overheat. This led to meltdowns and hydrogen explosions, releasing around 520 petabecquerels (PBq) of radioactive iodine and cesium. A lot of land and parts of the Pacific Ocean were contaminated (Steinhauser et al., 2014). At Chernobyl, 31 people died right away, and many others got sick later, especially from thyroid cancer caused by radioactive iodine (Saenko et al., 2011). At Fukushima, there were no direct deaths from radiation, but more than 1,600 people died from stress and problems related to evacuation (Maeda and Oe, 2017). Both disasters forced large numbers of people to leave their homes, about 350,000 in Chernobyl and 150,000 in Fukushima (Ohba et al., 2021). These events showed the importance of strong safety rules. Chernobyl showed how dangerous poor design and human error can be, while Fukushima revealed how vulnerable nuclear plants can be to natural disasters.

2.3 Bibliometric Analysis of Research on Major Nuclear Accidents

Bibliometric analysis is a quantitative method used to evaluate the body of literature within a specific research field by analyzing publication patterns, citation trends, and collaborative networks. It provides insights into the volume of research output, influential authors and studies, geographic distribution of contributions, and emerging areas of focus. By examining metrics such as citation counts, co-authorship networks, and keyword occurrences, bibliometric analysis helps identify research gaps, track the evolution of scientific inquiry, and assess the impact of studies on a field. This method is widely used to evaluate the progression of topics, compare regional and institutional contributions, and guide future research directions (Donthu et al., 2021).

Within the context of current thesis, bibliometric analysis examines studies on major nuclear accidents, primarily the Chernobyl accident (1987) and the Fukushima accident (2011) to highlight the research output, main thematic areas, and evolution of scientific inquiry over time.

2.3.1 Research questions, objectives, and contribution of the study

The aim of bibliometric analysis is to conduct a statistical quantitative analysis of the scientific literature on nuclear accident research. This involves addressing three key research questions (RQs): (RQ1) how the period of scientific production has changed; (RQ2) what the most important research topics are; and (RQ3) which countries are

most interested in nuclear research. Each RQ is linked to specific objectives and motivations, forming a comprehensive framework for bibliometric analysis.

The first research question (RQ1) seeks to examine how the period of scientific production has evolved over time. The objective is to track the development of ideas and methods, as well as to identify emerging trends in the field. This helps analyze significant patterns in historical data and provides insights into the evolution of research focus over time. The second research question (RQ2) focuses on identifying the most important topics studied in nuclear accident research. The objective here is to highlight foundational and impactful themes, including the most productive journals, frequently cited papers, and key thematic trends revealed through keyword analysis. This allows researchers to familiarize themselves with landmark studies and subject areas while identifying potential gaps and opportunities for future exploration. The third research question (RQ3) explores the global engagement in nuclear accident research by determining which countries are most active in this domain. The objective is to assess the spatial distribution of leading countries, analyze geographical interactions, and investigate the relationship between scientific productivity and driving factors. This understanding can help improve research productivity and clarify what drives the global scientific community's interest in nuclear accidents.

To achieve these objectives, bibliometric study employs a three-part methodological framework. First, performance analysis is used to address RQ1 by evaluating metrics such as the total number of publications, research trends, the number of active years, and productivity per year. This is conducted using the VOSviewer tool for bibliometric data analysis. Second, science mapping is applied to RQ2, focusing on foundational themes through an analysis of the most productive journals, the most cited papers, and thematic keyword patterns, again using VOSviewer. Lastly, spatial regression is used to answer RQ3 by assessing the spatial distribution of leading countries, their geographical interactions, and the relationship between scientific production and its driving indicators. This part combines bibliometric data analysis with spatial statistics and visualization using both VOSviewer and ArcGIS software. VOSviewer is a free software tool used to create and visualize bibliometric networks (Arruda et al., 2022). It helps researchers analyze relationships between authors, journals, keywords, or publications based on data from sources like Scopus or Web of Science. With VOSviewer, one can build maps that show how topics or researchers are connected,

making it easier to understand trends, collaborations, and key areas of research in a particular field. The tool is especially known for its easy-to-read visualizations, like network maps and density views (Arruda et al., 2022).

2.3.2 Data collection and research methodology

The research methodology employed in bibliometric analysis is structured into three distinct steps, as depicted in the Figure 2.2, each tailored to systematically gather, prepare, and analyze data on the bibliometric and geospatial aspects of publications related to the Chernobyl and Fukushima nuclear disasters.

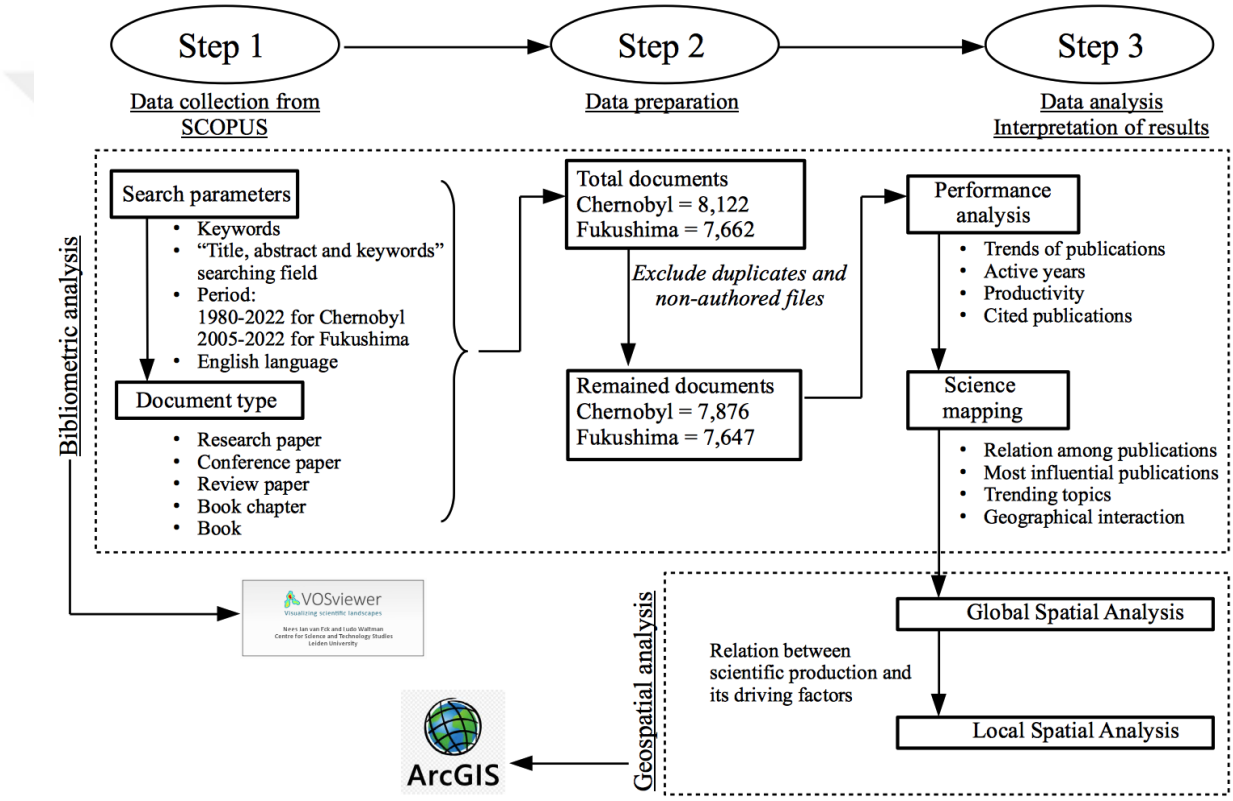

Figure 2.2 : Research methodology.

The data collection process begins with extracting bibliographic records from the Scopus database using a well-defined set of search parameters. Keywords such as 'Fukushima', 'Fukushima Daiichi', 'Chernobyl', 'Nuclear accident', and 'Nuclear disaster' were utilized in the "Title, abstract, and keywords" fields to ensure comprehensive coverage of relevant literature. The temporal scope of the data collection spans from 1980 to 2022 for Chernobyl-related studies and from 2005 to 2022 for Fukushima-related studies, reflecting the years of these respective nuclear

events and their scientific discourse. The search was restricted to documents in the English language to maintain uniformity and accessibility. The document types considered include research papers, conference papers, review papers, book chapters, and books, ensuring a broad inclusion of scientific contributions across various formats. Once the initial set of bibliographic records was gathered, the data underwent a refinement process to ensure reliability and relevance. From the total number of documents retrieved that were 8,122 for Chernobyl and 7,662 for Fukushima, duplicates and non-authored files were excluded to eliminate redundancy and non-scientific content. This filtering resulted in a final dataset comprising 7,876 Chernobyl-related and 7,647 Fukushima-related documents, which formed the basis for subsequent analyses. The analysis phase involved two key dimensions: bibliometric analysis and geospatial analysis. For the bibliometric analysis, two primary subcategories were considered: performance analysis and science mapping. Performance analysis focused on identifying trends in publication output, determining active research years, assessing productivity metrics, and highlighting the most frequently cited publications. Science mapping explored the relationships among publications, identified the most influential studies, uncovered trending research topics, and investigated geographical interactions in the literature. To complement the bibliometric analysis, geospatial analysis was conducted to examine the spatial distribution of scientific activity related to the nuclear disasters. This step investigated the relationship between the geographical distribution of scientific production and its driving factors, providing insights into the global and local research dynamics.

2.3.3 Geographically weighted regression: methodological framework

Geographically Weighted Regression (GWR) is a local spatial statistical technique that extends traditional regression analysis by allowing model parameters to vary geographically (Sisman and Aydinoglu, 2022). Unlike global regression methods, such as ordinary least squares (OLS), which assume that relationships between variables are constant across the study area, GWR captures spatial heterogeneity by estimating regression coefficients for each location in the dataset (Isazade et al., 2023). This makes GWR particularly useful for understanding how relationships between dependent and independent variables change across space.

GWR consists of six main steps: (1) data preparation; (2) Kernel selection; (3) weighting scheme; (4) model estimation; (5) output analysis; and (6) model diagnostics (Wheeler 2021).

At the first step, the dependent variable (Y) and independent variables (X_1, X_2, …, X_k) are defined. Spatial coordinates (u, v) are also prepared for each observation so that their geographical locations can be used in the model. At the second step, a kernel type is selected. This determines how spatial proximity is handled. Either a fixed kernel is chosen (the bandwidth is constant throughout the study area) or an adaptive kernel is used (bandwidth is adjusted based on the density of observations). At the third step, weights are assigned to observations based on their distance from the location being analyzed. A kernel function such as the Gaussian kernel, is commonly used for this. The weight is calculated using Equation 2.1

$$w_{ij} = exp\left(-\frac{d_{ij}^2}{h^2}\right) \tag{2.1}$$

where w_{ij} is the weight for observation *j* relative to location *i*, d_{ij} is the distance between *i* and *j*, and *h* is the bandwidth.

At the fourth step, a local regression model is fitted then to each location (i), where the coefficients are estimated using weighted least squares (Equation 2.2):

$$\beta(u_i, v_i) = (X^T W_i X)^{-1} X^T W_i y \tag{2.2}$$

where $\beta(u_i, v_i)$ are the local regression coefficients at location i; X is the matrix of independent variables; Wi is a diagonal matrix of weights for location i; and y is the vector of dependent variable values.

The estimated coefficients $\left(\beta(u_i, v_i)\right)$ for each location are examined at the fifth step to identify spatial patterns. Maps are often created to visualize how relationships change across the study area, which can help in identifying clusters or trends that may not be seen in a global model. Finally, at the sixth step, the quality of model fit is assessed using measures such as the Akaike Information Criterion (AIC) or adjusted R^2. The GWR model is often compared to a global regression model to determine whether a better explanation of the data is provided by accounting for spatial variation.

The basic form of the GWR model can be expressed as (Equation 2.3):

$$y_i = \beta_0(u_i, v_i) + \sum_{k=1}^{p} \beta_k(u_i, v_i) x_{ik} + \epsilon_i \tag{2.3}$$

where y_i is the dependent variable at location i; $\beta_0(u_i, v_i)$ is the intercept at location i; $\beta_k(u_i, v_i)$ are the coefficients for the k-th independent variable x_{ik} at location i, (u_i, v_i) are the spatial coordinated of location i; and ϵ_i is the error term.

The local coefficients $\beta_k(u_i, v_i)$ are estimated using the weighted least squares formula mentioned earlier. The weights W_i are determined by the distance-based kernel function, ensuring that closer observations exert a stronger influence on the regression at each location.

2.3.4 Temporal data exploration

The graphs in Figure 2.3 illustrate research trends related to the Chernobyl and Fukushima nuclear accidents, emphasizing the annual number of publications and cumulative growth over time.

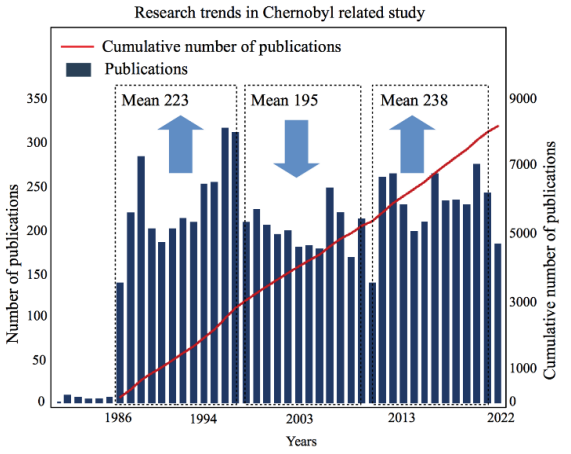

(a)

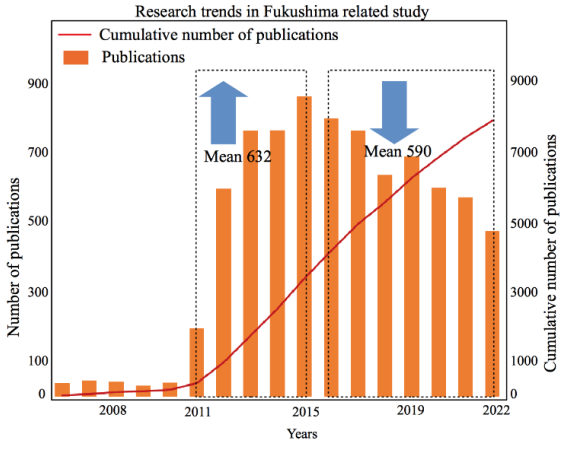

(b)

Figure 2.3 : Research trends: a) Chernobyl accident related documents, b) Fukushima accident related documents.

The left graph (Figure 2.3 a), focusing on Chernobyl-related studies, spans the years 1986 to 2022. It shows three distinct phases characterized by the mean number of annual publications: an initial period with a mean of 223, followed by a slight decline to a mean of 195, and finally a resurgence to a mean of 238 in the most recent years. The red line representing cumulative publications shows a steady increase, indicating sustained academic interest in Chernobyl despite fluctuations in yearly outputs.

The right graph (Figure 2.3 b), examining Fukushima-related studies, covers the years 2011 to 2022 and demonstrates a different pattern. Following the 2011 disaster, there was a rapid spike in publications, peaking at a mean of 632 during the initial years of research activity. Subsequently, a slight decline is observed, with a mean of 590 in recent years. The cumulative publication curve in this case also grows sharply, reflecting the immediate and intensive focus on Fukushima after the incident. Comparing the two graphs highlights differences in research dynamics: Chernobyl research has evolved over decades with periodic fluctuations, while Fukushima research saw a concentrated surge of activity in its early years. These trends suggest differences in the immediacy and longevity of scientific engagement with the two events, shaped by factors such as the timing, nature of the accidents, and ongoing socio-environmental impacts.

2.3.5 Statistics and trending topics

2.3.5.1 Top productive journals

The Table 2.2 and Table 2.3 summarize the top journals that have published papers related to the Chernobyl and Fukushima nuclear accidents, providing insights from a bibliometric analysis. Each table ranks journals by the number of publications and citations, alongside their percentage contributions to the total body of literature. This analysis reveals key publishing platforms and their influence within the academic discourse surrounding these two major nuclear disasters.

For the Chernobyl-related studies (Table 2.2), the top journal is the “Journal of Environmental Radioactivity” (Elsevier, Q2), accounting for 3.4% of publications and 7.6% of total citations, indicating its significant contribution to the field. Other notable journals include “Health Physics” (Wolters Kluwer Health, Q2) and “Radiation Protection Dosimetry” (Oxford University Press, Q3), which contribute 2.7% and 1.9% of publications, respectively. Despite some journals such as “Problemly

Radiatsiinoi Medytsyny ta Radiobiolohii" (Q4) having relatively low citation percentages, they provide niche contributions to Chernobyl research. The inclusion of journals such as "Nature" (Springer Nature, Q1) reflects the broader interdisciplinary interest in this topic. Overall, the journals listed are varied in scope, encompassing environmental radioactivity, health physics, radiation protection, and biophysical sciences, which highlights the multidisciplinary approach taken in Chernobyl research.

Table 2.2 : Top journals on Chernobyl accident related study.

No.	Journal information	Publications	Citations
		(%) of total	
1	Journal of Environmental Radioactivity (Elseiver; Q2)	3.4	7.6
2	Health Physics (Wolters Kluwer Health; Q2)	2.7	4.8
3	Radiation Protection Dosimetry (Oxford University Press; Q3)	1.9	2.4
4	Problemy Radiatsiinoi Medytsyny ta Radiobiolohii (Naukovyi Tsentr Radiatsiinoi Medytsyny; Q4)	1.8	0.2
5	Radiation and Environmental Biophysics (Springer Nature; Q2)	1.0	0.2
6	Nature (Springer Nature; Q1)	1.0	1.8
7	Atomic Energy (Springer Nature; Q3)	1.0	3.4
8	Radiation Research (Radiation Research Society; Q1)	0.9	2.8
9	Science of the Total Environment (Elseiver; Q1)	0.7	2.8
10	Hydrobiological Journal (Begell House; Q4)	0.6	0.1

For the Fukushima-related studies (Table 2.3), the "Journal of Environmental Radioactivity" again leads, contributing a significantly higher percentage of publications (6.4%) and citations (24%), underscoring its central role in the dissemination of Fukushima-related research. Unlike Chernobyl, the "International Conference on Nuclear Engineering Proceedings ICONE" (Q4) ranks second, demonstrating the relevance of conference proceedings for the Fukushima context, particularly for technological and engineering aspects. Other prominent journals include "Scientific Reports" (Springer Nature, Q1) and the "Journal of Radioanalytical and Nuclear Chemistry" (Springer Nature, Q2), which highlight the focus on analytical

and nuclear sciences in studying Fukushima's impacts. Notably, "Health Physics" also appears on this list, indicating its continued importance across both nuclear accidents.

Table 2.3 : Top journals on Fukushima accident related study.

No.	Journal information	Publications	Citations
		(%) of total	
1	Journal of Environmental Radioactivity (Elseiver; Q2)	6.4	24.0
2	International Conference on Nuclear Engineering Proceedings ICONE (Organization country is Japan; Q4)	2.6	0.4
3	Scientific Reports (Springer Nature; Q1)	2.2	8.9
4	Journal of Radioanalytical and Nuclear Chemistry (Springer Nature; Q2)	2.1	2.7
5	Journal of Nuclear Science and Technology (Taylor&Francis; Q3)	1.8	5.0
6	Radiation Protection Dosimetry (Oxford University Press; Q3)	1.7	1.5
7	Plos One (Public Library of Science; Q1)	1.7	1.6
8	Journal of Radiological Protection (Institute of Physics Publishing; Q3)	1.5	3.0
9	Health Physics (Wolters Kluwer Health; Q2)	1.5	1.6
10	Annals of Nuclear Energy (Elseiver; Q2)	1.4	1.5

A key observation is the larger role played by journals with high impact factors and broader scopes in Fukushima studies compared to Chernobyl. For instance, "Scientific Reports" and "Plos One" (both Q1) signify an increasing trend toward open-access and interdisciplinary platforms in more recent nuclear accident research. Additionally, journals like "Annals of Nuclear Energy" (Elsevier, Q2) demonstrate the emphasis on energy systems and nuclear engineering for Fukushima.

The bibliometric differences between the two events highlight shifts in academic priorities and methodologies over time. While Chernobyl research was heavily rooted in environmental, health, and radiological studies, Fukushima research incorporates a stronger engineering and multidisciplinary focus, reflecting the technological advancements and varied challenges associated with modern nuclear disasters. These

trends also emphasize the evolving role of journals in shaping the direction of nuclear accident research.

2.3.5.2 Top productive documents

The Table 2.4 and Table 2.5 highlights the most influential documents in the academic discourse surrounding the Chernobyl and Fukushima nuclear accidents, as revealed by bibliometric analysis.

Table 2.4 : Top cited documents on Chernobyl accident related study.

No.	Reference	Citations	Journal/Publisher name	Research area	Type of document
1	*Thyroid cancer after Chernobyl*				
	(Kazakov et al., 1992)	637	Nature	Medicine	Letter
2	*Life exposed: biological citizens after Chernobyl*				
	(Petryna, 2013)	987	Princeton University Press	Multidisciplinary	Book
3	*Human minisatellite mutation rate after the Chernobyl accident*				
	(Dubrova et. al., 1996)	347	Nature	Medicine	Article
4	*Pattern of radiation induced RET and NTRK1 rearrangements in 191 post-Chernobyl papillary thyroid carcinomas: biological, phenotypic, and clinical implications*				
	(Rabes et al., 2000)	328	Clinical Cancer Research	Medicine	Article
5	*Pediatric thyroid cancer after the Chernobyl disaster: Pathomorphologic study of 84 cases (1991-1992) from the republic of Belarus*				
	(Nikiforov and Gnepp, 1994)	252	Cancer	Medicine	Article
6	*Post-Chernobyl thyroid carcinoma in Belarus children and adolescents: comparison with naturally occurring thyroid carcinoma in Italy and France*				
	(Pacini et al., 1997)	234	Journal of Clinical Endocrinology and Metabolism	Medicine	Article

For Chernobyl-related studies (Table 2.4), the top-cited works predominantly focus on the medical and biological impacts of the disaster, particularly thyroid cancer. Kazakov et al. (1992), with 637 citations, explores thyroid cancer incidence following the Chernobyl accident and is published in “Nature”, reflecting its high scientific

significance. Similarly, Petryna (2013) provides a multidisciplinary perspective on the long-term health and societal impacts in her book, which has garnered 987 citations, making it the most cited document in this category. Other notable studies include Dubrova et al. (1996), which investigates genetic mutations, and Rabes et al. (2000), focusing on the molecular pathology of thyroid cancers, published in reputable journals like Clinical Cancer Research. These works emphasize the lasting medical and genetic consequences of Chernobyl, solidifying the focus on human health and molecular research.

Table 2.5 : Top cited documents on Fukushima accident related study.

No.	Reference	Citations	Journal/Publisher name	Research area	Type of document
1	*Preliminary estimation of release amounts of 131I and 137Cs accidentally discharged from the Fukushima Daiichi nuclear power plant into the atmosphere*				
	(Chino et al., 2011])	788	Journal of Nuclear Science and Technology	Environmental Science	Article
2	*Comparison of the Chernobyl and Fukushima nuclear accidents: a review of the environmental impacts*				
	(Steinhauser et al., 2014)	612	Science of the Total Environment	Environmental Science	Review
3	*CS-137 deposition and contamination of Japanese soils due to the Fukushima nuclear accident*				
	(Yasunari et al., 2011)	508	Proceedings of the National Academy of Sciences	Environmental Science	Article
4	*Xenon-133 and caesium-137 releases into the atmosphere from the Fukushima Daiichi nuclear power plant: determination of the source term, atmospheric dispersion, and deposition*				
	(Stohl et al., 2012)	428	Atmospheric Chemistry and Physics	Environmental Science	Article
5	*Impacts of the Fukushima nuclear power plants on marine radioactivity*				
	(Buesseler et al., 2011)	390	Environmental Science and Technology	Environmental Science	Article

In contrast, the top-cited documents for Fukushima-related studies (Table 2.5) predominantly address environmental impacts. The most cited work, by Chino et al. (2011), with 788 citations, estimates the release of radionuclides like I-131 and Cs-

137 into the atmosphere, underscoring its critical role in early response and environmental assessments. Steinhauser et al. (2014) and Yasunari et al. (2011) analyze environmental contamination, including soil deposition and broader ecological consequences, published in “Science of the Total Environment” and the “Proceedings of the National Academy of Sciences”, respectively. These papers highlight the global significance of environmental science in studying Fukushima. Additionally, Stohl et al. (2012) and Buesseler et al. (2011) provide key insights into atmospheric dispersion and marine radioactivity, emphasizing the event’s wide-ranging ecological impact. The comparison between the two accidents reveals a clear thematic divergence: while Chernobyl research centers on human health and biological consequences, Fukushima studies are heavily focused on environmental contamination and its global ramifications. This distinction reflects evolving academic priorities and the distinct nature of these nuclear disasters.

2.3.5.3 Keywords analysis

Figure 2.4 presents a comprehensive keyword analysis of academic studies on the Chernobyl and Fukushima nuclear accidents, conducted using VOSviewer, a tool designed for building and visualizing bibliometric networks such as co-authorship, co-occurrence, and citation networks. This analysis relies on the co-occurrence of keywords within indexed academic literature to identify research themes and group them into clusters. In VOSviewer, nodes (represented as circles) signify keywords, while the edges (lines) indicate the strength of relationships between them based on their co-occurrence frequency. The clustering algorithm assigns colors to different thematic groupings, where each color represents a specific cluster, and the circle sizes reflect the frequency of a keyword’s appearance in the literature, with larger circles signifying greater importance or centrality.

The analysis highlights distinct clusters for both the Chernobyl (left) and Fukushima (right) nuclear accidents. For Chernobyl, the keyword clusters reveal several key research themes. Cluster 1 (red) focuses on radionuclide dispersion, exploring the spread of radioactive materials such as CS-137 and their environmental contamination.

Cluster 2 (blue) emphasizes radiation dose estimation and includes studies on dosimetry and individual radiation exposure, forming the basis for risk assessment and epidemiology. Cluster 3 (green) examines health effects, particularly thyroid cancers

in children, linking exposure to long-term health risks. Cluster 4 (yellow) centers on the fallout of CS-137, a persistent concern due to its long half-life. Cluster 5 (purple) investigates radiation-induced mutations and genetic impacts, exploring the broader biological effects of the disaster. Cluster 6 (cyan) addresses thyroid and other cancers, providing critical insights into the epidemiology of radiation-induced diseases. Finally, Cluster 7 (orange) delves into the socio-environmental aspects of the exclusion zone, including its use in dark tourism and the cultural legacy of the disaster.

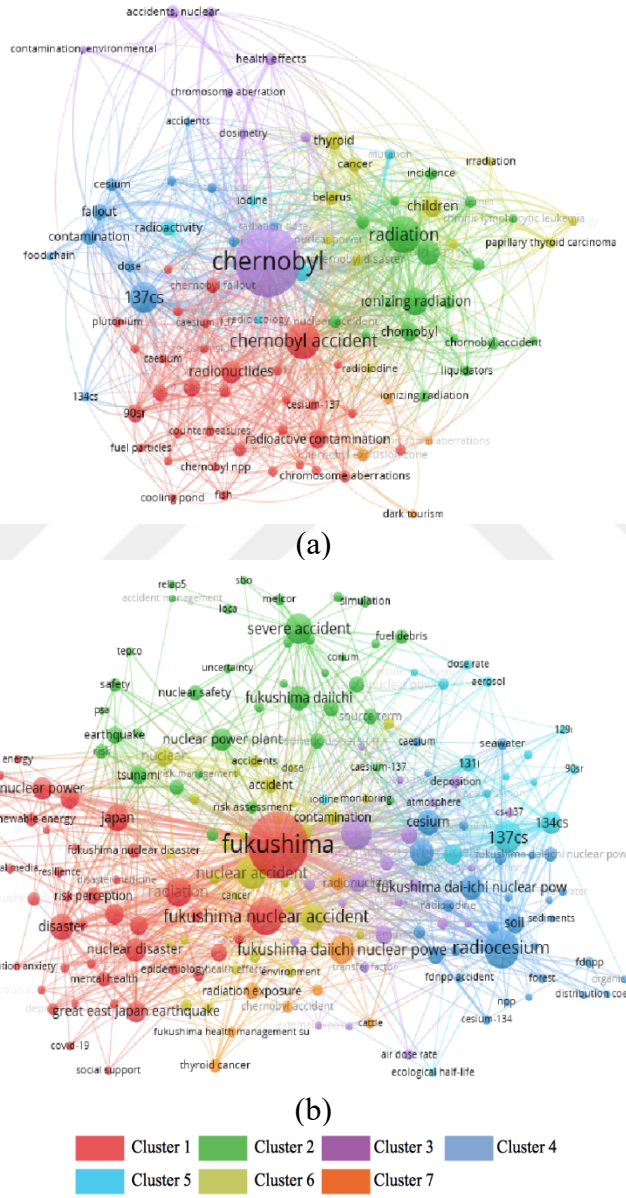

Figure 2.4 : Core research areas: a) Chernobyl accident related keywords, b) Fukushima accident related keywords.

The Fukushima analysis reveals a broader range of themes, reflecting its unique circumstances and comparisons with Chernobyl. Cluster 1 (red) focuses on the

sequence of events leading to the accident, including the earthquake, tsunami, and reactor failures. Cluster 2 (blue) emphasizes nuclear safety, emergency response, and evacuation measures, highlighting the need for improved protocols. Cluster 3 (green) examines the contamination and deposition of radionuclides, echoing themes from Chernobyl while addressing site-specific environmental impacts. Cluster 4 (yellow) expands on environmental contamination, exploring its broader effects on ecosystems and soil. Cluster 5 (purple) focuses on the radiological concerns of isotopes such as I-131 and CS-137, addressing both immediate and long-term risks. Cluster 6 (cyan) investigates health effects, including cancer and other radiation-induced diseases, mirroring concerns from Chernobyl while offering Fukushima-specific insights. Cluster 7 (orange) highlights comparative studies between the two accidents, providing lessons learned and opportunities for cross-learning to enhance nuclear safety and mitigation strategies.

Therefore, Chernobyl research primarily focuses on radionuclide dispersion, dosimetry, and health impacts, while Fukushima studies demonstrate a more diverse range of themes, including accident sequences, environmental contamination, and safety protocols. A shared focus is evident in health effects and comparative studies, emphasizing the integration of lessons learned to guide future nuclear safety measures.

2.3.6 Geographical distribution of research

The spatial distribution maps (Figure 2.5) illustrate the geographical productivity of nations in publishing literature on the Chernobyl and Fukushima accidents. These maps are essential for identifying which countries are most actively involved in addressing the consequences of these events.

For Chernobyl-related studies (Figure 2.5 a), the highest productivity is observed in Ukraine, Belarus, and the Russian Federation, emphasizing the proximity of these nations to the disaster site and their direct involvement in managing its aftermath. Additionally, countries like the United States, Germany, and France contribute significantly, reflecting their leadership roles in global nuclear research and mitigation strategies.

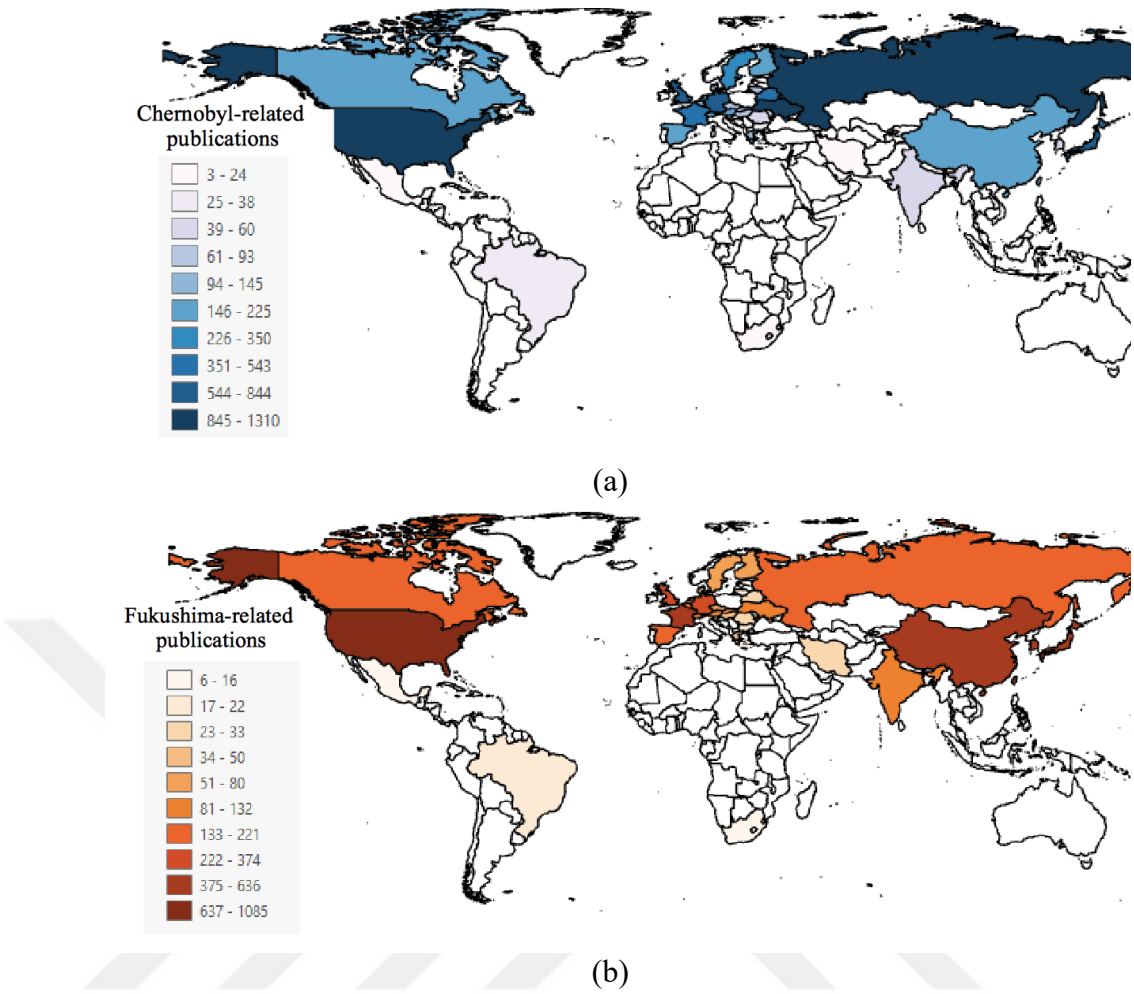

Figure 2.5 : Spatial distribution of scientific documents: a) Chernobyl accident related documents, b) Fukushima accident related documents.

In contrast, the Fukushima map (Figure 2.5 b) highlights Japan's dominant role in research, as the directly affected country, with substantial contributions from nations such as the United States, Germany, South Korea, and China. This regional concentration of research underscores the importance of understanding the local context of the disaster while incorporating global perspectives to develop comprehensive strategies for nuclear safety. The comparison between the two maps demonstrates how geographical distribution analysis can reveal different research dynamics: Chernobyl studies exhibit broader international engagement, whereas Fukushima research is more concentrated in East Asia.

The global collaborative networks (Figure 2.6) further emphasize the value of geographical distribution analysis by mapping co-authorship patterns between

countries. These networks, constructed using VOSviewer, provide a deeper understanding of the international partnerships driving nuclear disaster research.

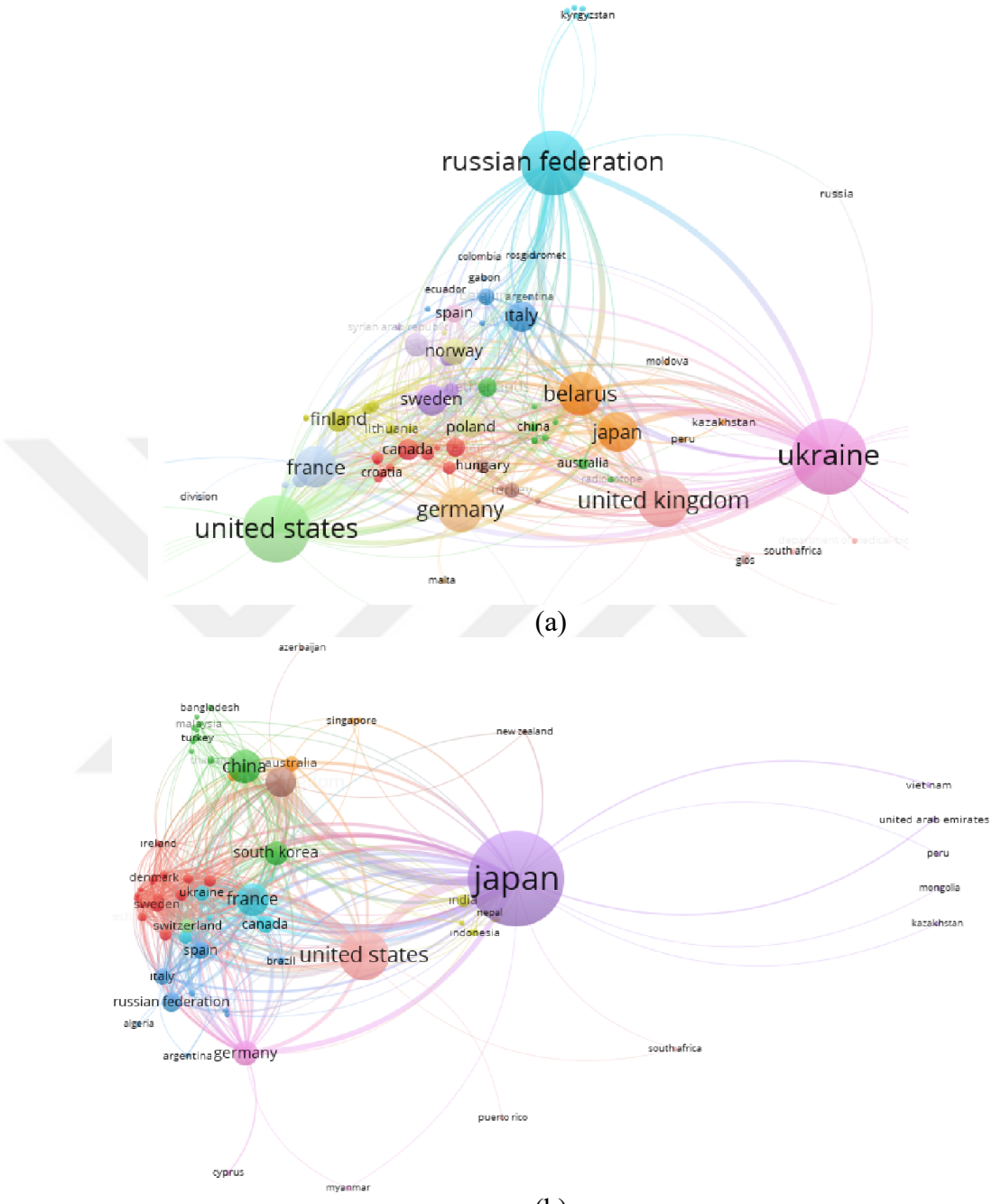

Figure 2.6 : Global collaborative network between the most productive countries: a) Chernobyl accident related collaboration, b) Fukushima accident related collaboration.

For Chernobyl-related studies (Figure 2.6 a), strong collaborations among Ukraine, Belarus, and the Russian Federation are evident, underscoring the shared historical and geographical ties to the disaster. At the same time, countries like Germany, the United

Kingdom, and the United States feature prominently, reflecting the global interest in nuclear safety and cross-border cooperation.

For Fukushima-related studies (Figure 2.6 b), Japan occupies a central position in the collaborative network, highlighting its pivotal role in research efforts. Strong links with the United States and collaborations with other nations, including South Korea, China, and European countries, showcase the global engagement with this disaster and its far-reaching implications for nuclear energy policies.

2.3.7 Geospatial analysis results

The presented workflow shown in Figure 2.7 outlines a geospatial analysis framework designed to examine the relationship between scientific production, represented by Chernobyl- and Fukushima-related publications (dependent variables), and a range of driving indicators (independent variables). The analysis is divided into two main components: Global Spatial Analysis and Local Spatial Analysis, aiming to identify the factors influencing research outputs and to assess their spatial variability.

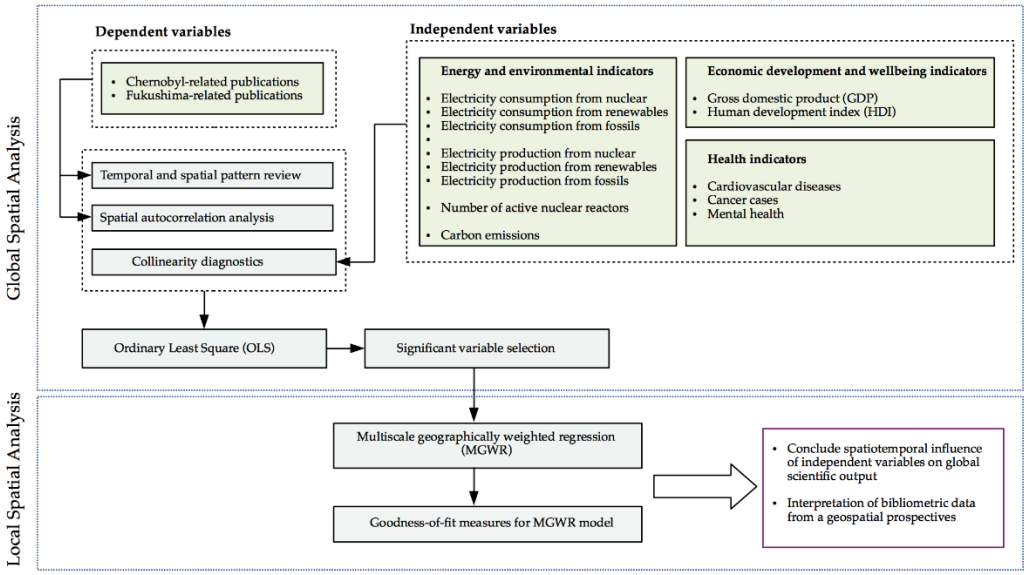

Figure 2.7 : Geospatial analysis: the framework of the research design.

The first step in the global spatial analysis involves a temporal and spatial pattern review, which evaluates the distribution of publications over time and space, providing a baseline understanding of publication trends. Following this, spatial autocorrelation analysis is conducted to detect clustering or dispersion patterns in the geographical distribution of scientific output. This step identifies whether spatially adjacent regions

exhibit similar research productivity. The next step involves collinearity diagnostics to evaluate the relationships between independent variables and remove multicollinearity that might distort the analysis.

Table 2.6 : Independent variables and their potential influence on scientific research related to nuclear accidents.

Independent variable	Explanation of influence
Electricity consumption from nuclear	Regions with high nuclear reliance may prioritize research on nuclear safety and accident mitigation.
Electricity consumption from renewables	Reflects a shift in energy policies, which may influence reduced focus on nuclear research in favor of alternatives.
Electricity consumption from fossils	Indicates energy dependence, potentially highlighting gaps in nuclear accident preparedness research.
Electricity production from nuclear	Higher nuclear energy production may drive scientific efforts to address safety, risk management, and accident scenarios.
Electricity production from renewables	A shift toward renewables may lead to reduced focus on nuclear accident studies and increased emphasis on cleaner energy transitions.
Electricity production from fossils	Regions dependent on fossil fuels may deprioritize nuclear-related accident research in favor of other energy concerns.
Number of active nuclear reactors	A greater number of reactors increases the likelihood of research on accident prevention, response, and impacts.
Carbon emissions	High emissions may spur comparative studies, positioning nuclear energy as a safer alternative to mitigate climate risks despite accident concerns.
Gross Domestic Product (GDP)	Wealthier regions may allocate more resources toward nuclear accident prevention, response planning, and health-related studies.
Human Development Index (HDI)	Higher development levels are often associated with increased investments in nuclear accident preparedness and resilience research.
Cardiovascular diseases	Areas with higher rates of cardiovascular issues may focus on understanding and mitigating radiation-related health risks from accidents.
Cancer risk	Regions with significant cancer prevalence may prioritize nuclear accident research to evaluate long-term radiation exposure impacts.
Mental health	Psychological trauma linked to nuclear accidents may drive localized studies on mental health impacts and recovery strategies.

After preprocessing, an OLS regression model is applied to establish the statistical relationship between dependent and independent variables globally. Significant variables identified through this step are then further analyzed using a Multiscale Geographically Weighted Regression (MGWR). This localized regression model allows for the exploration of spatial heterogeneity, revealing how the influence of independent variables varies across different regions. The final step evaluates the goodness-of-fit measures for the MGWR model, ensuring the robustness of the localized analysis. Table 2.6 below lists independent variables and their potential influence on scientific production.

The analysis presented in Table 2.7 highlights the spatial autocorrelation of various dependent variables using Global Moran's I Index, which provides a measure of spatial clustering in data. Moran's I is calculated for different variables, with their respective data sources outlined in the first table. Specifically, scientific publications were sourced from the Scopus database, while energy and environmental indicators, economic indicators and wellbeing data, and health indicators were extracted from platforms such as Our World in Data and the International Agency for Research on Cancer.

Table 2.7 : Summary statistics for Global Moran's I.

Dependent variables	Moran's Index	Expected Index	z-score	p-value
Scientific publications	0.259055	-0.032258	4.221900*	0.03469**
Fukushima-related publications	0.156400	-0.032258	7.942000*	0.04213**
Total publications (Chernobyl and Fukushima)	0.175694	-0.032258	6.386527*	0.02584**

*The critical z-score values for 95% confidence level are -1.96 and +1.96 standard deviations

**The results are significant at $p<0.05$

Summary statistics showed in Table 2.7 emphasize three dependent variables: scientific publications, Fukushima-related publications, and the total publication volume combining both Chernobyl and Fukushima. For each variable, the Moran's I Index, Expected Index, z-score, and p-value are reported. The results indicate statistically significant spatial autocorrelation for all three variables, as demonstrated by the positive Moran's I values and p-values less than 0.05. For scientific

publications, the Moran's I value is 0.259055, with an expected index of -0.032258, a z-score of 4.221900, and a p-value of 0.03469. These values suggest significant clustering of scientific publications, implying that areas with high publication output tend to be geographically close to other such areas. Similarly, Fukushima-related publications show a Moran's I of 0.156400, a z-score of 7.942000, and a p-value of 0.04213, indicating significant spatial patterns, possibly reflecting regional interests or proximity to the disaster site. The total publication count, encompassing both Chernobyl and Fukushima, yields a Moran's I of 0.175694, a z-score of 6.386527, and a p-value of 0.02584, further supporting the hypothesis of spatial clustering. The interpretation of these findings involves recognizing the broader implications of spatial autocorrelation in the distribution of academic research. For example, the positive Moran's I values across all three variables could indicate that research activity is concentrated in certain regions due to factors such as access to academic institutions, funding availability, or the proximity to disaster-affected areas. The statistically significant results further validate the presence of non-random spatial patterns, emphasizing the need to account for geographical factors when studying the impact of scientific knowledge.

The results from the OLS regression analysis presented in the Table 2.8 provide insights into the significant independent variables influencing the dependent variable under consideration.

Table 2.8 : Summary statistics for coefficients estimates and OLS regression model analysis.

Independent variables	Coefficient	Standard error	p-value	VIF
GDP	0.0022	0.0005	0.021	2.6166
Number of nuclear reactors	10.9567	2.4797	0.027	2.4421
Electricity production from nuclear	983.3767	338.0172	0.042	1.9782
Electricity consumption from nuclear	983.5089	338.0178	0.042	2.2022
R-squared		0.8541		
Adjusted R-squared		0.8369		
AIC		24.4690		

From Table 2.8, the variables include GDP, the number of nuclear reactors, electricity production from nuclear energy, and electricity consumption from nuclear energy. The

coefficients, standard errors, p-values, and Variance Inflation Factor (VIF) values are reported, alongside key model metrics such as R-squared, adjusted R-squared, and the AIC. GDP shows a coefficient of 0.0022 with a standard error of 0.0005 and a p-value of 0.021, indicating a significant positive relationship. The number of nuclear reactors exhibits a coefficient of 10.9567 and a p-value of 0.027, suggesting that countries with more reactors tend to contribute significantly to the model. Similarly, electricity production and consumption from nuclear energy have coefficients of 983.3767 and 983.5089, respectively, both with p-values of 0.042, reflecting their strong influence on the dependent variable. The VIF values for all variables are below the threshold of 5, indicating no multicollinearity issues. The high R-squared (0.8541) and adjusted R-squared (0.8369) values signify that the model explains a substantial proportion of the variance in the dependent variable. The spatial distribution maps (Figure 2.8) complement these findings by illustrating the global patterns of the independent variables.

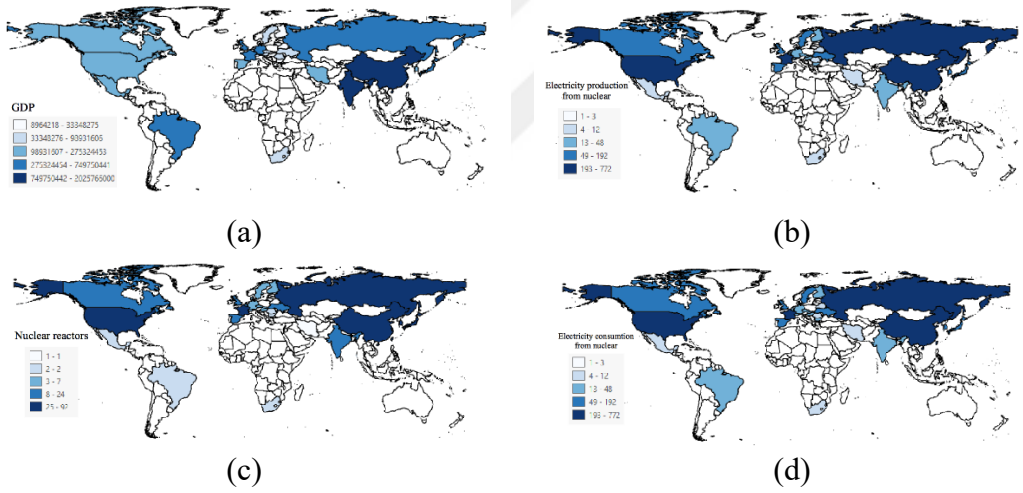

Figure 2.8 : Spatial distribution of selected independent variables at the country level across the world: a) GDP, b) Electricity production from nuclear, c) Nuclear reactors, d) Electricity consumption from nuclear.

The GDP map (Figure 2.8 a) reveals that economically advanced countries, particularly in North America, Europe, and parts of Asia, dominate higher GDP categories. Similarly, the number of nuclear reactors (Figure 2.8 c) is geographically concentrated in these regions, reflecting their historical investment in nuclear infrastructure. The maps for electricity production and consumption from nuclear sources (Figure 2.8 b and Figure 2.8 d) align with these trends, highlighting countries

like the United States, France, and China as leading contributors. These visualizations emphasize the uneven global distribution of nuclear energy-related activities, driven by economic, technological, and policy factors.

The results of the MGWR models are shown in Figure 2.9 and they illustrate the spatial heterogeneity in the relationships between key indicators (GDP, the number of nuclear reactors, electricity production from nuclear energy, and electricity consumption from nuclear energy) and their impacts on the dependent variable under consideration. By analyzing the maps, significant regional variations in the coefficients of these independent variables are evident, indicating localized effects rather than a uniform global pattern.

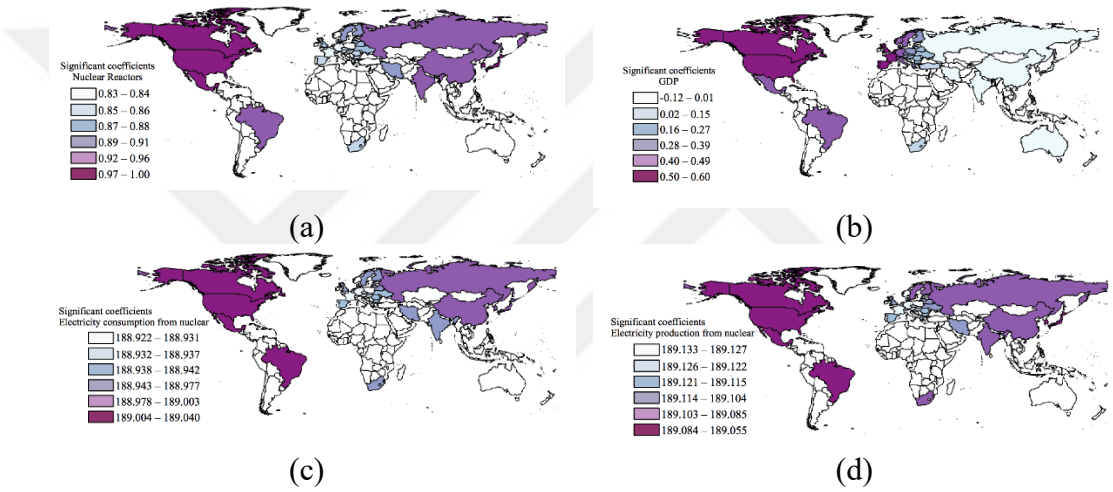

Figure 2.9 : Compound impact of energy and economic indicators on the spatial distribution of global scientific production: a) MGWR model for GDP, b) MGWR model for electricity production from nuclear, c) MGWR model for active nuclear reactors, d) MGWR model for electricity consumption from nuclear.

In the MGWR model for GDP (Figure 2.9 a), the coefficients demonstrate higher values in North America and parts of Europe, signifying a stronger positive association between GDP and the dependent variable in these regions. This reflects the economic capacity of these countries to invest in and sustain scientific advancements, infrastructure, or energy-related projects. In contrast, the weaker coefficients in regions like Africa and parts of Asia highlight a relatively smaller contribution of GDP to the dependent variable, potentially due to limited resources or differing national priorities.

The MGWR model for electricity production from nuclear energy (Figure 2.9 b) indicates strong coefficients in countries such as the United States, Canada, and parts

of Europe, which are major producers of nuclear energy. These findings highlight the critical role of nuclear energy production in shaping the dependent variable, possibly through its contribution to national energy independence, economic growth, or global scientific outputs. Regions with weaker coefficients, such as parts of South Asia and Africa, emphasize the minimal impact of nuclear energy production in these areas due to limited infrastructure or reliance on alternative energy sources.

The MGWR model for the number of active nuclear reactors (Figure 2.9 c) shows significant coefficients concentrated in regions such as the United States, France, and Japan, where nuclear infrastructure is well-developed. The high coefficient values in these areas underline the substantial role of nuclear reactor operations in influencing the dependent variable, likely due to their contribution to energy production, scientific innovation, or economic output. Conversely, regions with low coefficients, such as parts of Africa and South America, reflect the limited role of nuclear infrastructure in these areas.

Similarly, the MGWR model for electricity consumption from nuclear energy (Figure 2.9 d) reveals higher coefficients in regions where nuclear energy forms a significant part of the energy mix, such as North America and Europe. This suggests that nuclear energy consumption is a key determinant of the dependent variable in these regions, likely through its implications for energy efficiency, industrial activities, or societal advancements. Lower coefficients in other regions suggest a reduced dependency on nuclear energy for consumption purposes.

The Figure 2.10 shows the performance of the MGWR model in analyzing the relationships between various explanatory variables and their spatial impact on a global scale.

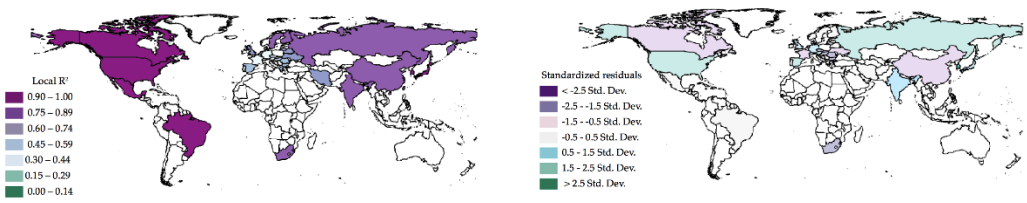

(a) (b)

Figure 2.10 : Performance of the MGWR model: a) Spatial distribution of local R^2, b) Spatial distribution of standard residuals.

The map on the Figure 2.10 a illustrates the spatial distribution of local R^2 values, which indicate how well the model explains variations in the dependent variable at

specific geographic locations. Higher local R^2 values (depicted in dark purple, ranging from 0.90–1.00) suggest that the MGWR model provides a strong explanatory power in regions such as parts of Europe, North America, and Eastern Asia, while lower values (light green, 0.00–0.14) show weaker explanatory power in regions such as parts of Africa and South America. The map on the Figure 2.10 b shows the spatial distribution of standardized residuals, which measure the difference between observed and predicted values standardized by the residuals' standard deviation. Most regions fall within ±1.5 standard deviations, shown in neutral tones, indicating a good fit overall. However, areas with residuals exceeding ±2.5 standard deviations (deep purple or blue) highlight locations where the model performs poorly or fails to capture specific local nuances.

The Table 2.9 provides summary statistics for the coefficients, standard errors, and p-values of the explanatory variables in the model, alongside broader performance metrics.

Table 2.9 : Summary statistics for coefficients estimates and MGWR model analysis.

Independent variables	Coefficient	Standard error	p-value
GDP	0.2760	0.4008	0.048
Number of nuclear reactors	0.8725	0.4866	0.010
Electricity production from nuclear	188.9736	100.6243	0.006
Electricity consumption from nuclear	189.1147	98.4534	0.006
R-squared		0.9721	
Adjusted R-squared		0.9573	
AIC		15.2118	

From Table 2.9, four key variables are analyzed: GDP, the number of nuclear reactors, electricity production from nuclear sources, and electricity consumption from nuclear sources. GDP, with a coefficient of 0.2760 and a p-value of 0.048, indicates a positive but modest relationship with the dependent variable and is statistically significant at the 5% level. The number of nuclear reactors exhibits a stronger association, as shown by its coefficient of 0.8725 and a highly significant p-value of 0.010. Electricity production from nuclear sources and electricity consumption from nuclear sources have the highest coefficients, 188.9736 and 189.1147, respectively, with low standard errors and p-values of 0.006, signifying their strong and significant impact on the

model's outcomes. Additionally, the overall model performance metrics are robust, with an R-squared value of 0.9721 and an adjusted R-squared of 0.9573, indicating that the MGWR model explains over 95% of the variance in the dependent variable when adjusting for the number of predictors. The AIC value of 15.2118 reflects the model's parsimony and goodness of fit, where lower AIC values signify better model performance. Taken together, the maps shown in Figure 2.10 and the results shown in Table 2.9 underscore the MGWR model's ability to capture spatial heterogeneity effectively while identifying key drivers influencing the dependent variable. The maps' visualizations (Figure 2.10) further enhance understanding of regional disparities in model performance and variable impacts.

2.3.8 Discussions on bibliometric analysis

Figure 2.11 schematically represents the evolving frame of nuclear accident research.

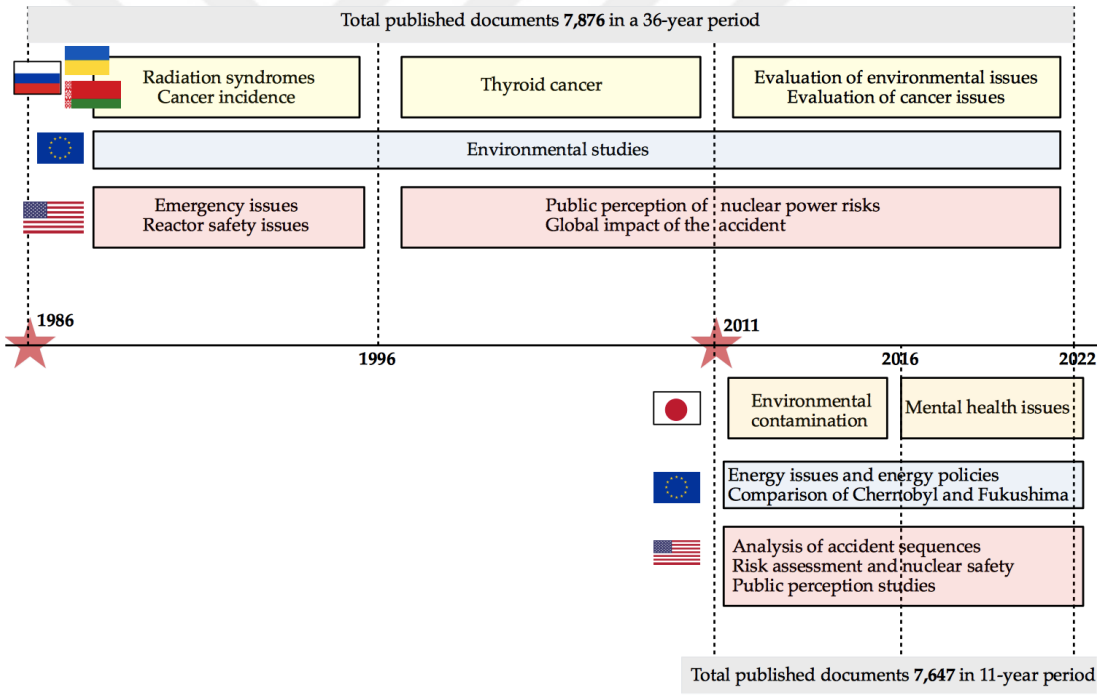

Figure 2.11 : Evolution of nuclear accident research (red stars indicate Chernobyl 1986 and Fukushima 2011 accidents, respectively).

Following the Chernobyl disaster in 1986, research efforts primarily centered on understanding the immediate health effects, such as radiation syndromes, cancer incidence, and thyroid cancer. These studies were predominantly driven by the need to assess and mitigate acute health impacts of radiation exposure (Tronko et al., 2010).

During this period, the scientific community also began examining reactor safety issues and emergency management, emphasizing the technical and procedural gaps exposed by the disaster (Espinosa-Paredes et al., 2008). Research on these topics was largely concentrated in Europe, reflecting the proximity and severity of the incident's impact on the region.

In the decades following Chernobyl, the focus of nuclear accident research expanded significantly. By the late 1990s and early 2000s, environmental studies gained prominence, as long-term ecological contamination and environmental recovery efforts became key concerns. There was a growing interest in the public perception of nuclear risks, as the global implications of the Chernobyl disaster influenced energy policies and public debates on nuclear power. During this period, research also addressed global impacts, reflecting the transboundary nature of nuclear accidents and their broader socio-political consequences (Slovik et al., 2000; Steinhauser et al., 2014).

The Fukushima nuclear disaster in 2011 marked another significant turning point in nuclear accident research. In the immediate aftermath, the focus shifted back to acute challenges, such as environmental contamination and analysis of accident sequences, with an emphasis on risk assessment and the lessons learned from both Chernobyl and Fukushima (Ohba et al., 2021). This period also saw the emergence of new topics, such as mental health issues, reflecting the psychological and social dimensions of nuclear accidents (Maeda and Oe, 2017). Notably, comparative studies between Chernobyl and Fukushima highlighted both commonalities and differences in the response to these disasters, providing valuable insights for future preparedness and mitigation strategies (Svendsen et al., 2016).

The analysis highlights regional contributions to the body of literature, with distinct thematic priorities:

- European research predominantly addressed environmental studies and energy policy implications (Moller and Mousseau, 2006; Wittneben 2012).
- Japanese studies post-Fukushima focused on environmental contamination and mental health issues (Maeda and Oe, 2017).
- Research from the United States placed significant emphasis on reactor safety, risk assessment, and public perception studies (D'Auria et al., 2017).

The publication volume over the two periods (1986-2011 and 2011-2022) reveals an interesting trend: despite the similar number of documents published in both intervals (~7,800 and ~7,600), the focus has diversified over time. While earlier research was driven by immediate technical and health concerns, recent studies have increasingly integrated multidisciplinary perspectives, including psychological, social, and policy-related dimensions.

In conclusion, this analysis underscores the dynamic nature of nuclear accident research, shaped by the lessons of past events and the evolving understanding of their consequences.

2.4 Lessons from Chernobyl and Fukushima

2.4.1 Emergency response

2.4.1.1 The Chernobyl disaster

The Chernobyl disaster, which took place in 1986 at the Chernobyl NPP, is widely regarded as the most severe nuclear accident in history (Evangeliou et al., 2016). Located in the town of Pripyat in the former Soviet Union, the plant was 104 kilometers north of Kyiv, Ukraine's capital, and just 7 kilometers south of the border with Belarus (Figure 2.12 a). The facility consisted of four reactors, each with a capacity of 1,000 MW, supplying approximately 10% of Ukraine's electricity at the time. The disaster occurred during a safety test in the early hours of April 26, 1986, when a technical failure led to a series of explosions that destroyed one of the reactors (Figure 2.12 b). The explosions released vast quantities of radioactive material into the atmosphere, spreading over large distances with the wind. While one reactor was obliterated, the other three were eventually restarted and operated for several years before the last reactor was shut down in 2000, marking the plant's final closure (Mullner 2019).

Initial efforts to contain the disaster focused on extinguishing the fire and halting nuclear reactions. Over 100 firefighters from the NPP facility battled the blaze, with many of them sustaining injuries and being exposed to dangerously high levels of radiation (Kortov and Ustyantsev, 2013). The radiation levels in parts of the plant were so extreme that monitoring equipment failed to measure them. Emergency teams and plant engineers also worked to prevent molten radioactive uranium from penetrating

the ground, as contamination of groundwater was a major concern (Filburn et al., 2016).

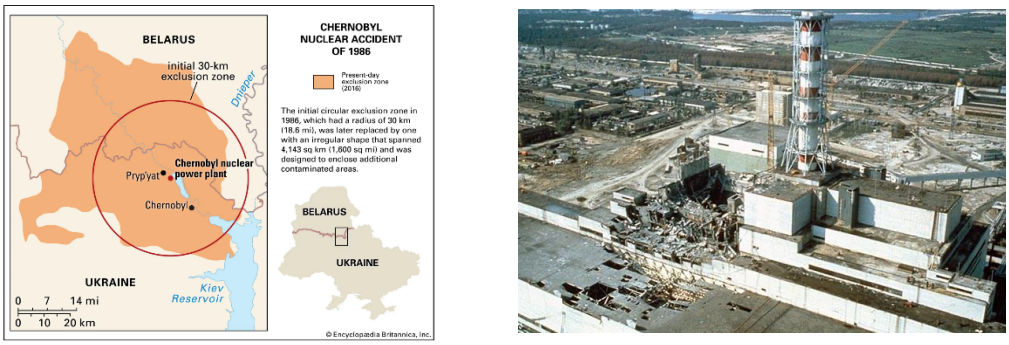

(a) (b)

Figure 2.12 : Chernobyl disaster: a) Chernobyl exclusion zone, b) Chernobyl's reactor after the explosion (both pictures are taken form Encyclopedia Britannica).

On April 26, after the injured firefighters and plant staff were evacuated, a government commission was formed to investigate the disaster and manage its consequences. However, the residents of Pripyat were not immediately informed of the danger. Public warnings were delayed, and no immediate measures were taken to reduce exposure to radiation. It wasn't until April 27 that the authorities announced a mandatory evacuation with the following statement (Naoum and Spyropoulos, 2021):

> "Attention! Attention! In connection with the accident at the Chernobyl atomic power station, unfavorable radiation conditions are developing in the city of Pripyat. In order to ensure complete safety for residents, children first and foremost, it has become necessary to carry out a temporary evacuation of the city's residents to nearby settlements of Kyiv province. For that purpose, buses will be provided to every residence today, April 27, beginning at 14:00 hours, under the supervision of police officers and representatives of the city executive committee. It is recommended that people take documents, absolutely necessary items and food products to meet immediate need. Comrades, on leaving your dwellings, please do not forget to close windows, switch off electrical and gas appliances and turn off water taps. Please remain calm, organized and orderly."

The evacuation of Pripyat began 36 hours after the explosion. Approximately 45,000 residents, mainly plant workers and their families living within a 3-kilometer radius of the NPP, were relocated using government buses. In the days that followed, the evacuation zone was extended first to a 10-kilometer radius and then to 30 kilometers,

eventually involving about 116,000 people over six months (Figure 2.13 a and Figure 2.13 b). Table 2.10 outlines the timeline of evacuation operations. A 30-kilometer exclusion zone was established around the plant, later expanded to include other highly contaminated areas (Figure 2.13 a). Experts predict the region will remain uninhabitable for thousands of years due to the high levels of radioactive contamination.

The Chernobyl disaster had far-reaching consequences, contaminating extensive areas across Ukraine, Belarus, and Russia and affecting millions of people. Over 150,000 square kilometers remain heavily contaminated, and by the end of 1986, more than 8 million individuals faced severe restrictions on land use (Saenko et al., 2011). In total, the disaster directly caused at least 28 deaths and over 100 injuries, according to the World Health Organization (WHO). Additionally, approximately 600,000 rescue workers and firefighters were exposed to significant radiation levels (Annex and UNSCEAR 2000) (Figure 2.13 c and Figure 2.13 d).

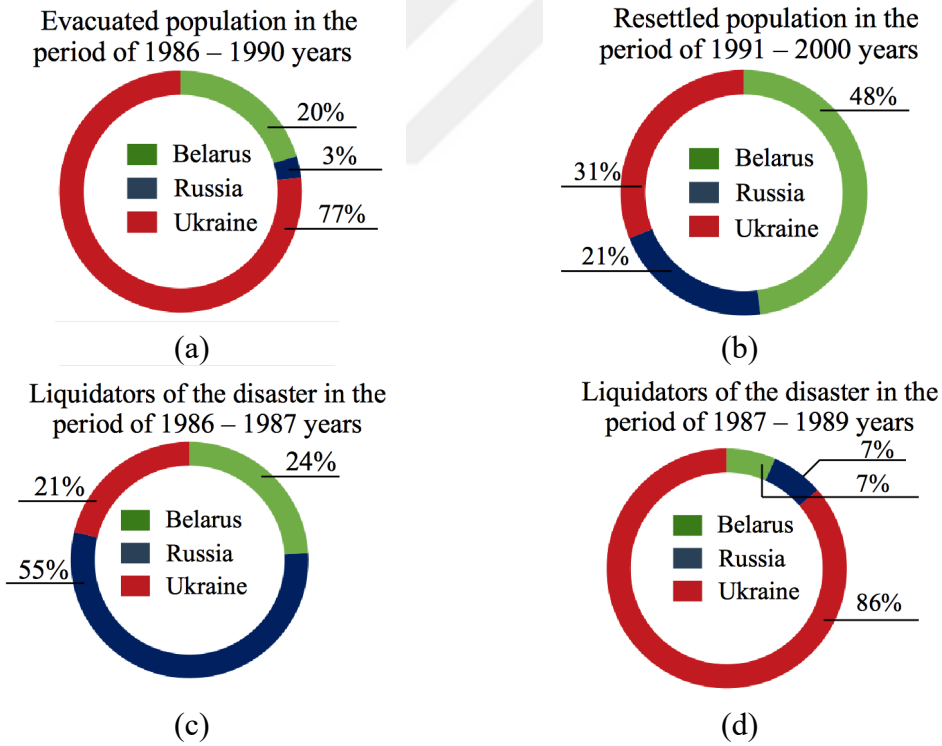

Figure 2.13 : Percent distribution of people affected by the Chernobyl accident: a) Distribution of evacuated population in the period of 1986 – 1990 (Waddington et al. 2017), b) Distribution of resettled population in the period of 1991 – 2000 (Waddington et al. 2017), c) Distribution of liquidators in the period of 1986 – 1987 (World Health Organization 2006), d) Distribution of liquidators in the period of 1987 – 1989 (World Health Organization 2006).

Table 2.10 : Timeline of evacuation orders related to the Chernobyl accident.

Date and local time	Details and description
April 26, 1986, at 01:23	The accident happened.
April 27, 1986, at14:00	The start of mass evacuation from the Pripyat town.
April 27, 1986, at 17:00	Evacuation of Pripyat was finished resulting in relocation of nearly 45,000 residents.
April 28, 1986, at 21:00	The first official announcement of the accident was made in the local news: *"There has been an accident at the Chernobyl NPP. One of the nuclear reactors was damaged. The effects of the accident are being remedied. Assistance has been provided for any affected people. An investigative commission has been set up."* (Geist 2015)
April 30 – May 03, 1986	Around 10,000 people were evacuated from 10-km radius zone.
May 03 – May 07, 1986	Residents of Ukraine (28,000 people) and Belarus (11,000) from the 30-km radius zone were evacuated.
May – September, 1986	Nearly 3,500 people from Ukraine, more than 14,000 people from Belarus, and 186 residents from the most contaminated Russian city named Bryansk were evacuated. These were the zones outside of 30-km radius.
1986 – 2000	The total number of permanently displaced individuals from the most polluted zones were about 350,000.

The long-term impact on regional demographics has been profound. Table 2.11 shows how population trends in affected regions have declined due to migration and the loss of economic opportunities.

Table 2.11 : Demographic data of towns and regions affected by the Chernobyl accident and located out of an exclusion zone (State Statistical Service of Ukraine, 2023).

Urban settlement	1985	2000	2015	2022	Decrease in population over 1985-2022, (%)
Ovruch	23,121	19,818	16,515	15,250	34%
Luhyny	6,099	5,439	4,121	3,868	36%
Korosten	70,690	65,454	65,454	61,496	13%
Radomyshl	17,020	16,572	14,930	13,685	20%
Korostyshiv	27,645	26,878	25,845	24,129	13%
Narodychi	4,062	3,437	2,604	2,907	28%
Honcharivske	4,900	4,279	3,451	3,289	33%
Korop	8,150	6,899	5,433	4,990	39%
Desna	12,004	9,890	7,550	7,297	39%
Ivankiv	13,245	12,079	10,596	9,999	24%

Industries such as agriculture, forestry, and food production, which are particularly vulnerable to radioactive contamination, could no longer function after the accident. Migration away from the contaminated areas was significant, and the population has continued to decline over time, with no signs of return.

2.4.1.2 The Fukushima disaster

Despite Japan's reputation for advanced disaster preparedness, the Fukushima-Daiichi nuclear accident posed an unprecedented challenge to the nation. This catastrophe profoundly disrupted the lives of hundreds of thousands of people and had a significant societal impact. The crisis was triggered by a combination of a devastating earthquake and tsunami, culminating in the most severe nuclear disaster since Chernobyl (Figure 2.14).

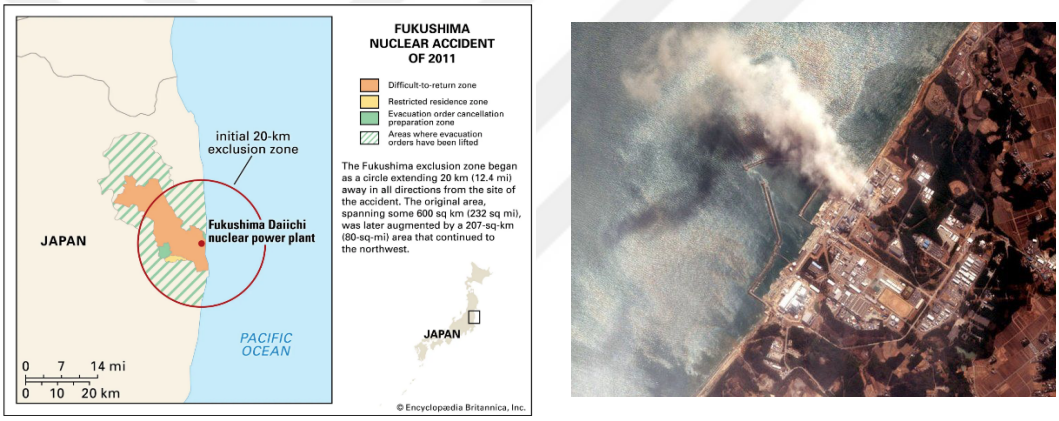

(a) (b)

Figure 2.14 : Fukushima-Daiichi disaster: a) Aerial image taken after the disaster (taken from Encyclopedia Britannica), b) Fukushima exclusion zone (taken from Encyclopedia Britannica).

The Fukushima-Daiichi NPP, situated in the towns of Okuma and Futaba along Japan's eastern coastline, housed six reactors with a combined electricity output of 4.7 GW, making it one of the largest nuclear facilities in the world (The National Diet of Japan, 2012; Kurokawa, 2013; Duffield, 2016). On March 11, 2011, the Mw 9.0-9.1 Tohoku earthquake struck, followed by a 15-meter tsunami that overwhelmed the plant's power supply and severely damaged the cooling systems of three reactors, initiating the nuclear disaster (Funabashi and Kitazawa, 2012).

Research reveals that neither the authorities nor the local population were sufficiently prepared for an accident of such magnitude. Consequently, residents had to evacuate

with no clear understanding of the duration of their displacement. The initial response to the Fukushima disaster included a combination of mandatory and voluntary evacuations, sheltering-in-place directives, restrictions on food and water consumption, and subsequent relocations (Thielen, 2012). The Japanese government acted swiftly, issuing a series of orders and guidelines to address the crisis (The National Diet of Japan, 2012; IAEA, 2015). A detailed timeline of these events is provided in Table 2.12.

Table 2.12 : Chronology of orders related to the response to the Fukushima Daiichi accident (The National Diet of Japan, 2012).

Date and local time	Details and description
11 March, 14:46	Epicenter of Mw 9.0 – 9.1 earthquake in the Pacific Ocean, 72 km east of the Tohoku region, Japan
11 March, 15:27	The first wave of the tsunami hit the NPP
11 March, 15:46	A 14-meter tsunami wave exceeded the barrier dam, flooding the facilities of the Fukushima NPP. Tsunami disabled the generators intended for emergency cooldown of the reactors.
11 March, 20:50	Mandatory evacuation for 0 – 2 km radius zone
11 March, 21:23	Mandatory evacuation for 2 – 3 km radius zone
11 March, 21:23	Sheltering in place for 3 – 10 km radius zone
12 March, 05:44	Mandatory evacuation for 3 – 10 km radius zone
12 March, 18:25	Mandatory evacuation for 10 – 20 km radius zone
15 March	Sheltering in place for 20 – 30 km radius zone
25 March	Mandatory evacuation continued for 10 – 20 km radius zone
25 March	Voluntary evacuation for 20 – 30 km radius zone
22 April	Restricted area for 0 – 20 km radius zone
22 April	Evacuation prepared area in case of emergency for 20 – 30 km radius zone
22 April	Deliberate evacuation area for 20 – 55 km radius zone
30 June	Restricted area for 0 – 20 km radius zone
30 June	Evacuation prepared area in case of emergency for 20 – 30 km radius zone
30 June	Deliberate evacuation area for 20 – 55 km radius zone
30 June	Specific spots recommended for evacuation for 20 – 55 km radius zone
30 September	Restricted area for 0 – 20 km radius zone
30 September	Specific spots recommended for evacuation for 20 – 55 km radius zone
30 September	Lifting the order of evacuation in evacuation prepared area for 20 – 30 km radius zone

In the hours following the accident, mandatory evacuation began for residents within a 2-km radius of the plant. Over the course of the day, this zone was expanded to a 20-

km radius, which was subsequently designated as a restricted area with no public access allowed (Figure 2.14 a). After evacuating all individuals within the initial 2-km zone, local authorities issued evacuation orders for those residing between 2 km and 3 km from the plant. At the same time, residents within the 3-10 km zone were instructed to shelter in place. The next day, evacuation orders were extended to cover the entire 20-km radius.

On March 15, five days after the disaster, the government advised residents in the 20-30 km zone to shelter in place. This directive remained in effect for several days, after which residents in this area were permitted to evacuate voluntarily. Mass evacuation efforts continued until June, at which point authorities identified specific "hot spots" with high radiation levels outside the 30-km radius. These areas, located between 20 km and 55 km northwest of the plant, led to the evacuation of nearly 15,000 additional residents.

Research has consistently shown that evacuees were not adequately informed about the severity of the Fukushima accident or the associated radiation risks (Kim and Kim, 2017). This communication breakdown, caused by disruptions to the information system following the earthquake, left many residents in fear and confusion, leading to rushed evacuations. This disorganized response caused severe traffic congestion along evacuation routes and, in some cases, individuals unknowingly moved into areas with higher radiation levels, particularly in the northwest.

Guidelines established by the Nuclear Safety Commission (NSC) (Cousins et al., 2011; Ohba et al., 2021) designated an 8-10 km zone around NPPs as the Emergency Planning Zone (EPZ), intended to facilitate preparedness for nuclear disasters. In the case of Fukushima, preparedness measures were limited to this zone, leaving the surrounding areas unprepared for the scale and speed of the required evacuation.

Within the 20-km radius evacuation zone, there were 17 medical facilities and 7 hospitals (Ohba et al., 2021). By March 13, when the evacuation of this zone was completed, approximately 2,000 elderly patients remained in care centers (Hasegawa et al., 2016). The evacuation of these patients was carried out hastily, often without adequate medical supplies on transport vehicles or the presence of medical personnel. Tragically, this disorganized effort resulted in the deaths of 60 patients during or shortly after their evacuation (Hasegawa et al., 2016).

The WHO reported that individuals evacuated in the initial stages received radiation doses of up to 6 mSv, whereas those evacuated later experienced exposure levels as high as 10 mSv (World Health Organization, 2021). For context, the average annual radiation dose from natural sources for a Japanese resident is approximately 4 mSv (Harada et al., 2014). These figures underscore the dangers posed by an unprepared and chaotic evacuation process, which, in some cases, caused more harm than the immediate risk of radiation exposure.

The disaster led to the displacement of over 160,000 individuals, accounting for 45% of those forced to evacuate by the combined effects of the earthquake and tsunami (Ohtsuru et al., 2015). Of these evacuees, 113,000 were relocated under mandatory orders, while 47,000 left voluntarily. In total, 11 municipalities were affected (Sun et al., 2022). In the years following the disaster, extensive decontamination efforts enabled the return of some evacuees. However, survey data revealed that many individuals were hesitant to return due to persistent concerns about radiation exposure (Murakami et al., 2020).

As of late 2020, the average return rate of evacuees was 14%. However, higher return rates were observed in municipalities such as Kawamata (78%), Kawauchi (72%), Minamisoma (83%), and Tamura (87%). Table 2.13 provides detailed information on the lifting of evacuation orders and demographic trends in Fukushima Prefecture. By October 2020, environmental contamination levels had decreased by 80% compared to November 2011, and most affected areas had undergone significant cleanup and restoration efforts (The Japan Times, 2023).

Table 2.13 : Demographic data of Fukushima prefecture before and after the accident and dates of lifting the evacuation orders (City Population, 2020).

Japan's regions	2010	2015	2020	The lifting of evacuation order
Futaba	6,932	0	0	March 2020
Katsuaro	1,530	18	420	June 2016
Kawamata	15,569	14,452	12,170	March 2017
Kawauchi	2,820	2,021	2,044	October 2014
Litate	6,209	41	1,318	March 2017
Minamisoma	70,878	57,797	59,005	July 2016
Namie	20,905	0	1,923	March 2017
Naraha	7,700	975	3,710	September 2015
Okuma	11,570	0	847	April 2019, March 2020
Tomioka	16,000	0	2,128	April 2017, March 2020
Tamura	40,422	38,503	35,169	April 2014

2.4.2 Environmental consequences

2.4.2.1 Chernobyl accident

The Chernobyl nuclear disaster released unprecedented amounts of radioactive materials into the environment, causing widespread and long-lasting ecological damage. The explosion of Reactor 4 at the Chernobyl NPP contaminated ecosystems not only in Ukraine, Belarus, and Russia but also across Europe and other parts of the world (Saenko et al., 2011). The immediate area surrounding the plant, particularly the 30-kilometer Exclusion Zone, suffered the most severe impact. This zone, encompassing parts of northern Ukraine and southern Belarus, experienced significant fallout from isotopes such as CS-137, I-131, and Strontium-90. Agricultural lands became heavily polluted, with radioactive particles embedding deeply in soil layers, rendering vast tracts of farmland unusable. In Belarus, approximately 22% of agricultural land was deemed unsuitable for cultivation, severely affecting food security and rural livelihoods. The contamination persists due to the long half-life of radionuclides, with some areas still unfit for farming decades after the disaster (Saenko et al., 2011).

Forests within the Exclusion Zone were similarly devastated, most notably the “Red Forest”, where radiation killed or severely damaged trees, leaving them with a reddish-brown hue. Over time, these forests became hotspots for radioactive accumulation in the ecosystem, affecting leaf litter, mushrooms, and wildlife. The water systems were also significantly impacted, with radioactive materials contaminating rivers, lakes, and groundwater. The Pripyat River, a major tributary of the Dnieper, carried radioactive particles downstream, compromising water supplies for millions of people. Although sedimentation has reduced contamination levels in some areas, many hotspots remain problematic (Thiry et al., 2009).

Beyond the immediate vicinity, the radioactive plume from the explosion spread across much of Europe, contaminating over 200,000 square kilometers of land. Scandinavian countries, including Sweden and Norway, experienced significant deposition of CS-137, which contaminated grazing lands and food sources such as reindeer and sheep (Alinaghizadeh et al., 2016). Figure 2.15 shows the land contamination in Ukraine and Europe. In these areas, radionuclides entered the food chain, leading to restrictions on meat consumption and ongoing challenges in

managing contaminated ecosystems. Central and Eastern European countries, such as Poland, Hungary, and Austria, faced similar issues, with widespread agricultural contamination affecting crops, dairy products, and wild game (Schwaiger et al., 2004). Even in Western Europe, fallout hotspots in countries like Germany and the UK created localized ecological disturbances, with species at the top of the food chain facing higher radiation exposure due to bioaccumulation (Schwarz 2025).

The global reach of the Chernobyl disaster became evident as radioactive materials were carried by atmospheric currents across the Northern Hemisphere. Traces of I-131 and CS-137 were detected as far away as Asia, the Middle East, and North America (Bilgic and Gunduz, 2022). Although the concentrations were much lower at these distances, the event underscored the global implications of nuclear accidents. Radionuclides eventually entered oceans through rivers and atmospheric deposition, and while their overall impact on marine ecosystems was less severe than on terrestrial environments, radioactive contamination was detected in fish, plankton, and other marine life (Mousseau 2021).

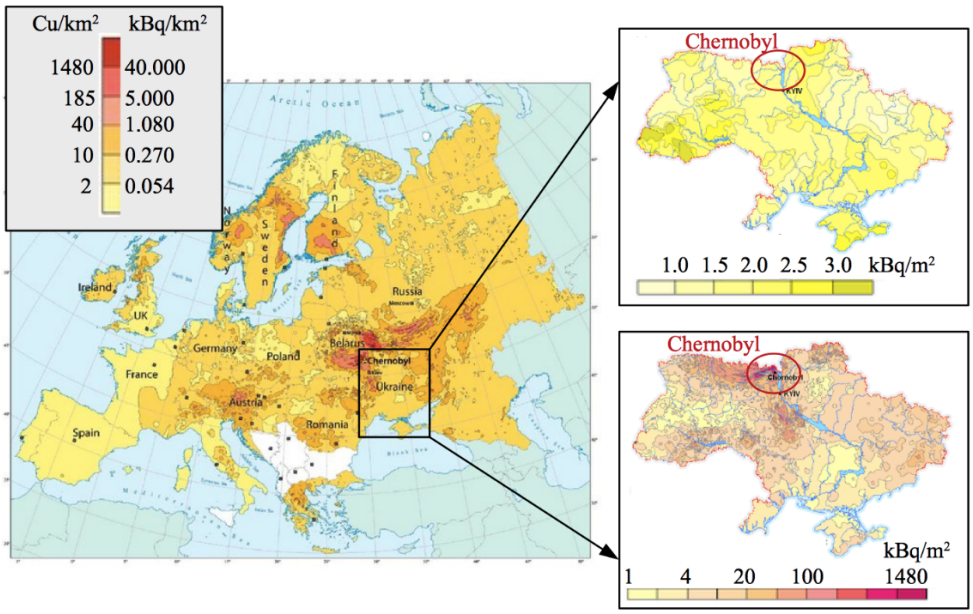

Figure 2.15 : Environmental contamination due to Chernobyl disaster: Maps showing radioactive contamination of the Europe by Cs137 after the accident (modified from Moller and Mousseau 2006) and radioactive contamination of the territory of Ukraine by Cs137 before and after the disaster (1985 year) (modified from Skrynyk et al. 2010).

Efforts to mitigate the environmental impact of Chernobyl have been ongoing, but significant challenges remain. Long-lived isotopes like CS-137 and St-90continue to

pose risks, especially in ecosystems where bioaccumulation occurs. Forests, in particular, are likely to remain contaminated for decades, and the accumulation of radionuclides in soil and water requires continuous monitoring. Advances in environmental science have improved understanding of radionuclide behavior, but the long-term ecological consequences of such widespread contamination are still not fully understood.

2.4.2.2 Fukushima accident

The immediate and long-term environmental consequences after Fukushima accident were profound, affecting not only Japan but also ecosystems and marine environments globally. The release of radioactive isotopes, including I-131, cesium-134, and CS-137, led to extensive contamination of soil, water, and vegetation, particularly in Fukushima Prefecture and surrounding regions. Farmland in these areas was severely affected, as radionuclides such as CS-137 bound strongly to soil particles, rendering large tracts of land unsuitable for cultivation. Farmers faced challenges as crops like rice and vegetables absorbed radiation, leading to bans on agricultural products and long-term impacts on food security and rural livelihoods. While decontamination efforts, such as the removal of surface soil layers and crop washing, were undertaken, certain areas remain unfit for farming even after more than a decade (Nihey 2023).

Forests in the fallout zone absorbed large amounts of radioactive cesium, leading to persistent contamination in tree bark, leaf litter, and soil. This created a cyclical problem as radionuclides re-entered the environment through natural processes such as leaf fall and water runoff (Sakai et al., 2021). Wildlife in these forests, including boars and deer, accumulated high levels of radiation through their diets, raising concerns about hunting and the consumption of game meat (Hashimoto 2023). Rivers, lakes, and groundwater systems were also significantly impacted, with radioactive runoff from the damaged plant contaminating water bodies such as the Abukuma River (Igarashi et al., 2022). This contamination affected drinking water supplies and irrigation systems, with radionuclides like cesium and iodine detected in reservoirs. Although natural dilution and sedimentation reduced radiation levels in some areas, localized hotspots of contamination remain problematic.

The disaster also had a significant impact on biodiversity. Radiation exposure caused mutations in butterflies, reduced populations of bird species, and affected the

reproductive health of aquatic organisms. While some species have shown resilience and even a resurgence in numbers due to reduced human activity in affected areas, others continue to suffer from the effects of prolonged exposure to low-level radiation (Sakauchi and Otaki, 2023). Beyond the terrestrial impacts, the Fukushima disaster's marine contamination was one of its most concerning aspects, as large amounts of radioactive materials entered the Pacific Ocean through direct discharges, surface runoff, and leaks from damaged storage tanks. Figure 2.16 shows the spatial distribution of Cs-137 in the Pacific Ocean after the accident. It is estimated that approximately 80% of the radioactive material released entered the ocean, with isotopes like CS-137, cesium-134, and St-90dispersing rapidly through ocean currents (Han et al. 2013). This contamination affected marine ecosystems as radioactive isotopes were absorbed by plankton, fish, and shellfish, leading to bioaccumulation through the food chain. Large fish, such as tuna, showed elevated cesium levels even thousands of kilometers from Japan, raising global concerns about seafood safety (Wakamatsu and Miyata, 2021). Seafloor contamination also became a long-term issue, as radioactive particles settled and created persistent hotspots, affecting bottom-dwelling organisms and the broader marine food web.

Globally, the Fukushima disaster had far-reaching environmental consequences. Radioactive isotopes released into the atmosphere during the initial explosions were carried by prevailing winds across the Northern Hemisphere, with traces of I-131 and CS-137 detected as far as North America and Europe (Cooke et al., 2022). Although concentrations were low and posed minimal risks to public health, the widespread dispersion underscored the transboundary nature of nuclear accidents. Ocean currents, particularly the Kuroshio Current, transported radioactive materials across the Pacific, with detectable levels of CS-137 reaching the western coasts of North America within two years of the accident (Han et al. 2013).

2.4.3 Health consequences

2.4.3.1 Chernobyl accident

The Chernobyl nuclear disaster led to severe and far-reaching health consequences that continue to be studied decades later. The massive release of radioactive materials exposed various groups, including workers, emergency responders, and the general population, to different levels of radiation. These exposures resulted in a range of acute

and chronic health effects, encompassing radiation-induced illnesses, psychological stress, and secondary health issues. The highest radiation doses were received by workers and emergency responders, known as liquidators, who were tasked with managing the immediate aftermath of the explosion and the subsequent cleanup (Onopriyenko et al., 2024). Other affected groups included evacuees from nearby areas, residents of contaminated regions, and, to a lesser extent, populations across Europe who were exposed to radioactive fallout (Panov et al., 2024). The magnitude of exposure and associated health impacts varied among groups, as outlined in Table 2.14.

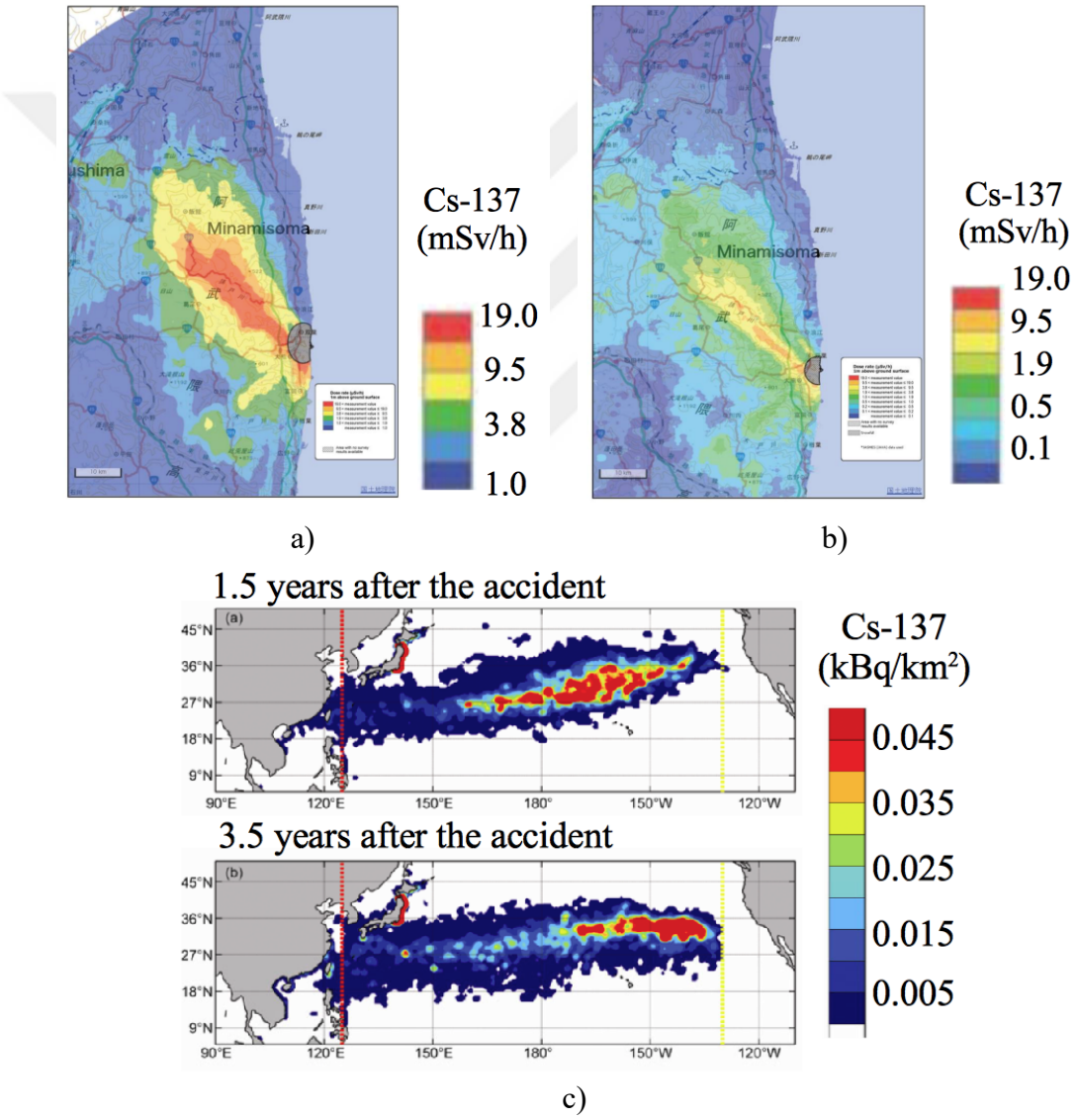

Figure 2.16 : The spatial distribution of radiation after the Fukushima disaster: a) Contamination of Japan as of April 2011 (modified from Feldhoff 2018), b) as of November 2016 (modified from Feldhoff 2018), c) Contamination of the Pacific Ocean at years 1.5 and 3.5 (modified from Han et al. 2013).

Table 2.14 : Radiation doses and associated health impacts across affected groups after the Chernobyl disaster (World Health Organization 2006).

Group	Average dose (mSv)	Range of doses (mSv)	Health impact
Reactor operators and firefighters	6,000 – 16,000	>10,000 for many; fatal doses	ARS; 28 fatalities within three months; long-term cancer risk.
Liquidators (1986 – 1990)	120	10 – 500	Elevated cancer risk, particularly leukemia; increased mortality from non-cancer diseases.
Evacuees (1986)	33	3 – 500	Increased incidence of thyroid cancer, especially in children; psychological stress.
Residents of highly contaminated areas	15 – 50	10 – 200	Thyroid cancer, cataracts, and potential cardiovascular effects.
General population in Europe	0.3	<1	No significant increase in cancer or other health risks detected.

Among the immediate health consequences, ARS was the most prominent, affecting 134 individuals, including firefighters and plant workers, who were exposed to extremely high doses. ARS caused symptoms such as nausea, vomiting, diarrhea, and severe burns, with 28 individuals succumbing to radiation within the first three months. Survivors of ARS often faced long-term health problems, including chronic fatigue, reduced immunity, and an elevated risk of cancer (Mettler et al., 2007).

One of the most extensively studied health effects of the Chernobyl disaster is the dramatic increase in thyroid cancer cases, particularly among children and adolescents. Exposure to radioactive I-131 was the primary cause, as children were more vulnerable due to their smaller thyroid glands and higher consumption of contaminated milk and food. Over 5,000 cases of thyroid cancer have been directly attributed to the disaster, with the highest rates observed in Belarus, Ukraine, and Russia. Although most cases were treatable, the physical and psychological burden on affected individuals remains significant (Leenhardt and Aurengo, 2000).

Additionally, liquidators faced an increased risk of leukemia due to their substantial radiation exposure, with epidemiological studies showing a dose-dependent rise in

incidence (Howe 2007). Other cancers, such as breast, bladder, and lung cancer, were also reported, though the evidence for these is less robust compared to thyroid cancer and leukemia (Hatch et al., 2005). Beyond cancer, radiation exposure was linked to non-cancerous conditions, including cataracts, cardiovascular diseases, and immune system disorders. Cataracts were observed among individuals exposed to doses as low as 250 mSv, while studies have suggested a possible connection between radiation and cardiovascular diseases, though further research is needed (Worgul et al., 2007).

The psychological and social effects of the disaster were profound, particularly among evacuees and residents of contaminated areas. Displacement, fear of radiation, and societal stigma contributed to high rates of anxiety, depression, and post-traumatic stress disorder (PTSD). For many, these mental health challenges have had a greater impact on their quality of life than direct radiation effects (Bromet and Havenaar, 2007).

Reproductive health also suffered in the wake of Chernobyl. Some studies reported increased rates of stillbirths, miscarriages, and congenital malformations in highly contaminated areas, though results varied. For example, an 80% rise in congenital malformations was observed in the most contaminated regions of Belarus, though stress and healthcare access disparities likely played a role (Korsakov et al., 2020).

The health impacts of Chernobyl were not confined to the immediate vicinity of the disaster. Radioactive fallout was detected across Europe, exposing populations to low levels of radiation (Drozdovitch et al., 2007). Although the doses were too small to cause significant health effects, the widespread dispersion of radionuclides highlighted the transboundary nature of nuclear disasters. The psychological impact extended globally, as fear of radiation influenced public attitudes toward nuclear power and prompted changes in energy policies (Bisconti 2018).

2.4.3.2 Fukushima accident

The Fukushima Daiichi nuclear disaster had significant health implications for workers, residents, and even global populations. Although the scale of radioactive release was lower than that of Chernobyl, the complex nature of the accident and the widespread contamination raised profound concerns about radiation exposure and its long-term health consequences.

One of the primary challenges in assessing the health impact of Fukushima is the lower radiation doses received by most affected groups compared to other major nuclear accidents (Ishikawa 2017). This was largely due to successful emergency responses, such as the evacuation of over 150,000 people from high-risk areas, restrictions on food and water consumption, and decontamination efforts (Hasegawa et al., 2016). Despite these measures, the disaster caused acute and chronic health effects, including psychological stress and potential long-term risks of radiation-induced diseases (Tsujiuchi et al., 2016).

The doses received by different groups varied depending on their proximity to the plant, duration of exposure, and adherence to safety protocols. Table 2.15 summarizes the estimated doses for key groups affected by the Fukushima disaster.

Table 2.15 : Estimated Radiation Doses and Associated Health Impacts Across Affected Groups After the Fukushima Disaster (Ishikawa et al., 2015).

Group	Average dose (mSv)	Range of doses (mSv)	Health impact
Plant workers (emergency response)	12	<1 – 679	Minor cases of radiation sickness; no deaths due to acute radiation exposure; increased cancer risk for higher doses.
Residents of evacuation zones	4	1 – 50	Negligible short-term health effects; potential increase in thyroid cancer risk, especially in children.
Residents outside evacuation zones	<1	<1 – 20	Radiation exposure below levels associated with significant health effects.
General population in Japan	<0.1	<0.1 – 1.0	No measurable increase in cancer or other health risks expected.
Global population	<0.01	<0.01 – 0.10	Insignificant health impact due to very low levels of fallout.

The workers at the Fukushima plant received the highest doses of radiation during emergency response and containment efforts. Approximately 174 workers were exposed to doses exceeding 100 mSv, a level associated with an increased risk of cancer, particularly leukemia. The highest recorded dose, 679 mSv, was received by a worker who participated in venting operations. While no fatalities occurred due to ARS, these workers face potential long-term health risks that require ongoing medical monitoring (World Health Organization 2012).

Residents of the evacuation zones experienced varying levels of exposure, with the average dose for those in highly contaminated areas estimated at 4 mSv in the first year. The exposure levels were significantly reduced after evacuation, highlighting the effectiveness of early protective measures. However, children in the region were particularly vulnerable due to their susceptibility to thyroid cancer from radioactive I-131 (I-131) released during the accident. Extensive screening programs identified a small increase in thyroid cancer cases, though the causal relationship with the disaster remains a subject of debate. The low overall doses have made it difficult to distinguish radiation-induced cases from the naturally occurring baseline (World Health Organization 2012).

For residents outside evacuation zones, radiation doses were generally below 20 mSv, a level considered safe for the general population. Comprehensive monitoring programs conducted in Fukushima Prefecture and neighboring areas consistently showed radiation levels well below thresholds associated with significant health risks. Nonetheless, the psychological impact of perceived radiation exposure has been substantial, with many residents experiencing anxiety, depression, and stress-related illnesses (World Health Organization 2013).

Globally, the fallout from Fukushima resulted in minimal radiation exposure due to the ocean's capacity to dilute contaminants and atmospheric dispersion. The majority of radionuclides released into the environment, such as Cs-137 and I-131, were carried into the Pacific Ocean, raising concerns about marine ecosystem contamination. Studies have shown that radioactive materials entered the food chain, with measurable levels detected in seafood. However, the doses received by seafood consumers worldwide were far below levels associated with health risks (Fisher et al., 2013).

The psychological and social impacts of the Fukushima disaster have been profound and long-lasting. The sudden evacuation, displacement, and stigma faced by evacuees have led to high rates of mental health disorders, including PTSD, depression, and anxiety. Elderly populations, in particular, faced increased mortality due to the stress of relocation and disrupted medical care. Furthermore, concerns about radiation exposure have resulted in behavioral changes, such as reduced outdoor activities and avoidance of locally produced food, further contributing to health and social challenges (Yabe et al., 2014).

2.4.4 Economic impact

2.4.4.1 Chernobyl accident

The economic consequences of the Chernobyl disaster were far-reaching and devastating, not only for the immediate region surrounding the nuclear plant but also for the broader Soviet Union and the world at large.

In the immediate aftermath of the disaster, the Soviet Union, which was responsible for the Chernobyl plant, faced an enormous financial burden. The costs associated with evacuation, emergency response, and the initial stages of containment and decommissioning were immense. More than 100,000 people were evacuated from the most contaminated areas, primarily in the Ukrainian Soviet Union, Belarus, and Russia. These individuals required relocation assistance, temporary housing, and ongoing compensation for the loss of their homes and livelihoods. The Soviet government provided financial support for the resettlement of evacuees, but this came at a substantial cost, both in terms of government expenditure and the loss of productivity in the affected areas (Samet and Seo, 2016).

The costs associated with the cleanup and decommissioning of the Chernobyl site itself were monumental. A large number of workers, including liquidators who were drafted from all over the Soviet Union, were involved in the immediate response efforts. These workers, many of whom received significant doses of radiation, undertook hazardous tasks such as clearing debris, constructing a concrete sarcophagus around the reactor, and decontaminating the surrounding area. The cost of these efforts was substantial, and estimates of the total cost of the Chernobyl cleanup range from $18 billion to $22 billion. The financial burden of these activities was further compounded by the need for long-term monitoring, decommissioning, and site restoration, which continues to this day (Beresford et al., 2016; Sagara et al., 2020).

The agricultural sector was one of the hardest-hit industries, with large swaths of farmland contaminated by radioactive fallout. The Soviet Union was forced to abandon entire agricultural regions in Ukraine, Belarus, and Russia, including significant portions of their fertile soil. The contamination led to the loss of crop yields, particularly in the production of grain, vegetables, and livestock. The areas surrounding Chernobyl, known as the “Chernobyl Exclusion Zone”, became uninhabitable, and much of the region’s agricultural production was halted. This not

only led to a reduction in domestic food supplies but also resulted in lost export revenues (Sagara et al., 2020).

The fishing industry was also severely impacted by the disaster. Radioactive contamination of rivers, lakes, and reservoirs in the affected regions led to the destruction of local fisheries and a sharp decline in fish stocks. Fish caught in contaminated waters showed elevated levels of radioactive cesium, leading to widespread restrictions on the consumption and sale of fish from these areas. The fishing industry in Ukraine and Belarus faced significant economic losses, with restrictions on both domestic and international markets for contaminated products. In the long run, the economic damage to the agricultural and fishing sectors caused by Chernobyl was estimated to be in the tens of billions of dollars, further exacerbating the economic strain on the Soviet Union (Morita et al., 2020).

One of the most enduring economic consequences of the Chernobyl disaster was the loss of public confidence in nuclear energy. Prior to Chernobyl, the Soviet Union had heavily invested in nuclear energy as a key part of its energy strategy. However, the disaster severely undermined the public's trust in the safety of nuclear power, both within the Soviet Union and globally. The global reaction to Chernobyl resulted in a reevaluation of nuclear energy policies in many countries. Several nations, including Italy, Germany, and Austria, abandoned or scaled back their nuclear energy programs following the disaster (Eiser et al., 1990). This shift in global energy policy had a lasting impact on the nuclear industry, leading to higher costs for nuclear energy projects, the delayed construction of new plants, and increased safety regulations. The longer-term financial effects of the Chernobyl disaster on the nuclear industry were significant, with billions of dollars in lost investment and increased operational costs for existing plants.

In addition to the direct economic costs, Chernobyl had significant social and political consequences that further contributed to the economic strain in the affected regions. The health impacts of the disaster, including the long-term effects of radiation exposure, resulted in additional economic costs related to healthcare. Many of the workers involved in the cleanup efforts, as well as residents of the contaminated areas, developed health problems, including cancers, thyroid diseases, and other radiation-related illnesses. These health impacts not only led to a reduction in the labor force but

also placed additional pressure on the already strained healthcare system (Lehmann and Wadsworth, 2011).

The economic consequences of Chernobyl were not limited to the Soviet Union. The disaster had ripple effects on global markets, particularly in the agricultural and energy sectors. Many European countries experienced heightened concerns about food safety, particularly with regard to the contamination of crops, livestock, and dairy products. For example, countries like Sweden, Finland, and Norway reported significant contamination of agricultural products, leading to trade restrictions and market disruptions (Liland et al., 2009). These nations were forced to impose bans on the import of certain food products from the affected regions and to implement costly measures to monitor and decontaminate contaminated foodstuffs. The European Union also established new regulations concerning the safety of food imports, which affected agricultural trade between the Soviet Union and Western Europe (Belyakov 2015).

Additionally, the Chernobyl disaster had an impact on global energy markets. The accident led to a temporary decline in the demand for nuclear energy, as countries reassessed the risks associated with nuclear power. This shift in energy policy, particularly in Europe, contributed to a rise in the demand for alternative energy sources such as coal, natural gas, and oil. The long-term consequences of this shift were seen in the higher energy costs for countries that reduced or abandoned nuclear power and turned to fossil fuels, which contributed to the global energy market fluctuations (Csereklyei 2014).

2.4.4.2 Fukushima accident

The immediate aftermath of the Fukushima disaster saw significant financial costs associated with the evacuation, emergency response, and containment efforts. In the first few years, the Japanese government and the Tokyo Electric Power Company (TEPCO), the operator of the Fukushima plant, incurred substantial expenditures. The evacuation of more than 150,000 people from the affected areas resulted in costs related to housing, relocation, and compensation. In total, the Japanese government allocated billions of dollars for these immediate measures. The government also provided financial support to businesses and industries in the affected regions to mitigate the economic shock, particularly for those in agriculture, fishing, and tourism (Yasutaka and Naito, 2016; Yanovskiy et al., 2020).

One of the most significant economic impacts of the Fukushima disaster was felt by Japan's energy sector. Following the accident, all of Japan's nuclear reactors were shut down for safety inspections, and many remain offline years later. This led to a sharp reduction in the country's nuclear power generation capacity, which had previously supplied around 30% of Japan's electricity. In the absence of nuclear power, Japan was forced to rely more heavily on fossil fuels, particularly natural gas, coal, and oil, to meet its energy needs. As a result, Japan's import bill for fossil fuels skyrocketed, increasing energy costs and contributing to a trade deficit. This shift also led to higher electricity prices for consumers and businesses, further straining the country's economy (Taghizadeh-Hesary et al., 2017).

In addition to the increased costs of energy imports, the Fukushima disaster severely impacted Japan's agricultural and fishing industries. Agricultural lands in the surrounding areas were contaminated with radioactive materials, leading to widespread restrictions on food production and consumption. The Fukushima prefecture, which had once been a major agricultural hub, saw a sharp decline in crop yields, particularly for rice and vegetables. The contamination also led to a loss of consumer confidence in the safety of Japanese food products, both domestically and internationally. This had long-term repercussions for Japan's food export industry, as key markets such as China, South Korea, and the European Union imposed restrictions on the import of Japanese agricultural goods (Bachev and Ito, 2013).

Similarly, the fishing industry in the affected regions faced significant challenges. Radioactive contamination of seawater and marine life led to a decline in fish catches, particularly for species such as tuna and squid. The fishing industry, particularly in Fukushima and neighboring prefectures, experienced a sharp drop in both domestic consumption and international demand. In 2011, Japan's fishing industry lost an estimated $2.5 billion due to the combined effects of contamination and reduced demand. The industry faced additional costs related to decontamination efforts, including the monitoring and testing of fish for radiation levels, and in some cases, the disposal of contaminated catches (Morita et al., 2020).

Tourism, another important sector of Japan's economy, was also severely impacted by the disaster. In the months following the Fukushima accident, Japan experienced a sharp decline in both domestic and international tourism. Fears of radiation exposure, compounded by media coverage of the disaster, led to a significant drop in visitors to

Japan, particularly in the Tokyo metropolitan area and regions near the Fukushima plant (Handler 2016; Kim 2016).

The economic consequences of the Fukushima disaster were not confined to Japan. The global effects were primarily felt in the energy sector, particularly in countries that relied on Japan for energy imports or that had nuclear energy policies influenced by the disaster. Many countries reassessed their nuclear energy strategies in the wake of Fukushima, leading to a shift away from nuclear power in some regions. In Germany, for example, the government made the decision to phase out nuclear power entirely, with the last nuclear reactor scheduled for closure by 2022 (Kharecha and Sato, 2019). Other countries, such as Italy and Switzerland, also reconsidered or delayed plans to develop nuclear energy (McLellan et al., 2013). This shift in energy policy had significant implications for global energy markets, particularly in terms of the demand for alternative energy sources such as natural gas and renewable energy.

The Fukushima disaster also had an impact on global supply chains, particularly in industries reliant on Japanese manufacturing. Japan is a major producer of high-tech components and electronics, and the disruption caused by the disaster affected the production of goods ranging from automobiles to semiconductors. For example, the automotive industry saw disruptions in the supply of key components, such as microchips and wiring, which led to production delays and higher costs for manufacturers in other countries (Arto et al., 2015).

In the longer term, the economic consequences of Fukushima have been marked by a shift in Japan's energy policy. The country has moved toward increasing its reliance on renewable energy sources such as solar, wind, and geothermal power, although this transition has been slow and costly (Nesheiwat and Cross, 2013). The Japanese government has also made efforts to reinstate some of its nuclear reactors, but the public remains divided on the issue, with strong opposition from local communities near nuclear plants and environmental groups (Polleri 2020). The cost of decommissioning the Fukushima plant itself remains a significant economic burden. Estimates of the total cost of decommissioning Fukushima, including the cleanup, compensation, and rebuilding efforts, run into the hundreds of billions of dollars, with no clear timeline for completion.

In conclusion, the economic consequences of the Fukushima Daiichi nuclear disaster have been profound and long-lasting. While Japan faced immediate economic losses

in agriculture, fishing, tourism, and energy, the global effects were more indirect, primarily impacting energy policies and supply chains. The long-term costs, particularly those associated with decommissioning the Fukushima plant and transitioning to alternative energy sources, remain substantial.

2.4.5 Lessons and future directions

The Chernobyl and Fukushima nuclear accidents have provided profound lessons in emergency response, environmental and health consequences, and economic impacts, offering critical insights for shaping future directions. Both incidents underscored the importance of timely evacuation in reducing radiation exposure. In Chernobyl, delayed evacuation significantly increased health risks, while in Fukushima, rapid evacuations demonstrated the importance of pre-planned strategies. However, confusion and logistical challenges during Fukushima highlighted the need for improved communication and coordination. These events emphasize the necessity of regular emergency drills and robust preparedness measures tailored specifically to nuclear incidents. Clear and transparent communication, delivered in multiple languages, is vital to managing public response and preventing panic during such crises.

The environmental and health consequences of these accidents reveal the long-lasting effects of radioactive contamination. Chernobyl's exclusion zone and Fukushima's contaminated regions illustrate the persistence of radionuclides in the environment, necessitating sustained monitoring and decontamination efforts. Health impacts, including increased thyroid cancer rates near Chernobyl and mental health challenges stemming from displacement in both regions, highlight the importance of long-term health surveillance for affected populations. Additionally, the ecological effects on biodiversity and ecosystems show a complex interplay, with some species adapting while others experience significant declines. These findings underscore the need for comprehensive longitudinal health studies, the development of effective decontamination technologies, and proactive ecological restoration strategies.

The economic burden of nuclear accidents is immense, as seen in the costs of evacuation, compensation, and decades-long cleanup operations in both incidents. These financial demands strain national budgets and have far-reaching implications for energy policies. Fukushima, in particular, prompted many nations to reevaluate

their nuclear energy strategies, with some, such as Germany, choosing to phase out nuclear power.

Cross-cutting recommendations emerge from these lessons. Strengthening global collaboration through international organizations like the IAEA can enhance safety standards and foster shared research, technology, and response strategies. Transparent risk communication is essential to building public trust, while designing nuclear infrastructure to withstand combined natural and human-made hazards is critical to preventing future accidents. Incorporating advancements in artificial intelligence, robotics, and DA technologies can improve monitoring, mitigation, and recovery efforts.

Overall, the Chernobyl and Fukushima accidents serve as stark reminders of the risks associated with nuclear energy. By integrating the lessons learned and focusing on innovation and collaboration, the global community can better prevent, manage, and respond to potential nuclear crises in the future.

2.5 Spatial Modelling and Vulnerability Assessment

2.5.1 Vulnerability and hazard mapping

Vulnerability and hazard mapping are the critical components of spatial modeling, providing essential insights into the spatial distribution of risks and susceptibilities within a given area. This process plays a pivotal role in disaster risk management and mitigation by identifying regions that are most at risk from specific hazards and understanding the factors contributing to their vulnerability. The methodology integrates various spatial datasets and analytical techniques to produce comprehensive maps that guide decision-making and resource allocation. This section describes the theoretical and methodological approaches, and practical applications of vulnerability and hazard mapping, emphasizing its importance in addressing complex environmental challenges.

2.5.1.1 Theoretical foundations of vulnerability and hazard mapping

Social vulnerability refers to the degree to which individuals, communities, or social systems are susceptible to harm due to exposure to hazards, emphasizing the social, economic, and demographic factors that influence resilience and recovery (Singh et

al., 2014). This concept is particularly critical in the context of nuclear accidents, where the intersection of human and environmental risk factors magnifies the potential consequences. Social vulnerability is shaped by a variety of determinants, including income levels, education, access to resources, health status, and social cohesion, all of which can accelerate or mitigate the impacts of a nuclear disaster. Unlike physical vulnerability, which focuses on the structural aspects of risk, social vulnerability highlights the inequities and systemic weaknesses that increase the susceptibility of certain populations to harm.

Hazard mapping, in the context of nuclear accidents, focuses on identifying the spatial extent and intensity of potential radiological hazards (Demiryay 2022). It is a critical tool for visualizing areas of high exposure, enabling targeted interventions such as evacuation planning, resource distribution, and risk communication. Nuclear accidents, such as those at Chernobyl and Fukushima, demonstrate the importance of understanding not only where hazards are likely to occur but also how social factors influence the severity of their impacts. Hazard mapping in this context must incorporate radiological dispersion models, population density, and infrastructure networks to accurately depict risk zones and prioritize emergency response efforts.

Despite their individual strengths, social vulnerability and hazard mapping are often treated as separate analytical domains, leading to significant gaps in risk assessment and disaster preparedness. Theoretical frameworks such as the Pressure and Release (PAR) model emphasize that vulnerabilities are the result of dynamic interactions between root causes, dynamic pressures, and unsafe conditions (Hammer et al., 2019). However, these frameworks frequently lack the spatial specificity needed to integrate social vulnerability directly into hazard mapping processes. Similarly, traditional hazard maps, while adept at identifying exposure zones, often fail to account for the underlying social disparities that influence the distribution and magnitude of risk (Fox et al., 2024). Bridging this gap requires a comprehensive approach that combines social vulnerability analysis with hazard mapping to provide a holistic view of risk in the context of nuclear accidents. The Vulnerability-Resilience Indicators Model (VRIM) offers a useful framework for such integration by highlighting the interplay between vulnerability and resilience (Frazier et al., 2014). By incorporating spatial data on social factors such as population demographics, access to healthcare, and

community networks alongside radiological dispersion models, researchers can produce maps that reflect both the physical and social dimensions of risk.

Advancements in Geographic Information Systems (GIS) technologies have created new opportunities for integrating social vulnerability into hazard mapping. For instance, GIS-based multi-criteria decision analysis (MCDA) allows for the weighting of social indicators alongside hazard data to identify areas where vulnerabilities and risks intersect (Fatemi et al., 2017). This approach is particularly relevant for nuclear accidents, where the rapid dissemination of risk information is essential for effective emergency response. Moreover, machine learning and big data analytics provide powerful tools for analyzing complex relationships between social and physical factors, enabling the development of dynamic, real-time risk maps (Zhang et al., 2023).

The need for integrated social vulnerability and hazard mapping is underscored by the unique challenges posed by nuclear accidents. These events often result in long-lasting environmental contamination, mass evacuations, and profound social disruptions, disproportionately affecting marginalized and vulnerable populations. By combining social vulnerability assessments with detailed hazard mapping, researchers and policymakers can better understand the multifaceted nature of risk and design interventions that address both immediate and long-term needs.

2.5.1.2 Methodological approaches to social vulnerability and hazard mapping

A variety of methodological frameworks have been developed to quantify and map social vulnerability in the context of environmental and technological hazards. One of the most widely used methods for assessing social vulnerability is the development of composite indices (Kim et al., 2025). The SVI, pioneered by (Cutter et al., 2003), aggregates various socio-economic and demographic variables, such as income levels, age, disability, and minority status, to produce a single vulnerability score. While SVI has been extensively applied in natural hazard studies (Jahan et al., 2011; Guillard-Goncalves and Zezere, 2018), its adaptability to technological disasters, including nuclear accidents, has also been demonstrated (Cope and. Slack, 2017; Fekete 2022; Fekete and Neuner, 2023). Similar indices, such as the Disaster Risk Index (DRI) and the Vulnerability-Resilience Indicators Model (VRIM), have been applied in various contexts to assess community resilience and vulnerability (Islam et al., 2013; Angeon and Bates, 2015).

GIS have become indispensable tools for social vulnerability assessment. GIS enables the spatial visualization and analysis of vulnerability indicators, providing a clear depiction of at-risk populations (Frigerio et al., 2016). Catter et al. (2000) highlighted the advantages of GIS in integrating diverse datasets, such as population density, evacuation routes, and shelter locations, to create comprehensive vulnerability maps. Advanced GIS methods, such as dasymetric mapping and spatial interpolation, have further enhanced the precision of vulnerability assessments by refining population distribution estimates (Eicher and Brewer, 2001; Mennis 2009). These methods are particularly useful in areas with uneven population distribution, such as rural regions near nuclear facilities.

Hazard mapping is a critical component of nuclear emergency preparedness, as it identifies areas at risk of radiological exposure and contamination (Demiryay 2022). Atmospheric dispersion models, such as Gaussian Plume Models (GPM), Lagrangian particle models, and Eulerian grid models, are commonly used to simulate the spread of radioactive materials following a nuclear accident (Kim et al., 2008; Cao et al., 2020; Merigoux 2022). These models incorporate meteorological data, source term characteristics, and terrain features to predict the spatial extent of radiological contamination. For example, the RIMPUFF model was used during the Fukushima Daiichi accident to provide real-time hazard maps for emergency response (Zhuang et al., 2022). Multi-hazard mapping can be also integrated with the radiological hazard and other risks, such as seismic activity, flooding, and extreme weather, which may exacerbate the consequences of a nuclear accident. Gill and Malamud (2014) emphasized the importance of multi-hazard approaches in identifying compound risks and developing robust mitigation strategies. Additionally, remote sensing technologies, including satellite imagery and aerial surveys, have been increasingly utilized for hazard mapping (Alarifi et al., 2022). These technologies provide high-resolution data on land use, vegetation cover, and infrastructure, which are essential for assessing contamination and planning evacuation routes.

Recent research has emphasized the integration of social vulnerability assessments with hazard mapping to develop comprehensive risk profiles (Chelariu et al., 2024). This approach enables emergency planners to prioritize interventions in areas where high social vulnerability coincides with significant hazards. For example, Chakraborty et al. (2023) demonstrated the utility of overlaying SVI with hazard maps to identify

socially vulnerable populations at risk of flooding and other disasters. Similar methodologies have been applied to other contexts to enhance evacuation planning and resource allocation (Lapietra et al., 2024).

2.5.2 Evacuation modelling

Evacuation modeling is a critical aspect of disaster management and urban planning, encompassing the study of human behavior, transportation networks, and decision-making processes during emergency scenarios to ensure the safe and efficient relocation of at-risk populations (Wachtel et al., 2021). While modeling evacuation, understanding human behavior is paramount, as evacuation dynamics are influenced by factors such as risk perception, social connections, and decision-making under stress (Bakhshian and Martinez-Pastor, 2023). Individuals' responses can be categorized into three phases: threat recognition, decision to evacuate, and actual movement (Ohba et al., 2021).

Traffic flow theory forms the backbone of transportation-based evacuation models by studying the movement of individuals and vehicles under different traffic conditions. Fundamental diagrams, such as speed-density and flow-density relationships, help simulate and predict traffic behavior during evacuations (Romanowska and Jamroz 2021). Additionally, evacuation planning often involves optimization to minimize evacuation time, maximize resource allocation, or balance multiple objectives (Bera et al., 2023). Theoretical frameworks such as game theory, multi-objective optimization (MOO), and decision analysis are frequently employed, helping to address trade-offs between competing priorities such as safety, cost, and equity (Khalilpourazari and Pasandideh 2021).

Methodologically, agent-based models (ABMs) simulate the behavior of individual agents (e.g., pedestrians or vehicles) and their interactions with the environment (Kaur and Kaur 2022). This bottom-up approach enables detailed analysis of complex evacuation scenarios, as demonstrated by Dumitrescu et al. (2024) in their study on panic-driven crowd dynamics. Macroscopic models aggregate populations and treat them as flows with the Lighthill-Whitham-Richards (LWR) model serving as a classic example for large-scale traffic simulations (Fan et al., 2024). Conversely, microscopic models focus on individual entities, capturing granular details such as acceleration,

lane changes, and interactions, with techniques such as cellular automata and car-following models (Feng et al., 2023).

Graph theory is central to network-based evacuation models, where nodes represent locations and edges represent routes. In this theory, algorithms like Dijkstra's or A* are used to determine optimal evacuation paths (Sun et al., 2021). Given the uncertainties inherent in evacuations, including unpredictable human behavior and environmental factors, fuzzy logic provides a robust framework for modeling such uncertainties. Recent studies have integrated fuzzy systems with optimization models to enhance decision-making during evacuations (Bozhenyuk et al., 2023).

Recent advancements in evacuation modeling have been transformative. GIS have revolutionized the field by providing spatial context and real-time data integration, facilitating route planning, resource allocation, and risk assessment (Stoia et al., 2022). Machine learning algorithms are increasingly being used to predict evacuation behaviors, optimize routes, and improve decision support systems. For instance, reinforcement learning has been applied to dynamic traffic management during evacuations (Noaeen et al., 2022). Advances in computational power and sensor technologies now enable real-time evacuation modeling, incorporating live data such as traffic conditions and weather updates to provide actionable insights (Kashinath et al., 2021). Hybrid models that combine different methodologies, such as ABMs and network-based models, offer a more comprehensive understanding of evacuation dynamics by enhancing the strengths of each approach (Yaagoubi et al., 2023).

2.6 Discussions on Literature Review

The Chernobyl disaster of 1986 and the Fukushima Daiichi accident of 2011 stand as two of the most catastrophic nuclear accidents in human history. Both incidents have provided critical insights into nuclear safety, emergency preparedness, and long-term societal impacts. Chernobyl, resulting from a reactor design flaw and human errors during testing, released large amounts of radioactive materials into the environment, affecting vast regions across Europe. Fukushima, triggered by an earthquake and tsunami, underscored the vulnerabilities of NPPs to natural disasters, despite advanced technology and strict regulatory oversight. The health impacts of Chernobyl were severe, with thousands of cases of thyroid cancer attributed to radioactive iodine exposure, particularly among children. Acute radiation sickness affected plant workers

and emergency responders. In Fukushima, while acute radiation effects were largely avoided, mental health issues, stress-related illnesses, and long-term cancer risks have been areas of concern. Both accidents caused extensive environmental contamination. Chernobyl's exclusion zone remains a testament to the enduring ecological effects, with soil, flora, and fauna showing elevated radiation levels even decades later. Fukushima's contamination affected agricultural lands and marine environments. Cleanup and decontamination efforts have proven challenging and resource-intensive in both cases. The financial toll of these disasters has been immense. Chernobyl imposed long-term economic burdens on Ukraine and surrounding regions, while Fukushima's cleanup costs are estimated in the hundreds of billions of dollars. Compensation for affected communities, decommissioning of reactors, and waste management are ongoing challenges.

A bibliometric analysis of research on these accidents reveals growing academic interest in nuclear safety, risk management, and mitigation strategies. Trends in publication data indicate a shift from purely technical studies to multidisciplinary approaches that consider social, environmental, and policy dimensions. However, significant gaps remain in integrating social vulnerability and community resilience into nuclear emergency planning. Research on social vulnerability highlights the unequal distribution of risks and impacts during nuclear accidents. Vulnerable populations, including the elderly, disabled, and economically disadvantaged, often face greater challenges in evacuation and recovery. Hazard mapping has been employed to predict the spatial distribution of radiological risks, but these maps frequently lack consideration of the human dimensions of vulnerability.

Evacuation modeling is critical for effective emergency response, providing insights into optimal evacuation routes, timing, and population movement dynamics. While significant advancements have been made, these models often prioritize logistical efficiency over social equity and community-specific needs. A notable research gap is the limited integration of social vulnerability assessments with hazard mapping to inform evacuation prioritization. Existing hazard maps typically focus on physical and environmental factors, neglecting the social and demographic characteristics of affected populations. However, by incorporating social vulnerability indicators into hazard mapping, emergency planners can better identify high-risk communities and allocate resources more effectively. Moreover, evacuation modeling can benefit from

greater emphasis on the needs of vulnerable groups, such as developing tailored communication strategies and ensuring accessible evacuation routes. Addressing these gaps requires a multidisciplinary approach that combines insights from social science, engineering, and public health.

The critical role of emergency response cannot be overstated. Timely and coordinated actions during nuclear accidents can significantly mitigate health risks and economic losses. Lessons from Chernobyl and Fukushima underscore the need for comprehensive preparedness plans that integrate hazard mapping, social vulnerability assessments, and robust evacuation models. Continuous training, community engagement, and scenario-based drills are essential to ensure that emergency responses are both efficient and suitable. In conclusion, integrating social vulnerability with hazard mapping and evacuation modeling represents a crucial step toward enhancing nuclear emergency preparedness. Addressing this research gap will contribute to more effective and adequate responses, ultimately safeguarding public health and reducing the long-term consequences of nuclear accidents.

3. METHODOLOGY

3.1 Social Vulnerability Assessment

Assessing social vulnerability is an important part of preparing for and responding to nuclear accidents. It helps identify which people are most at risk from radiation and its wider effects. Unlike technical assessments that focus only on radiation levels and infrastructure, social vulnerability looks at factors like age, income, education, and access to resources. These factors affect how well a community can respond, evacuate, and recover from a nuclear disaster (Singh et al., 2014). This kind of analysis is especially important in areas near NPPs, where not everyone has the same ability to evacuate or get help. Groups such as the elderly, children, low-income families, and people without transportation may face higher risks. These differences mean that special actions are needed to protect them (Ohba et al., 2021).

This thesis employs a structured multi-criteria decision-making (MCDM) approach to estimate and map social vulnerability to nuclear accidents by using both the Best Worst Method (BWM) and the Analytic Hierarchy Process (AHP). Figure 3.1 illustrates a methodological framework.

The process begins with the selection of relevant indicators based on literature and expert opinions. After data collection, normalization techniques ensure comparability across different scales and units, followed by the construction of a hierarchical structure to categorize indicators into meaningful groups. To derive the relative importance of each indicator, both BWM and AHP are applied. In BWM, the most important (Best) and least important (Worst) criteria are identified, and a preference vector is constructed by comparing these criteria against all others. The optimal weights are then computed by minimizing inconsistencies, and a consistency ratio is assessed for reliability. Meanwhile, AHP involves creating a pairwise comparison matrix to evaluate the relative importance of criteria, deriving the largest eigenvalue to determine priority weights, and assessing the consistency ratio to ensure judgment reliability. By employing both methods, a comparative analysis of weighting results

enhances robustness and accuracy. Once the weights are determined, they are integrated into a GIS to generate a spatial representation of social vulnerability, highlighting areas at higher risk during a nuclear emergency. The final step involves comparing the results of BWM and AHP to assess variations in weight assignments and their impact on vulnerability mapping. Based on these findings, policy recommendations are formulated to improve nuclear disaster preparedness and emergency response strategies.

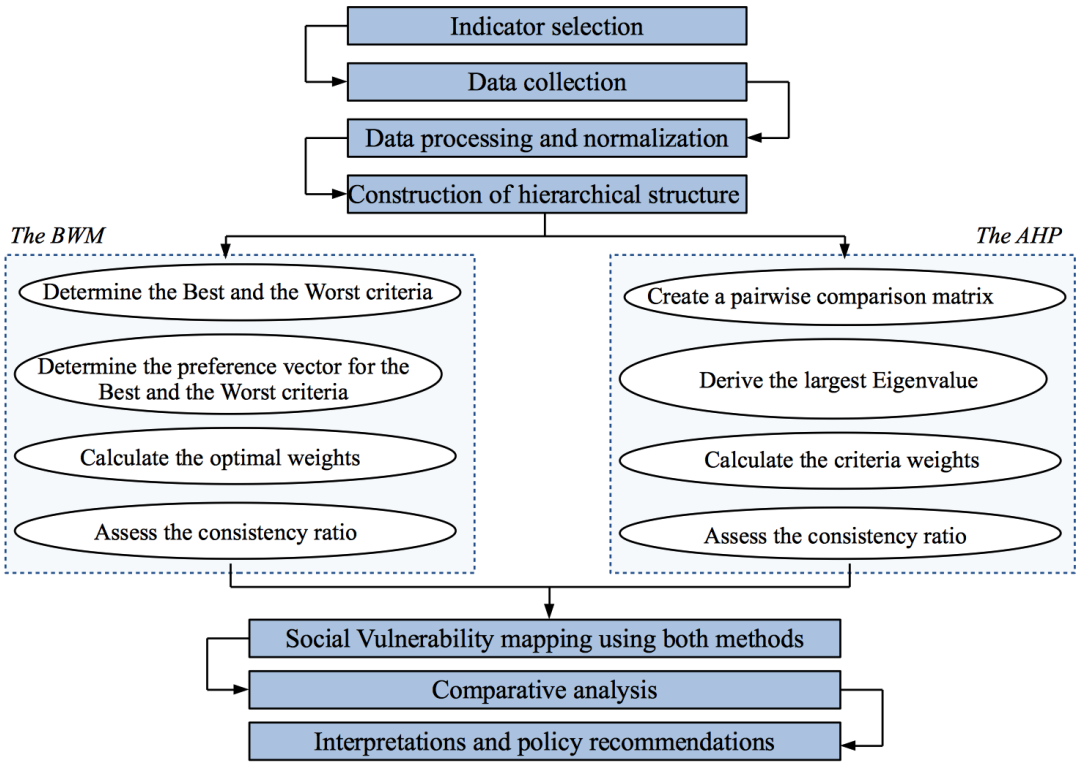

Figure 3.1 : Research framework for estimation and mapping of social vulnerability to nuclear accident.

3.1.1 Selection of criteria and data collection

Figure 3.2 illustrates the structured hierarchy of criteria used to assess vulnerability to nuclear accidents in this study. The study employs a hierarchical framework to assess social vulnerability to nuclear accidents, structuring the SVI into two major components: physical exposure and resistance. Each component is further divided into sub-components that encapsulate key vulnerability factors. Physical exposure represents the inherent susceptibility of a population to nuclear accidents based on demographic characteristics and the built environment. The Demography sub-

component includes factors such as gender, marital status, population density, and education level, which influence how different population groups are affected during a disaster. The building and environment system sub-component consider building density and LULC, as these aspects determine the spatial distribution of people and infrastructure at risk. On the other hand, resistance reflects the capacity to prepare for, respond to, and recover from a nuclear accident. It is divided into three key sub-components: preparedness, emergency response, and coping capacity. Preparedness accounts for the role of institutional and logistical support systems, including meteorological services, evacuation services, logistics, psychosocial support, and government agencies such as the Ministry of Agriculture and Forestry. Emergency response measures immediate response capabilities, focusing on evacuation time and the efficiency of emergency services. Coping capacity captures the ability to sustain essential services and support networks during a crisis, incorporating resources such as police, firefighters, reception centers, health facilities, hospitals, social participation, and food, water, and medicine supplies.

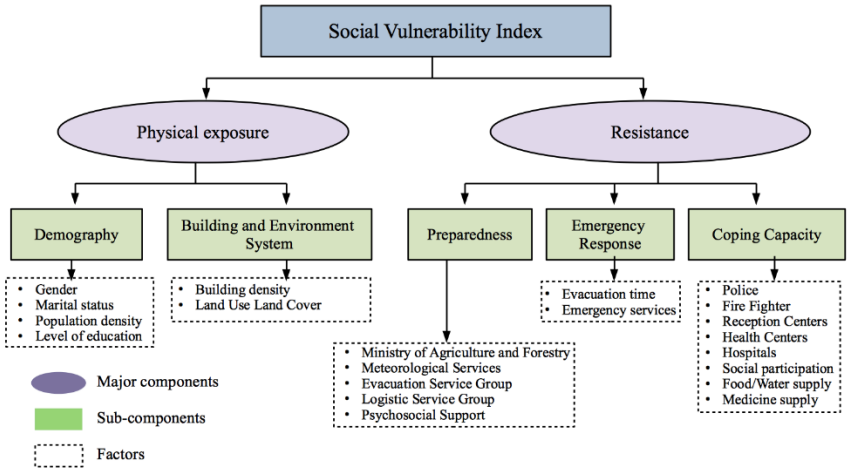

Figure 3.2 : The hierarchical structure of the nuclear accident vulnerability criteria used in the study.

Various data sources were utilized to assess the SVI, incorporating existing, objective, and subjective data. Existing data, such as census-based population demographics and environmental factors like LULC maps, were sourced from governmental agencies. Objective data encompassed measurable indicators, including the number of hospitals,

police stations, and fire stations, obtained through government records and GIS. Subjective data, gathered through surveys of subject-matter experts, was used to determine the weighting of research criteria. The raw data was transformed into indices and ratios, such as population density (expressed in persons per square kilometer) and the illiteracy rate (calculated as the proportion of the illiterate population). Each neighborhood's data was then analyzed individually using ArcGIS software. To ensure consistency across datasets, the min-max normalization method was applied, scaling values between 0 and 1. The initial step in this process involved determining the relationship between each factor and social vulnerability. For instance, higher population density was associated with increased vulnerability, signifying a positive correlation, whereas greater medical supply availability reduced vulnerability, indicating a negative correlation.

Normalization was performed following Equations 3.1 and 3.2 as outlined by (Kumar and Bhattacharjya 2020).

For positive correlation:

$$X_n = \frac{X - X_{min}}{X_{max} - X_{min}} \tag{3.1}$$

For negative correlation:

$$X_n = \frac{X_{max} - X}{X_{max} - X_{min}} \tag{3.2}$$

where X_n represents the normalized value of the factor, X is the actual value of the factor, X_{min} and X_{max} are the minimum and maximum values of the factor, respectively.

Table 3.1 presents the subcomponents and factors chosen for the study, detailing their representation and their correlation with vulnerability.

Including gender as a factor in the SVI for nuclear accident studies is important because gender affects how people experience and cope with disasters. For example, women often face higher risks due to their social roles, financial dependence, and physical needs. Studies show that women usually have fewer resources and less access to emergency services than men, which makes them more vulnerable during and after disasters (Muller et al., 2011; Ajtai et al., 2023). Women also often take care of children, elderly family members, and people with disabilities. In a nuclear accident,

these caregiving responsibilities can increase their stress and make it harder for them to protect themselves and others. Therefore, considering gender in emergency planning helps create better support and protection for everyone.

Table 3.1 : Factors and their functional relationship with vulnerability.

Subcomponent	Factor	Representation	Correlation
Demography	Gender	% women = (population of women/total population) × 100	Positive
	Marital status	% single = (not married population/total population) × 100	Positive
	Population density	P.D. = total population/area	Positive
	Level of education	% illiterate = (population without education/total population) × 100	Positive
Building and Environmental System	Building density	% of buildings = (number of buildings/total area) × 100	Positive
	LULC	% agricultural areas = (agricultural areas/total area) × 100	Positive
Preparedness	Ministry of agriculture and forestry	Number per neighborhood population = ((number + (1/near distance)) / total neighborhood population	Negative
	Meteorological services		Negative
	Evacuation service group		Negative
	Logistic service group		Negative
	Psychosocial support		Negative
	Emergency services		Negative
Emergency response	Evacuation time	The time needed for individuals to reach safety areas, considering traffic congestion, was derived from network analysis conducted in a GIS environment.	Positive
Coping capacity	Social participation	Number per neighborhood population = ((number + (1/near distance)) / total neighborhood population	Negative
	Food/water supply		Negative
	Medicine supply		Negative
	Police		Negative
	Firefighter		Negative
	Reception centers		Negative
	Health centers		Negative
	Hospitals		Negative

Marital status is also an important factor that affects vulnerability in disasters. It influences how people live, share responsibilities, and access support. Married or cohabiting people often share caregiving tasks, which can help them respond and recover more easily during a disaster. On the other hand, single individuals may have to manage everything alone, which can make them more vulnerable. From a financial point of view, married couples usually have two incomes, giving them more stability and resources to deal with the effects of a disaster. Marital status also affects who people live with and how they share basic resources, which can influence how well they cope during emergencies (Gayen et l. 2020).

Population density is another important factor when assessing social vulnerability in a nuclear accident. Areas with high population density face big challenges during evacuation. Traffic can become very heavy, slowing down or blocking people trying to leave. Hospitals, shelters, and supplies can quickly run out, causing delays in getting help. High building density also makes things harder. In places with many closely packed buildings, evacuation is more difficult, and emergency teams may struggle to move around. Narrow streets and crowded layouts can slow down rescue efforts and increase the risk of more people getting hurt (Furlan et al., 2021; Ajtai et al., 2023).

Education level is an important factor in how people understand and respond to emergencies. People with higher education are usually better at understanding warnings and safety rules, which is very important during a nuclear accident. They can follow instructions more easily and make better decisions (Zurovec et al., 2017). On the other hand, people with lower education levels, especially those who cannot read, may not fully understand how serious the situation is. This can make it harder for them to take the right actions. They often depend on family, friends, or the community for help and information. If these support systems are not available during a crisis, their risk becomes even higher (Arvin et al., 2023).

Land Use and Land Cover (LULC) characteristics also play a vital role in determining exposure to radiation hazards. Agricultural areas, for instance, are particularly vulnerable to radioactive contamination, which can threaten food security and disrupt local livelihoods (Zurovec et al., 2017). In contrast, urban areas dominated by commercial and industrial activities may face economic losses and increased unemployment due to disruptions in business operations. The extent to which different

land uses are affected further underscores the need for targeted response strategies based on regional characteristics (Fatemi et al., 2017).

Preparedness is a critical component in reducing vulnerability, involving proactive planning, education, and resource allocation before a nuclear accident occurs (Isia et al., 2023). In this study, preparedness encompasses multiple government agencies, including the Ministry of Agriculture and Forestry, Meteorological Services, Evacuation and Logistics Service Groups, and Psychosocial Support Groups. The Ministry of Agriculture plays a crucial role in ensuring food security and protecting agricultural livelihoods by maintaining safe food production. Meteorological Services contribute by providing accurate weather forecasts, which are essential for identifying affected areas, planning evacuation routes, and designating shelter locations. Evacuation and Logistics Service Groups oversee the safe relocation of populations and manage post-disaster recovery, while Psychosocial Support Groups address the mental and emotional well-being of affected individuals, ensuring a more compassionate and effective response (Ohba et al., 2021).

Emergency response efforts during a nuclear accident require a well-coordinated approach to mitigate both immediate and long-term consequences (Ohba et al., 2021). Key components of this response include emergency services and evacuation time. Emergency services consist of police, firefighters, hospitals, and health centers, all of which play vital roles in crisis management (Isia et al., 2023). The police ensure public safety and maintain order, while firefighters handle physical hazards, assist in rescue operations, and support medical teams. Hospitals and health centers provide immediate care, specialized treatment, and long-term medical support for individuals affected by radiation exposure. Additionally, two critical timeframes define the emergency response: evacuation time and plume arrival time. Evacuation time refers to how long it takes to move individuals from high-risk areas to safer locations, directly impacting public health and safety (Park et al., 2021). Plume arrival time measures how quickly the radioactive cloud reaches surrounding areas, making it imperative for evacuation to be completed before exposure occurs (Smith et al., 2015). Assessing and improving evacuation time enhances preparedness efforts, particularly for vulnerable populations.

Coping capacity, which encompasses preparedness, responsive infrastructure, community support, healthcare services, and long-term recovery strategies, is essential

for mitigating disaster impacts. Strengthening these elements allows individuals and communities to handle crises more effectively and recover more efficiently (Ohba et al., 2021; Isia et al., 2023). In addition to emergency services, coping capacity involves the efforts of volunteer organizations and community groups responsible for ensuring access to food, water, and medicine (Anderson et al., 2016).

3.1.2 Best-Worst method

The Best-Worst Method (BWM) is a powerful multi-criteria decision-making (MCDM) approach that has been widely applied in assessing social vulnerability, particularly in the development of the SVI. Originally introduced by Rezaei (2015), BWM provides a structured way to assign weights to multiple criteria by reducing inconsistencies that commonly arise in traditional methods like the AHP. Unlike other approaches, BWM requires decision-makers to identify the most and least important criteria before performing pairwise comparisons, ensuring a more consistent and robust weighting process (Rezaei 2015). The method begins by defining the relevant criteria influencing social vulnerability, such as population density, poverty rate, disability rate, access to transportation, etc. (Sharifi and Yamagata, 2016). Decision-makers then select the most critical criterion (best) and the least critical criterion (worst) based on expert knowledge and contextual considerations. Once these key criteria are identified, comparisons are made by evaluating how much more important the best criterion is relative to each of the other criteria, using a scale from 1 to 9 (Rezaei 2015). This results in a best-to-others (BO) comparison vector. A similar process is followed to compare all criteria against the worst criterion, forming an others-to-worst (OW) comparison vector. With these pairwise comparisons established, the next step involves solving an optimization problem to determine the optimal weights of the criteria. The objective is to minimize the maximum deviation (ξ) in judgments, ensuring consistency in the weight distribution. This is achieved through the following mathematical formulation Equations 3.3-3.6 (Rezaei 2015):

$$min_{\xi, w_i}\ \xi \tag{3.3}$$

Subject to:

$$\left|w_B - a_{Bj} w_j\right| \leq \xi, \forall_j \tag{3.4}$$

$$\left|w_j - a_{jw} w_w\right| \leq \xi, \forall_j \tag{3.5}$$

$$\sum_{j=1}^{n} w_j = 1, w_j \geq 0, \forall_j \quad (3.6)$$

where w_B and w_w are the weights assigned to the best and worst criteria, respectively, and a_{Bj} and a_{jw} are the relative importance values from the pairwise comparisons. By solving this optimization model, the final weights are determined in a way that ensures minimal inconsistency.

BWM has been widely used in social vulnerability assessments across various domains. For instance, Ozay and Orhan (2023) applied BWM to evaluate flood vulnerability in Turkiye, integrating socioeconomic and environmental indicators to prioritize resource allocation effectively. Similarly, Sahu and Mishra (2021) utilized BWM to assess pandemic vulnerability during COVID-19, focusing on factors such as healthcare accessibility and demographic sensitivity. Ozmen (2023) used the method for earthquake risk assessment, highlighting the role of infrastructure resilience and emergency preparedness in mitigating seismic impacts. In nuclear emergency planning, Zhang et al. (2014) presented an assessment model for eco-environmental vulnerability, which can be adapted for scenarios like ranking evacuation priorities within nuclear emergency zones by considering factors such as population density, road infrastructure, and social disparities.

3.1.3 Analytic Hierarchy Process

Another widely used method for social vulnerability assessment is the AHP. Unlike BWM, which relies on selecting the most and least important criteria before making pairwise comparisons, AHP systematically breaks down complex problems into a hierarchical structure, enabling decision-makers to evaluate multiple criteria at different levels (Vaidya and Kumar, 2006). Originally developed by Saaty (1980), AHP provides a more detailed framework for assessing social vulnerability by allowing comparisons not just between criteria but also among sub-criteria and alternative options. The process begins by defining the main objective, followed by identifying relevant criteria that influence social vulnerability, such as economic status, population density, infrastructure robustness, and access to emergency services (Grave et al., 2022). These criteria are structured in a hierarchy, where the top level represents the overall goal, intermediate levels contain key influencing factors, and the lowest level includes decision alternatives. AHP then employs pairwise comparisons, similar to BWM, but instead of comparing only the best and worst criteria, AHP

requires comparisons between all pairs of criteria. Decision-makers assign importance values using a numerical scale from 1 (equal importance) to 9 (extreme importance), forming a pairwise comparison matrix where each element a_{ij} represents the relative importance of criterion i over criterion j (Bozoki and Rapcsak, 2008). Once the matrix is constructed, the next step is to normalize it and compute the priority vector, which represents the relative weights of the criteria. This is done by calculating the eigenvector of the matrix, satisfying the Equation 3.7 (Saaty 2004):

$$Ap \times w = \lambda_{max} \times w \tag{3.7}$$

where Ap is the pairwise comparison matrix, w is the eigenvector containing the weights, and λ_{max} is the maximum eigenvalue. A key difference between AHP and BWM lies in the consistency check: AHP explicitly calculates a consistency index (CI) to measure the reliability of pairwise comparison, using the Equation 3.8 (Saaty 1980):

$$CI = \frac{\lambda_{max} - n}{n-1} \tag{3.8}$$

where n is the number of criteria. This value is then divided by the random consistency index (RI) to obtain the consistency ratio (CR) as shown in Equation 3.9:

$$CR = \frac{CI}{RI} \tag{3.9}$$

If the consistency ratio is below 0.1, the pairwise comparisons are considered reliable; otherwise, adjustments may be needed to improve consistency. This feature differentiates AHP from BWM, as the latter inherently reduces inconsistency by limiting the number of required comparisons.

AHP has been widely applied in social vulnerability assessments, similar to BWM but with greater flexibility in handling multiple levels of decision-making. Cutter et al. (2003) used AHP to construct the SVI, incorporating socio-economic and demographic indicators to assess community resilience. Banica et al. (2017) applied AHP for earthquake risk assessment, considering urban infrastructure, population density, and emergency response capabilities. Lyu et al. (2020) used AHP to prioritize flood-prone regions in China by integrating environmental and socio-economic indicators. In nuclear emergency planning, AHP has been utilized in optimizing evacuation strategies during radiological emergencies. By weighing factors such as road accessibility, population density, and emergency response times, the AHP tool

aids local health departments in California and Hawaii in making informed decisions for effective disaster response (Dalnoki-Veress et al., 2014).

3.1.4 Statistical assessment

3.1.4.1 Statistical comparison of BWM and AHP

To determine whether there is a statistically significant difference between the results obtained using the Best-Worst Method (BWM) and AHP, the Wilcoxon Signed-Rank test was applied. This non-parametric test is particularly useful for comparing two related samples when the data do not follow a normal distribution or when the sample size is small (Ogie and Pradhan, 2020). Unlike parametric tests such as the paired t-test, which assume normality, the Wilcoxon Signed-Rank test ranks the differences between paired observations, making it a robust alternative for evaluating differences in decision-making methods (Kitani and Murakami, 2022). The test operates on the assumption that if two methods yield similar results, the differences between their paired values should be symmetrically distributed around zero. If one method consistently assigns higher or lower weights than the other, the test will detect a statistically significant deviation. The process begins by computing the differences between corresponding values from BWM and AHP, denoted as $d_i = x_i - y_i$, where x_i represents the weight assigned by BWM and y_i represents the weight assigned by AHP for the same criterion. Any differences equal to zero are removed, reducing the effective sample size. The absolute values of the remaining differences are then ranked from smallest to largest, with tied values assigned an average rank. Each rank is given a positive or negative sign based on whether d_i is positive or negative, forming the signed ranks R_i^* (Rosner et al., 2006).

The test statistic is calculated by summing the positive ranks (W^+) and the negative ranks(W^-), with the smaller of the two taken as the test statistic W. If the sample size is small (<25), the test statistic is compared against critical values from Wilcoxon distribution tables. For larger sample sizes, the test statistic is approximated using a normal distribution, where the standardized test statistic is computed using Equation 3.10 (Rey and Neuhauser, 2011):

$$Z = \frac{W - \frac{n'(n'+1)}{4}}{\sqrt{\frac{n'(n'+1)(2n'+1)}{24}}} \qquad (3.10)$$

The corresponding p-value is then obtained from the standard normal distribution. If the p-value is below the chosen significance level (e.g., α=0.05), the null hypothesis is rejected, indicating a significant difference between the two methods. Conversely, if the p-value is above the threshold, the null hypothesis is not rejected, suggesting that BWM and AHP produce comparable results (Arda et al., 2025).

In the context of this thesis, the Wilcoxon Signed-Rank test was applied to compare the weight distributions derived from BWM and AHP across multiple criteria. By examining whether the two methods assign statistically different weights, the test provides valuable insights into their relative performance and consistency. If a significant difference is found, it may indicate that one method systematically favors certain criteria over the other, highlighting potential methodological biases. Conversely, if no significant difference is detected, it suggests that both methods are equally effective in assigning weights for social vulnerability assessment.

3.1.4.2 Sensitivity analysis in Multi-Criteria Decision-Making

In multi-criteria decision-making (MCDM) processes, sensitivity analysis plays a crucial role in assessing the robustness and reliability of results by evaluating how variations in input parameters affect the final outcomes (Demir et al., 2024). Given that methods such as the Best-Worst Method (BWM) and the AHP rely on subjective expert judgments and weighting schemes, sensitivity analysis helps determine whether small changes in criteria weights significantly alter the rankings or decisions (Maletic et al., 2014). If the results remain stable despite variations in input values, the model is considered robust; otherwise, adjustments may be needed to improve its reliability. Sensitivity analysis typically involves systematically modifying the weights assigned to different criteria while observing the impact on the final ranking of alternatives or solutions. One of the most effective ways to visualize these changes is through a tornado chart, which graphically represents how variations in each criterion's weight influence the overall ranking (Chadly et al., 2024). The tornado chart displays horizontal bars corresponding to different criteria, with the length of each bar indicating the extent to which changes in that criterion affect the final result. Criteria with longer bars exert a greater influence on the decision, highlighting key factors that drive the outcome. This visualization is particularly useful in identifying which parameters require the most careful consideration during decision-making.

Mathematically, sensitivity analysis can be performed by introducing a perturbation factor Δw_j to the original weight w_j of each criterion and recalculating the final scores. If the weighted sum method (WSM) is used, the new score for an alternative A_i is given by Equation 3.11 (Pianosi et al., 2016):

$$S_i' = \sum_{j=1}^{n} \left(w_j + \Delta w_j\right) \times v_{ij} \tag{3.11}$$

where v_{ij} represents the performance value of alternative A_i with respect to criterion j, and Δw_j is the incremental change applied to the weight w_j. The effect of these perturbations is analyzed by measuring how much the ranking of alternatives changes when different Δw_j values are applied.

3.1.4.3 Hot and Cold spot analysis

Understanding the spatial distribution of social vulnerability is crucial for effective disaster risk management and emergency planning. While composite indices provide an overall measure of vulnerability, they do not capture how vulnerability is spatially clustered or dispersed within a study area. To address this, a hot and cold spot analysis can be conducted using the Getis-Ord G_i^* statistic, which identifies statistically significant spatial clusters of high (hot spots) and low (cold spots) values in the composite SVI (Manap et al., 2019). This method helps reveal geographic patterns, allowing decision-makers to prioritize areas that require immediate attention in disaster preparedness and resource allocation.

The Getis-Ord G_i^* statistic measures local spatial autocorrelation, determining whether high or low values of a variable, such as social vulnerability, are clustered in space (Figueiredo et al., 2022). Unlike global spatial autocorrelation measures such as Moran's I, which evaluate overall spatial dependence, the Getis-Ord G_i^* statistic focuses on local variations, identifying specific regions where social vulnerability is significantly high or low. Mathematically, the G_i^* statistic for a given location i is computed using Equation 3.12 (Manap et al., 2019; Figueiredo et al., 2022):

$$G_i^* = \frac{\sum_{j=1}^{n} w_{ij} x_j}{\sum_{j=1}^{n} x_j} \tag{3.12}$$

where x_j represents the SVI value at location j; w_{ij} is the spatial weight between locations i and j; n is the total number of locations in the study area.

To determine the statistical significance of hot and cold spots, the G_i^* statistic is standardized using a Z-score, calculated by Equation 3.13 (Manap et al., 2019; Figueiredo et al., 2022):

$$Z(G_i^*) = \frac{G_i^* - E(G_i^*)}{StdDev(G_i^*)} \tag{3.13}$$

where the expected value $E(G_i^*)$ and standard deviation $StdDev(G_i^*)$ are defined as Equations 3.14 and 3.15 (Manap et al., 2019; Figueiredo et al., 2022):

$$E(G_i^*) = \frac{\sum_{j=1}^{n} w_{ij}}{n} \tag{3.14}$$

$$StdDev(G_i^*) = \sqrt{\frac{\sum_{j=1}^{n} w_{ij}^2}{n} - \left(\frac{\sum_{j=1}^{n} w_{ij}}{n}\right)^2} \tag{3.15}$$

A positive Z-score indicates clustering of high social vulnerability values (hot spots), while a negative Z-score suggests clustering of low values (cold spots). The significance of the clustering is assessed using p-values, where a low p-value ($p<0.05$) confirms that the identified hot or cold spot is statistically significant and unlikely to have occurred by chance (Figueiredo et al., 2022).

Applying the Getis-Ord statistic to the SVI allows for the identification of geographic areas where social vulnerability is concentrated. Hot spots indicate regions with significantly high vulnerability, often characterized by high population density, poor infrastructure, low socioeconomic status, and limited access to emergency services. These areas require prioritized intervention in disaster mitigation strategies. Cold spots, on the other hand, signify regions with relatively lower vulnerability, often associated with better infrastructure, economic stability, and higher resilience to disasters (Chowdhuri et al., 2022). In the context of nuclear emergency planning, hot spots represent communities that may face the greatest challenges during an evacuation or disaster response, necessitating targeted policies such as improved shelter allocation, enhanced transportation networks, and optimized resource distribution. Cold spots, while less vulnerable, may serve as potential locations for evacuation centers or logistical hubs.

3.2 Hazard Mapping

Hazard mapping is a critical step in assessing the potential risks associated with NPP accidents. This process involves modeling the dispersion of radioactive materials released during an accident, determining the extent of contamination, and evaluating the associated health impacts. For this purpose, the GPM is widely used to simulate the transport and dispersion of airborne pollutants, including radioactive releases. In this section, a detailed theoretical framework of the GPM is provided, the worst-case scenario for a nuclear accident is identified, and calculations to assess the Total Effective Dose Equivalent (TEDE) and cancer risk are performed.

3.2.1 Gaussian Plume Model theory

Gaussian Plume Theory is a widely used mathematical model for predicting the dispersion of pollutants in the atmosphere from a continuous point source (Yang et al., 2013). It provides a quantitative framework for assessing how pollutants disperse, depending on meteorological conditions, source characteristics, and the nature of the terrain. Figure 3.3 illustrates the conceptual framework of the Gaussian plume dispersion model.

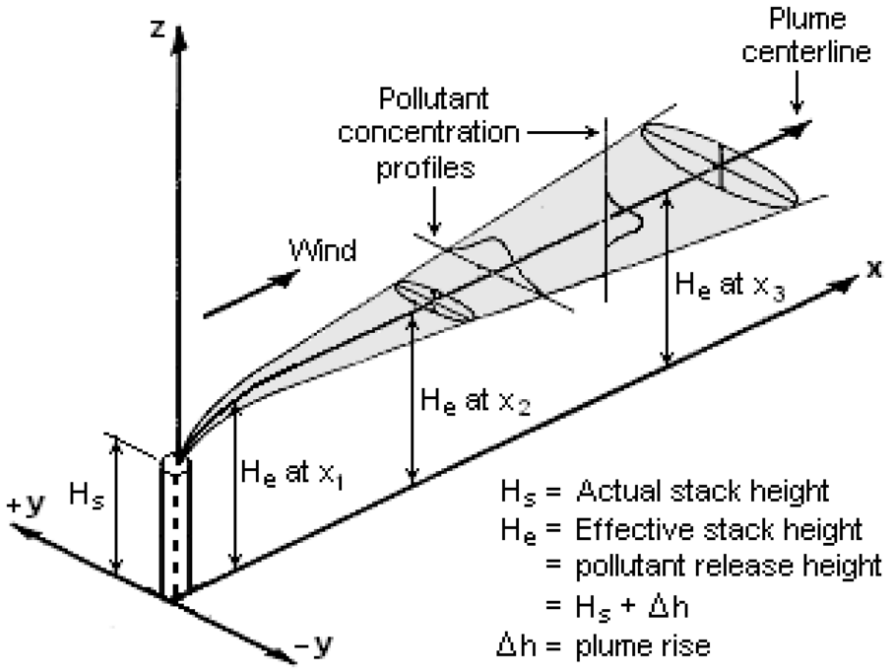

Figure 3.3 : A representation of a GPM (Johnson 2022).

The model operates in a three-dimensional Cartesian coordinate system with x-axis representing the wind direction (downwind), y-axis that is horizontal and perpendicular to wind direction (crosswind), and z-axis that is vertical height above the ground level. A continuous release from a source is assumed, and pollutants are transported by a steady wind in the x-direction, with dispersion occurring in the y- and z-directions.

The general Equation 3.16 for the pollutant concentration $C(x, y, z)$ at any point (x, y, z) due to a continuous release at height H is (Mohamed et al., 2013):

$$C(x, y, z) = \frac{Q}{2\pi u \sigma_y \sigma_z} exp\left(-\frac{y^2}{2\sigma_y^2}\right)\left[exp\left(-\frac{(z-H)^2}{2\sigma_z^2}\right) + exp\left(-\frac{(z+H)^2}{2\sigma_z^2}\right)\right] \quad (3.16)$$

where:

$C(x, y, z)$ is the concentration of the radioactive material (g/m^3) at a downwind location (x, y, z), where x is the downwind distance from the source (m), y is the crosswind distance from the centerline of the plume (m), and z is the vertical distance from the ground (m);

u is the wind speed in the x-direction (m/s);

Q is the release rate of the radioactive material (Bq/s);

σ_y and σ_z are the dispersion parameters (m), which depend on atmospheric conditions such as wind speed and stability class;

H is the release height (m).

Lateral and vertical distributions are shows in Equations 3.17 and 3.18, and the reflection of the plume at the ground surface is given by Equation 3.19 (Mohamed et al., 2013).

$$exp\left(-\frac{y^2}{2\sigma_y^2}\right) \quad (3.17)$$

$$exp\left(-\frac{(z-H)^2}{2\sigma_z^2}\right) \quad (3.18)$$

$$exp\left(-\frac{(z+H)^2}{2\sigma_z^2}\right) \quad (3.19)$$

Dispersion coefficients σ_y and σ_z describe the spread of the plume in the lateral and vertical directions. They depend on atmospheric stability and downwind distance (x). Empirical relationships are often used as shown in Equations 3.20 and 3.21 (Mohamed et al., 2013):

$$\sigma_y = a \times x^b \tag{3.20}$$

$$\sigma_z = c \times x^d \tag{3.21}$$

Where a, b, c, and d are stability-dependent constants which are shown in Table 3.2.

Effective stack height H combines the physical stack height H_S and plume rise ΔH in Equation 3.22 (Mohamed et al., 2013):

$H = H_S + \Delta H$ (3.22)

Table 3.2 : Stability-dependent constants used in GPM.

Stability class	a	b	c	d
A	0.22	0.92	0.20	0.92
B	0.16	0.92	0.12	0.92
C	0.11	0.92	0.08	0.92
D	0.08	0.92	0.06	0.92
E	0.06	0.92	0.03	0.92
F	0.04	0.92	0.016	0.92

3.2.2 Identification of the worst-case scenario

The worst-case scenario occurs when a combination of unfavorable meteorological, source, and dispersion conditions maximizes the pollutant concentration or its impacts on health and the environment (Mazur 2019). These conditions depend on several factors, including atmospheric stability, wind speed, release rate, release height, and proximity to the source.

Atmospheric stability classes describe the degree of turbulence and mixing in the atmosphere, which significantly influences the dispersion of pollutants from a source. Three classes, developed by Pasquill and later refined by Gifford, categorize the atmospheric stability into six classes: A, B, C, D, E, and F. Each class reflects specific meteorological and environmental conditions that determine how pollutants disperse

vertically and horizontally (Ahangari and Noori-Kalkhoran, 2019). Table 3.3 lists the stability classes.

Table 3.3 : Characteristics of stability classes.

Stability class	Condition	Turbulence	Dispersion characteristics
A	Very unstable (daytime with strong solar radiation and low wind speed)	High	Rapid dispersion in all directions
B	Unstable (daytime with moderate solar radiation)	Moderate to high	Strong vertical and horizontal mixing
C	Slightly unstable (daytime with weak solar radiation or moderate wind speed)	Moderate	Decent dispersion
D	Neutral (overcast conditions or high wind speed regardless of time)	Moderate	Balanced dispersion
E	Stable (nighttime with light wind and clear skies)	Low	Limited vertical mixing, horizontal spread
F	Very stable (nighttime with calm wind and clear skies)	Very low	Confinement near the ground, slow dispersion

Lower wind speeds usually reduce horizontal dispersion, causing pollutants to accumulate near the source. Conversely, high wind speeds lead to rapid dilution, lowering concentrations (Ahangari and Noori-Kalkhoran, 2019). A higher release rate corresponds to a greater quantity of pollutants being emitted into the atmosphere per unit time, which directly increases the concentration of pollutants in the surrounding environment. Conversely, the release height determines the initial altitude at which pollutants enter the atmosphere. When pollutants are released from a lower height, they tend to remain closer to the ground, increasing the potential for human and environmental exposure near the source. In contrast, a higher release height allows the pollutants to travel further and disperse more widely due to wind and atmospheric turbulence before they reach the ground, often resulting in lower concentrations at ground level but potentially affecting areas farther from the source (Birikorang et al., 2015). Concentrations peak at certain distances where dispersion and dilution balance. For GPMs, this typically occurs a short distance downwind of the source under stable atmospheric conditions. In the GPM, the pollutant concentration $C(x, y, z)$ is a function of wind speed u, dispersion coefficients σ_y and σ_z, and release height H. The

worst-case concentration at ground level (y=0, z=0) is given by Equation 2.23 (Essa and Saied, 2023).

$$C_{worst} = \frac{Q}{2\pi u \sigma_y \sigma_z} exp\left(-\frac{H^2}{2\sigma_z^2}\right) \tag{3.23}$$

where Q is the emission rate (Bq/s), u is the wind speed (m/s), σ_y and σ_z are the dispersion coefficients, and H is an effective release height.

In the current worst-case scenario analysis, the input data reflects parameters carefully chosen to represent realistic conditions, derived from the Fukushima nuclear accident as a reference (Table 3.4) (Chino et al., 2011). These inputs ensure that the modelling accurately simulates plausible extreme conditions for atmospheric dispersion, aiding in risk assessment and emergency planning. Using fixed values for release rate and height ensures comparability across scenarios and highlights the impact of meteorological variations (wind speed and stability).

Figure 3.4 shows pollutant concentrations as a function of wind speed for different atmospheric stability classes.

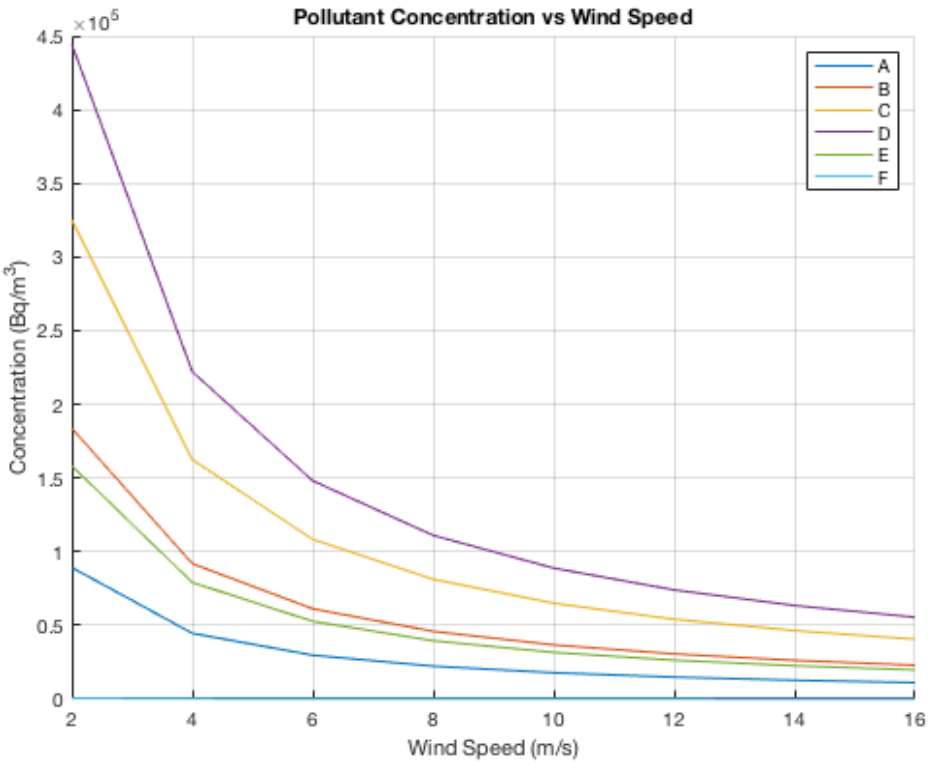

Figure 3.4 : Worst-case scenario results.

Table 3.4 : Input data parameters to identify the worst-case scenario.

Parameter	Value	Source	Significance
Cs-137 release rate	6.25×10^{13} (Bq/h)	This parameter is based on estimations from the Fukushima disaster, scaled to represent the radionuclide emission rate under catastrophic conditions.	The release rate quantifies the total radioactive material entering the atmosphere per hour; It directly affects pollutant concentrations, with higher values resulting in increasing ground-level exposure.
Release height	40 m	The height corresponds to the physical height of the stack or reactor building during the Fukushima release.	Release height influences the initial dispersion of the plume; A higher release height generally allows for more dispersion before the plume reaches ground level, reducing near-source concentrations.
Wind speed	2, 4, 6, 8, 10, 12, 14, 16 (m/s)	These wind speeds cover a realistic range of meteorological conditions observed in the vicinity of the Akkuyu NPP.	Wind speed determines the rate of horizontal transport of the plume; Lower wind speeds result in slower transport and higher concentrations near the source, while higher wind speeds promote dilution but spread the plume farther.
Atmospheric stability class	A, B, C, D, E, F	Stability classes are based on standard Pasquill-Gifford classifications, encompassing a spectrum of atmospheric conditions.	Stability class controls the dispersion coefficients, and consequently, the plume's spread; Stable classes (E, F) confine the plume close to the ground, increasing ground-level concentrations, whereas unstable classes (A, B) enhance dispersion, reducing near-source impact.

Form Figure 3.4, pollutant concentration decreases as wind speed increases for all stability classes. This can be explained by the fact that higher wind speeds lead to faster horizontal transport of the plume, which dilutes the pollutant concentration at any given point. Conversely, lower wind speeds result in slower dispersion and higher concentrations near the release point. Concentrations are highest under stability class D and lowest under stability class A. Stability class D represents neutral atmospheric conditions, where vertical mixing is moderate, leading to a balance between dispersion and confinement of pollutants. This results in relatively higher ground-level

concentrations compared to more unstable or stable conditions. On the other hand, stability class A corresponds to very unstable atmospheric conditions, characterized by significant vertical mixing, which disperses the pollutants over a larger volume and reduces concentrations at ground level. The combination of low wind speed and neutral atmospheric conditions results in the highest ground-level pollutant concentration, that is more than 4.0×10^5 Bq/m^3. These conditions pose the greatest risk to public health and the environment because ground-level pollutant concentrations are maximized and dispersion is limited, leading to localized hotspots of radioactive exposure.

3.2.3 Data assimilation techniques for hazard mapping

3.2.3.1 Data assimilation for nuclear emergency management

DA is a powerful computational technique that merges real-time observations with numerical models to improve prediction accuracy (Carrassi et al., 2018). In the context of nuclear emergencies, DA can be applied for refining atmospheric dispersion forecasts and supporting decision-making processes for response efforts. The integration of DA into emergency response systems enables authorities to better understand the spatial and temporal distribution of radioactive contaminants, especially under rapidly evolving meteorological conditions. Thus, during nuclear incidents DA supports real-time emergency response by enabling dynamic updates to dispersion forecasts as new data become available. Systems such as the National Atmospheric Release Advisory Center (NARAC) in the United States exemplify this application (Nasstrom et al., 2007). NARAC integrates meteorological observations with predictive models using DA to provide near real-time forecasts of radiological plume behavior, facilitating immediate protective actions. Moreover, DA is embedded in comprehensive decision support systems like Real-time Online Decision Support (RODOS). This platform utilizes DA to assimilate environmental radiation measurements and meteorological updates. As a result, emergency planners can access more accurate and timely information on plume dispersion, contamination zones, and exposure risks (Bartzis et al., 2000; Xiao et al., 2024).

Accurate estimation of the source term is another capability of DA. Direct measurements of radiation are often limited or unavailable during the early stages of an event. DA enables the use of inverse modeling techniques to estimate source terms

based on downwind observations of radiation levels. Eleveld et al. (2006) implemented a variational DA framework in a nuclear emergency response system to infer source term parameters, showing that assimilated models closely matched observed dispersion patterns. These techniques significantly reduce the uncertainty surrounding the origin and scale of releases, enabling more targeted emergency responses. Recent research has introduced machine learning-based DA approaches for enhancing nuclear emergency modeling. Klampanos et al. (2017) proposed the use of autoencoder-driven weather clustering to improve source term estimation during radiological events. By reducing the dimensionality of meteorological data, this method aids in faster and more efficient assimilation processes, which is crucial in time-sensitive emergency scenarios.

3.2.3.2 Improving atmospheric dispersion modelling

Traditional dispersion models, while valuable, often face limitations due to uncertainties in meteorological inputs. For example, widely used models such as Hybrid Single-Particle Lagrangian Integrated Trajectory (HYSPLIT) primarily rely on pre-processed or archived meteorological datasets rather than real-time observational data, which may limit their responsiveness to rapidly changing atmospheric conditions during an emergency. Similarly, the simple GPM is based on steady-state meteorological assumptions, assuming constant wind speed and direction over time, which can oversimplify the complex and dynamic nature of atmospheric dispersion following a nuclear release. DA techniques can address these challenges by integrating observational data into model simulations, thereby enhancing forecast accuracy and reliability. For instance, Jeong et al. (2008) demonstrated that applying DA to the CALPUFF dispersion model significantly improved forecasting accuracy when real meteorological data were assimilated. This integration led to better estimations of plume trajectories and ground-level concentrations of radioactive isotopes.

Advanced DA techniques, such as the ensemble Kalman filter (KF), have also been applied to atmospheric dispersion modeling. For example, a study by Zhang et al. (2014) utilized a modified ensemble KF in conjunction with a Lagrangian puff model to improve short-range dispersion predictions during nuclear accidents. The method effectively enhanced predicted concentration distributions and successfully reconstructed source term parameters. Several other studies have also leveraged KF variants to enhance the estimation of radioactive release parameters. For instance, the

authors in (Kundu et al., 2025) employed a KF to predict the release rate, subsequently refining it using observational data under varying wind conditions. Similarly, (Becerra et al., 2020) utilized an array of radiation sensors to estimate the release rate, comparing the efficacy of ensemble, unscented, and cubature KFs. The study in (Di Ronco et al., 2020) applied a KF to data from mobile radiation detectors to infer both the source location and the intensity of the release. In (Zhang et al., 2014), a modified ensemble KF was adopted to estimate not only the source term but also the plume rise height, thereby improving predictions of radioactive material transport. The research in (Cao et al., 2020) advanced a real-time KF-based estimation framework, underscoring the critical influence of stack height and wind speed on dispersion accuracy. Furthermore, (Wanf et al., 2017) introduced a hybrid DA approach combining PF with expectation-maximization techniques to enhance atmospheric dispersion modeling using synthetic drone observations.

While these contributions have substantially improved the performance of dispersion models, a notable limitation persists across them: the assumption of stable wind conditions. Although wind is universally acknowledged as a primary driver in atmospheric dispersion, these methodologies largely fall short in reconciling the static assumptions inherent to traditional dispersion models with the inherently dynamic nature of atmospheric flows. Concurrently, the field of wind forecasting particularly within the context of wind energy has made significant progress in real-time wind prediction through DA methods (Li and Zou, 2022; Karar et al., 2024). These techniques, which integrate observational meteorological data with predictive models, have proven effective in producing high-resolution, temporally adaptive wind field estimates (Zhang et al., 2015; Lean et al., 2021). Their application in dispersion modeling remains limited, despite their clear relevance. Given that accurate wind inputs are critical for modeling plume transport and diffusion. Incorporating dynamically updated wind data into GPMs is imperative for improving the realism and reliability of pollutant dispersion simulations. By assimilating real-time meteorological observations, GPMs can more accurately represent atmospheric transport processes and thereby enhancing predictions of pollutant advection, diffusion, and deposition. This, in turn, supports more effective environmental impact assessments and informed decision-making during nuclear emergencies.

3.2.3.3 Model formulation and framework

This study presents an integrated framework that combines a Particle Filter (PF)-based wind speed prediction model with the GPM to improve the real-time estimation of radionuclide dispersion. The proposed methodology dynamically updates wind speed estimates using PF and subsequently incorporates these refined values into the GPM to calculate airborne radionuclide concentrations. As illustrated in Figure 3.5, the framework is composed of two core computational components: the PF loop and the GPM loop.

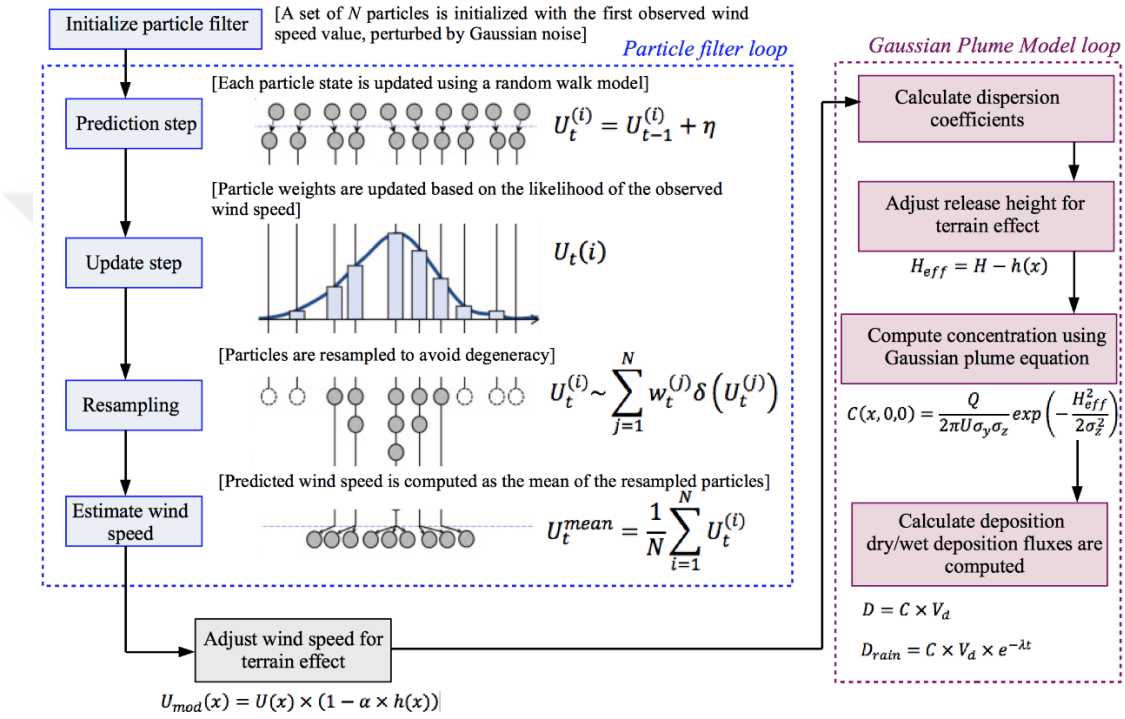

Figure 3.5 : Workflow of the proposed model on integration PF with GPM.

The PF algorithm is employed to generate real-time wind speed predictions while explicitly accounting for uncertainty and observational noise. The process begins by initializing a set of particles using the initial observed wind speed, with each particle perturbed by Gaussian noise to reflect inherent variability. During the prediction phase, particle states are evolved through a stochastic process governed by a random walk model, simulating the temporal dynamics of wind speed. In the subsequent update step, particle weights are recalibrated based on their likelihoods derived from newly observed wind speed measurements. To mitigate sample impoverishment and maintain population diversity, a resampling procedure is applied. The predicted wind speed is then obtained by computing the weighted average of the resampled particles.

To further enhance the accuracy of the prediction, terrain-induced modifications are applied, refining the wind speed estimates for use in dispersion modeling.

Once the wind speed is estimated and corrected, it is utilized as a key input for the GPM to assess radionuclide transport. The dispersion process begins with the calculation of the atmospheric dispersion coefficients, which are derived using Pasquill-Gifford stability classifications and corresponding empirical formulas (Nakajima et al., 2020). The effective release height is adjusted to incorporate terrain effects, thereby ensuring realistic representation of plume rise and atmospheric dynamics. Using the classical Gaussian dispersion formulation, radionuclide concentrations are then computed across varying downwind distances. Finally, the model estimates both dry and wet deposition fluxes, facilitating a comprehensive evaluation of environmental contamination and associated health risks resulting from radioactive fallout.

The PF is a sequential Monte Carlo technique designed for estimating the evolving states of dynamic systems under uncertainty and measurement noise (Jouin et al., 2016). Particularly well-suited for non-linear and non-Gaussian systems, the PF has been effectively applied to wind speed prediction in atmospheric dispersion modeling contexts (Cai et al., 2019). In essence, the PF approximates the posterior probability distribution of the system state (that is wind speed) using a set of weighted particles that are propagated over time in accordance with a defined dynamical model. The PF algorithm typically consists of four core stages: initialization, prediction, update (or weighting), and resampling (Chen 2003). A comprehensive overview of PF methodology is provided in the work of (Speekenbrink 2016).

Initially, a set of N particles is generated based on an initial wind speed observation. Each particle represents a plausible state estimate at the initial time step and is drawn from a normal distribution centered on the observed wind speed, introducing variability through a defined standard deviation. This is expressed in Equation 3.24:

$$U_0^{(i)} = U_{init} + N(0, \sigma^2) \tag{3.24}$$

Where $U_0^{(i)}$ denotes the wind speed of the i-th particle at time t = 0, U_{init} is the observed initial wind speed, and σ represents the standard deviation encapsulating initial uncertainty.

Each particle is initially assigned an equal weight, ensuring a normalized distribution of probabilities, as given in Equation 3.25:

$$w_0^{(i)} = \frac{1}{N} \tag{3.25}$$

where $w_0^{(i)}$ is the weight assigned to the *i-th* particle.

At subsequent time steps, particles evolve according to a dynamic model. In this study, a random walk model is employed to simulate the temporal variation in wind speed. The evolution of each particle is described in Equation 3.26:

$$U_t^{(i)} = U_{t-1}^{(i)} + \eta_t \tag{3.26}$$

Where $\eta_t \sim N(0, \sigma_p^2)$ represents Gaussian process noise with zero mean and variance σ_p^2, capturing inherent fluctuations in wind speed due to turbulence and other meteorological influences.

Following the propagation step, particle states are evaluated against real-time wind speed observations to compute their likelihood. The likelihood function forms the basis for updating particle weights, as shown in Equation 3.27:

$$w_t^{(i)} \propto p\left(Z_t | U_t^{(i)}\right) \tag{3.27}$$

where $p\left(Z_t | U_t^{(i)}\right)$ denotes the conditional probability of the observed wind speed Z_t given the estimated state $U_t^{(i)}$. This step enhances the influence of particles whose states align closely with actual observations.

As the algorithm progresses, weight degeneracy can occur, where most particles carry negligible weight. To address this, a resampling step is introduced to eliminate low-weight particles and replicate higher-weight ones. This step is formalized in Equation 3.28:

$$U_t^{(i)} = U_t^{(j)}, \quad j \sim multinomial\ (w_t) \tag{3.28}$$

Here, particles are resampled from the current distribution based on a multinomial draw over the normalized weights w_t, ensuring representation fidelity to the current state estimate. Post-resampling, all particles are re-initialized with equal weights (Equation 3.29):

$$w_t^{(i)} = \frac{1}{N} \tag{3.29}$$

The estimated wind speed at each time step is then obtained by averaging over the entire set of resampled particle states, providing a robust point estimate under uncertainty. This final step is captured by Equation 3.30:

$$U_t^{mean} = \frac{1}{N}\sum_{i=1}^{N} U_t^{(i)} \tag{3.30}$$

This aggregated estimate U_t^{mean} serves as the best approximation of the true wind speed at time t, reflecting both observational data and model dynamics within a probabilistic framework.

The classical GPM estimates ground-level concentration of airborne Cs-137 as shown in Equation 3.16. To account for terrain effect, the following modifications are applied: terrain-modified wind speed and adjusted effective plume height as shown in Equations 3.31 and 3.32, respectively:

$$U_{mod}(x) = max\big(U(x) \times \big(1 - \alpha \times h(x)\big), 0.1\big) \tag{3.31}$$

$$H_{eff} = H - h(x) \tag{3.32}$$

where $h(x)$ is the terrain height at location x (m), and α is an empirical scaling factor ($\alpha = 0.0001$) that represents the influence of topography on wind speed. While some studies detailing the exact value of α are limited, the concept aligns with established practices in atmospheric dispersion modeling. For instance, the CALMET meteorological model, used in conjunction with the CALPUFF dispersion model, incorporates algorithms that adjust wind fields based on complex terrain features, effectively modifying wind speeds in response to topographical variations (Liu et al., 2017; Rzeszutek 2019). In this study, selecting $\alpha = 0.0001$ (m^{-1}) serves as a reasonable mid-range estimate, reflecting moderate terrain complexity. Equation 3.31 imposes a minimum wind speed of 0.1 m/s to ensure numerical and physical stability in the model. Very low wind speeds like those approaching zero can lead to unrealistic concentration spikes and division by near-zero velocities in Gaussian plume calculations. The threshold value of 0.1 m/s is consistent with Environmental Protection Agency (EPA) guidelines and prior atmospheric dispersion models like AERMOD, which impose minimum wind speeds to prevent overconcentration and avoid misrepresentations (US EPA 2004).

Substituting $U_{mod}(x)$ and H_{eff} into general GPM yields the Terrain-Modified GPM (TM-GPM) as shown in Equation 3.33:

$$C_{TM}(x,0,0) = \frac{Q/3600}{2\pi U_{mod}(x)\sigma_y\sigma_z} exp\left(-\frac{(H-h(x))^2}{2\sigma_z^2}\right) \quad (3.33)$$

Where $C_{TM}(x,0,0)$ is a terrain-modified ground level concentration of CS-137 at downwind distance x measured in Bq/m^3; Q is an emission rate of Cs-137 from the source (Bq/h); $U_{mod}(x)$ is terrain-modified wind speed at location x (m/s); σ_y and σ_z are horizontal and vertical dispersion coefficients (m); H is a physical release height of the pollutant (m); $h(x)$ is a terrain elevation at location x (m). To ensure unit consistency in the Gaussian plume equation, the release rate Q given in Bq/h is divided by 3600 to convert it to Bq/s. This matches the wind speed unit (m/s) and allows the equation to yield concentrations in Bq/m^3.

3.3 Evacuation Priority Mapping

Evacuation priority mapping is a critical component of nuclear emergency planning, aiming to identify and prioritize areas with populations most at risk (Demiryay 2022). This mapping process involves the integration of multiple spatial datasets to optimize evacuation strategies based on both health risk and social vulnerability. In this thesis, combination of the SVI with a Cancer Risk Map (CRM) derived from simulated radioactive exposure was used, to produce a comprehensive evacuation priority assessment.

The SVI is a composite indicator that reflects the relative vulnerability of different regions based on demographic, socio-economic, and infrastructural characteristics. The SVI for each region is calculated using a weighted sum of normalized vulnerability indicators as shown in Equation 3.34 (Tate 2012; Pence et al., 2019).

$$SVI_i = \sum_{j=1}^{n} w_j X_{ij} \quad (3.34)$$

where SVI_i is the SVI for region i, X_{ij} represents the normalized value of the j-th vulnerability factor for region i, w_j is the weight assigned to each vulnerability factor based on its relative importance, and n is the total number of vulnerability factors.

The CRM represents the spatial distribution of long-term health hazards, specifically, the estimated lifetime cancer risk due to radioactive exposure following a nuclear accident. To integrate the CRM with the SVI and determine evacuation priorities, three different methods were employed: the WSM, the Geometric Mean Method, and the Maximum Value Approach.

The WSM involves assigning relative importance to cancer risk and social vulnerability through weights α and β, respectively, where the sum of these weights is equal to 1. The evacuation priority index for each neighborhood is calculated as a linear combination (Equation 3.35) (Marler and Arora, 2010):

$$EPI_i^{WSM} = \alpha \times CRM_i + \beta \times SVI_i \tag{3.35}$$

This method offers a flexible and balanced integration of both components and can be adjusted according to specific goals. For instance, prioritizing health risks more heavily or emphasizing social vulnerabilities depending on situation.

The Geometric Mean Method, on the other hand, computes the evacuation priority index by taking the geometric mean of the cancer risk and social vulnerability values (Escobar et al., 2004) (Equation 3.36):

$$EPI_i^{GMM} = \sqrt{CRM_i \times SVI_i} \tag{3.36}$$

This approach is more conservative, as it tends to assign high priority only to areas where both cancer risk and social vulnerability are simultaneously high. It avoids overestimating risk in locations where one factor dominates, thus emphasizing agreement between the two indicators.

Lastly, the Maximum Value Approach is computed by assigning the higher of the two criteria as the evacuation priority (Li et al., 2025) (Equation 3.37):

$$EPI_i^{MAZ} = max(CRM_i, SVI_i) \tag{3.37}$$

This method is particularly useful for urgent response scenarios, as it ensures that any area exhibiting high cancer risk or high social vulnerability, even if one of the factors is relatively low.

3.4 Discrete Event Simulation For Evacuation Time Estimates

3.4.1 Radius-based and priority-based evacuation strategies

Evacuation strategies are critical components of disaster management, particularly in scenarios involving large-scale emergencies such as hurricanes, wildfires, and industrial accidents including nuclear emergencies (Sadri et al., 2014; Beyki et al., 2023; He et al., 2024). Two prominent strategies for organizing evacuations are radius-based evacuation and priority-based evacuation. These strategies differ in their

approach to determining the order and timing of evacuations, as well as the criteria used to prioritize evacuees.

The radius-based evacuation strategy is a geographically driven approach that organizes evacuations based on the distance from the hazard source (Lu et al., 2014). This strategy divides the affected area into special zones or rings, with evacuation orders issued sequentially based on the proximity of each zone to the hazard. The Fukushima Daiichi nuclear disaster serves as a key example of this strategy in practice. The affected area was divided into three primary zones: (1) exclusion zone (0–20 km) where an immediate evacuation was mandated for all residents within a 20-kilometer radius of the plant due to the high risk of radiation exposure; (2) buffer zone (20–30 km) where residents in this zone were advised to remain indoors and prepare for potential evacuation, depending on the progression of the crisis and (3) outer zone (30+ km) where areas beyond 30 kilometers were considered low-risk, and no evacuation orders were issued unless conditions worsened (Hasegawa et al., 2016).

The priority-based evacuation strategy represents a more nuanced and sophisticated approach to disaster management by integrating social vulnerability and hazard mapping to identify and prioritize neighborhoods or populations for evacuation (Pence et al., 2019). Unlike the radius-based strategy, which relies solely on geographic proximity to the hazard source, the priority-based approach considers a broader range of factors, including demographic characteristics, infrastructure limitations, and the severity of the hazard. This strategy is a key contribution of this thesis and is specifically designed to address the shortcomings of traditional evacuation methods, offering a more equitable and efficient framework for managing large-scale evacuations. The foundation of the priority-based strategy lies in the integration of social vulnerability and hazard mapping. This process begins with a comprehensive assessment of the affected area, combining two critical datasets. The first is hazard mapping, which identifies areas with the highest risk of exposure to the hazard, such as radiation levels. The second is the SVI, a metric that quantifies the susceptibility of different populations to harm during a disaster. By overlaying these datasets, the model identifies high-priority neighborhoods like areas that exhibit both high hazard exposure and high social vulnerability and designates them as the first to be evacuated.

3.4.2 Modelling evacuation process using discrete event simulation

In this thesis, a comprehensive evacuation algorithm was developed using a discrete event simulation (DES) framework to estimate the total evacuation time (Song et al., 2009; Jafer and Lawler, 2016). The simulation framework incorporates two key evacuation strategies: radius-based evacuation and priority-based evacuation. These strategies are designed to optimize the evacuation process by considering the spatial distribution of evacuees and the urgency of their evacuation needs. The simulation model is structured around three core components: (1) events and state transitions, which define the sequence of activities during evacuation; (2) time calculation for each evacuation batch, which determines the duration of each phase of the evacuation process; and (3) traffic congestion modeling, which accounts for the impact of road capacity and vehicle flow on evacuation efficiency. The simulation model is designed to track a series of discrete events that represent critical issues in the evacuation process. These events are used to update the system state, which includes metrics such as the number of people evacuated, the number of individuals remaining in the danger zone, and the current level of traffic congestion. The following are the key events modeled in the simulation (Urbanik II 2000):

Event 1: Mobilization Start – this event marks the initiation of the evacuation process. It represents the moment when an evacuation order is issued, and evacuees begin preparing to leave the danger zone. The mobilization phase includes activities such as receiving the evacuation alert, gathering essential belongings, and moving to designated assembly points or vehicles.

Event 2: Loading Completion – this event occurs when evacuees have finished gathering their belongings and have entered their vehicles or transportation modes. The loading phase is influenced by factors such as the number of evacuees, the availability of vehicles, and the efficiency of loading procedures.

Event 3: Travel Start – this event signifies the beginning of the movement of vehicles or evacuees toward designated shelters or safe zones. The travel phase is critical, as it involves navigating through the transportation network, which may be affected by traffic congestion, road conditions, and the distance to shelters.

Event 4: Batch Arrival at Shelters or Safe Zones – this event marks the completion of an evacuation batch, where a group of evacuees successfully reaches the designated shelters. The arrival phase updates the system state by reducing the number of people in the danger zone and increasing the number of individuals in safe locations.

The evacuation process is modeled as a sequence of time-dependent phases, with each batch of evacuees following a specific timeline. The total evacuation time for a batch b, denoted as $T_{evac,b}$, is calculated using the Equation 3.38 (Bretschneider 2012; Deng et al., 2022):

$$T_{evac,b} = T_{mob} + T_{load} + max_{i \in D_b} T_{travel,i} + (b-1)G \tag{3.38}$$

where T_{mob} represents the mobilization delay, which is the time required for evacuees to prepare for evacuation after the order is issued; T_{load} represents the loading time, which is the duration required for evacuees to enter vehicles or transportation models; $max_{i \in D_b} T_{travel,i}$ is the maximum travel time for batch b, where D_b is the set of evacuees in the batch; and G represents the staggered delay between consecutive batches. This delay is introduced to prevent overcrowding and traffic congestion by spacing out the departure of evacuation batches.

The total evacuation time is then determined by the batch that takes the longest time to complete the evacuation process. This is expressed as Equation 3.39 (Bretschneider 2012):

$$T_{total} = max_{b \in B} T_{evac,b} \tag{3.39}$$

where B is the set of all evacuation batches.

Traffic congestion is another critical factor that can significantly impact the efficiency of the evacuation process. To account for this, the simulation incorporates a dynamic traffic flow model based on road capacity and the number of vehicles on the road. The congestion delay $T_{congestion}$ is calculated as shown in Equation 3.40 (Bretschneider 2012) :

$$T_{congestion} = \frac{N_v}{Q} \tag{3.40}$$

where N_v is number of vehicles on the road, which is derived from the number of evacuees N_p and the average vehicle occupancy (Equation 3.41) (Bretschneider 2012):

$$N_v = \frac{N_p}{occupancy} \tag{3.41}$$

here, Q represents the flow rate of vehicles, which is determined by the road capacity C and the number of lanes L (Equation 3.42) (Bretschneider 2012):

$$Q = C \times L \tag{3.42}$$

here, the road capacity C is defined as the maximum number of vehicles that can pass through a road segment per unit time, while the number of lanes L determines the overall throughput of the road network.

3.5 Evaluation of Nuclear Emergency Shelters

The evaluation of emergency shelters is a critical component of disaster preparedness and response planning (Wang et al., 2022). In the event of a nuclear accident, shelters serve as protective spaces that can significantly reduce radiation exposure and mitigate adverse health effects on affected populations (Farhat et al., 2024). Properly designed and strategically located shelters play a key role in minimizing casualties, ensuring the efficient evacuation of residents, and maintaining essential services during and after an incident (Farhat et al., 2024). Assessing the effectiveness of nuclear emergency shelters involves multiple factors, including their capacity, accessibility, proximity to high-risk areas, and ability to sustain occupants for extended periods (Ma et al., 2019). Additionally, factors such as evacuation time, shelter supply logistics, and environmental considerations must be incorporated into the evaluation process to optimize shelter placement and functionality (Safaei et al., 2020). A systematic evaluation of these shelters not only enhances emergency response efficiency but also supports decision-makers in refining shelter allocation strategies, improving infrastructure resilience, and ensuring compliance with safety regulations (Zou et al., 2018). This section presents an in-depth evaluation of nuclear emergency shelters, focusing on key performance metrics and optimization approaches to enhance their effectiveness in nuclear disaster scenarios.

3.5.1 Study framework: weighted sum method

The proposed methodology integrates GIS data, network analysis, and a MOO model to efficiently assign populations to shelters during an emergency.

MOO has been widely applied in disaster management, particularly in evacuation planning and shelter allocation (Yuan and Han 2010). Various studies have explored optimization techniques to balance conflicting objectives such as minimizing evacuation time, maximizing shelter accessibility, and ensuring fair resource distribution (Zhong et al., 2023). Classical approaches, including linear programming, heuristic algorithms, and metaheuristic methods like genetic algorithms and particle

swarm optimization, have been used to solve complex evacuation problems (Dulebenets et al., 2019; Obaid et al., 2024; Xiao et al., 2025). Recent advancements in GIS-based modeling and network analysis have further improved decision-making by integrating spatial data into optimization frameworks. Research has highlighted the importance of considering multiple criteria simultaneously in evacuation planning. Focusing solely on minimizing evacuation time can lead to overcrowded shelters, while prioritizing shelter accessibility might increase overall travel time. For instance, a study by Sotelo-Salas et al. (2024) developed a MOO model that balances evacuation time and shelter capacity, demonstrating the trade-offs involved in such planning decisions. The WSM is widely employed in MOO due to its straightforward approach of assigning different weights to competing objectives based on their relative importance. This method allows decision-makers to prioritize certain objectives over others, facilitating tailored evacuation strategies. Marler and Arora (2010) provide an in-depth analysis of the WSM, discussing its applicability and limitations in various optimization scenarios.

The process used in this thesis is illustrated in Figure 3.6 and consists of three main stages: input data, model formulation, and optimization process.

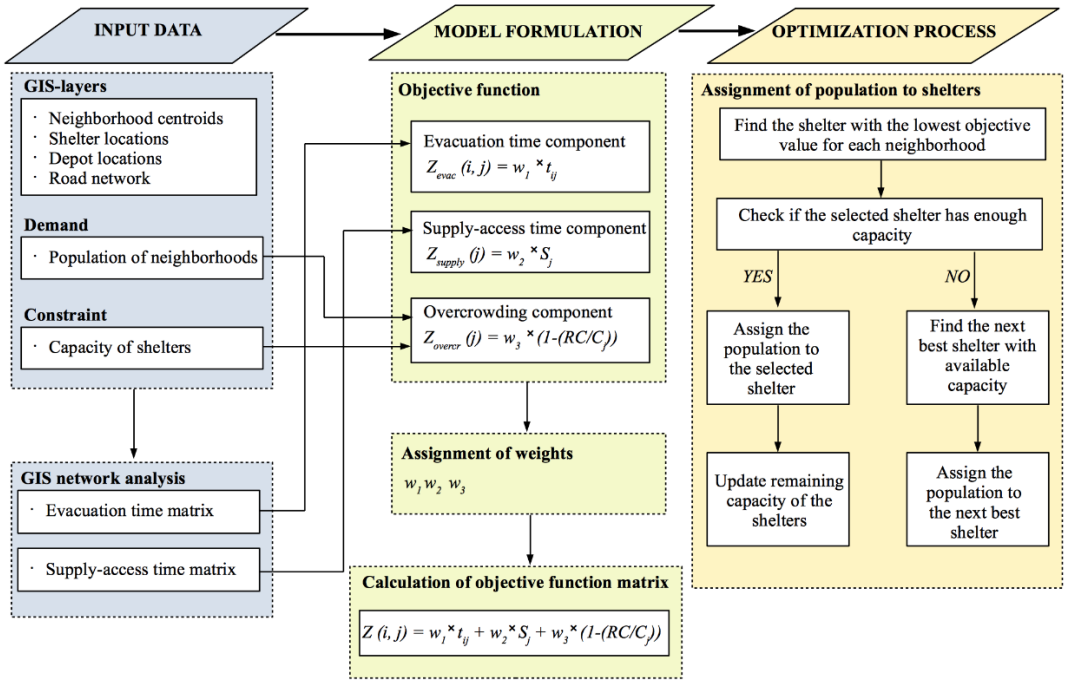

Figure 3.6 : Workflow of the proposed methodology.

The first stage involves collecting and organizing essential spatial and numerical data. GIS layers include neighborhood centroids, shelter and depot locations, and the road

network, all of which serve as fundamental inputs for the evacuation and supply distribution process. The population of each neighborhood represents the demand that must be allocated to shelters, while the capacity of shelters acts as a constraint, ensuring that no facility is overcrowded. Additionally, GIS network analysis is performed to generate an evacuation time matrix, which quantifies travel times between neighborhood centroids and shelters, as well as a supply-access time matrix, which measures the time required for emergency supplies to reach shelters from depots.

Once the input data is prepared, the second stage focuses on formulating the optimization model. The objective function is designed to balance three key components: evacuation time, supply-access time, and overcrowding. The evacuation time component minimizes travel time for evacuees, formulated as shown in Equation 3.43:

$$Z_{evac}(i,j) = w_1 \times t_{ij} \tag{3.43}$$

where t_{ij} represents the travel time from neighborhood i to shelter j, and w_1 is its assigned weight.

The supply-access time component accounts for the accessibility of emergency supplies to shelters, expressed as Equation 3.44:

$$Z_{supply}(j) = w_2 \times S_j \tag{3.44}$$

where S_j denotes the supply-access time for shelter j and w_2 is its corresponding weight.

To prevent overcrowding, the overcrowding component introduces a penalty for shelters approaching full capacity, formulated as Equation 3.45:

$$Z_{overc}(j) = w_3 \times (1 - RC/C) \tag{3.45}$$

where *RC* is the remaining shelter capacity and *C* is the total capacity.

The combined objective function, given by Equation 3.46 integrates all three factors, ensuring a balanced trade-off between evacuation efficiency, supply accessibility, and capacity utilization. The weights w_1, w_2, and w_3 allow for adjustments based on different emergency priorities.

$$Z(i,j) = w_1 \times t_{ij} + w_2 \times S_j + w_3 \times (1 - RC/C) \tag{3.46}$$

The final stage involves the optimization process, which systematically assigns populations to shelters based on the computed objective function values. For each neighborhood, the model selects the shelter with the lowest objective function value, prioritizing locations that optimize evacuation time, supply access, and capacity balance. If the chosen shelter has sufficient capacity, the population is assigned accordingly. Otherwise, the next best shelter with available capacity is selected. Once the assignment is made, the remaining shelter capacities are updated, and the process continues iteratively until all evacuees are allocated. This stepwise approach ensures that populations are distributed efficiently while minimizing evacuation time, ensuring supply accessibility, and preventing shelter overcrowding.

3.5.2 Origin-Destination cost matrix

The Origin-Destination (OD) Cost Matrix is a fundamental tool in transportation and evacuation modeling, representing the travel costs (such as time or distance) between a set of origins and destinations (Igbokwe and Ajie, 2023). In the context of emergency evacuation and shelter allocation, the OD cost matrix quantifies the cost of traveling from each neighborhood centroid (origin) to each potential shelter (destination), allowing for the selection of the most efficient evacuation routes.

An OD cost matrix is typically represented as a two-dimensional matrix where each element $C(i,j)$ denotes the cost of travelling from origin i to destination j. This cost can be computed using several distances or time-based measures, such as Euclidean distance or network-based travel time. If travel occurs in an open space, the cost between points can be calculated using Euclidean distance as shown in Equation 3.47 (Zhao et al., 2024):

$$C(i,j) = \sqrt{\left(x_i - x_j\right)^2 + \left(y_i - y_j\right)^2} \tag{3.47}$$

where (x_i, y_i) and $\left(x_j, y_j\right)$ are the coordinates of the origin and destination, respectively.

In real-world evacuation scenarios, travel occurs along a road network rather than in a straight line. Therefore, the cost between an origin i and a destination j is calculated as shown in Equation 3.48 (Musolino et al., 2013):

$$C(i,j) = \sum_{k=1}^{n} \frac{d_k}{v_k} \tag{3.48}$$

where d_k represents the distance of road segment k along the path, and v_k is the speed limit or estimated travel speed on that segment.

3.5.3 Statistical evaluation

K-fold cross-validation is a statistical technique used to assess a model's performance by dividing the dataset into k subsets, or folds (Zhang and Liu, 2023). Given a dataset $D = \{x_1, x_2, \dots, x_n\}$, it is randomly partitioned into k approximately equal-sized subsets, denoted as $D_1, D_2, \dots, D_k$. During each iteration i, the model is trained on all data except for the i-th fold, $D \backslash D_i$, while the holdout set D_i is used for validation. The performance error for each fold, represented as L_i, is computed based on the model's validation results. The overall model performance is then determined by averaging the errors across all folds, as expressed in Equation 3.49 (Zhang et al., 2019):

$$L_{avg} = \frac{1}{k}\sum_{i=1}^{k} L_i \tag{3.49}$$

Additionally, the variance of the model's performance across folds can be measured to evaluate its stability. The variance, denoted as σ^2, quantifies the consistency of the model's performance across different data partitions and is computed using Equation 3.50 (Zhang et al., 2019):

$$\sigma^2 = \frac{1}{k}\sum_{i=1}^{k}\left(L_i - L_{avg}\right)^2 \tag{3.50}$$

where σ^2 represents the variance, L_i is the error for the i-th fold, and L_{avg} is the mean error across all folds. A lower variance indicates more consistent performance, suggesting that the model generalizes well across different subsets of data.

3.6 Health and Environmental Impact Assessment

3.6.1 Health impact: Total effective dose equivalent and cancer risk estimation

The primary health concerns stem from exposure to ionizing radiation, which can damage Deoxyribonucleic acid (DNA) and increase the risk of cancer, genetic mutations, and other health effects. To quantify these risks, two key metrics are usually used: TEDE and cancer risk estimation (Raisali et al., 2006).

Nuclear accidents release a variety of radioactive isotopes, including CS-137 (Cs-137), I-131 (I-131), St-90(Sr-90), and Plutonium-239 (Pu-239) (Chaisan et al., 2013). These isotopes emit alpha particles, beta particles, and gamma rays, each with varying

penetration power and biological impact. For example, gamma rays can penetrate deep into tissues, causing widespread damage, while alpha particles are particularly harmful when inhaled or ingested. The health effects of these isotopes depend on factors such as the type of radiation, the duration of exposure, and the sensitivity of the exposed population (Choi et al., 2015).

The TEDE is a critical measure used to assess the overall radiation dose received by an individual. It accounts for both external and internal exposure pathways and is expressed in Sieverts (Sv) or Millis everts (mSv). External exposure refers to radiation from sources outside the body, such as gamma rays from radioactive fallout, while internal exposure results from the ingestion or inhalation of radioactive materials, such as I-131 accumulating in the thyroid or Sr-90 in bones (Wooten 2002). The TEDE is calculated by summing the contributions from these two pathways. For external exposure, the dose is calculated by considering the absorbed dose from each type of radiation, weighted by factors that account for the relative biological effectiveness of the radiation type and the sensitivity of the exposed tissue. For internal exposure, the dose is calculated based on the activity of the ingested or inhaled radionuclide and its corresponding dose coefficient, which varies by age group and exposure pathway (Wooten 2002). Therefore, the mathematical expression for TEDE is shown as Equation 3.51:

$$TEDE = External\ Dose + Internal\ Dose \tag{3.51}$$

External dose is expressed by Equation 3.52 (Wooten 2002):

$$External\ Dose = \sum_i (D_i \times w_R \times w_T) \tag{3.52}$$

where D_i is absorbed dose from radiation type i (in grays, Gy); w_R is radiation weighting factor (e.g., 1 for gamma rays, 20 for alpha particles); and w_T is tissue weighting factor (e.g., 0.12 for lungs, 0.04 for thyroid).

Internal dose is expressed by Equation 3.53 (Wooten 2002):

$$Internal\ Dose = \sum_j \left(A_j \times e_j\right) \tag{3.53}$$

where A_j is activity of radionuclide j ingested or inhaled (in becquerels, Bq) and e_j is dose coefficient for radionuclide j (in Sv/Bq), which depends on the age group and exposure pathway.

The cancer risk associated with radiation exposure is estimated using risk coefficients provided by organizations such as the International Commission on Radiological Protection (ICRP) and the EPA (Unver 2011). These coefficients vary by age group, sex, and organ, reflecting differences in biological sensitivity and expected lifespan. For example, newborns and children are at higher risk due to their rapid cell division and longer expected lifespan, with risk coefficients ranging from 0.15 to 0.20 per sievert. Adults generally have lower risk coefficients, with men at approximately 0.05 to 0.08 per sievert and women at 0.06 to 0.10 per sievert due to their increased susceptibility to breast and thyroid cancer. The lifetime cancer risk is calculated by multiplying the TEDE by the appropriate risk coefficient. For instance, an adult male exposed to a TEDE of 100 mSv would have a lifetime cancer risk of approximately 0.7% (Unver 2011; Hancerlioglu et al., 2019). Lifetime cancer risk is calculated as shown in Equation 3.54 (Unver 2011):

$$Lifetime\ Cancer\ Risk = TEDE \times Risk\ Coefficient \tag{3.54}$$

Table 3.5 lists risk coefficients by age group and sex.

Table 3.5 : Risk coefficients and health impact (Bellamy et al., 2019).

Age group	Risk coefficient (per Sv)	Key characteristics
Newborns	~0.15-0.20	Higher risk due to rapid cell division and longer expected lifespan
Children	~0.10-0.15	Increased sensitivity to radiation, particularly for thyroid cancer
Adults – men	~0.05-0.08	Increased risk of lung cancer and leukemia
Adults – women	~0.06-0.10	Slightly higher risk due to breast and thyroid sensitivity

3.6.2 Environmental consequences: Cs-137 deposition and decay modeling

CS-137 (Cs-137) is a radioactive isotope with a half-life of 30.17 years, commonly released into the environment during nuclear accidents. Understanding the environmental consequences of Cs-137 deposition and decay is critical for assessing its long-term impact on ecosystems, human health, and agricultural systems (Nurliati et al., 2024).

Cs-137 is released into the atmosphere as a particulate aerosol during nuclear events and is deposited onto the ground and vegetation through two primary mechanisms: dry deposition, which involves the direct settling of particles onto surfaces due to gravity

and turbulence, and wet deposition, which occurs when particles are scavenged by precipitation like rain or snow (EPA 2017). The total activity of Cs-137 deposited per unit area is referred to as the deposition density D, typically measured in kBq/m² or Bq/m² (EPA 2017). After deposition, Cs-137 can migrate vertically into the soil or be redistributed by wind, water, or biological activity. The migration rate depends on soil properties (e.g., clay content, organic matter) and environmental conditions (e.g., rainfall, erosion) (Zhu and Smolders, 2000). Over time, Cs-137 undergoes radioactive decay, reducing its activity in the environment. However, due to its long half-life (30.17 years), Cs-137 remains a concern for decades, contributing to external radiation exposure (from ground deposition) and internal exposure (via ingestion of contaminated food or water) (Ehlken and Kirchner, 2002). It can accumulate in plants, animals, and humans, leading to long-term ecological and health risks (Ehlken and Kirchner, 2002).

Deposition density is calculated from the time-integrated air concentration C_{int} and the deposition velocity v_d. The relationship is given by Equation 3.55 (Ehlken and Kirchner, 2002):

$$D = C_{int} \times v_d \tag{3.55}$$

Here, D is deposition density (Bq/m^2 or kBq/m^2), C_{int} is time-integrated air concentration (Bq×s/m^3), and v_d is deposition velocity (m/s).

The deposition velocity depends on the type of deposition and environmental conditions. For dry deposition, v_d typically ranges from 10^{-3} to 10^{-1} m/s, while for wet deposition, it ranges from 10^{-2} to 10^{-1} m/s. The activity of Cs-137 decreases over time according to the exponential decay law as shown by Equation 3.56 (EPA 2017):

$$A(t) = A_0 \times e^{-\lambda t} \tag{3.56}$$

where $A(t)$ is activity at time t (Bq or kBq), A_0 is an initial activity (Bq or kBq), λ is a decay constant ($\lambda = \frac{ln(2)}{T_{1/2}}$) and $T_{1/2}$ is a half-life of Cs-137 (30.17 years).

The uptake of Cs-137 by plants is modeled using the soil-to-plant transfer factor TF (Equation 3.57) (EPA 2017):

$$C_f = C_S \times TF \tag{3.57}$$

where C_f is an activity concentration in plants (Bq/kg), C_S is an activity concentration in soil (Bq/kg), and TF is a transfer factor (typically 10^{-3} to 10^{-1} for Cs-137).

The effective half-life T_{eff} accounts for both radioactive decay and environmental removal processes (Equation 3.58) (EPA 2017):

$$\frac{1}{T_{eff}} = \frac{1}{T_{1/2}} + \frac{1}{T_{env}} \tag{3.58}$$

where T_{env} is environmental half-life (years).

3.7 Economic Loss Assessment

A nuclear accident can have severe economic consequences, affecting multiple sectors and extending over different timeframes. The economic losses following such an event can be categorized into short-term and long-term impacts, as well as direct and indirect losses. Understanding these distinctions is crucial for policymakers, emergency planners, and economists to assess the full scope of damage and develop appropriate mitigation strategies (NEA 2000).

Short-term economic impacts arise immediately after a nuclear accident, primarily due to emergency response efforts, disruption of local economies, and direct damage to infrastructure. For instance, the Fukushima Daiichi nuclear disaster in 2011 led to the immediate evacuation of over 150,000 residents, halting economic activities in affected regions. The government and private sector had to allocate substantial resources for emergency response, temporary shelter, and decontamination efforts. Additionally, trade restrictions on Japanese agricultural and seafood exports caused immediate economic strain on local producers (Hasegawa et al. 2016).

Long-term economic impacts, on the other hand, persist for years or even decades after the accident. The Chernobyl disaster in 1986 resulted in long-lasting consequences, including the abandonment of entire towns and the loss of agricultural land due to radioactive contamination. The exclusion zone around the plant remains largely uninhabitable, limiting economic redevelopment. Moreover, the psychological and health-related effects on affected populations, including increased cancer rates, have led to sustained healthcare costs and loss of workforce productivity (Beresford et al 2020).

Direct economic losses refer to the immediate financial costs associated with a nuclear accident. These include damage to the power plant itself, costs of emergency response, compensation for affected individuals, and decontamination expenses. For example, after the Fukushima accident, TEPCO faced enormous financial liabilities, including billions of dollars in compensation payments and cleanup efforts (Feldman 2015).

Indirect economic losses arise as a ripple effect of the accident, affecting industries and economic activities beyond the directly impacted zone. A key example is the long-term decline in tourism and real estate values in areas near the Fukushima disaster site (Yorucu and Katircioglu 2014). Additionally, the global nuclear energy sector faced increased regulatory scrutiny, leading to delays in new reactor constructions and shifts in energy policies worldwide (Hayashi and Hughes 2013).

3.7.1 Direct economic losses assessment

Direct economic losses from a nuclear accident are the most immediate and quantifiable financial impacts. These losses stem directly from the event itself and primarily involve costs related to physical damage, emergency response, compensation, and decontamination (NEA 2000). Such losses are typically borne by the nuclear plant operator, government agencies, and, in some cases, the insurance sector. One of the most significant direct losses is the damage to the nuclear facility and associated infrastructure. The Fukushima Daiichi disaster in 2011 serves as a stark example: the tsunami triggered by the earthquake disabled the plant's cooling systems, leading to core meltdowns in multiple reactors. The physical damage to the reactors and ancillary systems was estimated to cost over $20 billion (Neureiter et al., 2014). TEPCO, the operator of the plant, faced unprecedented financial burdens, including reactor dismantling, long-term containment measures, and environmental remediation. In addition to structural damages, extensive resources are required for emergency response operations. These include mobilization of emergency personnel, provision of medical care, deployment of radiation detection equipment, and establishment of evacuation centers. For instance, the Japanese government allocated billions of yen in the immediate aftermath of the Fukushima disaster for rescue efforts and public safety. Compensation to affected individuals and communities also constitutes a major direct economic loss. Victims of the accident, including evacuees, received payments for displacement, loss of property, and psychological distress. TEPCO was mandated to provide compensation amounting to over $90 billion, illustrating the scale of financial

liability following such a catastrophe. Figure 3.7 shows the duration of compensations after Fukushima accident (Neureiter et al., 2014).

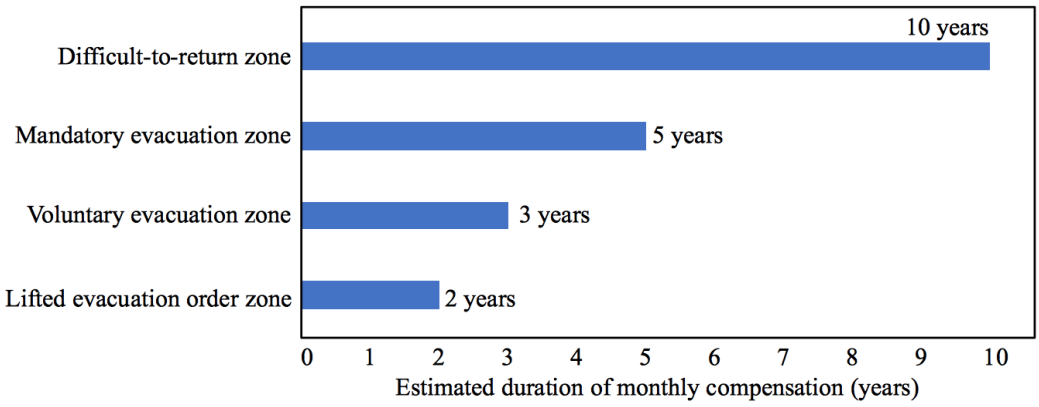

Figure 3.7 : Estimated duration of Fukushima evacuee monthly compensation by zone.

For residents of zones where evacuation orders were lifted, monthly compensation generally continued for approximately two years after the order was canceled. Voluntary evacuees received compensation for up to three years, while those from mandatory evacuation zones were compensated for as long as five years. In the most severely affected and so called “difficult-to-return” zones monthly compensation payments extended for up to ten years (Neureiter et al., 2014).

Finally, decontamination and environmental cleanup are critical yet costly components of the post-accident response. In Fukushima, decontaminating affected land including soil removal, storage of radioactive waste, and water treatment have cost the Japanese government and TEPCO tens of billions of dollars (Neureiter et al., 2014).

3.7.2 Indirect economic losses assessment

Indirect economic losses, while less immediately visible than direct costs, often represent the most extensive and enduring financial consequences of a nuclear accident. These losses arise from secondary impacts that disrupt economic systems, influence public perception, and hinder regional and national development over time (NEA 2000). One significant category of indirect loss is the long-term impact on property values and real estate markets. Areas surrounding the Fukushima Daiichi plant experienced a sharp decline in land and property prices due to contamination fears and stigma, even in locations with minimal radiological impact (Yamane et al.,

2013). Another major indirect loss involves the agricultural and fisheries sectors. In the aftermath of the Fukushima disaster, radioactive contamination led to strict government-imposed bans and international trade restrictions on food products from affected regions (Morita et al., 2020). This not only affected producers in the exclusion zone but also affected broader supply chains and market confidence across Japan. Many producers suffered long-term losses due to reduced demand and reputational damage.

Tourism, an important economic driver in many regions, also suffers significantly from nuclear accidents. For example, after both the Chernobyl and Fukushima incidents, nearby tourist destinations saw a sharp drop in visitor numbers (Handler 2016). Even areas located outside the contamination zones experienced reduced economic activity due to general public fear and travel cancellations. Recovery in the tourism sector is often slow and dependent on extensive public reassurance and rebranding efforts.

Moreover, the broader economic landscape can be affected through increased regulatory scrutiny and shifts in energy policy. The global nuclear industry experienced a downturn following the Fukushima accident, with several countries delaying or canceling nuclear projects. Germany, for instance, accelerated its nuclear phase-out, leading to economic losses in the energy sector and a realignment of energy infrastructure investments (Wittneber 2013). These shifts can lead to opportunity costs and a reallocation of resources that hinder economic growth.

Finally, the psychological and health effects of a nuclear accident can indirectly affect economic productivity. Persistent anxiety, stress-related illnesses, and the loss of workforce due to relocation or health impacts contribute to decreased economic output. In Chernobyl-affected regions, studies have linked chronic health issues and mental distress to long-term declines in labor force participation and productivity, compounding the indirect economic costs (Oe 2021).

3.7.3 Economic loss assessment methodology

In this thesis, the total economic losses resulting from a nuclear accident are calculated as the sum of six major cost components: cost of response, cost of decontamination, cost of health, cost of waste, cost of compensation, and cost of administration. These categories align predominantly with direct losses, though they may span both short-term and long-term timeframes depending on their nature (Bizet and Leveque 2017).

Therefore, the total costs are calculate using an Equation 3.59:

$$C_{total} = C_{response} + C_{decont} + C_{health} + C_{waste} + C_{compens} + C_{admin} \quad (3.59)$$

where:

Cost of response $C_{response}$ includes immediate emergency actions such as evacuation, firefighting, radiation monitoring, and logistics. This is a short-term direct cost, typically incurred within the first days to months following the incident (Bizet and Leveque 2017).

Cost of decontamination C_{decont} refers to the cleanup of contaminated areas, including removal of topsoil, washing of infrastructure, and safe handling of radioactive residues. This is a long-term direct cost, as decontamination efforts often continue for years or even decades (Bizet and Leveque 2017).

Cost of health C_{health} includes both immediate medical treatment for radiation exposure and long-term health monitoring and care for affected populations. It is considered a long-term direct cost, as radiation-related illnesses, including cancers, may develop many years after the exposure event (Li et al., 2022).

Cost of waste C_{waste} accounts for the treatment, transport, and final disposal of radioactive waste generated during accident and decontamination. This is classified as a long-term direct cost due to the complexity and duration of safe radioactive waste management (Drace et al., 2022).

Cost of compensation $C_{compens}$ encompasses payments to evacuees, farmers, businesses, and others adversely affected populations by the accident. It spans both short-term and long-term direct losses, depending on the duration of displacement and the nature of the affected party. For example, as discussed earlier, compensation payments in Fukushima ranged from 2 to 10 years depending on evacuation status (Ashlet et al., 2017).

Finally, cost of administration C_{admin}, calculated as 5% to 10% of the total of the five aforementioned categories, covers management, coordination, planning, and reporting activities. This too is a direct cost that supports both short-term emergency operations and long-term recovery efforts (NEA 2000).

4. CASE STUDY

4.1 History of Nuclear Power in Turkiye

Türkiye's interest in nuclear energy began in the 1950s, as the country looked for ways to support its development and energy needs (Agbulut 2019). In 1956, the Turkish Atomic Energy Authority (TAEA) was created to focus on nuclear research, make safety rules, and promote peaceful uses of nuclear energy. A year later, Türkiye joined the IAEA, showing its commitment to using nuclear technology safely (Jewell and Ates, 2015).

In the 1960s, Türkiye started doing research to see if building NPPs was possible. They looked for good locations that were near water for cooling, far from earthquake risks, and close to electricity networks. By the early 1970s, several places were considered, and Akkuyu in Mersin Province stood out as the best choice because of its safe and suitable location (Akcay 2009). In 1976, Türkiye made its first serious move to build a NPP in Akkuyu. It signed deals with international companies, but the project couldn't move forward due to money problems, political issues, and not having enough experts in nuclear technology. In 1983, the government started a new nuclear program to restart the Akkuyu project and look at other sites like Sinop, near the Black Sea. During this time, Türkiye tried to work with countries like Germany, Sweden, and Canada. However, progress was slow due to economic problems, changing political goals, and public fear about nuclear safety and especially after the Chernobyl disaster in 1986, which made many people more worried about nuclear power (Guler 2019). Things started to change in the 2000s. As Türkiye's economy grew and cities expanded, the country needed more electricity. The government saw nuclear power as a way to meet this demand, reduce pollution, and cut back on imported energy. Finally, in 2010, Türkiye and Russia signed a major agreement for Russia to build the Akkuyu NPP. Russia's Rosatom company agreed to build, own, and run the plant (Aydin 2020). Building started in 2018, with plans for four reactors using Russian VVER-1200 technology. The first one is expected to be ready in 2025, and the rest by 2028. Once finished, Akkuyu will provide about 10% of Türkiye's electricity (Uluer and Caglayan,

2021). Türkiye also planned other nuclear projects. One was the Sinop NPP on the Black Sea, another possible site is İğneada in Thrace.

4.2 Akkuyu Nuclear Power Plant: an Overview

The Akkuyu NPP represents a significant milestone in Türkiye's energy strategy, aiming to diversify energy resources and reduce reliance on imported fossil fuels. Located in the southern region of Türkiye, the plant is the country's first nuclear power facility and is poised to play a critical role in meeting the growing energy demands of the nation. This section provides a comprehensive overview of the Akkuyu NPP, encompassing its geographical features, design specifications, safety measures, and its potential environmental and socioeconomic impacts.

4.2.1 Geographical and demographic profile

The Akkuyu NPP is situated in the Mersin Province, near the Gulf of Mersin in the eastern Mediterranean region. Figure 4.1 shows the geographical location of Akkuyu NPP. The site is approximately 140 kilometers west of Mersin city and is located along the coastline, providing access to seawater for cooling purposes. The geographical selection of Akkuyu was influenced by several factors, including seismic stability, proximity to energy distribution networks, and minimal impact on densely populated areas (Kyriakides 2023).

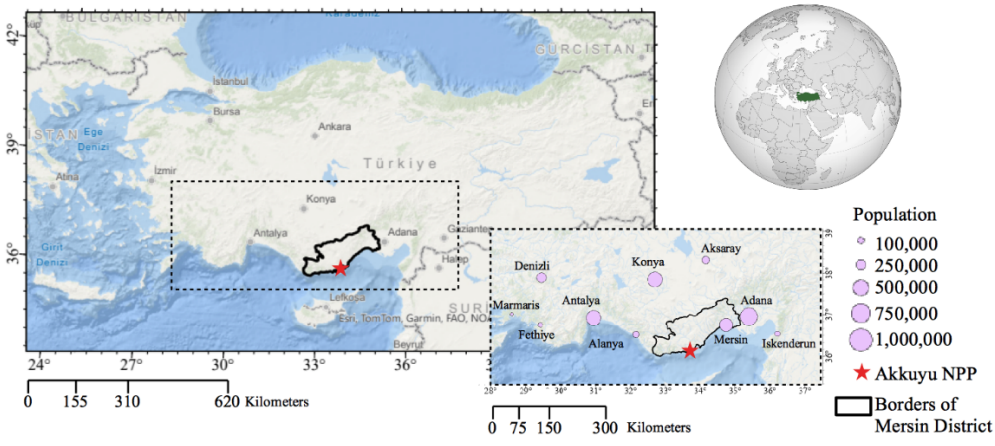

Figure 4.1 : Geographical location of Akkuyu NPP.

The population around Akkuyu is relatively small compared to urban areas, with a mix of villages and rural communities (Figure 4.2). The local economy mainly revolves around agriculture, fishing, and small trade. Most of the population is involved in

citrus farming and olive growing, while fishing provides additional income along the coast. Although there are no major urban settlements near Akkuyu, Mersin Province has over 1.8 million people, making it important for emergency planning in case of a nuclear accident (Kartancioglu 2018).

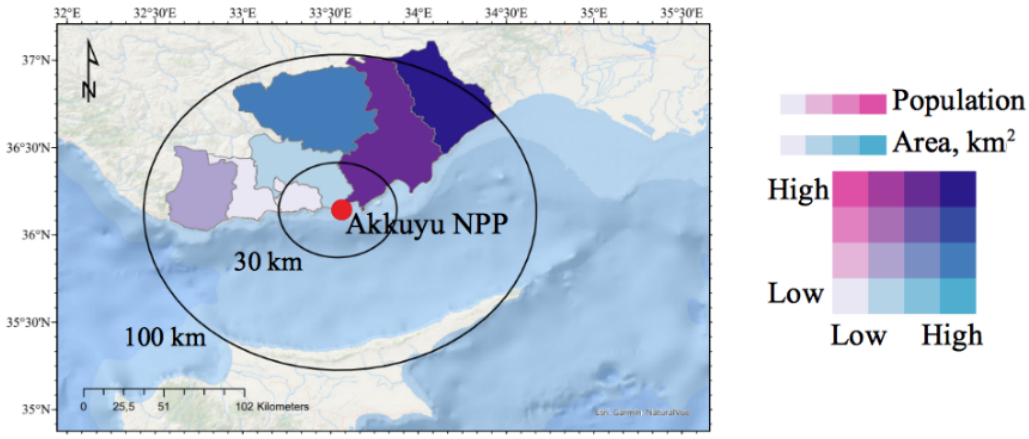

Figure 4.2 : Demographic profile of Mersin province.

The region features a Mediterranean climate, characterized by hot, dry summers and mild, wet winters. These climatic conditions are favorable for the operation of a NPP as they ensure year-round accessibility and stable environmental conditions for operational efficiency. The topography of the Akkuyu site includes a combination of coastal plains and gentle hills, providing a natural buffer against potential external risks such as flooding (Celik and Gulersoy, 2018).

The site's geological characteristics have been rigorously analyzed to ensure its suitability for nuclear operations. Detailed studies have indicated that the area is relatively stable, with a low likelihood of significant seismic activity (Kartal et al., 2014).

The area around the NPP has different types of land heights, as shown in the Digital Elevation Model (DEM) in Figure 4.3. The NPP is located near the coast, where the land is low and close to sea level, which is shown in green on the map. As go further inland, the land slowly gets higher, changing color from yellow to brown, and reaches up to about 3,487 meters. This means there are tall mountains in the north and northeast parts of the area. The 30 km and 80 km circles around the NPP include both flat land near the sea and hilly or mountainous areas further away. The shape of the land is

important because it can affect things like wind direction and how radiation might spread in an emergency.

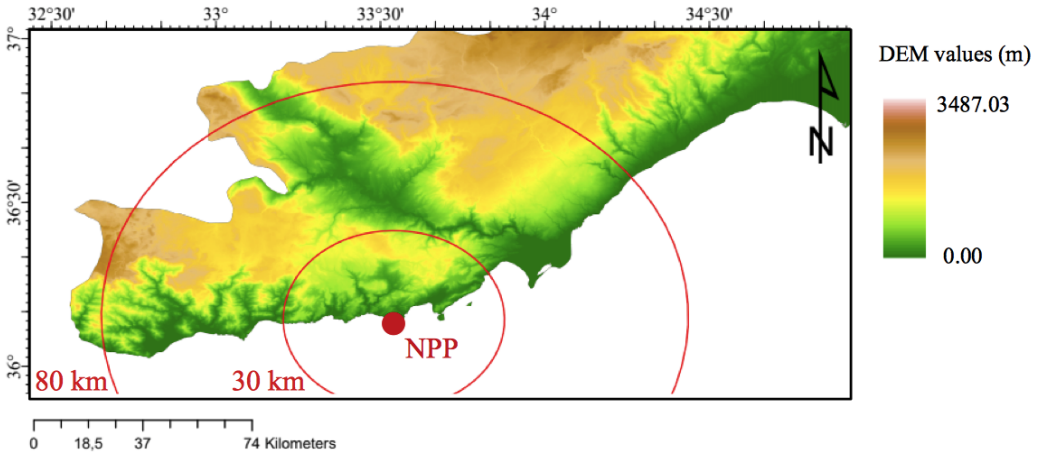

Figure 4.3 : Topographic features of study area.

4.2.2. Design and Technical Specifications

The Akkuyu NPP is being built using Russian VVER-1200 reactor technology, which is a type of pressurized water reactor (PWR). This design is known for being both safe and efficient (Wang et al., 2019). The plant will have four reactors, and each one will produce 1,200 megawatts (MW) of electricity. That adds up to a total capacity of 4,800 MW. When all four reactors are running, the plant is expected to generate about 35 billion kilowatt-hours (kWh) of electricity every year. This amount will cover around 10% of Türkiye's total electricity needs (Uluer and Caglayan, 2021).

The VVER-1200 comes with several important safety features. It has a double containment structure that protects the reactor from outside impacts and helps stop radioactive material from escaping. It also includes a core catcher, which is a special device that can safely trap and cool the reactor core in case something goes wrong, like a meltdown. The reactor also uses passive safety systems, which means it can cool down using natural forces like gravity, even if no one is actively controlling it (Kulikov et al., 2022).

4.2.2 Safety and Risk Mitigation

Safety is a top priority in the design and operation of the Akkuyu NPP. In addition to the safety features of the VVER-1200 reactors, the plant follows international safety standards from organizations like the IAEA and the World Association of Nuclear

Operators (WANO). Some key safety measures include seismic resilience, where the plant is built to withstand earthquakes, ensuring its structure remains intact during seismic events. Emergency preparedness is also a critical focus, with detailed response plans, evacuation procedures, early warning systems, and close collaboration with local authorities. Environmental monitoring is continuously carried out to track radiation levels and other environmental factors, ensuring that any abnormal conditions are quickly detected (Demiryay 2022).

4.2.3 Environmental and Socio-Economic Impact

The Akkuyu NPP is expected to bring major benefits to Türkiye's energy sector and economy, while also raising important environmental and social concerns. From an environmental perspective, the plant will help reduce carbon emissions by replacing fossil fuel-based energy production, supporting Türkiye's climate goals. However, the use of seawater for cooling could potentially affect the marine ecosystem, so measures like regulating thermal discharge and conducting impact assessments have been put in place to minimize these risks (Saylan and Aygun, 2024). Additionally, the plant will manage radioactive waste, including spent nuclear fuel, according to strict guidelines to limit environmental impact (Bilgilioglu 2022).

On the socio-economic side, the Akkuyu NPP is creating thousands of jobs, which boosts local economies. It will also improve energy security by reducing Türkiye's reliance on energy imports. Furthermore, the collaboration with international partners will promote technology transfer, advancing Türkiye's nuclear sector and building local expertise (Kaygusuz and Avci, 2021).

4.3 Review of Related Legislation Regarding Akkuyu-NPP

4.3.1 IAEA standards

The IAEA plays a key role in setting global safety standards for the development, operation, and decommissioning of NPPs (Omoto 2005). These standards serve as guidelines for countries with nuclear facilities, including Türkiye, where the Akkuyu NPP is located. The IAEA's safety standards cover many areas, such as site selection, design, construction, operation, and emergency preparedness.

When it comes to site selection and design, the IAEA emphasizes the importance of choosing locations that minimize risks from natural disasters like earthquakes, floods, and tsunamis. Akkuyu NPP is located in a seismically active area, so following these guidelines ensures that the plant can withstand major earthquakes (Yavuz 2023). The design of the plant must also include multiple safety layers to prevent radioactive releases, even in extreme conditions.

For operational safety, the IAEA sets standards that require a strong safety culture, regular training, and strict operational procedures. This includes ensuring that the reactor operates within safe limits, performing routine maintenance, and conducting regular safety audits (Bicakci and Evren, 2022).

Emergency preparedness is another critical area, and the IAEA provides guidelines in its General Safety Requirements (Demiryay 2022). These guidelines require countries to have emergency response plans that include effective communication, timely evacuations, and public protection measures.

Lastly, the safe handling and disposal of radioactive waste is essential for protecting the environment and public health. The IAEA's guidelines require detailed plans for managing spent nuclear fuel and other radioactive waste (Santana 2016).

4.3.2 National energy policies

Türkiye's national energy policies focus on ensuring energy security, diversifying energy sources, and reducing reliance on imported fossil fuels (Demirbas 2001). The construction of the Akkuyu NPP is an important part of the country's nuclear energy strategy and Türkiye meet its commitment to reducing greenhouse gas emissions. By investing in nuclear power, including the Akkuyu NPP, Türkiye is supporting its transition to a low-carbon economy, in line with the Paris Agreement (Avci and Kygusuz, 2020). The Akkuyu NPP project has also brought economic benefits, such as job creation, technology transfer, and infrastructure development, which align with Türkiye's broader goals of fostering industrial growth and technological innovation. Türkiye's nuclear energy policies are backed by a solid legal framework, including the Nuclear Energy Law and regulations from the TAEA. These laws regulate all aspects of nuclear energy development, ensuring safety, security, and environmental protection (Demiryay 2022).

4.3.3 National emergency plan and safety responsibilities

The establishment and implementation of a comprehensive National Emergency Plan (NEP) are essential for ensuring public safety in case of a nuclear incident at the Akkuyu NPP. The NEP outlines the roles and responsibilities of various stakeholders, such as government agencies, local authorities, and plant operators, to ensure an effective response during an emergency (Demiryay 2022). The NEP is designed to address all phases of a potential nuclear emergency, including preparedness, response, recovery, and mitigation. It follows international best practices and incorporates recommendations from the IAEA. Key components of the plan include a risk assessment, which involves a detailed hazard analysis to identify potential scenarios, like reactor malfunctions or external threats, and evaluates their likelihood and impact. The NEP also establishes EPZs around the Akkuyu NPP. These zones are divided into two categories: the Precautionary Action Zone (PAZ), where immediate protective actions such as sheltering and evacuation are implemented, and the Urgent Protective Action Planning Zone (UPZ), which requires rapid protective actions based on environmental monitoring and risk assessment (Matsunaga et al., 2021).

The TAEA plays a key role in overseeing the implementation of safety standards, conducting inspections, and ensuring compliance with the NEP. TAEA is responsible for monitoring nuclear facilities, enforcing regulatory frameworks, and coordinating with other stakeholders to mitigate risks. The Disaster and Emergency Management Authority (DEMA) is in charge of coordinating national and regional emergency response activities, such as evacuation planning, resource allocation, and ensuring clear communication with the public during a crisis (Demiryay 2022). Local authorities, especially municipalities, play a crucial role in executing evacuation plans, providing safe shelters, and raising community awareness. Their responsibilities also include organizing regular drills and ensuring that the public understands emergency procedures and can act promptly during an emergency. Within this scope, public communication and education are vital elements of the NEP, aiming to raise awareness about nuclear safety and create a culture of preparedness through training sessions and information campaigns (Ogul and Karaagac, 2019). The NEP also includes mechanisms for continuous monitoring and improvement, learning from past nuclear incidents like Fukushima and Chernobyl to make the plan more adaptable and resilient to new risks. Furthermore, the plan outlines the logistical needs for an effective

emergency response, such as having protective equipment, medical supplies, and transportation available (Kantarcioglu 2018).

4.4 Study Area Description

4.4.1 Meteorological data

The meteorological conditions at the Akkuyu NPP site in Mersin Province, Türkiye, play a crucial role in safety assessments, and emergency preparedness. The region's climatic characteristics, wind patterns, precipitation levels, and seasonal variations significantly influence dispersion modeling for potential radioactive releases and overall plant efficiency. This section provides a comprehensive overview of the climatic, weather, and meteorological conditions surrounding Akkuyu NPP.

4.4.1.1 Climatic Conditions

Akkuyu experiences a Mediterranean climate, characterized by hot, dry summers and mild, wet winters (Celik and Gulersoy, 2018; Cetin 2020). Figure 4.4 shows the average, minimum, and maximum temperatures, as well as averages sunshine hours inherent to this region.

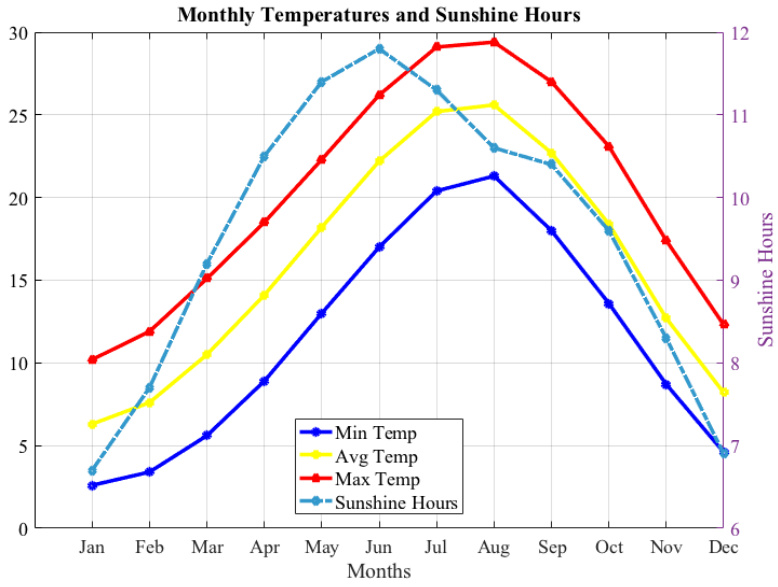

Figure 4.4 : Monthly temperatures and sunshine days.

The annual average temperature ranges from 6°C to 26°C, with summer highs often exceeding 35°C, particularly during July and August. Winters are mild, with temperatures rarely dropping below 5°C, even in January, the coldest month. The

moderate climate minimizes risks associated with extreme cold or heat, which could otherwise impact plant operations or structural integrity. The region benefits from long periods of sunshine, averaging approximately 2,800 hours annually, with minimal cloud cover during the summer months.

4.4.1.2 Wind Patterns

Wind dynamics are the most critical factor for nuclear safety, particularly in the context of potential atmospheric dispersion of radioactive materials. Figure 4.5 shows wind roses for each season independently.

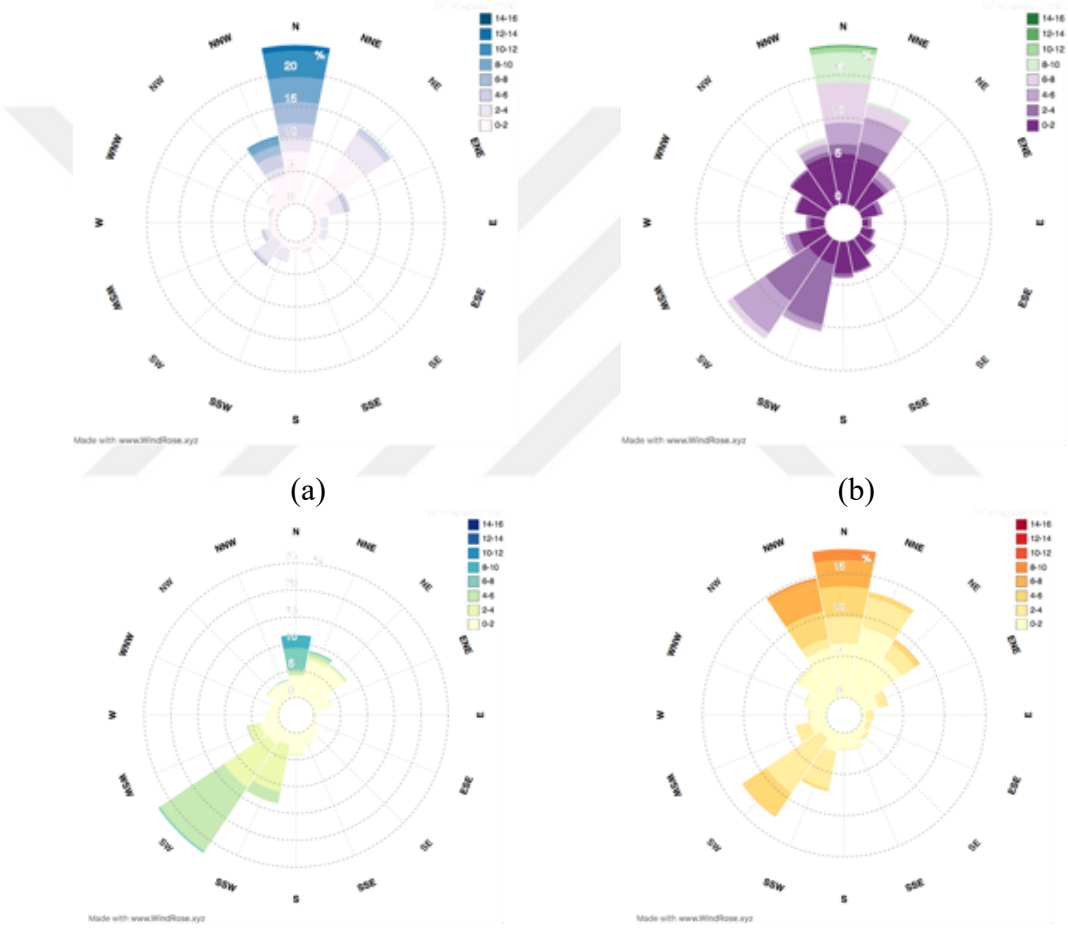

(a) (b)

(c) (d)

Figure 4.5 : Seasonal wind roses: a) Winter, b) Spring, c) Summer, d) Autumn.

The wind rose diagram in Figure 4.5 a illustrates the prevailing wind conditions during the winter observation period. The dominant wind direction is from the north (N), accounting for over 20% of occurrences, followed by northwest (NW) and northeast (NE), albeit with much lower frequencies. Wind speeds are predominantly within 2-8

m/s range, as shown by the light and medium blue shades, indicating moderate wind conditions. Higher wind speeds (10-14 m/s) are rare but also occur primarily from the north.

From Figure 4.5 b, the dominant wind direction is south-southwest (SSW), accounting for over 10% of occurrences, followed by south (S) and southwest (SW). the majority of wind speeds fall within the 0-4 m/s range, indicating of relatively calm wind conditions. However, sporadic high-speed winds (10-14 m/s) are observed, primarily associated with northern directions (N).

Figure 4.5 c illustrates wind rose diagram for summer period. The dominant wind direction shifts significantly to the south-southwest (SSW), with higher wind percentages observed at speeds between 2-8 m/s. Winds from the north (N) are less frequent in summer and tend to have lower speeds compared to other seasons.

In Figure 4.5 d, autumn wind rose diagram shows that the predominant wind direction is from the north (N), with a significant percentage of the wind occurring at speeds between 6-14 m/s. Additionally, some winds come from the south-southwest (SSW) but at lower frequencies and moderate speeds.

Figure 4.6 below provides a visual summary of the monthly wind speed data, enabling a comparative analysis of wind speed distribution over the yearly data.

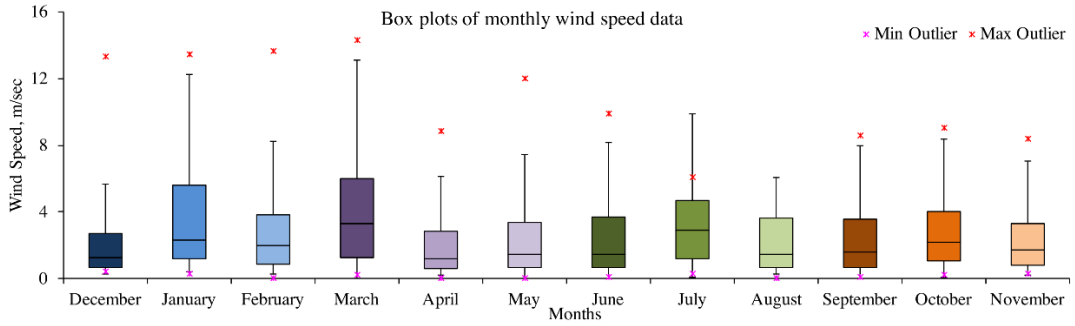

Figure 4.6 : Box plots of monthly wind speed data.

The bold horizontal line within each box represents the median wind speed for the respective month. For instance, March shows one of the higher median wind speeds, indicating stronger winds during this month compared to others. The height of each box indicates the spread of the central 50% of the wind speed data (from the 25th to

the 75th percentile). Months like March and July exhibit larger boxes, suggesting more variability in wind speeds compared to months like April and May. Red and magenta symbols represent outliers beyond the whiskers (minimum and maximum values within 1.5 times of the interquartile range (IQR). Red (maximum) outliers are seen frequently across months, suggesting occasional extreme wind events. The whiskers extend to the smallest and largest values within the 1.5 times IQR range. The long whiskers for months like March and July reflect a wide range of wind speed variations. As for the seasonal patterns, wind speeds appear higher and more variable during the winter months, possibly influenced by stronger atmospheric dynamics typical of that season. In contrast, months like May and June have lower median wind speeds and less variability, indicating calmer wind conditions. March stands out with a higher median and significant variability, suggesting it is the windiest month. Conversely, April and May have the lowest variability, likely indicating stable and moderate wind conditions.

The variability and extreme outliers in wind speed observed in months like March and July are critical for modeling the dispersion of radioactive materials in the event of a nuclear accident. High wind speeds can lead to rapid and far-reaching dispersion of radioactive plumes, increasing the affected area and complicating evacuation and containment strategies. Conversely, periods of lower wind speed (e.g., April or May) may result in localized accumulation, increasing exposure risks near the source.

Apart of wind speed, the stability class also plays a critical role in the dispersion of radioactive materials following a nuclear accident. Atmospheric stability determines the vertical mixing and dispersion characteristics of the atmosphere, classified into categories (A to F) based on turbulence and thermal stratification. Thus, categories from A to C represent unstable conditions with high turbulence, leading to strong mixing and faster dispersion. Category D represents neutral stability, common during overcast conditions or strong winds. Finally, categories from E and F represent stable conditions with low turbulence, leading to limited dispersion and higher localized concentrations of radioactive materials. Figure 4.7 illustrates the recurrences of stability categories and wind speeds for the current study area.

Figure 4.7 a shows the recurrence of wind speeds. Here, the wind speed range 1.6-3.5 m/s has the highest recurrence, occurring nearly 50% of the time, indicating that moderate winds are the most common conditions. Higher wind speeds (e.g., 5.6 – 10.5

m/s) have a much lower recurrence, signifying that strong winds are less frequent. Extremely low wind speeds (e.g., 0.0 – 0.5 m/s) are rare, occurring less than 5% of the time.

Figure 4.7 b shows the recurrence of atmospheric stability classes. Here, class C (unstable) has the highest recurrence (approximately 35%), indicating frequent conditions with strong vertical mixing. Categories D (neutral) and E (slightly stable) also occur frequently (25% - 30%), suggesting common conditions with moderate to low dispersion potential. Stable categories (F) have a moderate recurrence (10%), while highly unstable conditions (A and B) are rare.

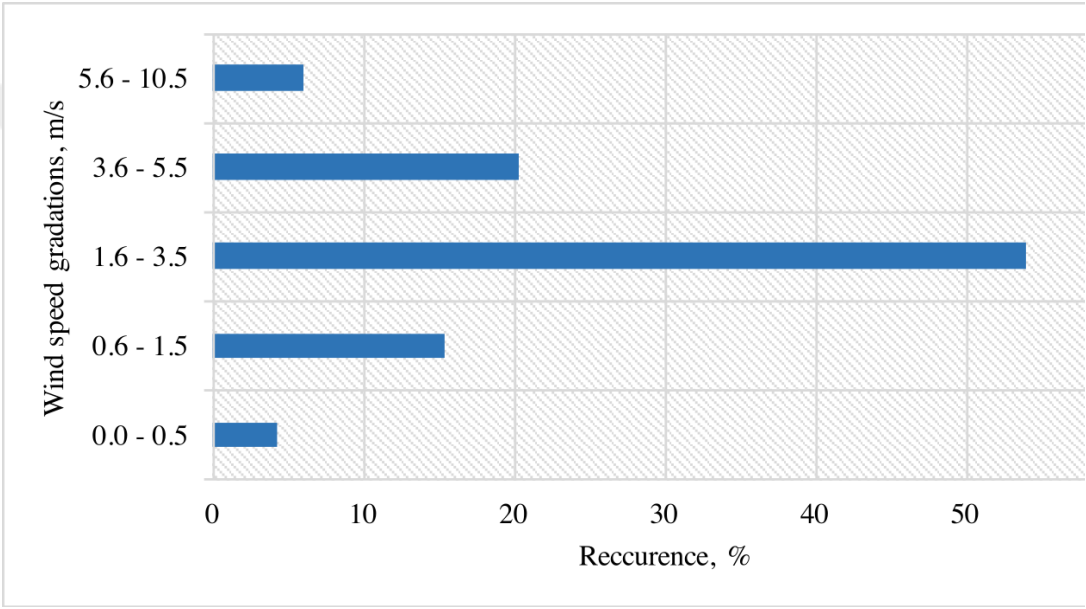

(a)

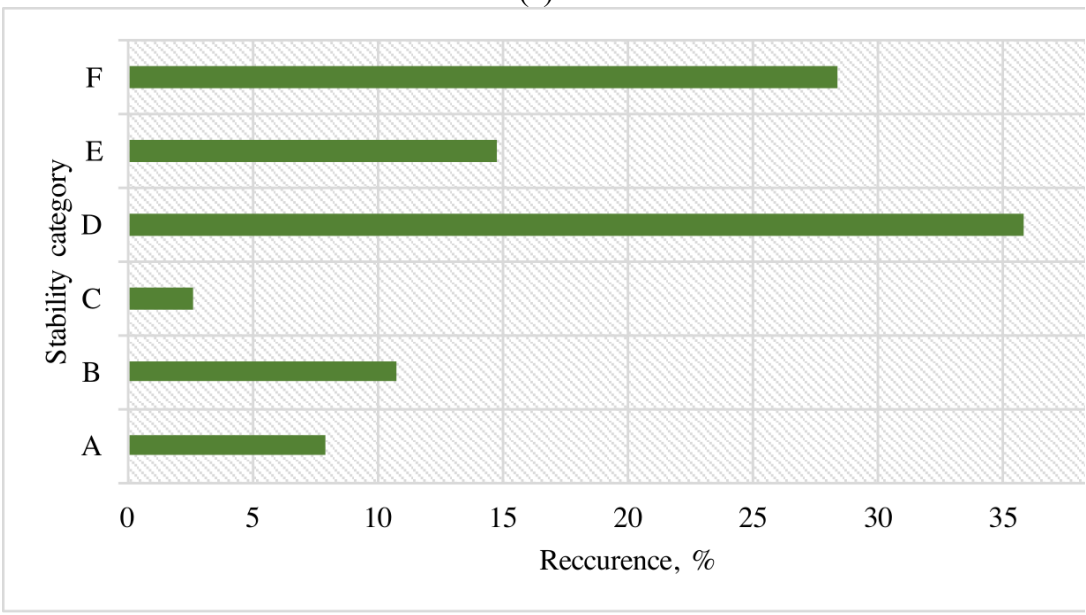

(b)

Figure 4.7 : Recurrence of atmospheric data: a) Stability categories, b) Wind speed.

4.4.1.3 Precipitation

Figure 4.8 illustrates the monthly precipitations and rainy days in the study area. The Akkuyu region receives an annual average precipitation of approximately 800 to 1,200 millimeters, with the majority of rainfall occurring between November and March. During the summer months, precipitation is minimal, often limited to isolated thunderstorms (Adiguzel 2023). Heavy rain events are rare but can lead to localized flooding in low-lying areas (Ozay and Orhan, 2023).

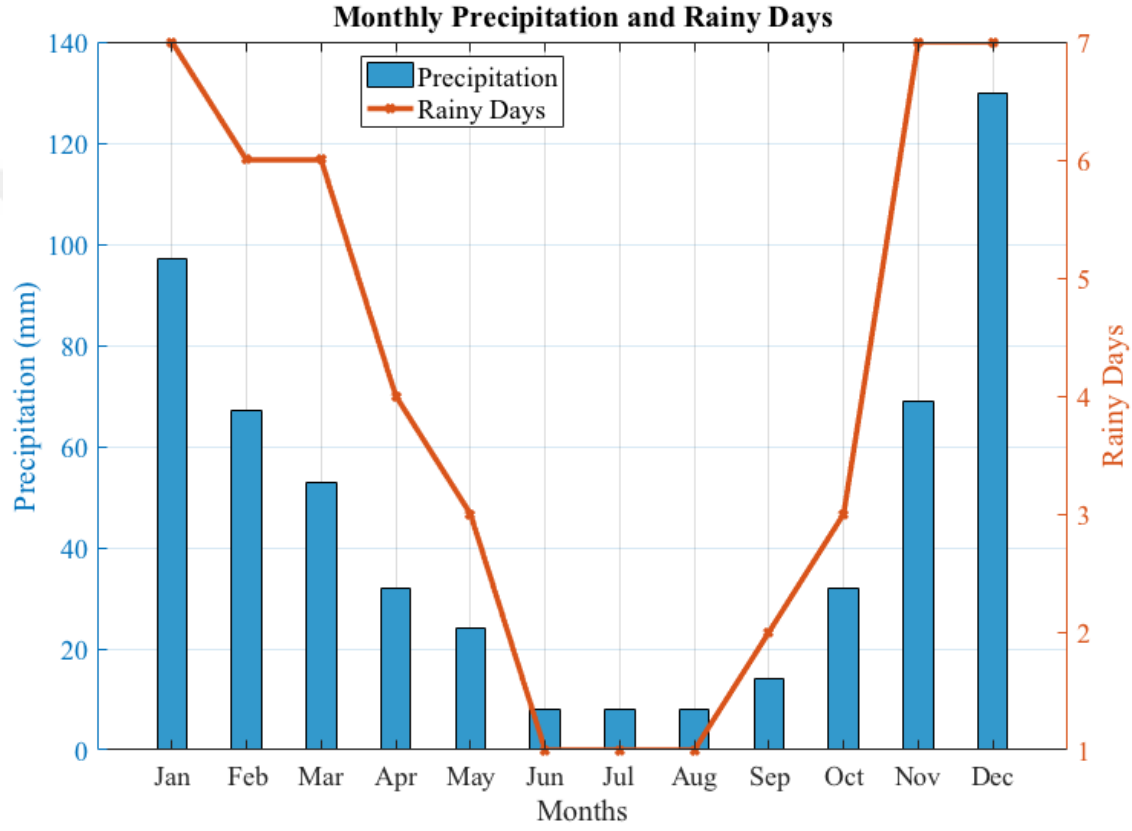

Figure 4.8 : Monthly precipitations and rainy days.

4.4.1.4 Humidity

Humidity levels in Akkuyu vary significantly between seasons. During the summer, relative humidity averages 60-70%. In winter, humidity levels can rise to 80-90% due to cooler temperatures and increased precipitation (Adiguzel 2023). Figure 4.9 shows the monthly humidity levels.

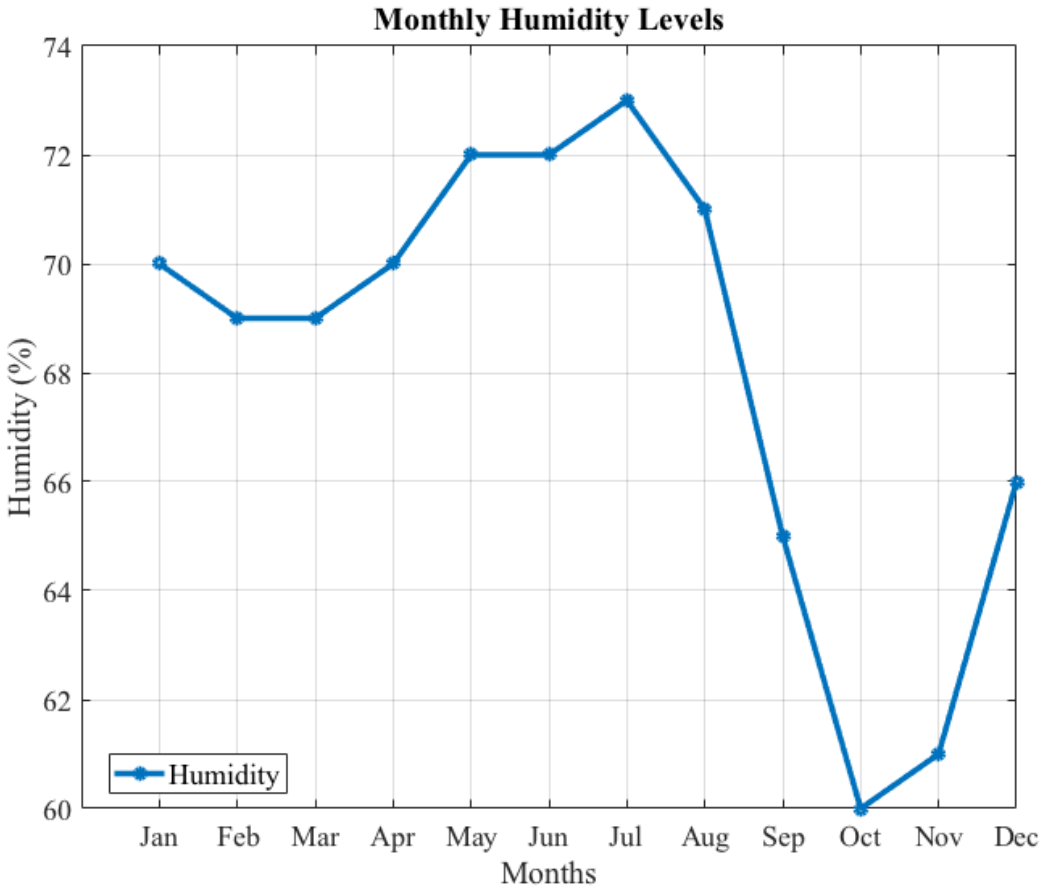

Figure 4.9 : Monthly humidity levels.

Although Akkuyu is usually protected from severe weather, it can still experience some extreme events from time to time. These include thunderstorms, especially in spring and autumn, which bring short but heavy rain. In summer, there can be heat waves with very high temperatures that increase the need for cooling water at the power plant. Storm surges are also rare but possible, caused by strong winds and changes in air pressure, so it's important to have coastal protection in place to keep the NPP safe (Kabatchenko et al., 2020).

4.4.2 Land use and agricultural activities

The Akkuyu region is characterized by a diverse array of land use and land cover (LULC) features that play a key role in shaping the local environment and agricultural activities. The landscape surrounding the Akkuyu NPP is predominantly rural, featuring a mix of agricultural lands, forested areas, and coastal ecosystems. These natural and human-modified land areas are integral to the region's ecological balance, economic productivity, and the overall sustainability of the NPP operations.

4.4.2.1 Land Use and Land Cover features

Mersin Province, including the area near Akkuyu, is known for its Mediterranean climate. This climate supports a variety of land uses, with agriculture being a primary activity in the low-lying areas (Figure 4.10).

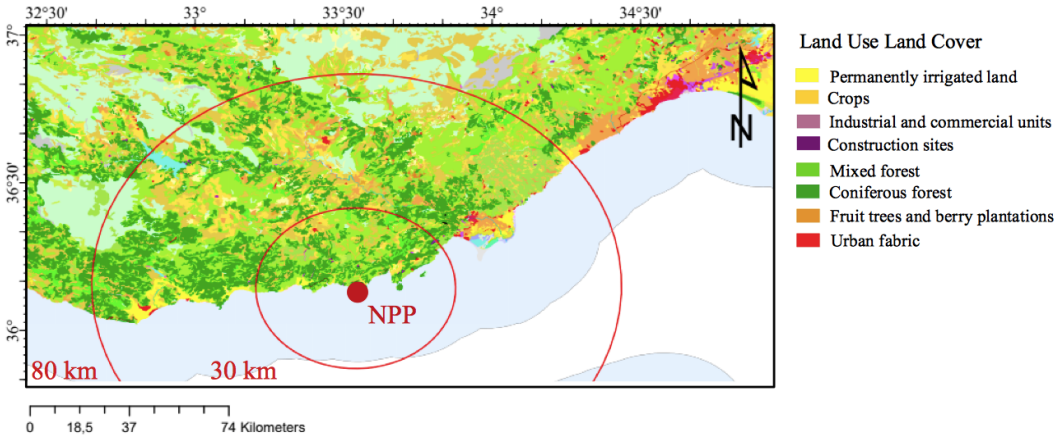

Figure 4.10 : Land Use and Land Cover of study area.

In Mersin, most of the agricultural land is found along the coastal plains, where the soil is fertile and there is good access to water for irrigation. About 33% of Mersin's land is used for farming, with a large part of it growing crops like citrus fruits, vegetables, and olives. Besides farming, the region also has large forested areas, mainly made up of pine and oak trees (Sandal et al., 2020; Iban and Sahin, 2022).

4.4.2.2 Agricultural activities in Mersin

Agriculture is very important for Mersin's economy, supporting many local families and making a big contribution to the province's GDP. Mersin is one of Türkiye's top agricultural regions, especially known for growing citrus fruits, olives, and vegetables. The fertile plains near Akkuyu, along with the Mediterranean climate, create great conditions for growing all kinds of crops. Farming in the area uses a mix of irrigation and natural rainfall, with irrigation systems helping farmers keep their crops healthy during the hot and dry summers (Orhan 2021).

Citrus fruit farming is one of the biggest agricultural activities in Mersin. The region grows a lot of oranges, lemons, and mandarins. About 50,000 hectares of land are used to grow oranges, which produce around 350,000 tons each year. Lemons are grown on about 30,000 hectares and bring in 200,000 tons annually, while mandarins are grown on 20,000 hectares and yield around 150,000 tons (Uysal et al., 2021).

Olive farming is also a major part of agriculture in Mersin, with around 25,000 hectares of olive trees producing about 40,000 tons of olives each year. These are often turned into olive oil and exported around the world. Vegetable farming is also common, with tomatoes, cucumbers, and peppers being the most popular. Tomatoes are grown on 10,000 hectares, producing around 100,000 tons a year. Cucumbers and peppers are each grown on about 5,000 hectares, with 30,000 tons of each crop harvested yearly. These vegetables are sold both locally and internationally (Bilgilioglu 2021).

Mersin also grows smaller amounts of other crops like cotton and corn. Cotton is planted on about 5,000 hectares and produces 10,000 tons per year. Corn covers roughly 4,000 hectares and gives around 15,000 tons each year. While not as large as citrus or vegetables, these crops still add value to the region's farming economy (Serim et al., 2023).

4.4.2.3 Economic and Environmental Impacts of Agricultural Land Use

Agriculture is very important for the local economy in Mersin. It makes up about 15-20% of the province's income and gives jobs to a large number of people. Around 25% of the workers in Mersin are involved in farming, raising animals, or working in food production (T.C. Çevre, Şehircilik ve İklim Değişikliği Bakanlığı, 2021).

The LULC around Akkuyu are important not only for making income but also for protecting the environment (Iban and Sahin, 2022). Farming, especially near the coast, needs to be managed carefully to avoid problems like land damage, water shortages, and pollution. Irrigation is very important for farming here. The irrigation system uses local rivers and modern technology to help grow crops even during dry weather. But now, because the Akkuyu NPP uses a lot of water, it's important to manage water use properly so that farmers still have enough.

Since farms are located close to the Akkuyu NPP, any changes in land use like new buildings or environmental effects from the plant could affect farming. For example, warm water from the plant's cooling system could harm the Mediterranean Sea's environment. This might hurt fishing and fish farming, which are also part of agriculture (Leng et al., 2024). Changes in soil or water supply could also reduce the growth of crops like citrus fruits, olives, and vegetables, which need good conditions to grow well (Xu et al., 2019)

5. RESULTS AND DISCUSSION

5.1 Social Vulnerability Index to Nuclear Accident

5.1.1 Research criteria

Figure 5.1 shows the spatial representation of the research criteria selected for the study. A region was divided into administrative units corresponding to neighborhoods. All data values were standardized using a normalization formula shown in Section 3.1.1 to ensure consistency across the study area. The normalization process adhered to methodologies established in prior research (e.g., Zurovec et al., 2017; Nazeer and Bork, 2019; Ajtai et al., 2023; Isia et al., 2023). Following normalization, the data in Figure 1 were classified into five categories: 0.00-0.20, 0.21-0.40, 0.41-0.60, 0.61-0.80, and 0.81-1.00, aligning with the approaches used in the referenced studies.

The population distribution map from Figure 5.1 a illustrates the spatial variation in population within the study area. Higher population concentrations are observed in some of the middle parts of the region, while other the areas exhibit lower populations. Figure 5.1 b and Figure 5.1 c represent the proportion of women in different areas and spatial distribution of non-married individuals, respectively. Both maps show a relatively even spread across the region, with slight variations near urban centers. Higher concentrations of illiterate individuals are observed in rural areas (Figure 5.1 d). Building density is given in Figure 1e and this map shows that densely build environments are concentrated in specific urbanized areas, whereas rural regions have sparse settlements. The agricultural land distribution (Figure 5.1 f) highlights regions where cultivation activities are dominant. The Figure 5.1 g integrates preparedness levels and coping capacity, depicting spatial variations in resilience. Areas with higher preparedness levels are generally located near urban centers, where infrastructure and emergency planning initiatives are more developed. However, more vulnerable zones with lower coping capacity are observed in rural and less accessible regions. The emergency response map (Figure 5.1 h) indicates the distribution of emergency services and estimated evacuation times. Regions with shorter evacuation times are

well-served by emergency infrastructure, while areas further from response centers exhibit prolonged evacuation durations. Overall, the spatial distribution of these factors provides a comprehensive understanding of regional vulnerabilities and strengths in the context of nuclear emergency preparedness.

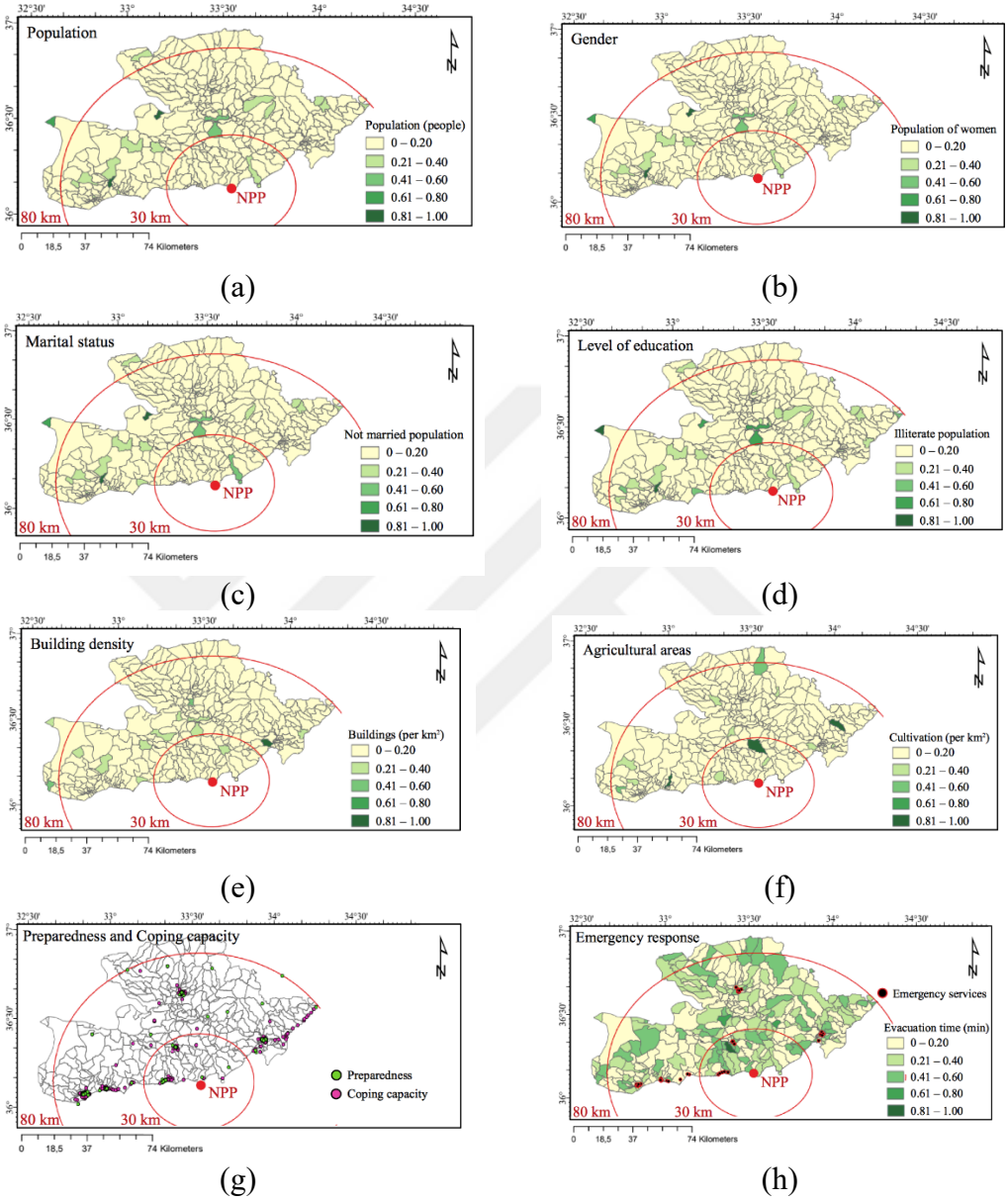

Figure 5.1 : Spatial representation of research criteria: a) Population, b) Gender, c) Marital status, d) Level of education, e) Building density, f) Agricultural areas, g) Services of preparedness and coping capacity, h) Emergency response capabilities.

5.1.2 Expert survey

The decision-making process in this study was guided by input from multiple experts, ensuring a comprehensive evaluation. In this context, an expert is defined as an individual with extensive knowledge and experience in SVI analysis and disaster

management, gained through both academic training and practical fieldwork. The development of the questionnaires was structured according to the hierarchical framework of nuclear accident vulnerability criteria. A total of 25 experts participated in the survey, primarily recruited from academic institutions. Of these, 77% were affiliated with Geomatics Engineering, encompassing specialists in GIS and Disaster Management, 14% had backgrounds in Environmental and Earth Sciences, and 9% were from Nuclear Engineering. This diverse composition facilitated a multidimensional assessment, mitigating the risk of a unilateral approach to decision-making. The responses were subsequently evaluated for consistency using the consistency ratio.

Figure 5.2 presents box plots illustrating the distribution of final weights assigned to each criterion, enabling a comparative analysis of two distinct weighting methods. Detailed descriptions of these criteria are provided in Table 5.1.

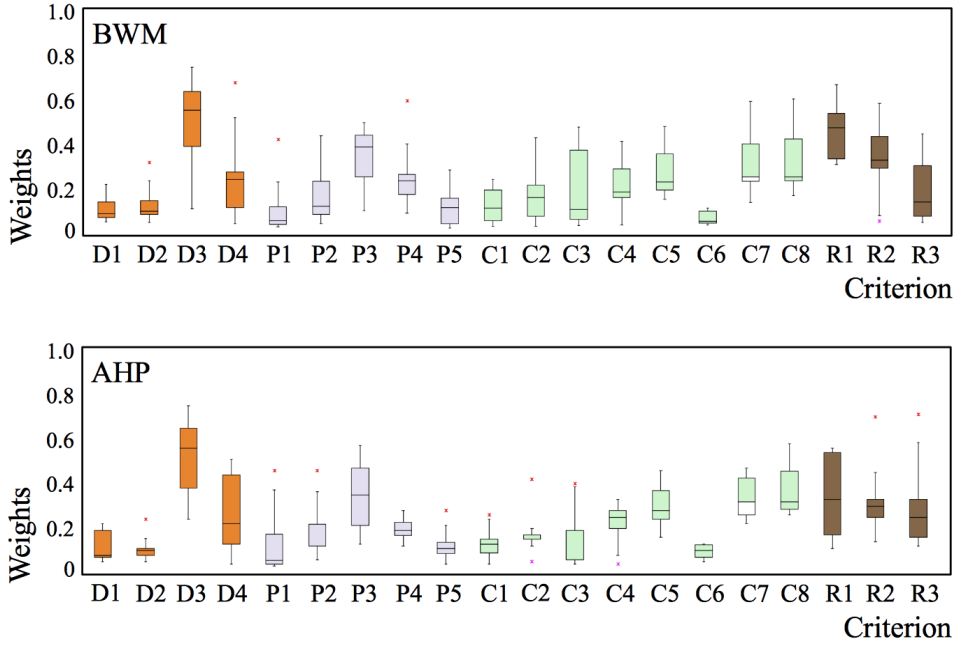

Figure 5.2 : Dispersion of weights for each criterion.

In the BWM, the assigned weights exhibit considerable variation across different criteria. Notably, criteria such as D3 and R1 receive higher weights with a broader dispersion, reflecting greater variability in their perceived significance. Conversely, criteria like P1 and P5 are associated with lower and more narrowly distributed weights, indicating a relatively lower perceived importance and a more consistent evaluation. Similarly, in the AHP, variability in weight distributions is observed,

though with some differences compared to BWM. While criteria such as D3 and R1 still retain higher weights, the overall spread of weight values may differ, reflecting methodological distinctions between the two approaches.

Table 5.1 : Description of criteria which shown in Figure 1.

Name	Description	Name	Description
D1	Gender	C2	Food/Water supply
D2	Marital status	C3	Medicine supply
D3	Population density	C4	Police
D4	Level of education	C5	Firefighter
P1	Ministry of agriculture and forestry	C6	Reception centers
P2	Meteorological services	C7	Health centers
P3	Evacuation service group	C8	Hospitals
P4	Logistic service group	R1	Preparedness
P5	Psychological support	R2	Emergency response
C1	Social participation	R3	Coping capacity

5.1.3 SVI obtained with BWM

The SVI map was developed by ranking vulnerable areas based on the factors and components detailed in Section 3.1.1. Social vulnerability is categorized into five levels: very low, low, moderate, high, and very high, which are visually distinguished using a color scale in Figure 5.3.

The demographic vulnerability map (Figure 5.3 a) reveals that the study region largely exhibits a low SVI. This outcome is influenced by factors such as a balanced gender distribution, a lower proportion of single individuals compared to married ones, a low illiteracy rate, and generally low population density. These demographic characteristics enhance the resilience of the population, reducing the potential impact of a nuclear accident. A similar pattern is evident in the building and environmental vulnerability map (Figure 5.3 b), which assesses infrastructure, land use, and environmental conditions. The findings indicate that most areas have low vulnerability levels, attributed to low-density housing. Consequently, the physical environment does not significantly heighten vulnerability in the event of a nuclear accident. The physical exposure map (Figure 5.3 f), integrating demographic and environmental data, also demonstrates predominantly low or very low SVI levels throughout the study area. Only a small portion of the region exhibits moderate to high vulnerability, suggesting that a limited number of areas are significantly affected by demographic or

environmental factors. In contrast, the preparedness, emergency response, and coping capacity maps (Figure 5.3 c, 5.3 d, 5.3 e) present the highest SVI values across the study region, exposing critical weaknesses in emergency management. The emergency response map, in particular, highlights high vulnerability due to prolonged evacuation times. In several areas, the time required for residents to evacuate exceeds the time needed for a radioactive plume to reach them, posing a serious public safety risk.

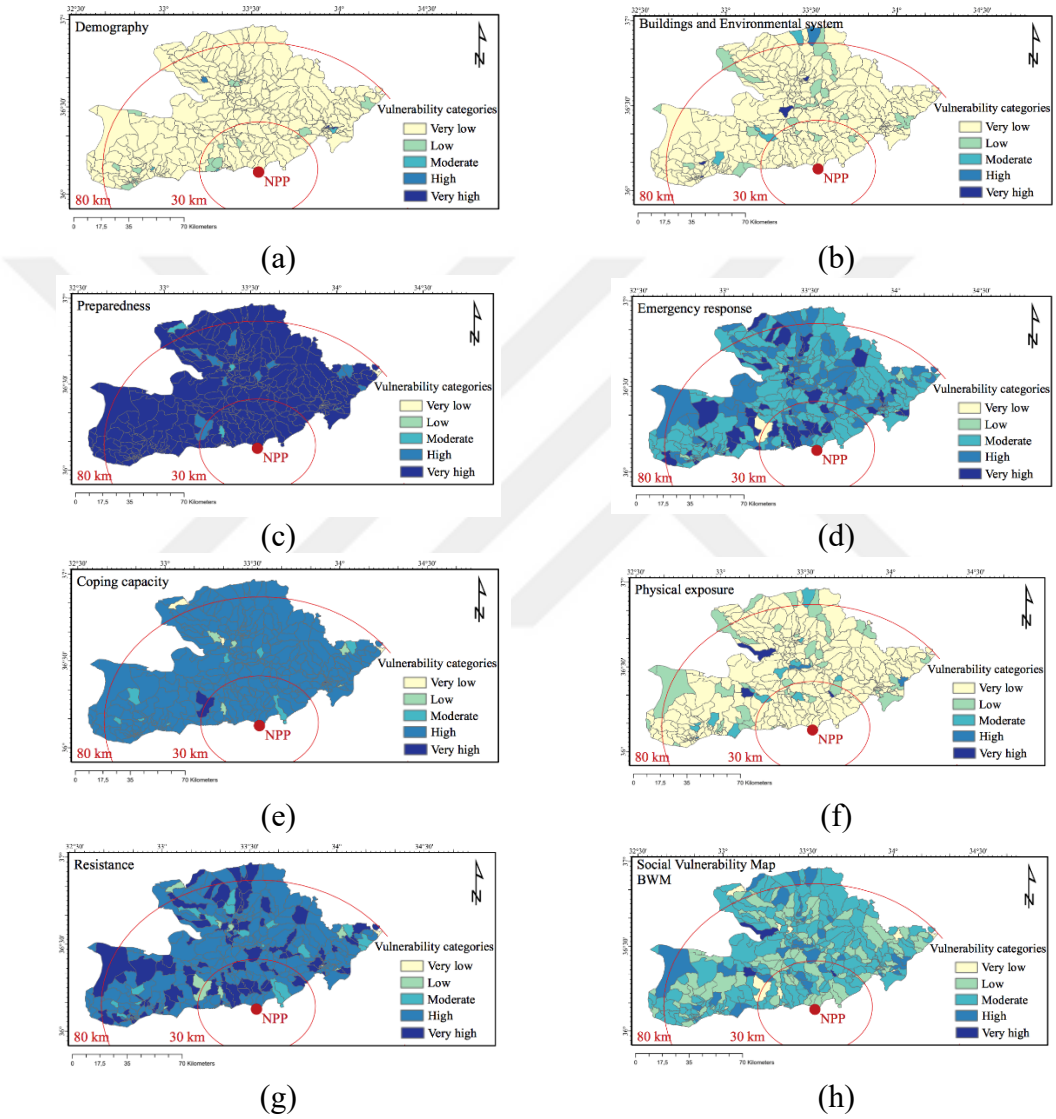

Figure 5.3 : Social vulnerability coefficient maps obtained with BWM: a) Demography map, b) Building and environmental system map, c) Preparedness map, d) Emergency response map, e) Coping capacity map, f) Physical exposure map, g) Resistance map, h) SVI map.

Furthermore, the resistance map (Figure 5.3 g), which assesses the region's ability to recover from adverse events, does not sufficiently compensate for these vulnerabilities. The high SVI values related to preparedness and coping capacity indicate that existing emergency strategies are inadequate for mitigating exposure

risks. The final SVI map (Figure 5.3 h) consolidates these insights, demonstrating that many neighborhoods within the study area are at moderate to high risk in the event of a nuclear accident.

5.1.4 SVI obtained with AHP

The SVI map, developed using the AHP method, is displayed in Figure 5.4.

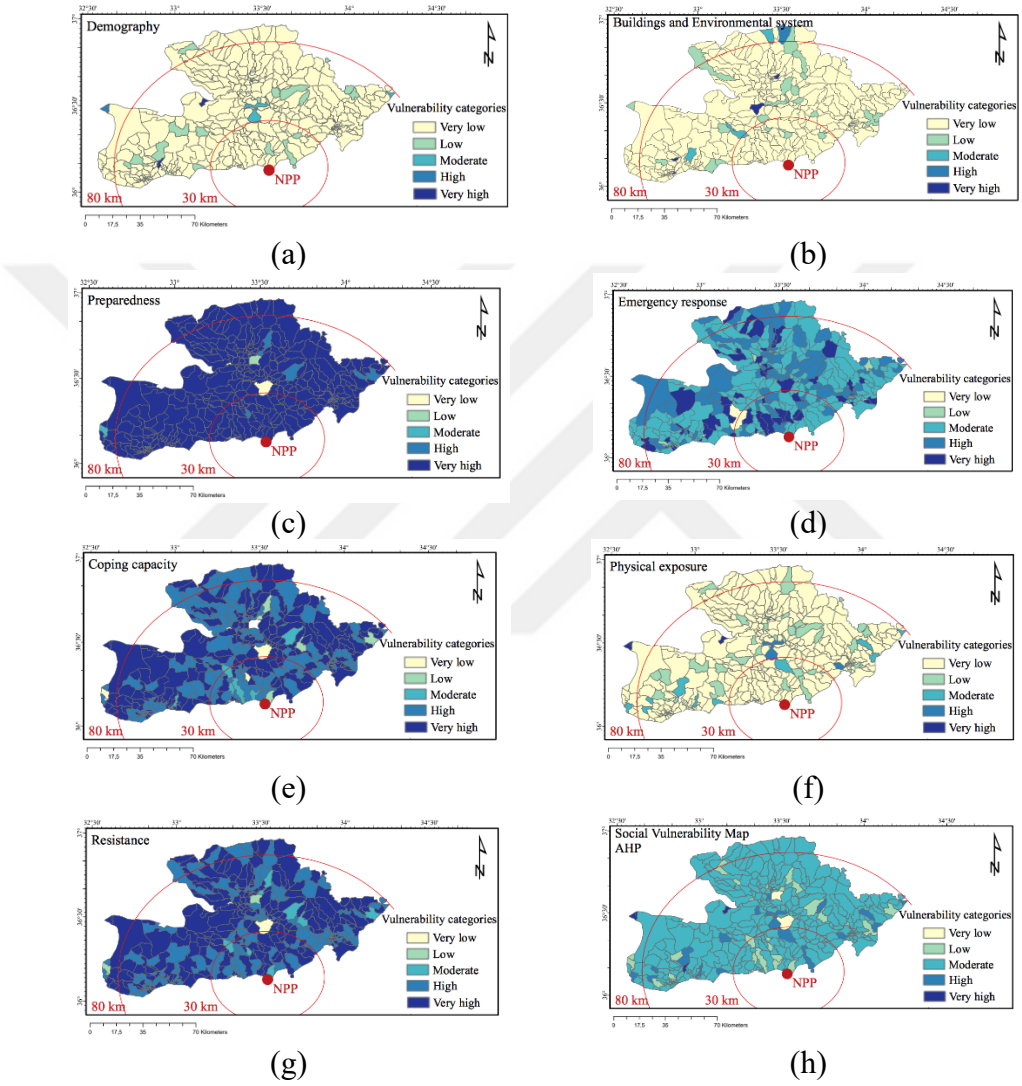

Figure 5.4 : Social vulnerability coefficient maps obtained with AHP: a) Demography map, b) Building and environmental system map, c) Preparedness map, d) Emergency response map, e) Coping capacity map, f) Physical exposure map, g) Resistance map, h) SVI map.

The physical exposure map (Figure 5.4f), which merges demographic and building/environmental maps (Figure 5.4a and 5.4b), closely aligns with results derived from the BWM. Areas with very low or low vulnerability are typically those with discontinuous urban fabric, as these zones tend to have lower population

densities, fewer structures, and reduced housing density, resulting in minimal contribution to overall social vulnerability. The resistance map (Figure 5.4g), which assesses an area's ability to endure or recover from adverse events, exhibits higher vulnerability levels than those determined by BWM. This is especially noticeable within a 30-kilometer radius of the NPP, where almost all regions are classified as highly vulnerable. Approximately 90% of the zones within this radius fall into the high or very high vulnerability categories, emphasizing the critical need for risk mitigation strategies in these areas. The final SVI map (Figure 5.4h) indicates that most regions have moderate vulnerability, with certain neighborhoods showing low vulnerability scores. Interestingly, some lower vulnerability zones are located near the NPP. This counterintuitive result can be explained by higher levels of regional development, including economic growth, dense road networks, and the presence of governmental institutions. These elements contribute to improved public infrastructure quality, thereby reducing vulnerability levels despite geographic proximity to the NPP. Economic advancements in these regions ensure better community services, enhanced disaster response capabilities, and overall resilience, mitigating potential vulnerabilities. The availability of well-developed public infrastructure, including hospitals, emergency services, and efficient transportation networks, plays a pivotal role in minimizing social vulnerability. Furthermore, well-established road networks enable faster evacuations and emergency access, while governmental institutions enhance disaster management efficiency. As a result, economically developed regions are more adept at responding to and recovering from nuclear incidents, reinforcing the necessity of ongoing infrastructure investment to reduce social vulnerability.

5.1.5 Statistical assessment

5.1.5.1 Results of Wilcoxon Signed-Rank test

To determine whether there is a statistically significant difference between the BWM and AHP methods, the Wilcoxon Signed-Rank test was conducted. The results of this test are summarized in Table 5.2.

The median values (0.42 for BWM and 0.46 for AHP) indicate that AHP generally yields higher results compared to BWM. The Z-score of 15.7 is notably large, suggesting a significant difference between the rankings of the two methods. Moreover, the p-value is below 0.001, implying that the likelihood of this difference

occurring due to random variation is less than 0.1%. Additionally, the large effect size confirms that the difference between the two methods is both statistically and practically significant.

Table 5.2 : Wilcoxon Signed-Rank test results.

Method	N	Median	Min	Max	Test statistic (Z)	p-value	Effect size (r)
BWM	347	0.42	Low	High	15.70	< .001	0.85
AHP	347	0.46	Very Low	Very High			

The observed variations in social vulnerability assessment between BWM and AHP stem from their distinct methodological frameworks. BWM relies on directly comparing the most and least important criteria, offering a stable but potentially less detailed evaluation, as it is less sensitive to minor fluctuations in ranking. In contrast, AHP involves pairwise comparisons among all criteria, providing a more detailed analysis of their relative significance. The increased sensitivity of AHP to variations in individual pairwise comparisons can lead to differing results, especially when criteria have closely ranked importance or when expert judgments exhibit slight inconsistencies. Comparative studies on BWM and AHP frequently highlight AHP's superior reliability due to its structured pairwise comparison process and built-in consistency checks. For example, Ortega et al. (2021) found that AHP produced more consistent and reproducible results in a facility location decision-making study. Likewise, Singh and Pant (2021) emphasized that AHP's ability to effectively model and validate complex decision-making structures makes it the preferred approach in multi-criteria evaluations.

5.1.5.2 Sensitivity analysis results

To evaluate the robustness of the BWM and AHP, a sensitivity analysis was conducted by adjusting the criteria weights and examining how the ranking of alternatives changed. Figure 5.5 presents a tornado diagram that illustrates the sensitivity of various factors affecting the model's output under both methods.

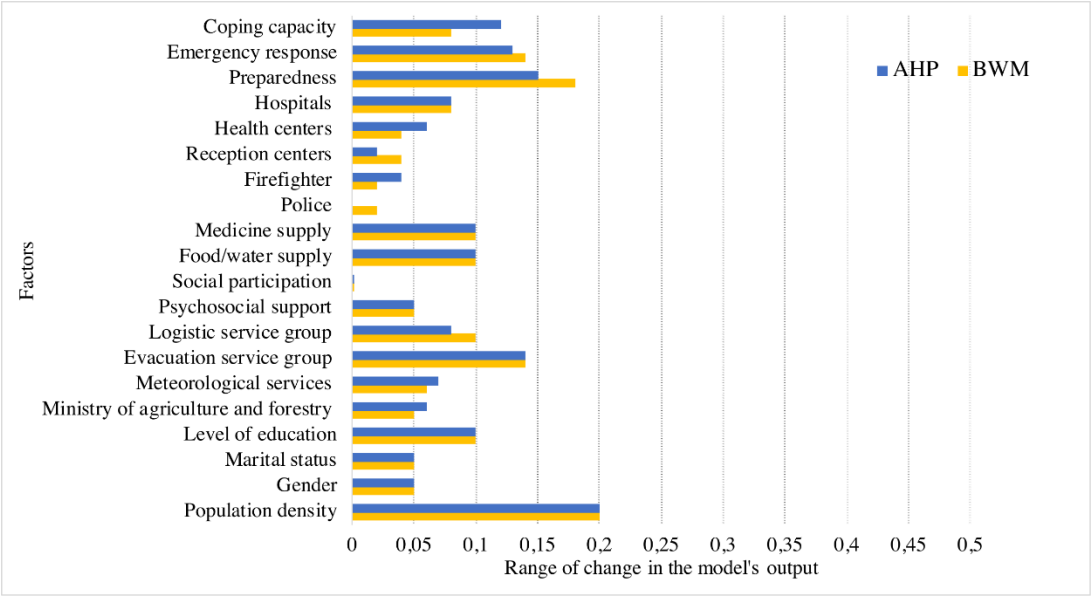

Figure 5.5 : Tornado chart.

The results indicate that coping capacity and emergency response exhibit the highest sensitivity in both methods, meaning these factors have the most substantial influence on the model's outcomes. Their critical role suggests they are essential in determining system performance under varying conditions. Additionally, the evacuation service group demonstrates relatively high sensitivity, highlighting its importance in assessing social vulnerability.

Overall, the sensitivity patterns of BWM and AHP are largely similar across most factors. However, slight variations exist in certain cases: preparedness shows higher sensitivity in BWM than in AHP, suggesting that BWM places greater emphasis on this factor. Conversely, social participation and police centers exhibit minimal impact in both methods, indicating that these factors contribute little to the overall model. These findings underscore the importance of focusing on highly sensitive factors, such as coping capacity and emergency response, in improving decision-making processes related to nuclear accident preparedness and response.

5.1.5.3 Hot and Cold spot analysis results

A hot and cold spot analysis was conducted on the composite SVI to assess the spatial correlation across the study area. The Getis-Ord Gi* statistic was applied to detect spatial clustering patterns, providing insights into regions with significantly high or low social vulnerability. Statistically significant z-scores were used to identify and visualize hot and cold spots at confidence levels of 99%, 95%, and 90%. The results

of this analysis are illustrated in Figure 5.6a and 5.6b, corresponding to the BWM and AHP methods, respectively.

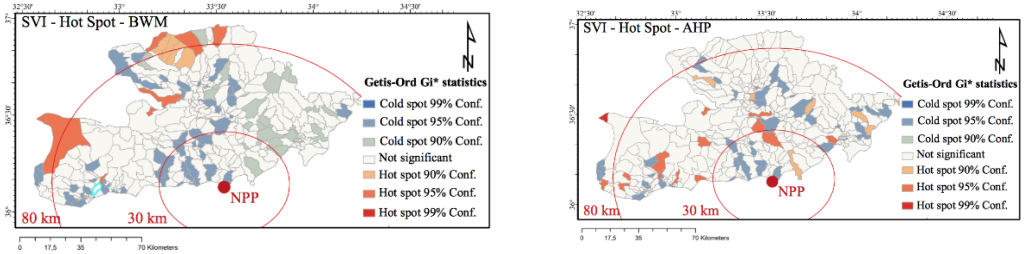

(a) (b)

Figure 5.6 : Hot and cold spots of social vulnerability: a) BWM, b) AHP.

In the maps, red areas represent statistically significant hot spots, indicating regions with a high concentration of social vulnerability at the 90% and 95% confidence levels. These areas are particularly concerning, as they highlight locations where populations are more susceptible to the impacts of a nuclear accident. Conversely, blue areas signify statistically significant cold spots, where social vulnerability is less concentrated, also identified at the 90% and 95% confidence levels. Meanwhile, gray regions exhibit no statistically significant clustering, suggesting a lack of strong spatial patterns in social vulnerability within these areas.

This analysis provides critical insights for regional planning, offering valuable information for resource allocation, risk mitigation, and policy formulation. Identifying hot spot areas allows decision-makers to prioritize interventions, such as strengthening emergency response systems, enhancing public preparedness programs, and improving infrastructure resilience in the most vulnerable regions. Furthermore, these findings underscore the need for targeted policy efforts and additional research to better understand the underlying factors contributing to social vulnerability.

5.1.6 Discussions

5.1.6.1 Significance of the SVI in the context of nuclear disaster management

The development of an SVI is particularly crucial for countries like Türkiye, where nuclear energy is being introduced for the first time. By quantifying the susceptibility of different populations to the adverse impacts of a nuclear incident, the SVI serves as a critical tool for enhancing disaster management across all phases: mitigation, preparedness, response, and recovery (Oktari et al., 2020).

In the mitigation phase, the SVI plays a vital role in identifying high-risk regions and populations that are most susceptible to nuclear accidents. It highlights areas with elevated social vulnerability, such as communities with limited healthcare access, low educational levels, and inadequate infrastructure, allowing policymakers to prioritize risk reduction strategies. Implementing targeted public awareness campaigns on nuclear safety and proactively addressing these vulnerabilities can significantly reduce the potential consequences of a nuclear disaster, thereby minimizing risks to society (Arifah et al., 2019).

Similarly, in the preparedness phase, the SVI informs the development of emergency response strategies and public safety initiatives by identifying socially vulnerable populations and enabling authorities to tailor communication, training, and resource distribution efforts accordingly. For instance, evacuation plans can be designed with special considerations for groups, such as based on age or those with mobility limitations, while the allocation of emergency resources can be optimized to ensure that shelters, medical facilities, and supplies remain accessible to those in greatest need (Oloruntoba et al., 2018).

During the response phase, the SVI becomes an essential tool for optimizing emergency interventions in the immediate aftermath of a nuclear accident. Emergency responders can use the index to prioritize aid distribution and ensure that the most vulnerable populations receive assistance first. This targeted approach could involve deploying medical teams to areas with high concentrations of vulnerable individuals or directing evacuation efforts toward regions where social vulnerability is most pronounced, thereby enhancing both the efficiency and equity of emergency response efforts (Arifah et al., 2019).

As the recovery phase begins, the SVI continues to play a crucial role by guiding long-term rehabilitation and reconstruction efforts. It helps identify communities requiring the most support to regain stability after a nuclear accident, enabling recovery strategies to be customized to meet the specific needs of vulnerable populations. Providing mental health services, restoring livelihoods, and rebuilding critical infrastructure are essential components of recovery efforts that ensure affected communities can rebuild resilience over time (Oloruntoba et al., 2018). By integrating the SVI into each phase of disaster management, policymakers and emergency

planners can make more informed decisions that ultimately reduce social vulnerability and improve resilience in the face of potential nuclear accidents.

5.1.6.2 Assessment of social vulnerability to nuclear accidents

This study utilized both the BWM and the AHP to assess social vulnerability to nuclear accidents at the neighborhood level. The analysis revealed various dimensions of vulnerability, particularly concerning the resilience capacities.

Results indicated low vulnerability scores related to physical exposure, primarily due to the geographical and demographic characteristics of these neighborhoods. Many are located in areas with low population density and sparse building distribution, which naturally results in reduced exposure to radiation and fallout in the event of a nuclear accident. Additionally, their spatial distribution that is being situated away a nuclear facility further minimizes the potential for direct exposure. These observations align with Fekete and Neuner (2023) study in Germany, which demonstrated that social vulnerability decreases with increasing distance from hazardous sites. However, despite low physical exposure, the study revealed high levels of vulnerability in terms of preparedness, response, and coping capacities. Many neighborhoods lack adequate emergency preparedness programs, such as public education on nuclear hazards, access to emergency supplies, and established evacuation routes. Similarly, local emergency response capacities are often constrained by limited resources and infrastructure, impairing their ability to act swiftly in the event of a nuclear incident. Furthermore, coping capacity is weakened by socioeconomic factors, such as inadequate healthcare access and weak social support systems. These deficiencies exacerbate overall vulnerability, despite the relatively low physical exposure risks. These findings are also consistent with previous research emphasizing the critical role of social determinants in disaster vulnerability. For instance, Cutter et al. (2003) highlighted that social factors, including socioeconomic status, significantly influence a community's ability to prepare for, respond to, and recover from disasters. Moreover, Karanci et al. (2005) underscored the importance of community engagement and psychosocial factors in enhancing disaster preparedness and resilience. The application of BWM and AHP in this study provided a nuanced understanding of social vulnerability by incorporating both quantitative and qualitative assessments. This approach aligns with the methodology employed by Lixin et al. (2014) in their analysis of social vulnerability in Tianjin, China, where multiple criteria decision-making

techniques were utilized to capture the complex interplay of factors contributing to vulnerability.

5.1.6.3 Key findings and policy implications

The results of this study highlight the complex and layered nature of social vulnerability in the context of nuclear accidents. Notably, limited physical exposure does not automatically translate to lower overall vulnerability. The identified weaknesses in preparedness, emergency response, and coping capacity point to critical areas where improvements are needed. To enhance neighborhood-level resilience, efforts should focus on practical measures such as community education initiatives to raise awareness of nuclear risks, improved access to emergency facilities and services, and the development of tailored disaster management strategies that reflect the specific characteristics and needs of each community. Strengthening these components could play a significant role in reducing vulnerability and enhancing public safety in areas at risk of nuclear incidents.

5.1.6.4 Comparison with existing literature

The findings of this study align with previous research emphasizing the critical role of socioeconomic, physical, and resistance factors in shaping social vulnerability. Demographic characteristics, such as high population density, a high percentage of women, and low educational levels, have been consistently identified as key contributors to vulnerability (Kumar & Bhattacharjya, 2020; Furlan et al., 2021; Ajtai et al., 2023). Additionally, building density and land use patterns significantly influence social vulnerability, as areas with high building concentrations tend to face greater risks (Shafapourtehrany et al., 2022; Zurovec et al., 2017). Beyond structural and demographic factors, a community's coping capacity, response, and preparedness are crucial in determining its overall vulnerability, shaping its ability to mitigate, adapt to, and recover from nuclear disasters (Isia et al., 2023).

5.1.6.5 Methodological considerations: BWM vs. AHP

Understanding the methodological differences between AHP and BWM is essential for accurately interpreting SVI results. The AHP method often produces higher vulnerability scores due to its pairwise comparison process, which can amplify subjective biases and increase sensitivity to criteria weighting (Abdrabo et al., 2023;

Xie & Meng, 2023). In contrast, BWM utilizes a more streamlined weighting approach, typically resulting in more balanced and moderate vulnerability assessments (Debnath et al., 2023).

5.1.6.6 Limitations and future research directions

Several limitations should be considered when interpreting the findings. Both BWM and AHP depend on expert judgment, making them susceptible to subjectivity, as variations in expertise, personal biases, or cognitive tendencies can lead to inconsistencies in criteria weighting (Kazibudzki, 2021; Starczewski, 2023). To enhance robustness, future research should explore hybrid decision-making models that combine qualitative expert input with quantitative machine learning techniques. Another challenge lies in validating SVI predictions, as limited real-world data exist to directly correlate SVI scores with actual disaster outcomes (Bakkensen et al., 2017). Conducting case studies or retrospective analyses of past nuclear incidents, such as Fukushima and Chernobyl, could help assess the predictive accuracy of SVI models (Rufat et al., 2019). Additionally, spatial and temporal limitations must be acknowledged. While neighborhood-level data facilitate regional analysis, they may obscure finer-scale variations in social vulnerability (Tate, 2012; He & Guan, 2024). Future research could integrate high-resolution demographic and mobility data or apply time-series modeling to capture the dynamic evolution of social vulnerability over time (Fekete, 2019).

5.2 Hazard Mapping

5.2.1 Simulation of Cs-137 release using GPM

HotSpot is a rapid assessment software developed by Lawrence Livermore National Laboratory (LLNL) for evaluating the radiological consequences of nuclear incidents (Kundu et al., 2022). The software employs Gaussian plume dispersion modeling, which allows for quick screening of radiation dose impacts from point or area sources. HotSpot is designed for emergency response and safety planning, providing near-instantaneous dose estimates for various release scenarios, including reactor accidents, RDDs, and nuclear detonations. The deposition calculations in HotSpot consider particle size, weather conditions, and fallout characteristics, while concentration estimations provide airborne radioactivity levels at different distances. TEDE

calculations integrate both external exposure (from ground shine and plume immersion) and internal exposure (from inhalation of radioactive material) to assess the total radiation dose received by individuals in affected areas (Zubair et al., 2022). The software requires several key input parameters related to the source term, meteorological conditions, and terrain characteristics, as summarized in the Table 5.3.

Table 5.3 : Input parameters for HotSpot software.

Category	Parameter	Units	Used values
Source term	Radionuclide type	-	Cs-137
	Activity released	Bq or Ci	1×10^{17}
	Particle size	μm	2
	Release height	m	40
	Release duration	S or Min	2 days
Meteorology	Wind speed	m/s	2
	Wind direction	Degree	0-337.5
	Atmospheric stability	From A to F	D
	Precipitation rate	mm/hr	0.20
Terrain and site	Ground roughness	m	0.1
	Deposition velocity	m/s	0.01
Exposure and dose	Inhalation rate	m^3/hr	0.5
	Shielding factor	-	1.0

Parameters under the Source Term category describe the characteristics of the radioactive release, such as the radionuclide type, which specifies the isotope involved (e.g., I-131, Cs-137), and the activity released, which represents the total radioactivity in becquerels (Bq) or curies (Ci). The particle size influences deposition behavior, with smaller particles remaining airborne longer, while the release height determines how far and how fast the plume disperses. The release duration defines the time over which the radioactive material is emitted, affecting concentration levels. The Meteorology section includes parameters like wind speed and direction, which control plume movement, and atmospheric stability, categorized by the Pasquill-Gifford stability classes (A – F), which affect turbulence and dispersion. Precipitation rate influences wet deposition, where rainfall removes radioactive particles from the atmosphere. The Terrain and Site parameters account for environmental factors, such as ground roughness, which impacts dispersion, and deposition velocity, which determines how quickly particles settle onto surfaces. Finally, the Exposure and Dose parameters include inhalation rate, which affects internal dose calculations based on human

breathing rates, and shielding factor, which accounts for the attenuation of radiation by buildings or terrain, reducing external exposure.

The particle size for Cs-137 depends on the source and release conditions, but typical values used in atmospheric dispersion models like HotSpot fall within the range of: 0.3 – 5 μm for aerosolized Cs-137 (e.g., from reactor accidents or fallout), 1 – 10 μm for resuspended Cs-137 from soil or contaminated surfaces, and 10 – 100 μm for larger fallout particles near the release site. For nuclear accidents like Chernobyl and Fukushima, the dominant Cs-137 particle size was found to be around 0.4 – 1.4 μm and 0.25 – 0.71 μm, respectively, meaning it remained airborne for long distances and deposited gradually (Ogorodnikov et al., 1998; Muramatsu et al., 2015). For Cs-137 and a precipitation rate of 0.20 mm/hr, the deposition velocity is influenced by both the particle size and the rainfall rate. Typically, Cs-137 particles in aerosolized form have a deposition velocity ranging from 0.001 to 0.1 m/s. Smaller particles, around 0.5 – 2 μm, which are common for Cs-137 in fallout scenarios, tend to have a deposition velocity on the lower end of this range. With a precipitation rate of 0.20 mm/hr, considered light to moderate rainfall, deposition velocity for Cs-137 might range from 0.005 to 0.02 m/s (Sportisse 2007).

The inhalation rate refers to the volume of air an individual breathes per unit of time, which is crucial for calculating the internal dose from inhaled radioactive particles. For adults, the typical inhalation rate ranges from 0.5 to 1.5 m^3/hr, with values higher during physical exertion and lower at rest (US EPA 2011). The shielding factor accounts for the reduction in radiation exposure due to barriers such as buildings or terrain. A shielding factor of 1 indicates no shielding, meaning the person is exposed to radiation without any attenuation, while lower values represent varying degrees of protection. In this PhD research, the inhalation rate was set for adults, and the shielding factor was chosen to be 1, assuming no shielding effects in the open environment for simplicity.

Ground roughness refers to the texture and structure of the Earth's surface, which influences the dispersion of airborne radioactive particles. It is typically represented by the roughness length, which affects the turbulence and vertical mixing of the atmosphere. Lower values (e.g., 0.001 m) are used for smooth surfaces like oceans or flat fields, while higher values (e.g., 1.0 m) are applied to urban or densely forested areas with significant obstacles (Di Nicola et al., 2022). For the Akkuyu region, the

terrain surrounding the facility is a mix of coastal plains and agricultural land, with relatively flat and open areas. Therefore, a moderate ground roughness value of around 0.1 m was found to be suitable for modeling atmospheric dispersion in this region, reflecting the mixed rural environment with some vegetation but no significant urban structures.

The results of simulation are shown in Figure 5.7 for air concentration, TEDE, and ground deposition as function of distance, respectively.

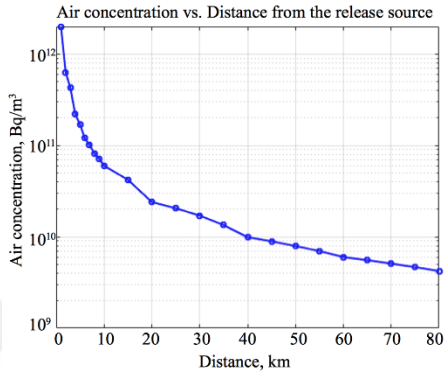

(a)

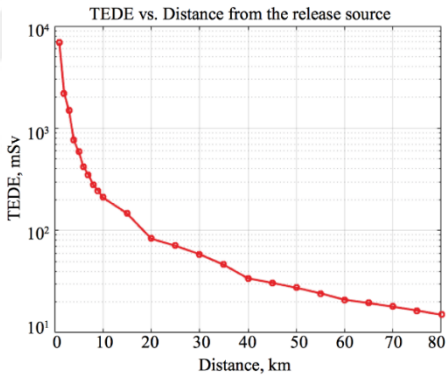

(b)

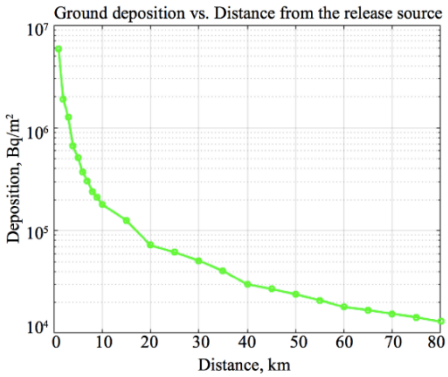

(c)

Figure 5.7 : Results of simulation: a) Air concentration, b) TEDE, c) Ground deposition.

Graphs on Figure 5.7 illustrate how radiation exposure (TEDE), airborne radioactive concentration, and ground deposition decrease as the distance from the release source increases. The Air Concentration (Bq/m³) vs. Distance graph (Figure 5.7a) represents how much radioactive material remains suspended in the air. At 1 km, the concentration is 2.00×10^{12} Bq/m³, posing a severe inhalation hazard. As the distance increases, the concentration declines, dropping to 4.20×10^{9} Bq/m³ at 80 km, indicating that individuals closer to the release site inhale significantly more radioactive particles, while those further away face much lower exposure. The TEDE vs. Distance graph (Figure 5.7b) shows the radiation dose a person would receive at different distances. Close to the release site, at around 1 km, the dose is extremely high (~6900 mSv), which is lethal. As distance increases, the dose drops significantly, reaching about 15 mSv at 80 km, following an inverse relationship where exposure decreases the farther one moves from the source. The Ground Deposition (Bq/m²) vs. Distance graph (Figure 5.7c) illustrates how much radioactive material settles on surfaces. At 1 km, deposition is around 5.90×10^{6} Bq/m², meaning the contamination of soil and surfaces is highest near the source. By 80 km, deposition decreases to 1.30×10^{4} Bq/m², showing that while contamination spreads over long distances, its intensity significantly diminishes. Therefore, the maximum deposition occurs at 1 km with 5.90×10^{6} Bq/m², while the lowest deposition, 1.30×10^{4} Bq/m², is observed at 80 km. Similarly, the highest airborne concentration, 2.00×10^{12} Bq/m³, is found near the release, while the lowest value, 4.20×10^{9} Bq/m³, is recorded at the farthest distance.

International and national nuclear emergency response guidelines establish different TEDE thresholds for protective actions such as sheltering, evacuation, and relocation. The IAEA recommends sheltering when TEDE is 10-50 mSv, evacuation when TEDE exceeds 50 mSv, and long-term relocation for TEDE levels above 100 mSv over the first year (IAEA, 2011). These thresholds are generally followed by national authorities, though some variations exist. For instance, EPA sets a lower evacuation threshold of 10 mSv over four days (EPA, 2017), while the Japanese post-Fukushima guidelines align closely with IAEA recommendations but apply a 20 mSv threshold for long-term relocation (NRA, 2013). European countries such as France, Germany, and the UK also adopt the 10–50 mSv range for sheltering and 50 mSv for evacuation, with a long-term relocation threshold of 100 mSv (ASN, 2021; SSK, 2014; PHE,

2019). The Russian guidelines (NRB-99/2009) and Türkiye's Nuclear Regulatory Authority (TAEA/NDK) follow similar thresholds to the IAEA, ensuring consistency in nuclear emergency planning (NRB-99/2009; TAEA, 2019). The Table 5.4 summarizes the TEDE limits used by different agencies and countries for protective actions. These thresholds serve as the basis for emergency planning and protective action decision-making in nuclear incidents. While international standards provide general guidance, national frameworks may adjust these levels based on local risk assessments, regulatory frameworks, and historical nuclear events.

Table 5.4 : Country-specific guidelines on emergency response.

Country/Agency	Sheltering (mSv)	Evacuation (mSv)	Relocation (mSv)	Reference
IAEA	10-50	>50	>100	IAEA, 2011
U.S. EPA	>10	10-50	>20	EPA, 2017
Japan (Post Fukushima)	10-50	>50	>20 (long-term)	NRA, 2013
France	10-50	>50	100	ASN, 2021
Germany	10	50	>100	SSK, 2014
UK	10	>30	100	PHE, 2019
Russia	10	>50	>100	NRB-99/2009
Turkiye	10-50	>50	100	TAEA, 2019

Based on the results and aligning with the emergency planning guidelines indicated in Table 5.4, evacuation is necessary within the 0 – 30 km zone due to the high levels of radiation exposure and associated health risks. Beyond this area, in the 30 – 80 km zone, sheltering is recommended as a protective measure to minimize radiation exposure while allowing for a more controlled response.

5.2.2 Simulation of Cs-137 release using particle filter integrated with terrain-modified GPM

Based on the wind data described in Section 4.4.1.2, three different meteorological scenarios were selected to understand how varying wind conditions affect the spread of radioactive materials. The first scenario reflects unstable, moderate wind conditions, with an average wind speed of 6 m/s and stability class C that is typical for winter. The second scenario represents stable, low wind conditions, with an average wind speed of 3 m/s and stability class E, which often occur during the summer. The third scenario simulates unstable, high wind conditions, with an average wind speed of 14 m/s and stability class A, meant to capture rare but extreme wind events. To better understand

how weather affects dispersion, rainfall was also included in each scenario. Other parameters such as source term were chosen as listed in Table 5.3. For model inputs, three months of historical hourly wind speed data was used. A three-month period was selected because it balances practical needs and scientific relevance for nuclear emergency planning, which focuses on short-term forecasts. Longer-term datasets might be better for general risk studies but are less useful for real-time decision-making in a crisis. This wind data was used in a PF model, which helps estimate real-time wind speed by combining observations with uncertainty handling. The wind speeds predicted by the PF model were then used as inputs for the TM-GPM, which calculated how radioactive materials spread in the air. The analysis was limited to a 10-kilometer radius around the plant, which represents the plume exposure zone. This is the area at highest risk for immediate radiation effects and where fast protective actions, like evacuation or sheltering, are most critical.

Figures 5.8, 5.9, and 5.10 show how Cs-137 concentration at ground level changes over time and distance from the NPP, using a log scale to make the patterns easier to see.

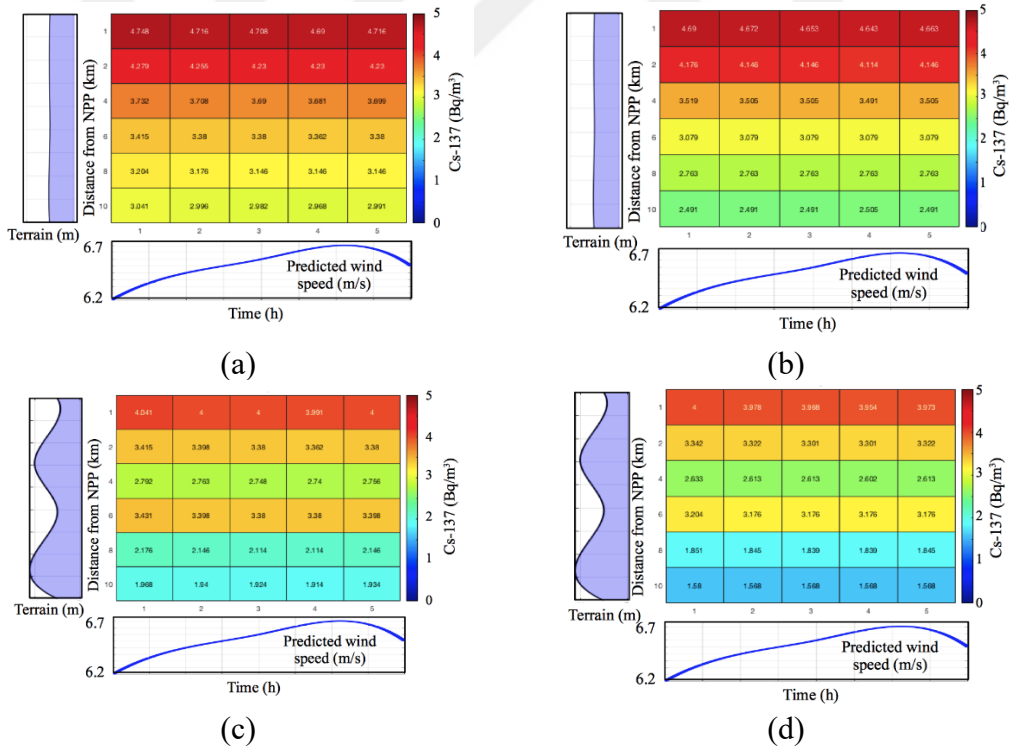

Figure 5.8 : Cs-137 ground-level log-transformed concentration values over time and distance (first scenario): a) no terrain and no rain, b) no terrain with rain, c) terrain and no rain, d) terrain with rain.

In the flat terrain and no-rain conditions (Figures 5.8a, 5.9a, 5.10a), the highest Cs-137 levels are found close to the NPP, with concentrations gradually decreasing as you move further away. This is a typical pattern predicted by GPM, where pollutants spread outward and become more diluted under steady wind conditions.

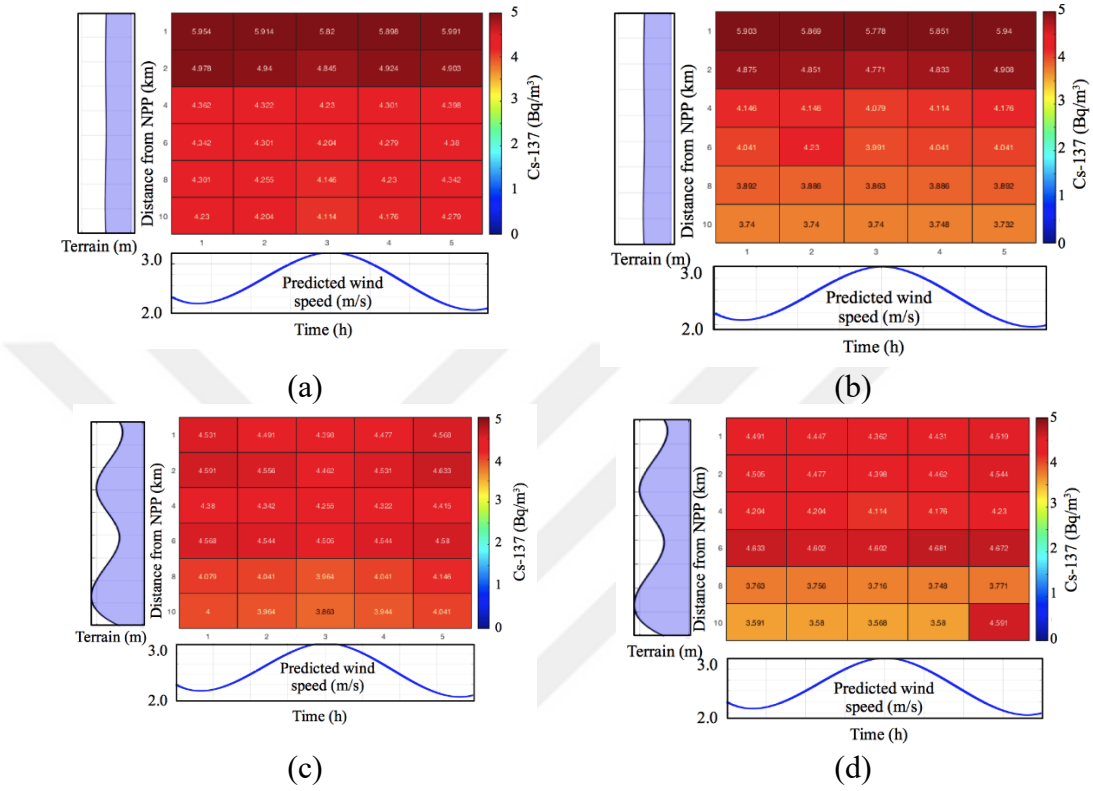

Figure 5.9 : Cs-137 ground-level log-transformed concentration values over time and distance (second scenario): a) no terrain and no rain, b) no terrain with rain, c) terrain and no rain, d) terrain with rain.

When rainfall is added (Figures 5.8b, 5.9b, 5.10b), the concentration drops more quickly. This is because rain helps remove radioactive particles from the air, depositing them on the ground. These results are similar to what was seen after the Chernobyl and Fukushima accidents, where rain played a key role in reducing airborne contamination and increasing ground deposition (Stepanenko et al., 2002; Kinoshita et al., 2011; Yasunari et al., 2011; Kalkan et al., 2021).

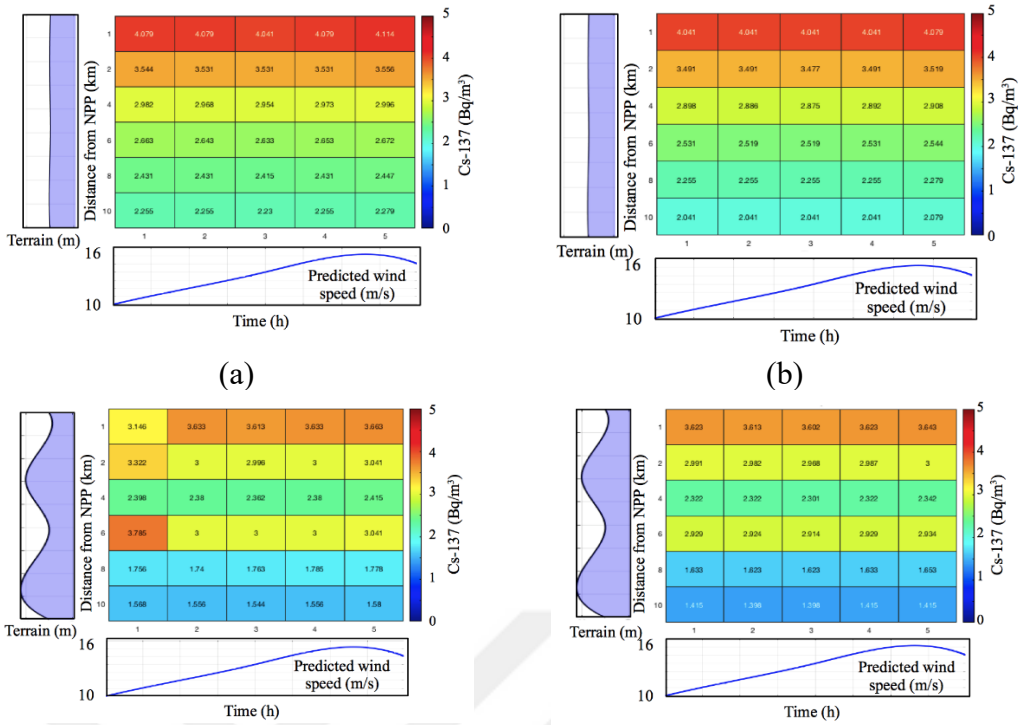

Figure 5.10 : Cs-137 ground-level log-transformed concentration values over time and distance (third scenario): a) no terrain and no rain, b) no terrain with rain, c) terrain and no rain, d) terrain with rain.

Adding terrain to the model (Figures 5.8c, 5.8d, 5.9c, 5.9d, 5.10c, 5.10d) makes the dispersion pattern more complex. In areas with higher elevation, the plume spreads and dilutes faster due to factors like increased vertical mixing, turbulence, and uplift caused by slopes (orographic effects). This results in lower Cs-137 concentrations in hilly areas. In contrast, valleys tend to collect radioactive particles especially when rain is present. This happens because valleys often have lower wind speeds, more water runoff, and airflow patterns that trap pollutants. Similar outcomes have been reported in previous studies from mountainous regions, where contaminants often accumulate in low-lying zones (Giovannini et al., 2020; Liao et al., 2025).

In some terrain-included cases (e.g., Figures 5.8c, 5.9c, 5.10c), a sharp drop was observed in concentration near the NPP, showing how terrain can interrupt the usual plume shape. When rain is included (Figures 5.8d, 5.9d, 5.10d), this effect becomes even more noticeable. Radioactive particles tend to wash off hillsides and settle in valleys, leading to uneven contamination patterns. This behavior has also been

documented after the Chernobyl accident, where Cs-137 was found to build up in floodplains and other low-lying areas (Ivanov et al., 2026; Mamikhin et al., 2016).

Wind speed also affects how the radioactive material spreads. In the second scenario (Figure 5.9), the wind is weaker and more variable, which leads to less predictable plume movement and higher concentrations closer to the source. In contrast, in the moderate and high wind scenarios (Figures 5.8 and 5.10), the wind is stronger and more stable. This helps transport the Cs-137 further away from the NPP, but it also spreads it out more, resulting in lower concentrations in individual areas.

5.2.3 Model assessment

To check the performance of PF-based wind speed prediction model, a cross-validation was used. For this, such standard error metrics as root mean square error (RMSE), mean absolute error (MAE), the coefficient of determination R^2, and Pearson's correlation coefficient were calculated.

The RMSE measures the average size of the prediction errors, but it gives more weight to larger errors since it uses squared differences. It is calculated using Equation 5.1:

$$RMSE = \sqrt{\frac{1}{n}\sum_{i=1}^{n}\left(y_i - y_i^p\right)^2} \tag{5.1}$$

where y_i represents observed values and y_i^p represents predicted values.

MAE, on the other hand, gives the average of the absolute differences between predicted and actual values. It treats all errors equally and is easier to interpret. It is given by Equation 5.2:

$$MAE = \frac{1}{n}\sum_{i=1}^{n}\left|y_i - y_i^p\right| \tag{5.2}$$

where y_i and y_i^p represents measured and predicted values, respectively.

R^2 shows how well the predicted values match the observed data in terms of explained variance. A value close to 1 means the model fits the data very well. It is calculated as in Equation 5.3:

$$R^2 = 1 - \frac{\sum\left(y_i - y_i^p\right)^2}{\sum(y_i - y^m)^2} \tag{5.3}$$

where y_i and y_i^p represents measured and predicted values, respectively, and y^m is the mean of the observed values.

Finally, Pearson's correlation coefficient tells how strongly the predicted and observed values are related in a linear sense. Values close to +1 mean there is a strong positive correlation. It is calculated using Equation 5.4:

$$r = \frac{\Sigma(y_i - y^m)(y_i^p - y_m^p)}{\sqrt{\Sigma(y_i - y^m)^2}\sqrt{\Sigma(y_i^p - y_m^p)^2}} \tag{5.4}$$

where y_i and y_i^p represents measured and predicted values, respectively; y^m is the mean of the observed values; y_m^p is the mean of predicted values.

The performance results are summarized in Table 5.5.

Table 5.5 : Statistical results of model evaluation.

RMSE	MAE	R^2	r
0.1620	0.0940	0.9770	0.9880

Figure 5.11 supports these findings visually. In Figure 5.11a, the predicted and observed wind speed values over time are shown. The two curves align closely, indicating that the model accurately follows real wind speed patterns. Figure 5.11b shows a scatter plot of predicted versus observed values. The points are tightly clustered along the diagonal line, with a correlation of 0.99, highlighting the strong agreement between actual and predicted data. Overall, these results confirm the model's effectiveness for short-term wind speed forecasting.

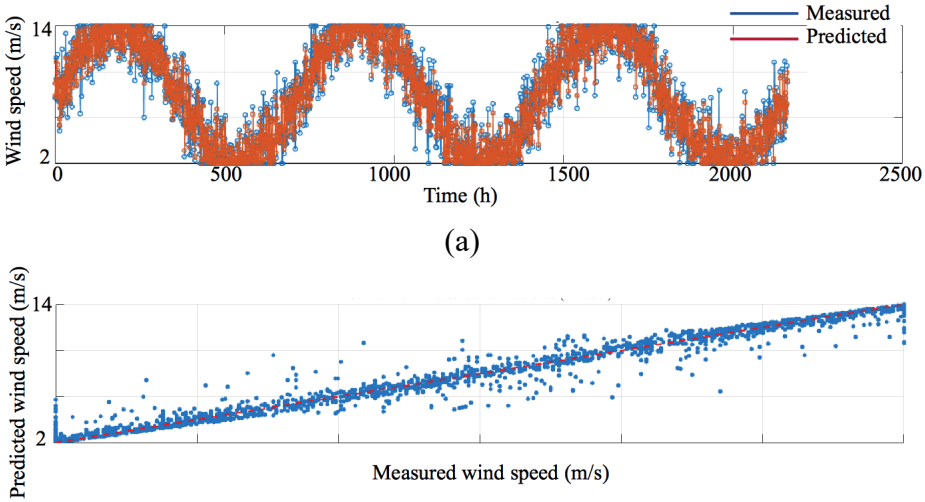

Figure 5.11 : Cross-validation of wind prediction using PF: a) Plot of measured versus predicted values of wind speed, b) Correlation plot between measured and predicted wind speed values.

The one-sample Kolmogorov-Smirnov test (KS) was then used to check whether the error values from the wind speed predictions follow a normal distribution. The test works by comparing the empirical cumulative distribution function (ECDF) of the sample errors with the cumulative distribution function (CDF) of a normal distribution that has the same mean and standard deviation as the sample. The main test statistic, D, measures the largest difference between these two distributions. This helps us understand how far the sample data deviate from a normal distribution. The p-value tells us if this difference is statistically significant. Also, the K statistic was included, which adjusts the D value for the sample size ($K = D\sqrt{n}$), giving a more normalized measure of deviation. The test results are shown in Table 5.6.

Table 5.6 : Results of the KS test.

D-statistics	K-statistics	p-value
0.0102	0.4564	0.9840

Based on these results, the D value is very small (0.0102), and the p-value is 0.9840, which is much greater than the commonly used threshold of 0.05. This means one fails to reject the null hypothesis, in other words, there is no strong evidence that the error values deviate from a normal distribution. The low D and K values support this conclusion, showing only a small difference between the actual and expected distributions and suggesting that the sample size did not exaggerate this difference. Overall, the KS test confirms that the errors from the wind speed prediction model are approximately normally distributed. To visually support this result, two plots were created: a histogram of the error values with a fitted normal curve (Figure 5.12a) and a quantile-quantile (Q-Q) plot (Figure 5.12b). These plots help further demonstrate that the error distribution closely follows a normal pattern.

The histogram of the error values (Figure 5.12a) shows the distribution of the prediction errors and gives a visual sense of how the errors are spread. A normal distribution curve is overlaid to help visually compare the actual error distribution with a theoretical normal distribution. Similarly, the Q-Q plot (Figure 5.12b) compares the quantiles of the observed errors with those of a normal distribution. If the points in the Q-Q plot lie close to the 45-degree line, it indicates that the error distribution is approximately normal.

(a)

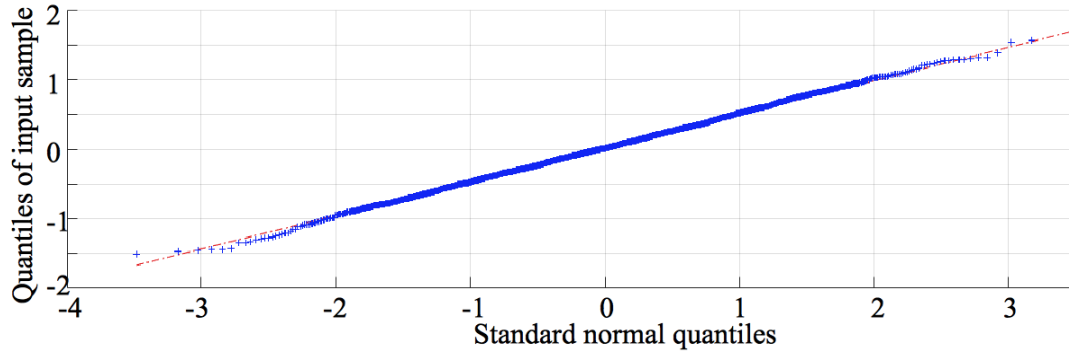

(b)

Figure 5.12 : Results of KS test: a) Histogram of errors, b) QQ plot of errors.

To evaluate the performance of the wind speed prediction model, a k-fold cross-validation was applied. This method helps prevent overfitting and gives a better idea of how well the model performs on unseen data. It is particularly useful for time-series data, like in this study, where data points are influenced by their position in time. Therefore, a 5-fold cross-validation was used to test the PF model for wind speed forecasting. This means the dataset was split into five equal parts (folds). For each round, one part was used to test the model, and the remaining four parts were used to train it. This process was repeated five times so that each part of the dataset served as the test set once. This way, all data points were used for both training and testing, leading to a more balanced and accurate evaluation of model performance. Using cross-validation in time-series prediction is important because it mimics real-world forecasting, where future values are predicted based on past data. It also avoids depending on a single train-test split, which might not represent the overall model performance accurately. The cross-validation results are shown in Figure 5.13. The PF model showed consistent performance across all five folds. Metrics like RMSE, MAE, R^2, and correlation stayed within a narrow range, indicating that the model is stable and reliable. RMSE and MAE increased slightly up to the third fold, then decreased again, showing only small changes in prediction error. The R^2 values also dropped

slightly until fold 3 but remained strong overall, indicating the model explains the variation in wind speed well. Correlation values were consistently high, showing the model effectively captures the relationship between the inputs and outputs. These results suggest that the PF model performs well across different subsets of the data, without signs of overfitting or underfitting.

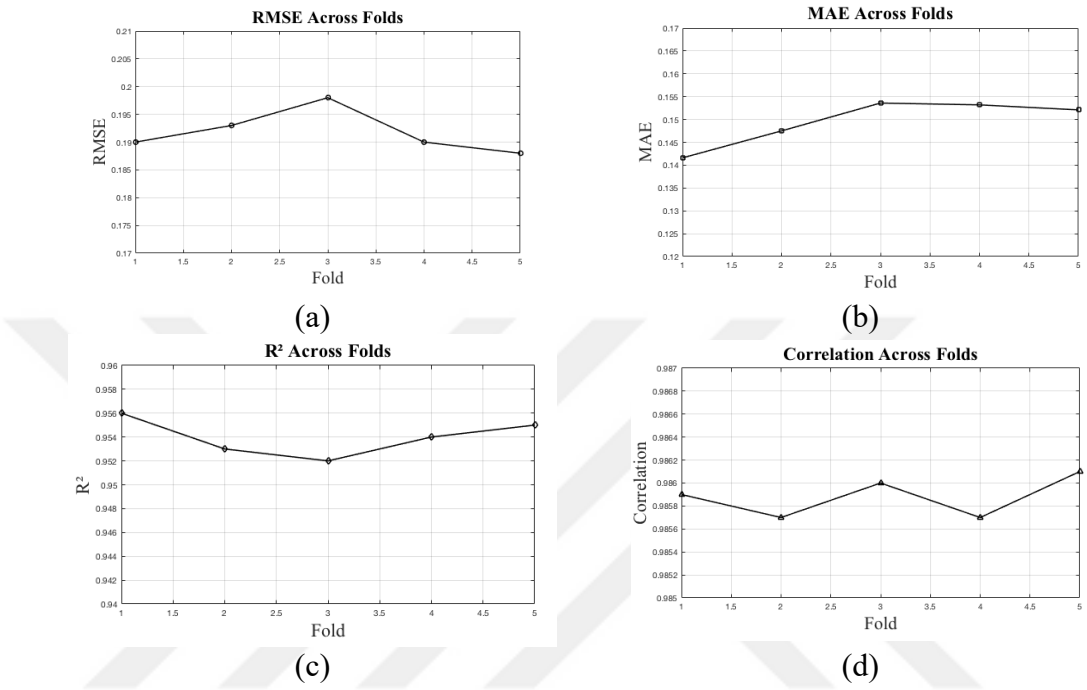

Figure 5.13 : K-fold cross-validation performance metrics.

5.3 Evacuation Priority Mapping

To identify the areas requiring prioritized evacuation planning in the event of a nuclear accident, cancer risk data was integrated with the SVI through three distinct approaches: the WSM, the Geometric Mean Method, and the Maximum Value Approach. The results are illustrated in the evacuation priority maps (Figure 5.14), with evacuation categories ranging from Very Low to Very High.

In the WSM map (Figure 5.14a), the integration is performed by assigning relative weights to the cancer risk and SVI layers, reflecting their perceived importance. In this study, equal weights of 50% were selected. This method produces a balanced spatial distribution of evacuation priorities. A notable concentration of High to Very High priority zones appears within and just beyond the 30 km radius zone from the NPP, with additional hotspots extending into the northeast and southern regions.

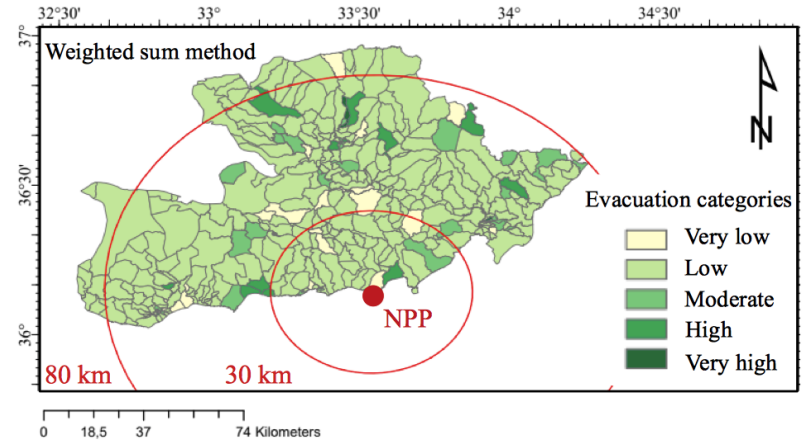

(a)

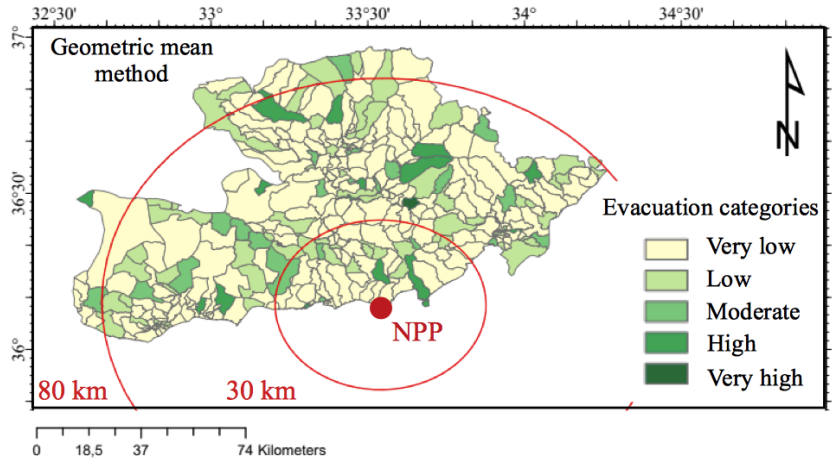

(b)

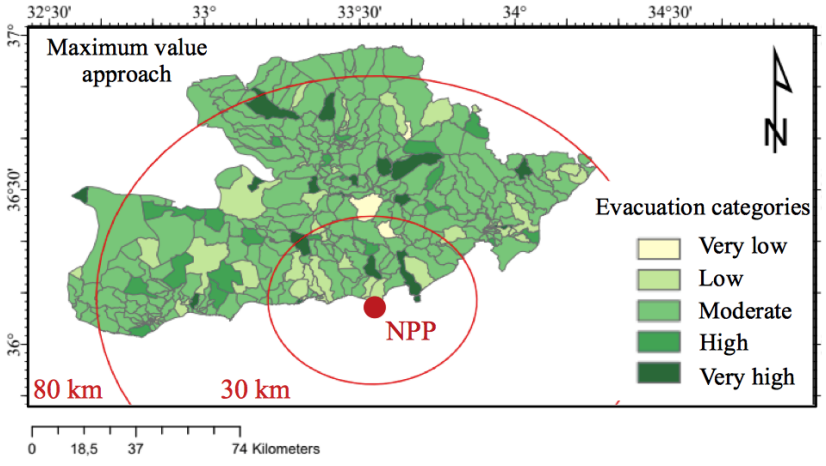

(c)

Figure 5.14 : Evacuation priority map: a) WSM, b) Geometric mean method, c) Maximum value approach.

The Geometric Mean Method map (Figure 5.14b) results in a more conservative distribution of priority zones. This method emphasizes consensus between criteria, meaning that high evacuation priority is assigned only to areas where both cancer risk

and social vulnerability are concurrently high. As a result, many areas fall into the Low and Moderate categories, with only a few distinct High and Very High zones scattered across the region. This approach minimizes overestimation of risk but may underrepresent areas where one criterion is dominant.

In contrast, the Maximum Value Approach map (Figure 5.14c) is based on calculations by assigning the highest category present in either of the input layers as the final evacuation priority. This method highlights a broader extent of High and Very High evacuation zones, particularly within the 30 km and 80 km buffers. It is especially useful in emergency contexts where rapid, conservative planning is necessary to avoid overlooking high-risk populations.

5.4 Evacuation Time Estimates Results

5.4.1 Comparison of radius-based and priority-based evacuation strategies

A discrete event-based approach is employed to calculate the evacuation time for the radius-based and priority-based evacuations of 56 districts based on predefined mobilization, loading, and travel parameters. Each district is assigned a population and an associated travel time to the evacuation point. The evacuation is executed in batches, with each batch comprising a group of districts prioritized according to a strategic evacuation order radius-based or priority-based.

The model assumes a fixed mobilization period of 10 minutes and a loading duration of 15 minutes per batch, after which the maximum travel time within the batch determines the final evacuation time. A timeframe of 5 minutes is introduced between batches to avoid logistical congestion. At each step, the cumulative evacuated population is updated, and the simulation proceeds continues until all districts have completed their evacuation. The results provide both numerical outputs such as the total evacuation time and the number of evacuees over time and a visual representation in the form of an evacuation curve (Figure 5.15).

Therefore, Figure 5.15 compares two evacuation strategies: radius-based and priority-based by tracking the cumulative number of people evacuated over time. The y-axis represents the number of evacuees in tens of thousands, while the x-axis shows the evacuation time in minutes.

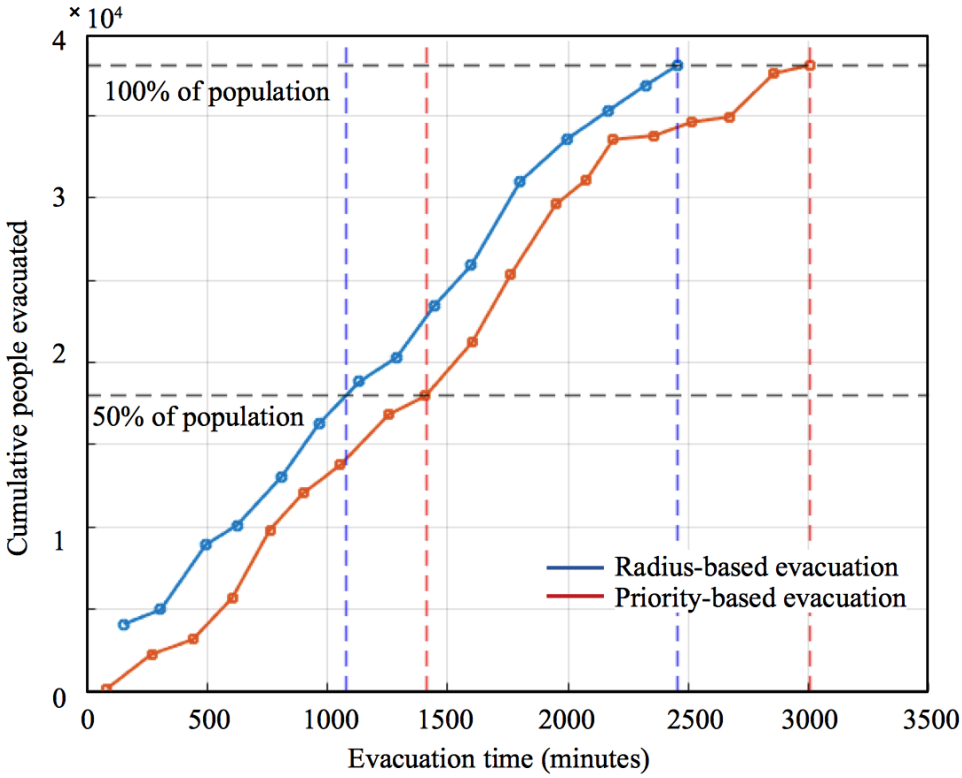

Figure 5.15 : Evacuation time estimates for radius-based and priority-based evacuations. Black dashed lines represent the 50% and 100% of population, blue and red dashed lines show the evacuation time when 50% and 100% of population is evacuated corresponding to radius-based and priority-based evacuations, respectively.

At first glance, both evacuation strategies seem to perform similarly, with their lines on the graph staying close to each other. However, there are some clear differences. The radius-based strategy (shown in blue) evacuates 50% of the total population in 1000 minutes (about 16.6 hours), while the priority-based strategy (shown in red) takes 1400 minutes (about 23.3 hours) to reach the same point. This shows that the radius-based approach is faster. After 1500 minutes, the blue line (radius-based evacuation) becomes steeper, which means people are being evacuated more quickly during that time. By the time 2500 minutes have passed, the radius-based method has evacuated everyone, but the priority-based method has only evacuated about 88% of the population. On average, the evacuation time is 21.8 hours for the radius-based strategy and 26.1 hours for the priority-based one. In terms of efficiency, the radius-based strategy evacuates about 930 people per hour, while the priority-based strategy manages around 760 people per hour.

Although the radius-based evacuation is clearly faster, it still raises an important question about who gets evacuated first. One major concern is whether this method

helps vulnerable districts such as those living in areas with insufficient disaster preparedness, response or coping capacities to be evacuated firstly. The priority-based strategy is basically designed to help these groups first. In contrast, the radius-based method mainly focuses on how close people are to the danger, without considering their social or physical needs. This means that some of the most vulnerable groups might have to wait longer to be evacuated. For this, the model was evaluated to see the proportion of vulnerable people evacuated first. The results are shown in Figure 5.16.

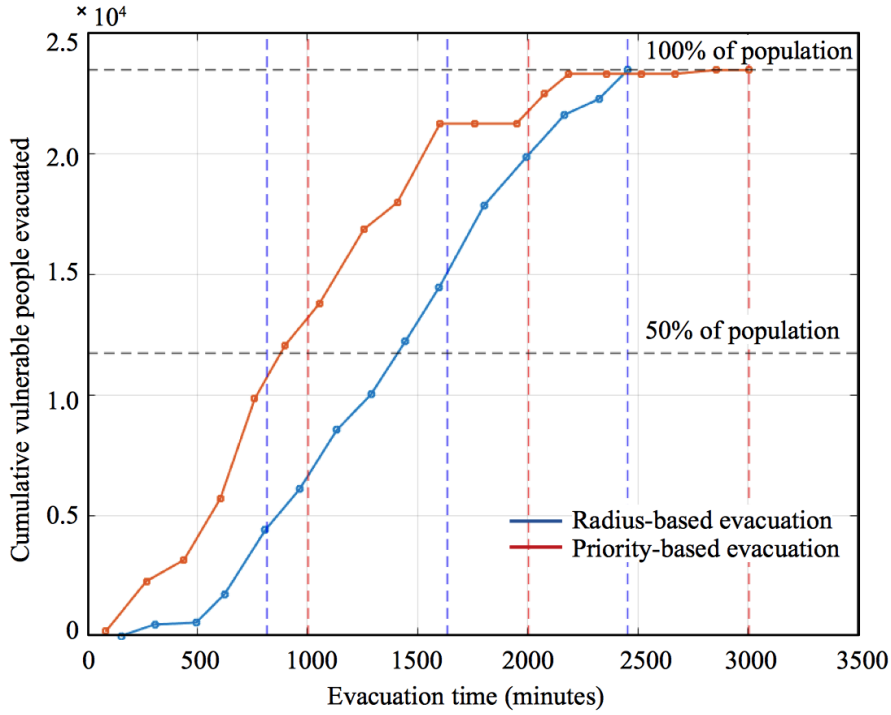

Figure 5.16 : Evacuation time estimates for radius-based and priority-based evacuations accounting for vulnerable population. Black dashed lines represent the 50% and 100% of population, blue and red dashed lines show the evacuation timeframe in three phases.

As previously discussed, the total evacuation time for the radius-based strategy is 2,454 minutes (approximately 40.9 hours), while for the priority-based strategy it is 3,003 minutes (50 hours). From Figure 5.16, if the total evacuation process is divided into three equal phases, each phase would span 818 minutes for the radius-based strategy and 1,001 minutes for the priority-based one. The total population to be evacuated is 38,048 individuals, of which 23,450 (or approximately 62%) are classified as vulnerable based on the evacuation priority map. Analyzing the distribution of vulnerable individuals evacuated during each phase reveals key differences between the two strategies. Under the priority-based approach, 55% of the

vulnerable population is evacuated in the first phase, 93% by the end of the second, and the full 100% by the end of the third phase. In contrast, the radius-based strategy evacuates only 19% of vulnerable individuals in the first phase, 64% by the second phase, and reaches 100% only by the final phase. These findings indicate that while the priority-based method increases total evacuation time by approximately 40% to evacuate the first half of the population and 22% for the remaining half it ensures that vulnerable groups are prioritized earlier in the process. This highlights a critical trade-off between evacuation speed and social equity that must be considered in emergency planning.

In addition to evacuation timing and prioritization of vulnerable populations, the health impact of each strategy was evaluated through average TEDE doses and estimated cancer risk. As shown in Figure 5.17, the average TEDE received per person across the initial timeframe of evacuation (first ten evacuation batches) is consistently lower under the priority-based approach. It means that in this evacuation strategy the priority in evacuation is first given to people who are at higher risk of developing cancer. As the result, the priority-based strategy reduces the overall TEDE dose by approximately 14% when compared to the radius-based evacuation.

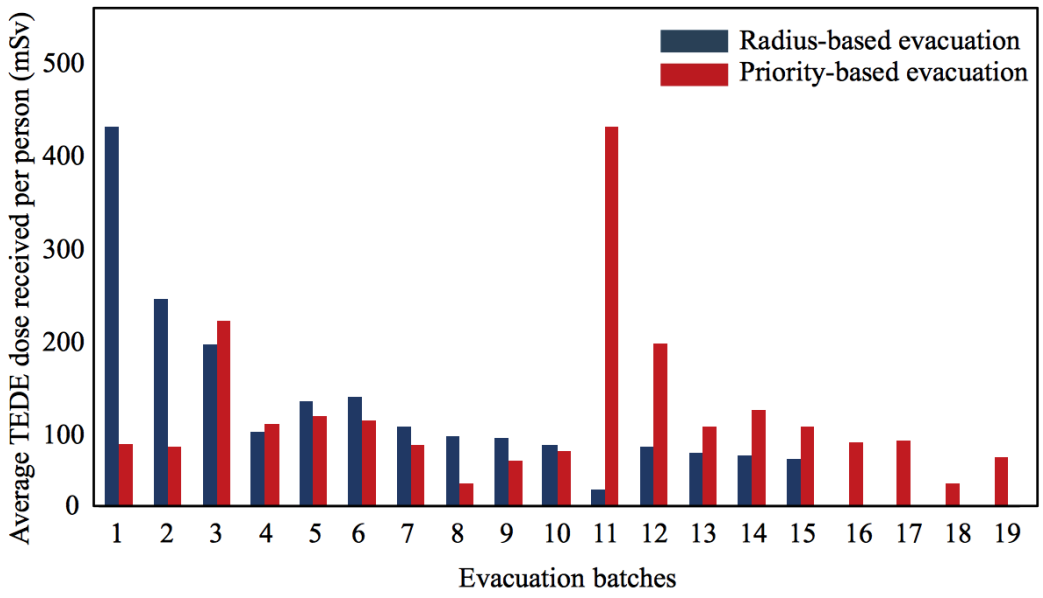

Figure 5.17 : Average TEDE doses received per person for each evacuation batch.

Furthermore, Table 5.7 summarizes the associated cancer risk metrics, indicating that the priority-based method results in lower collective radiation doses and, consequently, fewer estimated cancer cases. This results in relative reduction in cancer

risk of 20.61%. These findings emphasize that, beyond operational efficiency, the priority-based strategy offers clear public health benefits by minimizing radiation exposure and long-term health risks for the population.

Table 5.7 : Comparison of Collective Radiation Dose and Estimated Cancer Cases for Radius-Based and Priority-Based Evacuation Strategies.

Metric	Radius-based evacuation	Priority-based evacuation
Collective dose of TEDE (person-Sv)	2270.47	1802.52
Estimated cancer cases	113	90

5.4.2 Decision matrix and sensitivity analysis for evaluating evacuation strategies

To choose the best evacuation strategy, a decision matrix and sensitivity analysis were employed. This helps to compare the radius-based and priority-based methods by looking at important factors like how fast people are evacuated, how well vulnerable groups are protected, and how much radiation people are exposed to. Table 5.8 shows the decision matrix.

Table 5.8 : Decision matrix for evaluating radius-based and priority-based evacuation strategies across key performance criteria.

Criteria	Description	Radius-based evacuation	Priority-based evacuation	Goal
C1	Average evacuation time	21.8 hours	26.1 hours	Minimize
C2	Percent of vulnerable people evacuated first	19%	55%	Maximize
C3	Average TEDE dose received per person	172 mSv	140 mSv	Minimize
C4	Estimated cancer cases	113	90	Minimize
C5	Evacuation efficiency (evacuated people per hour)	930	760	Maximize

Criteria C1 (average evacuation time) reflects how long it takes to evacuate the population on average, where shorter times are preferred, so the goal is to minimize this value. Criteria C2 (percent of vulnerable people evacuated first) indicates how well each strategy prioritizes vulnerable groups; a higher percentage is better, so the

goal is to maximize. Criteria C3 (average TEDE dose received per person) measures the average radiation exposure during evacuation, therefore lower doses reduce health risks, making minimization is the goal. Criteria C4 (estimated cancer cases) represents the long-term health impact, where fewer cases are ideal, so this too should be minimized. Finally, criteria C5 (evacuation efficiency) calculates the number of people evacuated per hour, where higher values indicate faster evacuation, making maximization the goal.

Figure 5.18 shows the sensitivity analysis graphs. These graphs illustrate how the WSM scores for radius-based and priority-based evacuations change when the weight of each of the five criteria is adjusted. Each subplot in Figure 5.18 focuses on one particular criterion and shows what happens when its weight is increased, while making sure the total weight across all criteria always adds up to 100%.

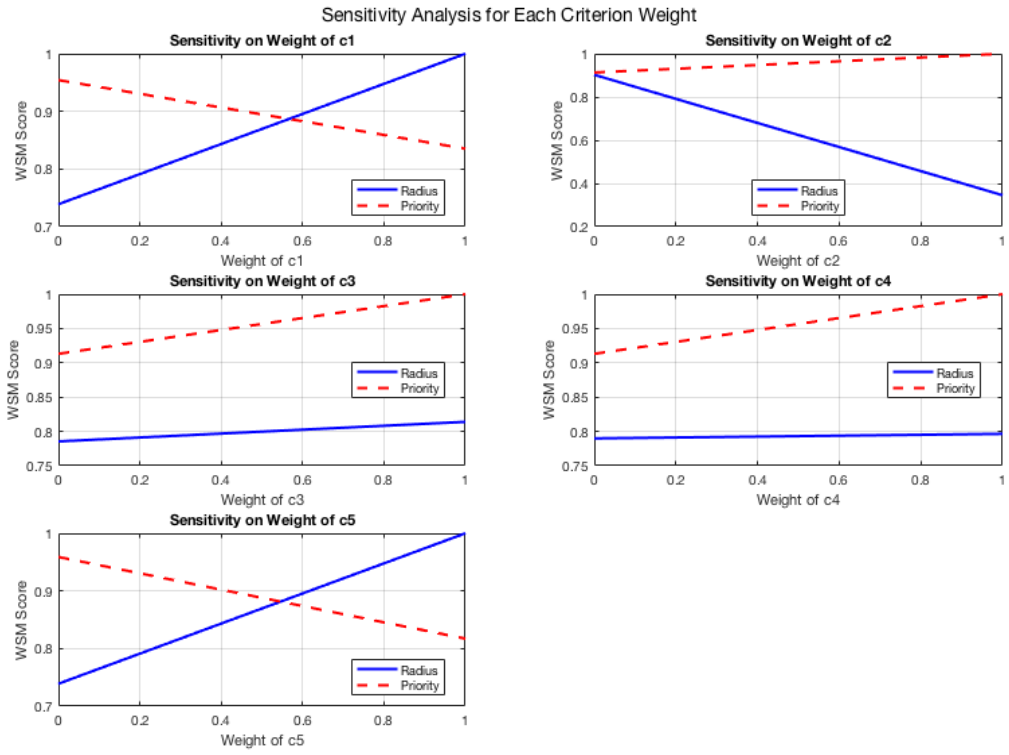

Figure 5.18 : Sensitivity results for evaluating evacuation strategies.

From the results, as more weight is given to C1, the score for radius-based evacuation goes up, while the score for priority-based goes down a bit. Around a weight of 0.55, their scores cross over. This means the "best" option changes depending on how important the score of C1. Therefore, C1 has a big influence on the final decision. The same can be said regarding the criterion C5 – this also important for the decision-

making. As for the criterion C2, the more weight is given to it, the worse radius-based method performs and the better priority-based method performs. As the lines do not cross each other, priority-based is always ranked higher than radius-based. This means C2 has some influence, but it is not strong enough to change the final decision. In criterion C3, both radius-based and priority-based get better scores when the weight is increased, but priority-based evacuation improves more. As lines do not cross, C3 helps improve scores but doesn't really affect the final ranking. Finally, adjusting the weight of C4 doesn't really change the scores. Therefore, this criterion doesn't have much impact on the decision at all.

The sensitivity analysis showed how changing the weight of each criterion affects the final ranking between radius-based and priority-based evacuations. Criteria C1 and C5 got the most weight because they can actually change which method wins. C2 got a medium amount of weight because it influences the scores but doesn't flip the ranking. Finally, C3 and C4 got the smallest weight because they don't matter much as changing their weights don't impact the final outcome. The weight's assigning is listed in Table 5.9.

Table 5.9 : Assigned weights for each criterion based on sensitivity analysis.

Criterion	Importance	Assigned weight
C1	Very important	0.30
C2	Medium importance	0.20
C3	Not important	0.10
C4	Not important	0.10
C5	Very important	0.30

Multiplying each normalized value of criteria by its corresponding weight and summing them up will show which of the method performs better. From calculation, radius-based evacuation score is 0.8216, and priority-based evacuation score is 0.9047. Therefore, the priority-based method performs better and should be preferred.

5.5 Shelter Suitability Analysis in Nuclear Emergency Scenario

5.5.1 Spatial data

The 30-kilometer EPZ encompasses 56 neighborhoods with a population of approximately 38,000 residents, including both urban and rural areas (Figure 5.19a). This zone was previously identified as feasible for evacuation in the event of a nuclear

accident. To mitigate these risks, a network of 59 designated shelters and 25 supply depots has been established within the EPZ (Figure 5.19b). These shelters were selected from existing buildings, each constructed with walls at least 0.7 meters thick, ensuring effective protection against gamma radiation exposure. Most shelters and depots are concentrated in the southern part of the EPZ, where population density is highest, highlighting the need for strategic evacuation planning and resource distribution. To improve evacuation efficiency and resource allocation, the study area was divided into three regions (Figure 5.19b). This division considers factors such as geographical features, population distribution, evacuation feasibility, and shelter capacity management. The population is evenly distributed across these regions, with 32% residing in regions A and C each, while region B accommodates the remaining 36%. This structured division enables a more precise and efficient emergency response strategy tailored to the unique characteristics of each region.

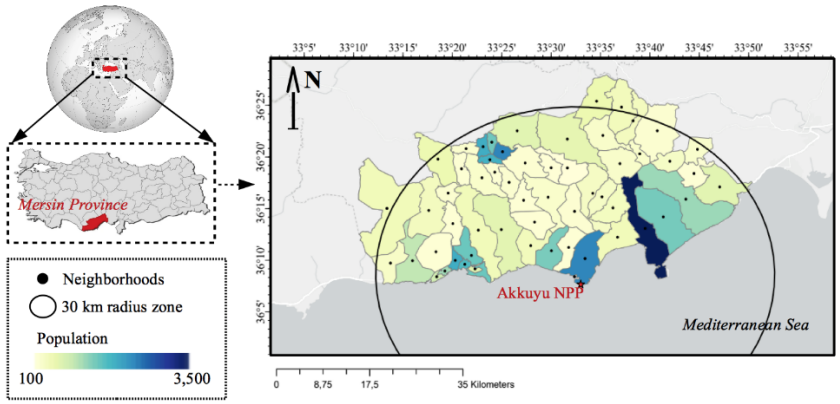

(a)

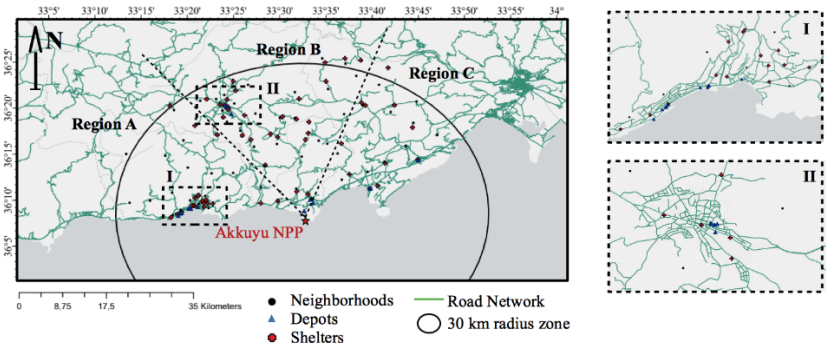

(b)

Figure 5.19 : Study area: a) Population within the 30-km radius zone, b) Location of shelters, depots, and neighborhoods' centroids, as well as road network.

In Mersin Province, Türkiye, road infrastructure is classified into various categories based on their function and traffic capacity, as outlined in Table 5.10. These classifications, which include state roads, regional highways, and urban/local roads, are crucial in defining evacuation routes and supply logistics, particularly in areas where road capacity and speed limits vary significantly.

Table 5.10 : Road description.

Type of road	Typical lane capacity (vehicles per hour per lane)	Speed limit for cars (km per hour)
State roads	1,800-2,200	90
Provincial roads	1,200-1,800	90
Local roads	500-1,000	50-90*
Highways	2,000-2,500	120
Urban roads	800-1,500	50

*Depending on the specific location and road conditions

5.5.2 Origin-destination analysis for evacuation route planning

Figure 5.20 presents the results of an OD Cost Matrix analysis, which evaluates evacuation routes between residential neighborhoods and emergency shelters. Evacuation times were calculated based on the road network, as described in Section, and analyzed for three different time thresholds: 75 minutes, 90 minutes, and 115 minutes.

The dashed black lines represent potential evacuation routes from each neighborhood to one or more shelters. Although depicted as straight connections, these routes reflect realistic travel paths, incorporating road curves and network constraints. The analysis reveals that as the time threshold increases, the number of viable evacuation routes grows, leading to a denser and more complex network. In the 75-minute scenario, only neighborhoods located near shelters have accessible evacuation routes. As the threshold extends to 90 and 115 minutes, more shelters become reachable, resulting in a higher route density and greater flexibility in evacuation planning.

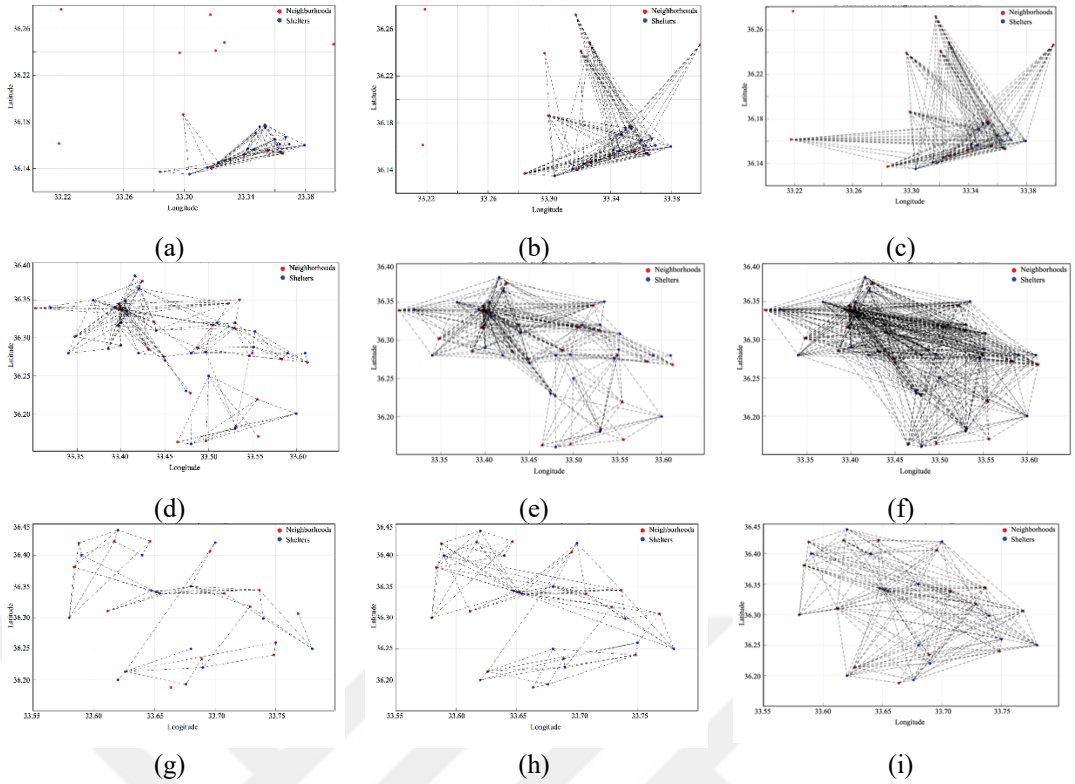

Figure 5.20 : OD analysis of evacuation routes to emergency shelters: a), b), c) Evacuation routes for Region A – thresholds 76 min, 90 min, and 115 min, respectively, d), e), f) Evacuation routes for Region B – thresholds 76 min, 90 min, and 115 min, respectively, g), h), i) Evacuation routes for Region C – thresholds 76 min, 90 min, and 115 min, respectively.

5.5.3 Origin-destination analysis of supply-access routes

Figure 5.21 presents an independent analysis of supply-access routes for emergency shelters across three distinct regions, evaluating the availability and geographic distribution of supply depots in relation to the shelters. In each graph, red dots represent supply depots, which act as starting points for distributing emergency supplies, while blue dots indicate emergency shelters, the final destinations where supplies are delivered to support evacuees. The black lines connecting depots to shelters depict potential supply routes, assessed based on factors such as distance, travel time, and road conditions during a nuclear emergency, following a methodology similar to the OD analysis described in Section.

The analysis examines supply accessibility under different time thresholds, tailored to each region. In Region A, the selected thresholds are 5, 15, and 20 minutes, while Region B is evaluated at 5, 50, and 90 minutes, and Region C at 15, 50, and 90 minutes. These thresholds reflect the minimum, average, and maximum travel times from depots to shelters within each region. For instance, in Region A, the longest necessary

travel time is 20 minutes, making extended thresholds, such as 90 minutes, unnecessary.

The findings highlight variations in supply accessibility across the three regions. In Region A, which contains 14 shelters and 12 depots, nearly all shelters can be reached within 15 to 20 minutes, indicating a well-distributed depot network that ensures efficient supply delivery, provided there are no major disruptions. In contrast, Region B, with 30 shelters and 10 depots, experiences significant delays in supply delivery for shelters located farther from depots, suggesting the need for additional depots in remote areas or optimization of transportation routes to reduce delays. Region C, with 15 shelters and only 3 depots, faces even greater logistical challenges due to the scarcity of depots and their distance from shelters, making it difficult to achieve adequate supply access within the 15-minute window. In this case, improving accessibility would require the establishment of new depots or the implementation of alternative strategies to expedite deliveries.

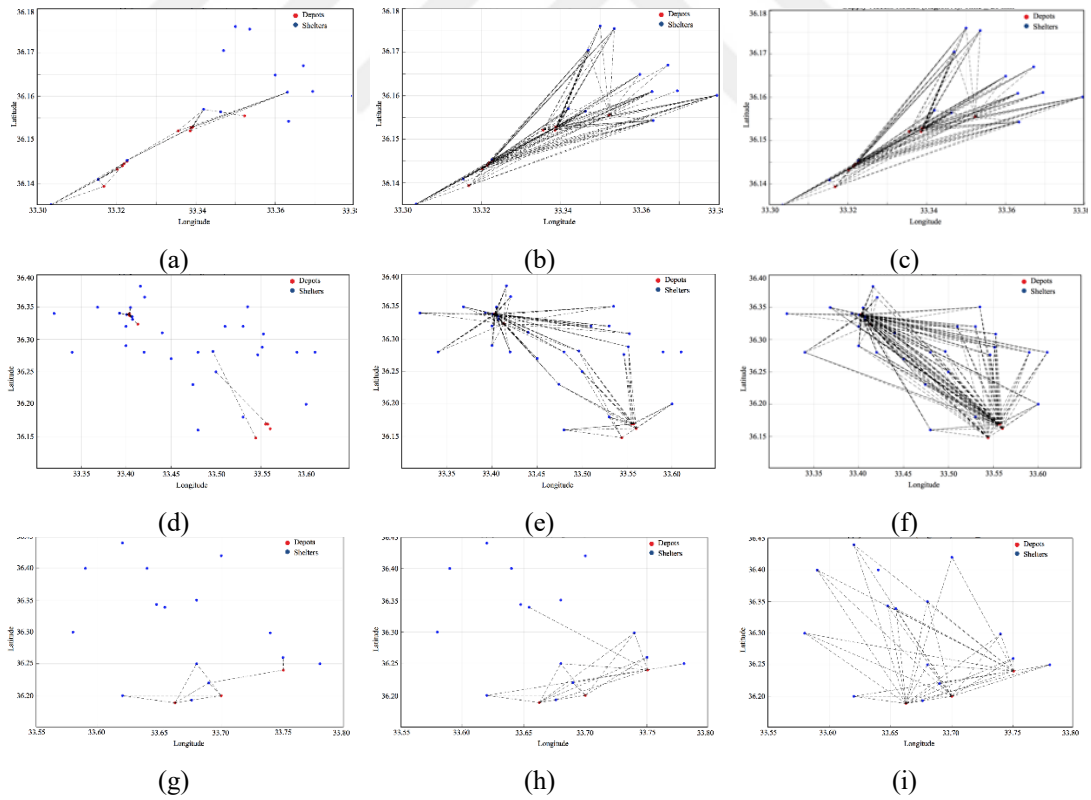

Figure 5.21 : OD analysis of supply-access routes to emergency shelters: a),(b), c) supply-access routes for Region A – thresholds 5 min, 15 min, and 20 min, respectively; d), e), f) supply-access routes for Region B – thresholds 5 min, 50 min, and 90 min, respectively; g), h), i) supply-access routes for Region C – thresholds 15 min, 50 min, and 90 min, respectively.

Overall, this analysis underscores the importance of strategic depot placement and route optimization in ensuring a reliable emergency supply chain, particularly in regions where existing infrastructure may not adequately support timely supply distribution.

5.5.4 Optimization process results

The optimization results for shelter allocation, presented in Figure 5.22, illustrate how populations from different regions are assigned to specific shelters. The map provides insight into the distribution of evacuees and highlights the utilization of shelters across Regions A, B, and C.

In Region A (Figure 5.22a), the assignment pattern reveals that certain neighborhoods rely heavily on a few shelters, while others remain unallocated. Notably, neighborhoods 1, 3, and 6 are assigned to shelter S4, with respective population assignments of 1,016, 1,231, and 604. This concentrated utilization of specific shelters suggests that the optimization process prioritizes minimizing evacuation time, resulting in the selection of shelters closest to the population centers. However, the presence of several unused shelters indicates that while some shelters efficiently serve evacuees, others remain unutilized due to their less favorable locations relative to high-density neighborhoods.

A similar trend is observed in Region B (Figure 5.22b), where significant unused shelter capacity exists. For example, shelter S2, with a capacity of 1,500, remains largely vacant, whereas shelters S3 and S4 are nearly at full capacity, with only 17 and 14 spaces remaining, respectively. This uneven evacuee distribution suggests that certain shelters are preferred due to their strategic locations and accessibility, while others, despite available capacity, are underused. Shelter S5 emerges as the optimal choice, achieving an objective value of 0.52 due to its balance of short evacuation routes, proximity to resources, and low congestion. In contrast, shelters S1 and S16, with objective values of 0.796 and 1.568, respectively, demonstrate higher inefficiencies due to longer evacuation times, increased congestion, or limited access to necessary resources.

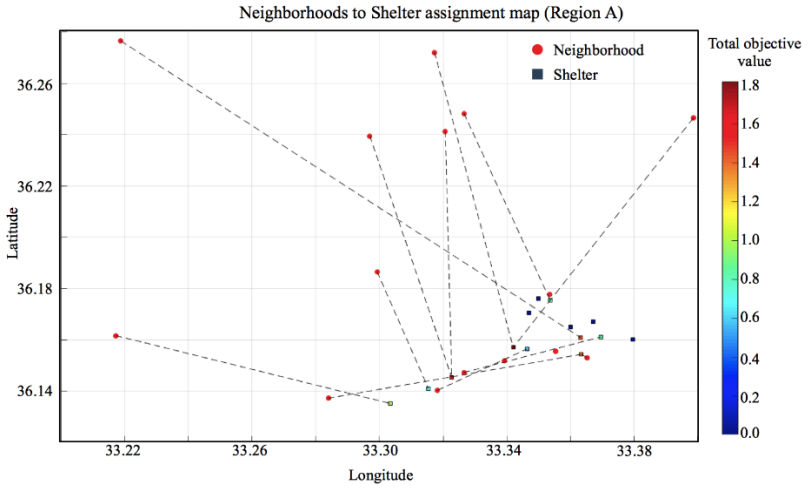

(a)

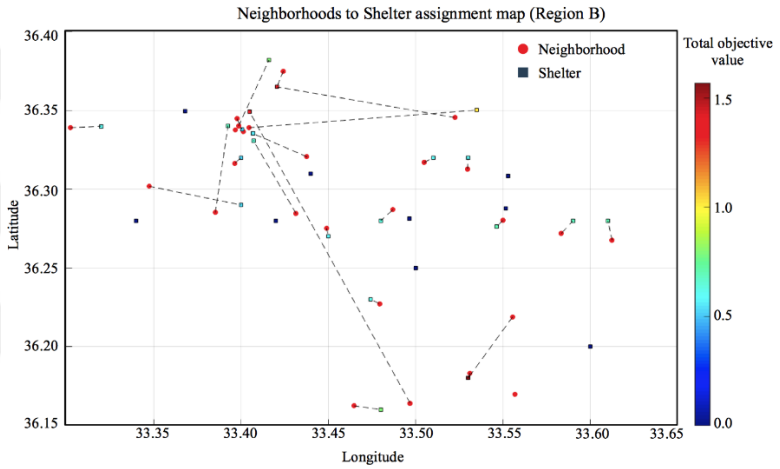

(b)

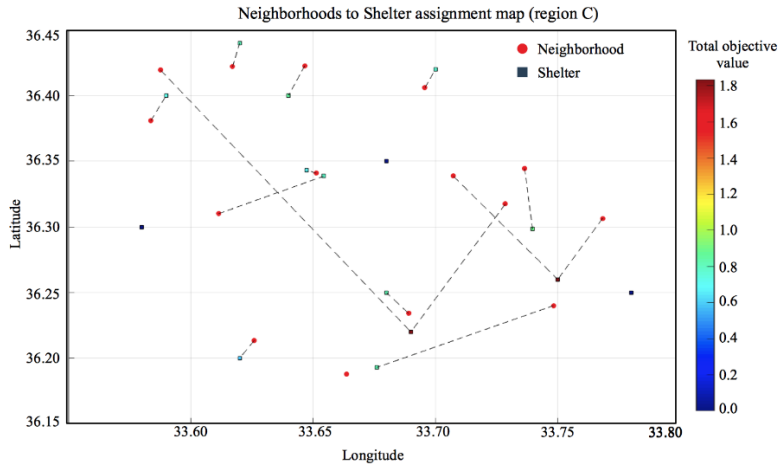

(c)

Figure 5.22 : Neighborhoods to shelter assignment map with shelter ranking: a) Region A, b) Region B, c) Region C.

In Region C (Figure 5.22c), the shelter assignment pattern further highlights the uneven utilization of available facilities. Shelters S2, S3, and S5 accommodate significant portions of the population, with respective assignments of 1,532, 1,268, and 634 individuals, whereas shelters S1, S6, and S7 remain largely underutilized. The disparity in remaining shelter capacities further emphasizes this imbalance, as shelters such as S12 have only three available spaces left, while others, like S2, still have 1,968 open spaces. The objective values for shelters in Region C range from 0.580 to 1.834, with shelter S1 identified as the optimal choice due to its lowest objective value of 0.58, indicating a well-balanced evacuation time, resource access, and crowd distribution. Conversely, shelters S4 and S5, with higher objective values of 1.834 and 1.824, respectively, reflect inefficiencies related to overcrowding or less effective evacuation routes.

Figure 5.23 further illustrates the population assignments alongside the remaining shelter capacities, providing a clearer view of the allocation discrepancies. The underutilization of certain shelters can be attributed to multiple factors inherent to the optimization model and study constraints. The primary objective of minimizing evacuation time drives evacuee assignments toward shelters located closest to their neighborhoods, which naturally results in some shelters remaining unoccupied despite their available capacity. More distant shelters are less likely to be selected as they do not contribute significantly to reducing evacuation time. Furthermore, the optimization process enforces capacity constraints to prevent overcrowding, meaning that once a shelter reaches its limit, additional evacuees cannot be assigned, even if the shelter is geographically proximate to other neighborhoods.

The geographic distribution of shelters also plays a crucial role in these outcomes. Higher population densities in the southern part of the study area correspond to a greater concentration of shelters, whereas less densely populated areas contain fewer shelters, often leading to their underutilization. As a result, shelters in sparsely populated regions may not reach full capacity simply because the number of evacuees in need is lower.

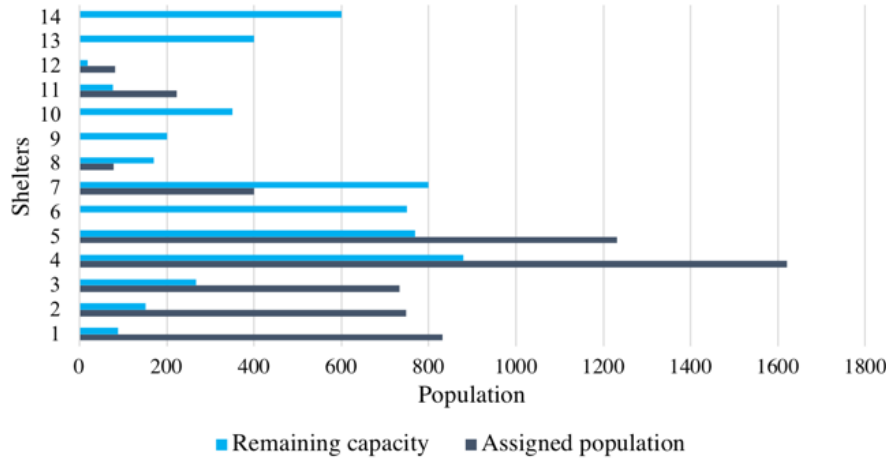

(a)

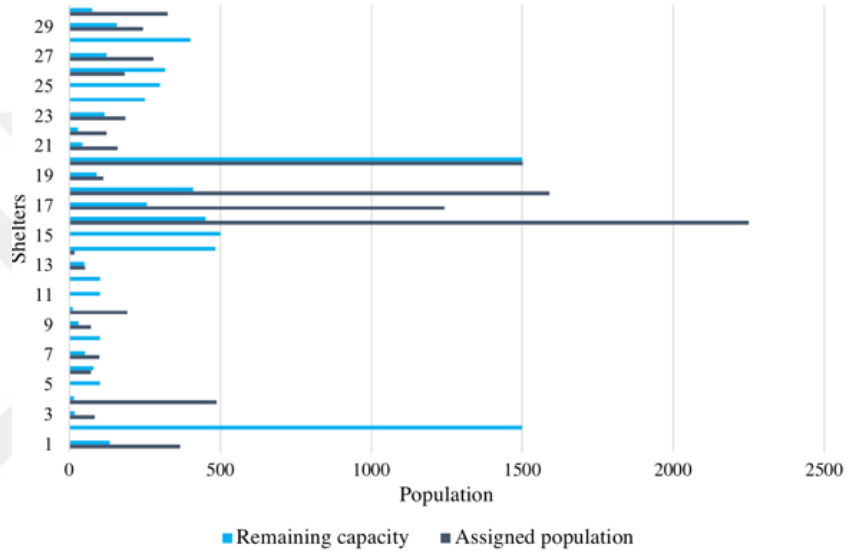

(b)

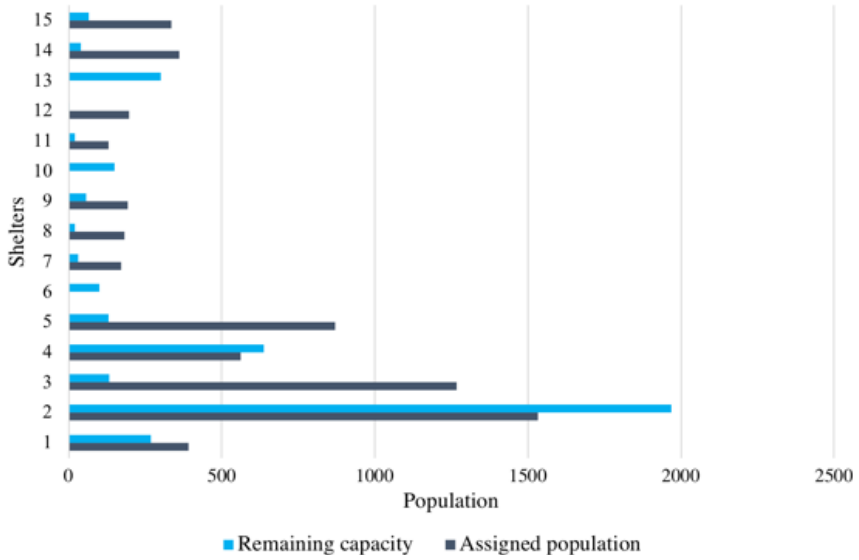

(c)

Figure 5.23 : Population assignment and remaining capacity in shelters: a) Region A, b) Region B, c) Region C.

Although minimizing evacuation time is the primary goal, other considerations, such as accessibility to essential supplies and avoiding overcrowding, influence the final allocation. Ultimately, the optimization model seeks to balance these competing factors, and the results underscore the complexity of shelter allocation in emergency evacuation scenarios, where efficiency, accessibility, and resource availability must be carefully managed.

5.5.5 Model evaluation

5.5.5.1 Sensitivity analysis

Figure 5.24 presents a sensitivity analysis of a multi-dimensional optimization problem that incorporates three weighted criteria: evacuation time (α), supply-access time (β), and overcrowding prevention (γ). The horizontal axis represents the weight assigned to evacuation time (α), while the vertical axis denotes the corresponding total objective value. Annotations within the plot indicate the weights for supply-access time (β) and overcrowding prevention (γ) for each data point. The analysis demonstrates how different weight combinations influence the total objective value, emphasizing the trade-offs among the criteria. For example, an increase in α generally results in higher total objective values, reflecting a prioritization of minimizing evacuation time. In contrast, assigning greater weights to β and γ leads to lower total objective values, highlighting their significance in the optimization process. The clustering of points further illustrates the interdependencies between weights and the model's overall performance.

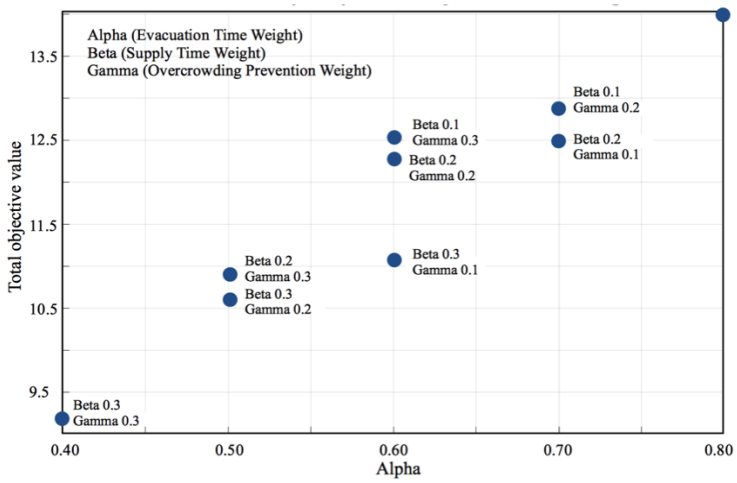

Figure 5.24 : Sensitivity analysis: total objective value vs. weights.

Ultimately, the sensitivity analysis provided a thorough understanding of how variations in the weights assigned to evacuation time, supply-access time, and overcrowding prevention influenced the model's total objective value. By systematically evaluating these trade-offs, the analysis identified the optimal balance required to achieve the most effective outcomes. Consequently, the final weight selection was based on these findings, ensuring a well-informed and robust decision-making process aligned with the specific priorities and constraints of the scenario.

5.5.5.2 Robustness and generalization

To assess the robustness and generalization ability of the developed models, k-fold cross-validation was performed. This method evaluates how consistently a model performs across different data subsets and determines its capacity to generalize to unseen conditions. The primary objective of this validation was to ensure that the models maintain stable performance in minimizing evacuation time, supply-access time, and overcrowding, even when faced with variations in population distribution, road conditions, or resource availability.

Robustness refers to the model's ability to produce consistent results across different folds, ensuring stable performance under changing conditions. Generalization, on the other hand, evaluates whether the model can reliably assess emergency shelter suitability when applied to new scenarios, such as different disaster regions, infrastructure setups, or population distributions. To measure these aspects, the mean objective values and standard deviations of the models were analyzed, with the coefficient of variation (CV) used as an indicator of performance stability.

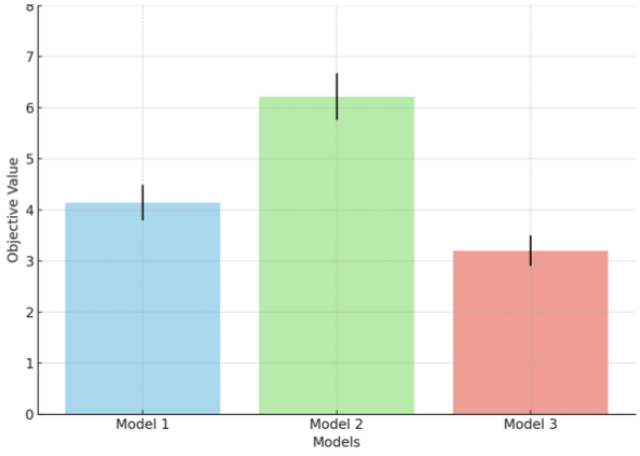

Figure 5.25 : Results of k-fold cross-validation: mean objective value with standard deviation.

Model 1 (Region A) achieved a CV of 8.5%, with a mean objective value of 4.14 and a standard deviation of 0.35, demonstrating reliable performance with low variability. Model 2 (Region B) exhibited a slightly lower CV of 7.4%, with a mean objective value of 6.22 and a standard deviation of 0.46, indicating good robustness but with room for further optimization. Model 3 (Region C) displayed the highest robustness, with the lowest variability (CV = 9.4%), a mean objective value of 3.20, and a standard deviation of 0.30, confirming strong consistency across folds.

The results indicate that Model 1 maintains stable performance, making it a dependable choice for Region A's characteristics. Model 2, though reliable, shows slightly higher variability, suggesting that fine-tuning could enhance its adaptability to specific conditions in Region B. Meanwhile, Model 3 stands out as the most robust and versatile model, excelling in both consistency and predictive capability, making it particularly well-suited for Region C.

Overall, the k-fold cross-validation results confirm that all models exhibit strong reliability and generalization ability. These findings validate their effectiveness in optimizing emergency shelter allocations under varying conditions, ensuring stable performance and reliable decision-making in disaster response scenarios.

5.5.6 Discussions: optimization results for shelter allocation

The results of this study provide valuable insights into the complexities and trade-offs involved in emergency evacuation planning, particularly in a nuclear emergency scenario. The optimization process successfully minimized evacuation time; however, it also resulted in an uneven distribution of evacuees and varying levels of shelter utilization. This highlights the inherent challenge of balancing multiple objectives – evacuation time, shelter capacity, and supply access – within the constraints of real-world emergency conditions.

In Region A, the optimization process led to a significant concentration of evacuees in shelter S4, particularly from neighborhoods 1, 3, and 6, while several other shelters remained underutilized. This outcome can be attributed to the prioritization of evacuation time, which favored assigning evacuees to the nearest shelters. Although this approach aligns with the model's highest-priority objective, it also indicates a potential risk of congestion in certain shelters while others remain largely vacant. A similar trend was observed in Region B, where shelters like S2 had considerable

unused capacity, whereas S3 and S4 were nearly full. Shelter S5 emerged as the most optimal, with an objective value of 0.52, due to its favorable location and accessibility. In contrast, shelters such as S1 and S16 had higher objective values, reflecting either longer evacuation times or limited accessibility. While the model effectively reduces evacuation time, introducing additional constraints or refinements could lead to a more balanced distribution of evacuees. Region C followed the same pattern, where certain shelters, including S2, S3, and S5, were heavily utilized, while others, such as S1, S6, and S7, remained underpopulated. This suggests a geographic bias in shelter selection, where those minimizing travel times were consistently preferred, potentially resulting in suboptimal resource allocation. Notably, shelter S1, which had the lowest objective value (0.58), was well-positioned to balance evacuation time, supply access, and crowd control. However, the higher values associated with shelters like S4 and S5 indicate inefficiencies similar to those observed in other regions.

The underutilization of many shelters can be primarily attributed to the optimization model's focus on minimizing evacuation time. Since evacuees were assigned to the closest available shelters, those located farther from population centers, despite having capacity, often remained unused. This prioritization of proximity over shelter capacity, while efficient in terms of evacuation time, raises concerns about resource distribution and potential overcrowding in the most optimal shelters. Another key factor influencing these results is the geographic distribution of shelters. The southern part of the study area, characterized by higher population density, contains a greater number of shelters. In contrast, sparsely populated areas have fewer shelters, which often remain underutilized due to the lower number of evacuees. This spatial imbalance results in an uneven distribution, where densely populated regions experience a concentration of evacuees in specific shelters, while others in less populated areas remain vacant.

These findings highlight the need for a more balanced approach to shelter placement and utilization, particularly in regions with varying population densities. In high-density areas, additional shelters may be required to prevent overcrowding and ensure adequate access to resources. Meanwhile, in sparsely populated regions, mobile or flexible shelters could be introduced to supplement existing facilities and ensure comprehensive coverage. The results of this study have significant implications for emergency planning, especially for nuclear accidents and large-scale disasters. While

proximity and evacuation time are crucial in determining shelter assignments, incorporating additional constraints such as real-time traffic conditions and shelter occupancy levels could enhance the optimization process and promote more effective shelter utilization. Furthermore, reevaluating the geographic distribution of shelters could help address disparities in population density and resource allocation. Increasing shelter capacity in densely populated areas and deploying mobile solutions in less populated regions could lead to a more resilient and efficient evacuation strategy.

5.6 Health and Environmental Implications from Postulated NPP Accident

5.6.1 TEDE and cancer risk calculations

The spatial distribution of TEDE and corresponding cancer risk across the study area are shown if Figure 5.26, with buffer zones of 30 km and 80 km radii centered around the NPP.

In Figure 5.26a, the TEDE values have been categorized into five classes: Very Low, Low, Moderate, High, and Very High. The highest TEDE values are concentrated around the immediate vicinity of the NPP, particularly within the 30 km radius zone. This is expected, as radioactive dispersion is typically most intense near the source. The gradient of dose values decreases with increasing distance from the NPP.

Figure 5.26b shows the cancer risk categories, which are directly inferred from the TEDE distributions using dose-response models and population data. The spatial pattern of cancer risk mirrors that of the TEDE to a significant extent, with highest risk categories also clustered around the NPP and gradually decreasing outward. However, discrepancies are noticeable in certain districts where cancer risk appears relatively elevated despite moderate TEDE levels. This variation are directly attributed to demographic factors.

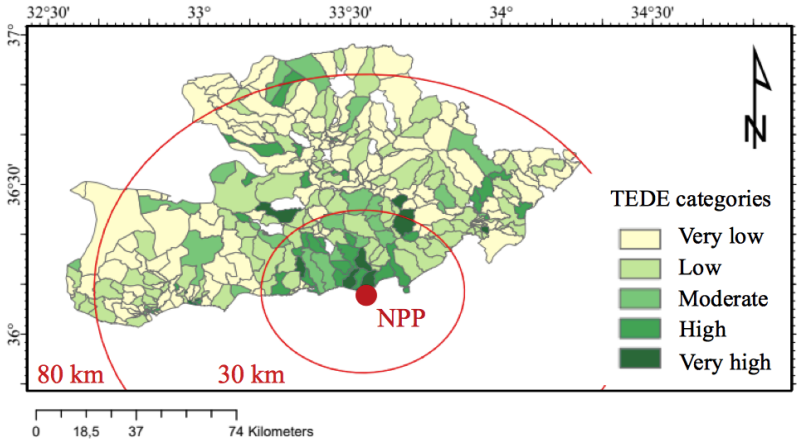

(a)

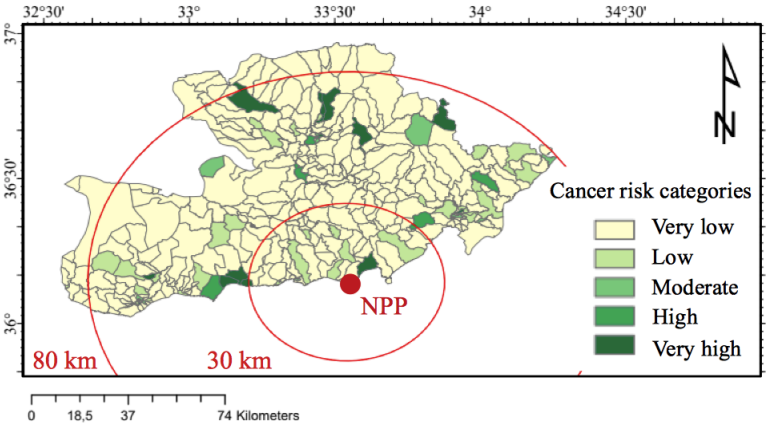

(b)

Figure 5.26 : Health consequences from hypothetical accident: a) TEDE, b) Cancer risk.

5.6.2 Results from modeling radioactive deposition and decay mechanisms

Radioactive deposition refers to the settling of radioactive particles onto the ground and other surfaces following a nuclear accident. These particles, in particular Cs-137, can pose long-term environmental and health risks due to their persistence and mobility in the ecosystem. Once deposited, radionuclides undergo radioactive decay that is a natural process by which unstable atoms lose energy by emitting radiation, gradually transforming into more stable elements. The rate of decay is characterized by a substance's half-life, which determines how long it takes for its activity to reduce by half.

Table 5.11 compares the action levels for radiation contamination in the aftermath of the Chernobyl and Fukushima nuclear accidents, highlighting the different thresholds

for relocation, agricultural restrictions, and monitoring measures in both regions. For mandatory relocation, both Chernobyl and Fukushima set the threshold at >1,480 kBq/m² (40 Ci/km²), although in Fukushima, this was specifically aimed at keeping the annual dose below 20 mSv/year. Voluntary relocation and strict land use controls applied to areas with radiation levels ranging from 555 to 1,480 kBq/m² in Chernobyl, while in Fukushima, this was based on the projected annual dose. Agricultural restrictions were more stringent in Chernobyl, where radiation levels of 37-555 kBq/m² prohibited farming and forest use, whereas in Fukushima, farming was restricted only at levels >250 kBq/m². Enhanced monitoring was applied at lower contamination levels, with zones established for soil and food monitoring, and areas with contamination below 37 kBq/m² were deemed safe for unrestricted use in both regions, though Fukushima set a stricter threshold of <5 kBq/m² for food and agriculture concerns.

Table 5.11 : Cs-137 ground deposition thresholds (kBq/m^2).

Protective action	Chernobyl accident	Fukushima accident	Reference
Mandatory relocation	>1,480	>1,480	
Voluntary relocation	555 – 1,480	Not formally defined, but based on annual dose >20 mSv	
Agricultural restrictions	37 – 555	>250	
Enhanced monitoring	Around 37	5 – 250	
Safe for use	<37	<5	

The Figure 5.27 illustrates the long-term environmental persistence of Cs-137 contamination based on initial ground deposition levels, categorized by recommended protective actions. As shown, areas with the highest deposition levels such as those requiring mandatory relocation remain above the safety threshold of 5 kBq/m² for over 240 years, highlighting the long-lasting consequences of severe nuclear contamination. Zones classified for voluntary relocation or agricultural restrictions exhibit decay timelines exceeding 160-200 years, indicating that land-use limitations may need to be enforced for multiple generations. Regions under enhanced monitoring, though relatively less contaminated, still require careful observation for over 150 years before reaching safe levels.

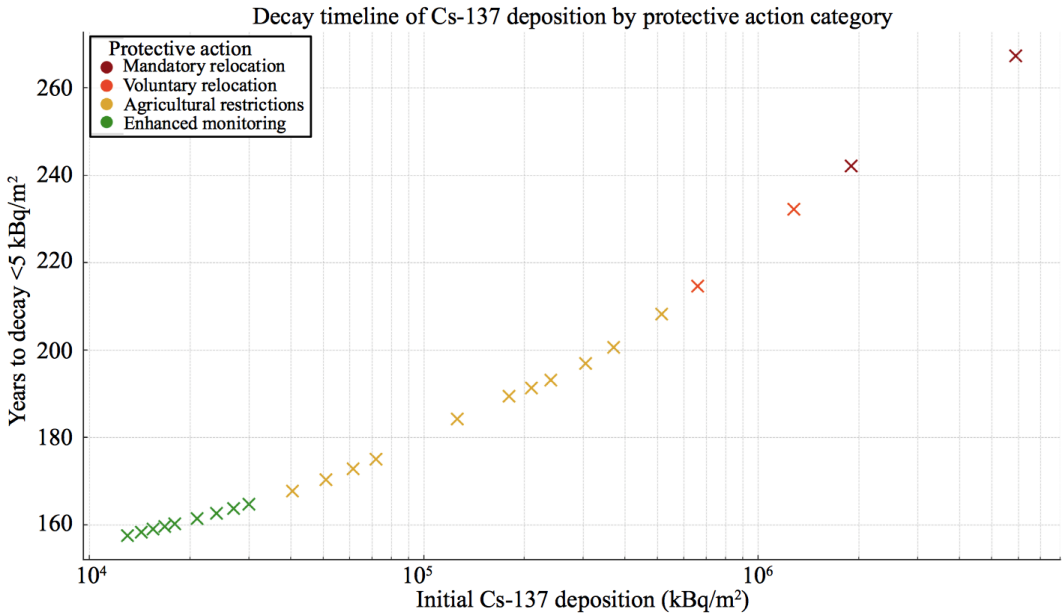

Figure 5.27 : Decay timeline of Cs-137 deposition by protective action category.

5.7 Results from Economic Loss Assessment

As it was stated in Section 3.7.3., the total economic losses resulting from a nuclear accident are calculated as the sum of six major cost components: cost of response, cost of decontamination, cost of health, cost of waste, cost of compensation, and cost of administration.

5.7.1 The emergency response cost estimation

The emergency response cost is calculated using an Equation 5.5 by multiplying the estimated cost per person by the population of the affected neighborhood.

$$C_{response} = \sum(P_n \times c_{person}) \tag{5.5}$$

where P_n is a population of a particular neighborhood and c_{person} represents costs for person.

This cost per person includes essential short- to medium-term support services such as temporary housing, provision of food and water, and first aid medical supplies. It is assumed that all residents are able to evacuate by their own vehicles. To estimate the per-person cost, this research references data from the Fukushima Daiichi nuclear disaster in 2011, where government reports indicate that the cost of emergency response per evacuee ranged from approximately $1,000 to $5,000 United States Dollar (USD) (NEA 2012). However, direct application of these values to the Turkish

context would not accurately reflect economic differences between the two countries. Therefore, the per capita GDP is used to adjust these figures proportionally, recognizing that the cost of living and service provision is closely tied to a country's economic output. Therefore, in 2011, Japan's per capita GDP was approximately $48,760 USD, while in 2023, Türkiye's per capita GDP was approximately $13,105 USD. The cost adjustment is made using the following Equation 5.6:

$$Adjusted\ Cost_{Turkiye} = Reference\ Cost_{Japan} \times \left(\frac{GDP_{Turkiye}}{GDP_{Japan}}\right) \quad (5.6)$$

where $Reference\ Cost_{Japan}$ is the cost of emergency response during Fukushima accident, GDP_{Japan} is GDP per capita of Japan corresponding to 2011 and $GDP_{Turkiye}$ is GDP per capita of Turkiye corresponding to 2023.

Applying this adjustment, the lower bound of $1,000 becomes approximately $270 USD, while the upper bound of $5,000 becomes approximately $1,345 USD for Turkiye. Thus, the emergency response cost per person in Turkiye is estimated to range from $270 to $1,345 USD, depending on the scale and duration of evacuation needs. These adjusted values are then multiplied by the affected neighborhood's population to calculate the total emergency response cost. Figure 5.28 illustrates the spatial distribution of emergency response costs within 80-km zone around the NPP.

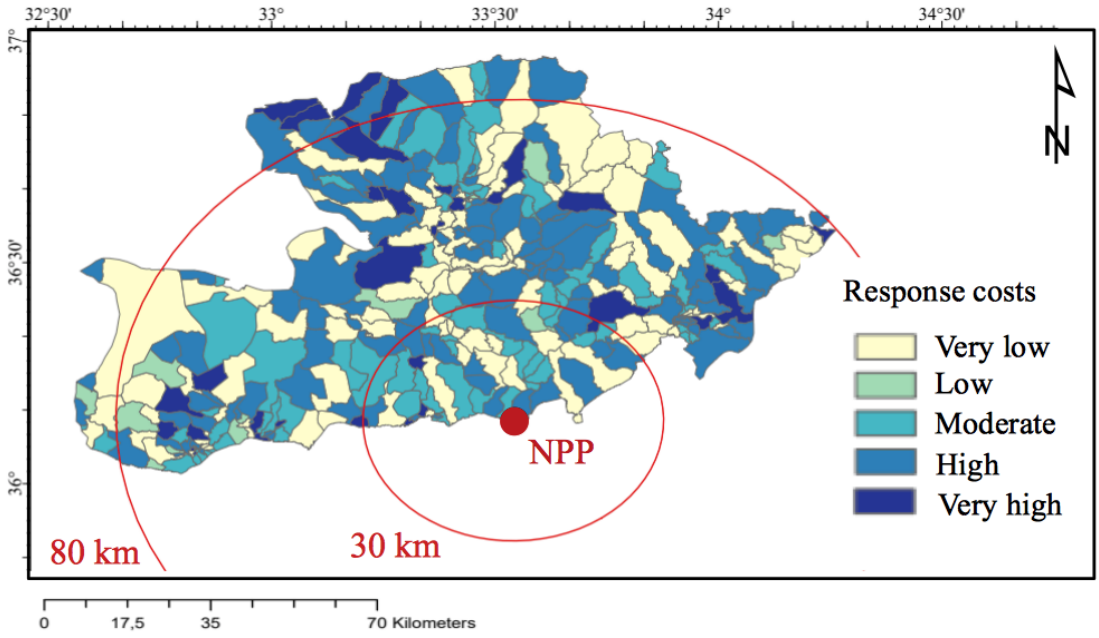

Figure 5.28 : The emergency response costs.

Areas in the northern and northeastern sectors exhibit higher costs despite having lower population densities compared to other regions. This occurs due to limited road infrastructure, which complicates the logistics of rapid emergency response. The lack of accessible routes increases travel times and resource requirements for deployment. In contrast, the southern and southwestern zones show lower costs, reflecting better road connectivity and closer proximity to essential infrastructure, which facilitate more efficient emergency operations.

5.7.2 The decontamination cost estimation

Decontamination costs are estimated using Equation 5.7:

$$C_{decont} = area_contaminated \times cost_per_km^2 \quad (5.7)$$

where $area_contaminated$ represents the contaminated area in km^2 and $cost_per_km^2$ is a cost in USD for each square kilometer to decontaminate the area.

The costs for each square kilometer to decontaminate the area were taken from official reports after the Fukushima accident and these are based on the decontamination intensity that is listed in Table 5.12.

Table 5.12 : Decontamination intensity (Yasutaka and Naito 2016).

Ground deposition (kBq/m^2)	Decontamination level	Description	Cost original	Adjusted cost for Turkiye
<40	Low	Minor intervention or natural decay only	$1M	$268,700
40 – 600	Medium	Partial decontamination (roads, roofs of buildings, etc.)	$3M	$806,100
>600	High	Full decontamination including soil removal	$7M	$1,880,900

*Adjusted cost for Turkiye is based on Equation 5.6.

Figure 5.29 represents the expected decontamination costs across the study region.

A clear pattern shows that areas with “very high” and “high” costs are mostly clustered near and northeast of the NPP. The gradual change from high to low costs across the map suggests that cleanup efforts may focus first on places with important infrastructure or sensitive environments. Some coastal areas are less affected, due to less valuable lands in terms of agriculture. Areas with “very low” patterns in north are less used for agricultural purposes and therefore are not expected to have high loses.

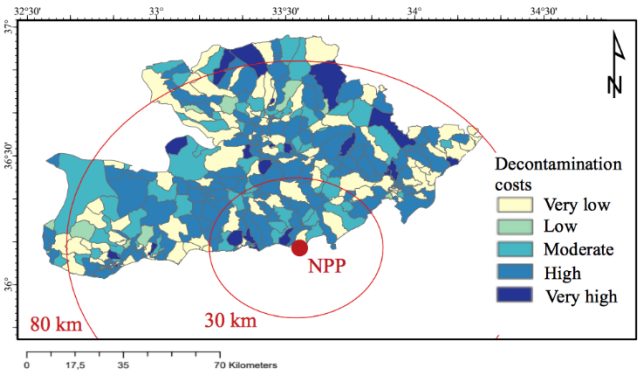

Figure 5.29 : The decontamination costs.

5.7.3 The health-related cost estimation

Health-related economic losses following a nuclear accident are estimated by multiplying the population of each affected neighborhood by the average medical cost per person. These costs account for both immediate and long-term medical needs resulting from radiation exposure and associated psychological impacts. Based on data from Fukushima, the per capita health cost ranged between $500 and $20,000 (NEA 2012, IAEA 2015). These figures encompass a wide range of health-related expenses, including radiation exposure screening and regular health monitoring, medical consultations and diagnostic tests, treatment of radiation-induced illnesses and secondary health effects, and mental health care services (e.g., therapy for trauma, stress-related disorders).

Applying Equation 5.6, the adjusted health costs for Turkiye are as follows: low estimate is $1,345 and high estimate is $5,375. Figure 5.30 shows a distribution of health related costs.

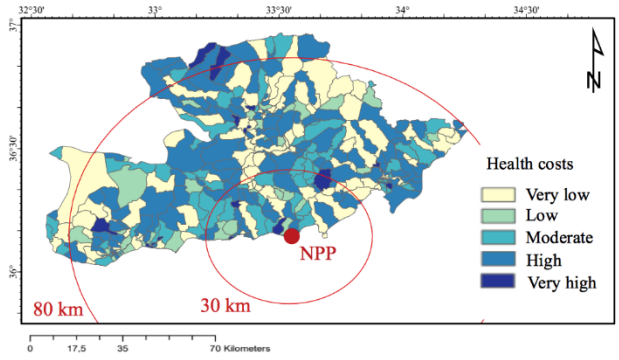

Figure 5.30 : The health-related costs .

The map depicting health-related costs shows significant variation within the EPZs. Populated regions, especially those closer to the NPP, exhibit higher health expenditures. These costs stem from increased exposure to radiation, leading to greater demand for medical services, long-term health monitoring, and treatment of radiation-induced illnesses. Outlying regions with "very low" costs correspond to sparsely inhabited but better-protected areas, suggesting a need to align health resource allocation with projected exposure risk and population vulnerability.

5.7.4 The radioactive waste-related cost estimation

Waste costs are calculated by multiplying the estimated volume of radioactive waste (measured in cubic meters, m^3) by the unit cost of waste processing and disposal (measured in USD per m^3) as shown in Equation 5.8:

$$C_{waste} = waste_volume \times unit_cost \tag{5.8}$$

where $waste_volume$ is the estimated volume of radioactive waste that is estimated by multiplying contamination area and factor; and $unit_cost$ is a cost of waste.

After the Fukushima accident, the volume of waste generated was closely linked to the level of decontamination required, as defined in Table 5.13.

Table 5.13 : Volume of radioactive waste (Yasutaka and Naito 2016; NEA 2021).

Decontamination level	Estimated waste volume factor
Low (ground deposition is less than 40 kBq/m^3)	1000
Medium (ground deposition is between 40 and 600 kBq/m^3)	2000
High (ground deposition is more than 600 kBq/m^3)	3000 – 5000

The unit cost for waste handling and disposal, based on post-Fukushima estimates, ranges from $500 to $2,000 per cubic meter, depending on factors such as storage requirements, transportation, shielding, and final disposal in secure facilities. Figure 5.31 illustrates spatial differences in the costs associated with managing radioactive waste following a nuclear accident.

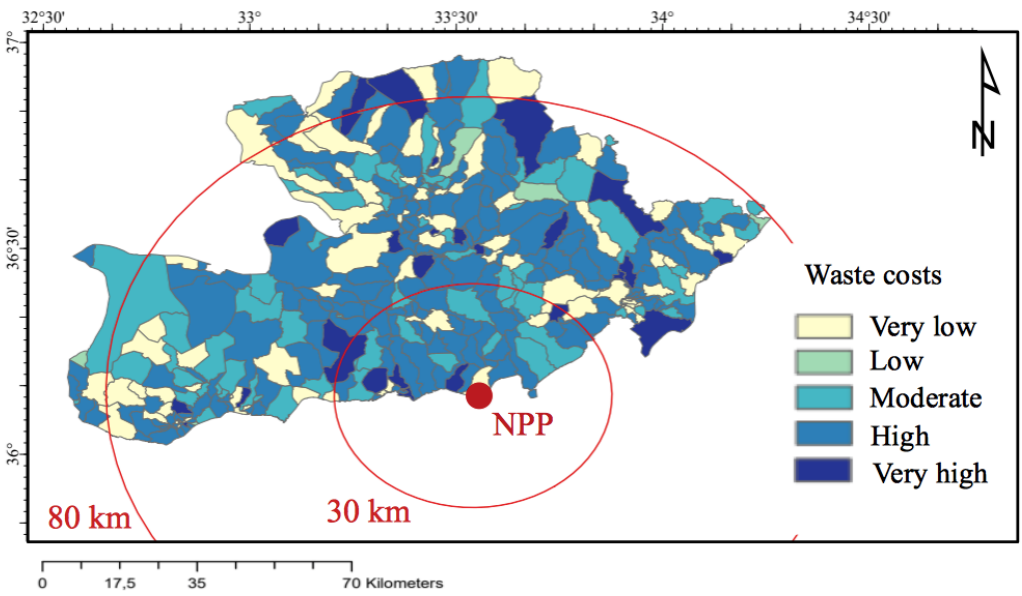

Figure 5.31 : The radioactive waste-related costs.

Areas surrounding the NPP, particularly within the 30-km zone, show higher costs due to greater contamination levels necessitating more complex waste handling and disposal procedures. The variation across regions reflect differences in terrain and the type of infrastructure, which influence the ease or difficulty of waste removal and containment. Lower-cost regions usually benefit from naturally lower contamination risks.

5.7.5 The compensation-related cost estimation

In this study, the total compensation cost is estimated by multiplying the population of the affected neighborhood by the average compensation per person as shown in Equation 5.9:

$$C_{compens} = P_n \times AVG \tag{5.9}$$

where P_n is a population of a particular neighborhood and AVG is the average compensation per person.

Based on data from the Fukushima Daiichi nuclear disaster, the average compensation per person was approximately $5,000 (NEA 2012). To adapt this cost to the economic conditions of Türkiye, a GDP-based adjustment is applied as shown in Equation 5.6. Thus, in the Turkish context, the estimated compensation cost per person is approximately $1,345. Figure 5.32 shows the compensation-related costs.

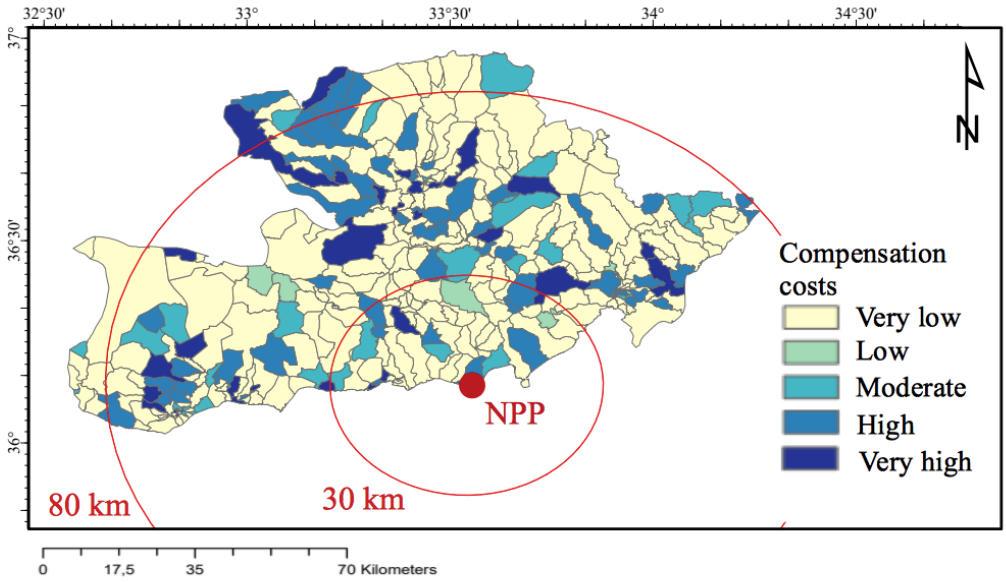

Figure 5.32 : The compensation-related costs.

Compensation-related costs are heavily concentrated in densely populated regions. These costs are associated with the displacement of residents, property loss, agricultural impacts, and other socio-economic disruptions. The high costs suggest a greater burden on authorities to compensate affected populations, particularly in areas with higher land value or agricultural activity. The spatial pattern highlights where financial assistance and legal claims would be most substantial in the aftermath of a nuclear incident.

5.7.6 The administration-related cost estimation

In the aftermath of a nuclear accident, a significant portion of total expenditures is allocated to administrative functions that support the implementation and coordination of emergency response, recovery, and long-term management activities. These administration-related costs include expenses for staffing, logistics coordination, information management, planning, legal and financial services, communication strategies, and overall governance of the crisis response.

To estimate these costs realistically, a percentage-based approach is adopted, consistent with previous disaster-related economic assessments (NEA 2012). In this study, administrative costs are assumed to constitute between 5% and 10% of the total of all other calculated cost components. Mathematically, the administration-related cost is calculated as shown in Equation 5.10:

$$C_{admin} = (5\% - 10\%) \times \left(C_{response} + C_{decont} + C_{health} + C_{waste} + C_{compens}\right) \quad (5.10)$$

where $C_{response}$ is the costs of emergency response, C_{decont} is the cost of decontamination, C_{health} is the health-related costs, C_{waste} is the radioactive waste costs, and $C_{compens}$ is the compensation.

Figure 5.33 displays the distribution of administrative costs. The spatial trend shows moderate to high costs near the NPP and in central areas. Regions with higher values in the other cost components show proportionally elevated administrative costs.

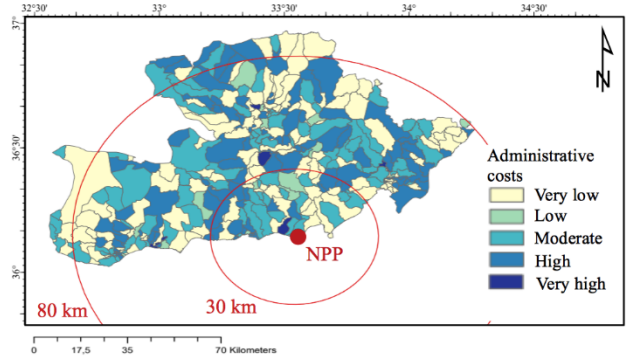

Figure 5.33 : The administration-related costs.

5.7.7 The total estimated economic loss assessment

The Figure 5.34 presents a spatial distribution of total costs resulting from a nuclear emergency, integrating six key categories: emergency response, decontamination, health, radioactive waste management, compensation, and administrative expenses. This map reveals not only where costs accumulate but also highlights areas of financial vulnerability that would demand the greatest recovery efforts.

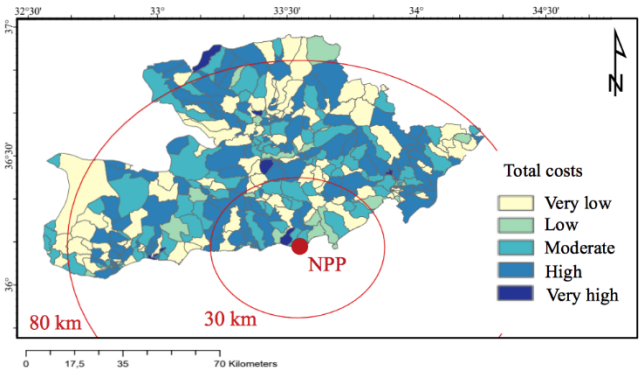

Figure 5.34 : The total estimated costs.

Based on area coverage across the map, the approximate distribution of cost categories can be summarized as follows: “very high” total costs are around 5% of the area,

“high” total costs are 30%, “moderate” total costs are approximately 45%, “low” total costs are nearly 5%, and “very” low total costs are 15%. These proportions suggest that while a substantial portion of the region (around 50%) experiences “low” to “moderate” costs, a significant segment (approximately 35%) falls into the “high” or “very high” cost categories. Spatially, the highest cost regions are clustered around the NPP, particularly to the northwest and west, reflecting dominant population density. Zones to the east and beyond the 30-km zone are exposed to the compounded burden of high health risks, decontamination challenges, and emergency management demands. In contrast, rural areas further from the NPP especially in the west and northwest out of 30-km tend to fall within the “low” or “very low” cost categories, this is due to lower exposure levels and sparse development.

6. CONCLUSIONS AND RECOMMENDATIONS

6.1 Major Findings

This research aimed to develop a spatial model that integrates vulnerability assessments and evacuation planning to enhance preparedness and response strategies during NPP accidents. To achieve this, the study pursued four key objectives: (1) assess social vulnerability in nuclear accident scenarios; (2) simulate evacuation strategies based on varying spatial and demographic parameters; (3) integrate spatial and temporal data into a comprehensive modeling framework; and (4) provide actionable policy recommendations to improve nuclear emergency preparedness. The study was also guided by three hypotheses, each of which was rigorously tested using real-world data, spatial modeling techniques, and scenario-based simulations.

Hypothesis 1: "Areas with higher SVI scores exhibit increased susceptibility to adverse outcomes during nuclear accidents."

The research strongly supports this hypothesis. The findings reveal that vulnerability is not solely dictated by physical proximity to the NPP or direct exposure levels. Rather, socio-economic factors such as limited access to resources, weak infrastructure, poor emergency response capacity, and insufficient preparedness significantly elevate a community's risk. Critically, even areas with lower radiation exposure can be highly vulnerable due to systemic disadvantages. These insights emphasize the importance of localized and socially-informed disaster planning. Targeted interventions such as public awareness campaigns, improved access to emergency services, and customized disaster preparedness strategies can meaningfully reduce vulnerability and increase community resilience.

Hypothesis 2: "The priority-based evacuation method, which integrates SVI data with hazard mapping, results in more effective and equitable evacuation outcomes compared to the traditional radius-based approach".

From the results, the radius-based approach evacuates 50% of the population within 1,000 minutes (approximately 16.6 hours), while the priority-based strategy requires 1,400 minutes (23.3 hours) to reach the same point. Overall, the average evacuation time is 21.8 hours for the radius-based method versus 26.1 hours for the priority-based method, indicating that the former is approximately 22% more time-efficient. However, this faster evacuation speed comes at a cost. The radius-based method, which primarily prioritizes proximity to danger zones, neglects the social and physical vulnerabilities of populations. In contrast, the priority-based approach explicitly prioritizes districts with lower disaster preparedness, response capacity, and coping mechanisms. When the evacuation timeline is divided into three equal phases, the priority-based strategy successfully evacuates 55% of vulnerable individuals in the first phase, 93% by the second, and 100% by the third. Conversely, the radius-based strategy only evacuates 19% of vulnerable populations in the first phase and reaches 64% by the second. Full evacuation of the vulnerable population is only achieved in the final phase. Despite the longer overall duration that is approximately 3,003 minutes (50 hours) compared to 2,454 minutes (40.9 hours), the priority-based method ensures that those most at risk are evacuated earlier. This represents a fundamental trade-off between operational efficiency and ethical responsibility in emergency management. In addition to social equity, public health impacts were evaluated through average TEDE and estimated cancer risk. The results show that the priority-based approach consistently yields lower TEDE levels during the early stages of evacuation. By prioritizing individuals most susceptible to radiation-related health outcomes, the strategy achieves a 14% reduction in average TEDE and a 20.61% relative decrease in estimated cancer risk compared to the radius-based method. These findings confirm that while the priority-based evacuation strategy may extend total evacuation time, it substantially improves outcomes for vulnerable populations and reduces health risks.

Hypothesis 3: “Regions with higher socioeconomic vulnerability experience greater indirect economic losses following a nuclear accident”.

Spatial cost assessments validated this hypothesis. While around 50% of the affected area fell into “low” to “moderate” cost categories, a significant portion (35%) experienced “high” to “very high” indirect economic losses. These areas, typically located closer to the NPP and characterized by denser populations and weaker socioeconomic conditions, are more susceptible to prolonged health impacts,

economic displacement, and infrastructural strain. Conversely, rural and less-developed regions farther from the plant incurred significantly lower indirect costs. These results underscore the uneven economic burdens nuclear disasters impose and the need for targeted mitigation measures including economic support, healthcare provision, and strategic investments in resilience-building infrastructure.

6.2 Limitations of Research

This study presents a novel spatial framework integrating social vulnerability and evacuation modeling during NPP accidents; however, several limitations must be acknowledged. First, the simulation operates under the assumption of a static population distribution, not accounting for dynamic human mobility patterns that typically occur during real emergencies. This limits the realism of evacuation scenarios, particularly in densely populated or highly mobile urban areas. Second, the transportation network used in the model is simplified and based on predefined travel time matrices rather than a detailed, real-time road network analysis. As a result, critical factors such as traffic congestion, road capacity, and route blockages could not be fully captured, potentially affecting the accuracy of evacuation time estimates.

Additionally, while TEDE and cancer risk estimates provided valuable insights into public health outcomes, these calculations relied on average environmental conditions and generalized biological response factors. This introduces uncertainty, as actual radiation dispersion and individual susceptibility may vary significantly depending on local meteorological conditions and population health characteristics. Another limitation lies in the development of the SVI, which, although comprehensive, was constrained by the availability and granularity of publicly accessible data. Key vulnerability indicators such as disability status, informal housing, or undocumented populations were either underrepresented or unavailable, potentially limiting the full scope of vulnerability assessment.

Addressing these limitations in future studies can significantly improve the robustness, accuracy, and usability of spatial models designed for nuclear disaster preparedness and response.

6.3 Policy Recommendations for Emergency Response in Turkiye

In Türkiye, when planning how to respond to a nuclear emergency, it's important to think about who is most at risk. Some people may not have access to transportation, health care, or good information. To make emergency plans fair and effective, the government should use the SVI. This helps identify communities that might need extra help during a nuclear accident. By including SVI in national emergency guidelines, authorities can better plan who should evacuate first, where shelters should be placed, and which areas need more support.

Not everyone can leave an area quickly in an emergency. Older adults, people with disabilities, families without cars, and those living in poverty may need more time and help. The government should update emergency laws to make sure these groups are evacuated first. This would make the process fairer and save more lives by helping the people who are in the most danger.

In places with higher social vulnerability especially near NPPs public services need to be stronger. This means making sure there are good roads for quick evacuation, strong communication systems to share warnings, and enough hospitals or health centers to help people. By investing more in these areas, the government can reduce the risks for people who might otherwise be left behind during an emergency.

Türkiye should build a national online map system that shows nuclear risks in real time. GIS, can track things like radioactive spread, population movement, and the condition of nearby shelters. It would help emergency teams make faster, smarter decisions. For example, if a nuclear leak happens, they can see where the wind is blowing and quickly decide which areas need to be evacuated first.

People living near NPPs should know what to do if an accident happens. The government should start public education programs to teach people about nuclear risks and safety steps. It's also important to organize regular practice drills. These drills help people stay calm and act quickly during a real emergency. The more prepared people are, the better they can protect themselves and their families.

6.4 Recommendations for Future Studies

In the future, it will be very helpful to use real-time information when planning and managing evacuations during a nuclear accident. For example, weather conditions like wind speed and direction can change quickly and affect where the radiation spreads. By using live meteorological data, one can better understand how dangerous materials move through the air.

Also, using mobile tracking systems like Global Positioning System (GPS) from smartphones or location data from cell towers like Global System for Mobile Communications (GSM data) can help to see how people are moving during an evacuation. This makes it possible to create live computer simulations that show both how radiation is spreading and how people are trying to leave the area. These live simulations can help emergency teams give better advice and manage traffic more effectively during real emergencies.

Right now, warning systems might not be fast enough to protect everyone in case of a sudden nuclear release. To fix this, future research should focus on more advanced early warning systems that work together with scientific models, like the Gaussian Plume or HYSPLIT models. These models use weather data to predict how far and in which direction radiation will spread. If these models are connected to the warning system, people can be informed faster and more accurately about where the danger is coming from and what actions they should take (like staying indoors or evacuating).

Sometimes, more than one type of disaster can happen at the same time. For example, a nuclear plant might be affected by an earthquake or flood, which can make the emergency even worse. That's why it's important to expand the current models and plans to consider more than just nuclear accidents. By including other hazards like earthquakes, floods, or wildfires one can build a stronger and more flexible emergency response system. This is called multi-hazard vulnerability mapping, and it helps understand which communities are at the highest risk from multiple dangers and what support they might need the most.

REFERENCES

Abdrabo, K. I., Kantoush, S. A., Esmaiel, A., Saber, M., Sumi, T., Almamari, M., Ghoniem, S. (2023). An integrated criteria-based approach for constructing an urban flood vulnerability index as an urban decision-making tool using the PCA and AHP techniques: A case study of Alexandria. Egypt. *Urban Climate,* 48: 101426.

Addo, E. K., Kabo-bah, A. T., Diawuo, F. A., Debrah, S. K. (2023). The role of nuclear energy in reducing greenhouse gas (GHG) emissions and energy security: a systematic review. *International Journal of Energy Research,* 1: 8823507

Adigüzel, F. (2023). Calculating the tourism climate index for urban planning: a case study of Mersin province. *Journal of Gastronomy, Hospitality and Travel (Joghat)*, 6(3): 1253-1266.

Ahangari, R. and Noori-Kalkhoran, O. (2019). A study of the protective actions for a hypothetical accident of the Bushehr nuclear power plant at different meteorological conditions. *Radiation and Environmental Biophysics,* 58: 277-285.

Ajtai, I., Ştefănie, H., Maloș, C., Botezan, C., Radovici, A., Bizău-Cârstea, M., Baciu, C. (2023). Mapping social vulnerability to floods. A comprehensive framework using a vulnerability index approach and PCA analysis. *Ecological Indicators,* 154: 110838.

Akcay, B. (2009). The case of nuclear energy in Türkiye: From Chernobyl to Akkuyu nuclear power plant. *Energy Sources, Part B,* 4(4): 347-355.

Alarifi, S. S., Abdelkareem, M., Abdalla, F., Alotaibi, M. (2022). Flash flood hazard mapping using remote sensing and GIS techniques in southwestern Saudi Arabia. *Sustainability,* 14(21): 14145.

Alinaghizadeh, H., Wålinder, R., Vingård, E., Tondel, M. (2016). Total cancer incidence in relation to 137Cs fallout in the most contaminated counties in Sweden after the Chernobyl nuclear power plant accident: a register-based study. *BMJ open,* 6(12): e011924.

Anderson, D., Prioleau, P., Taku, K., Naruse, Y., Sekine, H., Maeda, M., Yanagisawa, R. (2016). Post-traumatic stress and growth among medical student volunteers after the March 2011 disaster in Fukushima, Japan: implications for student involvement with future disasters. *Psychiatric quarterly,* 87(2): 241-251.

Angeon, V. and Bates, S. (2015). Reviewing composite vulnerability and resilience indexes: A sustainable approach and application. *World Development,* 72: 140-162.

Annex, D. and UNSCEAR. (2000). Sources and effects of ionizing radiation. *Investigation of I,* 125.

Arda, T., Bayrak, O. C., Uzar, M. (2025). Analyzing coastal vulnerability using analytic hierarchy process and best-worst method: a case study of the Marmara gulf region. *Arabian Journal for Science and Engineering,* 50(3): 1851-1869.

Arifah, A. R., Tariq, M., Juni, M. H. (2019). Decision making in disaster management cycle of natural disasters: a review. *Int J Public Health Clin Sci,* 6(3): 1-18.

Arruda, H., Silva, E. R., Lessa, M., Proença Jr, D., Bartholo, R. (2022). VOSviewer and bibliometrix. *Journal of the Medical Library Association: JMLA,* 110(3): 392.

Arto, I., Andreoni, V., Rueda Cantuche, J. M. (2015). Global impacts of the automotive supply chain disruption following the Japanese earthquake of 2011. *Economic Systems Research,* 27(3): 306-323.

Arvin, M., Beiki, P., Shahraki, S. Z. (2023). A neighborhood-level analysis of association between social vulnerability and COVID-19 in Ahvaz, Iran. *International Journal of Disaster Risk Reduction,* 85: 103504.

Ashley, S. F., Vaughan, G. J., Nuttall, W. J., Thomas, P. J., Higgins, N. A. (2017). Predicting the cost of the consequences of a large nuclear accident in the UK. *Process Safety and Environmental Protection,* 112: 96-113.

ASN. (2021). French Nuclear Safety Authority, Radiological Protection and Emergency Preparedness Framework, Paris, 07 July 2022.

Avci, A. C. and Kaygusuz, K. (2020). Renewable and sustainable energy policies in Türkiye after the Paris Agreement: economic and environmental analysis. *Journal of Engineering Research and Applied Science,* 9(2): 1618-1629.

Aydin, C. I. (2020). Nuclear energy debate in Türkiye: Stakeholders, policy alternatives, and governance issues. *Energy Policy,* 136: 111041.

Ayoub, A., Wainwright, H. M., Sansavini, G., Gauntt, R., Saito, K. (2024). Resilient design in nuclear energy: Critical lessons from a cross-disciplinary analysis of the Fukushima Dai-ichi nuclear accident. *Iscience,* 27(4): 109485.

Ağbulut, Ü. (2019). Türkiye's electricity generation problem and nuclear energy policy. *Energy Sources, Part A: Recovery, Utilization, and Environmental Effects,* 41(18): 2281-2298.

Bachev, H. and Ito, F. (2013). Impacts of Fukushima nuclear disaster on Japanese agriculture and food chains. *Agricultural Research Updates,* 6: 1-76.

Bakhshian, E. and Martinez-Pastor, B. (2023). Evaluating human behaviour during a disaster evacuation process: A literature review. *Journal of traffic and transportation engineering (English edition),* 10(4): 485-507.

Bakkensen, L.A., Fox-Lent, C., Read, L.K., Linkov, I. (2017). Validating resilience and vulnerability indices in the context of natural disasters. *Risk analysis,* 37(5): 982-1004.

Bartzis, J. Ehrhardt, J., French, S., Lochard, J., Morrey, M., Papamichail, K. N., … (2000). Rodos: Decision support for nuclear emergencies. In S. H. Zanakis, G. Doukidis, C. Zopounidis (Eds.), *Decision Making: Recent Developments and Worldwide Applications. Applied Optimization* (Vol. 45, pp. 381-395). Springer: Boston.

Becerra, V. M.; Vajpayee, V.; Bausch, N.; Santhosh, T. V.; Vinod, G.; Deng, J. (2020). Estimation of radioactivity release activity using non-linear Kalman filter-based estimation techniques. *Energies,* 13(15): 3985.

Bellamy, M. B., Dewji, S. A., Leggett, R. W., Hiller, M., Veinot, K., Manger, R. P., Stewart, D. J. (2019). External exposure to radionuclides in air, water, and soil. *Federal Guidance Report,* 15: 402.

Belyakov, A. (2015). From Chernobyl to Fukushima: an interdisciplinary framework for managing and communicating food security risks after nuclear plant accidents. *Journal of Environmental Studies and Sciences,* 5(3): 404-417.

Belyi, D., Kovalenko, A., Bazyka, D. (2013). Acute radiation syndrome survivors after chernobyl accident: History of irradiation, diagnostic mistakes and death reasons in long-term period. *Radiat Emerg Med,* 2(2): 5-12.

Bera, S., Gnyawali, K., Dahal, K., Melo, R., Li-Juan, M., Guru, B., Ramana, G. V. (2023). Assessment of shelter location-allocation for multi-hazard emergency evacuation. *International Journal of Disaster Risk Reduction,* 84: 103435.

Beresford, N. A., Fesenko, S., Konoplev, A., Skuterud, L., Smith, J. T., Voigt, G. (2016). Thirty years after the Chernobyl accident: What lessons have we learnt?. *Journal of environmental radioactivity,* 157: 77-89.

Beresford, N. A., Scott, E. M., Copplestone, D. (2020). Field effects studies in the Chernobyl Exclusion Zone: Lessons to be learnt. *Journal of environmental radioactivity,* 211: 105893.

Beyki, S. M., Santiago, A., Laím, L., Craveiro, H. D. (2023). Evacuation simulation under threat of wildfire – an overview of research, development, and knowledge gaps. *Applied Sciences,* 13(17): 9587.

Bhanot, K. (2000). Preliminary fact finding mission following the accident at the nuclear fuel processing facility in Tokaimura, Japan (Vienna: IAEA). *Journal of Radiological Protection,* 20(1): 73.

Bilgilioğlu, S. S. (2021). Land suitability assessment for Olive cultivation using GIS and multi-criteria decision-making in Mersin City, Türkiye. *Arabian Journal of Geosciences,* 14(22): 2434.

Bilgilioğlu, S. S. (2022). Site selection for radioactive waste disposal facility by GIS based multi criteria decision making. *Annals of Nuclear Energy,* 165: 108795.

Birikorang, S. A., Abrefah, R. G., Sogbadji, R. B. M., Nyarko, B. J. B., Fletcher, J. J., Akaho, E. H. K. (2015). Ground deposition assessment of radionuclides following a hypothetical release from Ghana Research Reactor-1 (GHARR-1) using atmospheric dispersion model. *Progress in Nuclear Energy,* 79: 96-103.

Bisconti, A. S. (2018). Changing public attitudes toward nuclear energy. *Progress in Nuclear Energy,* 102: 103-113.

Bizet, R. and Lévêque, F. (2017). The economic assessment of the cost of nuclear accidents. In Ahn, J., Guarnieri, F., Furuta, K. (Eds.) *Resilience: A New Paradigm of Nuclear Safety* (pp.79-96). Springer: Cham.

Bilgiç, E. and Gündüz, O. (2022). Radiological modeling of the impacts of the Chernobyl nuclear power plant accident on Türkiye and southwest Asia. *Atmospheric Pollution Research,* 13(2): 101308.

Bozhenyuk, A., Rodzin, S., Rodzina, L. (2023). Multi-Criteria group decision-making: a fuzzy algorithm for emergency evacuation tasks. In *2023 International Russian Automation Conference (RusAutoCon)*.

Bozóki, S. and Rapcsák, T. (2008). On Saaty's and Koczkodaj's inconsistencies of pairwise comparison matrices. *Journal of Global Optimization,* 42: 157-175.

Bretschneider, S. (2012). *Mathematical models for evacuation planning in urban areas.* Springer Berlin, Heidelberg.

Brian, L. (2011). A social vulnerability index for disaster management. *Journal of Homeland Security and Emergency Management,* 8(1): 1-22.

Bromet, E. J. and Havenaar, J. M. (2007). Psychological and perceived health effects of the Chernobyl disaster: a 20-year review. *Health physics,* 93(5): 516-521.

Buesseler, K., Aoyama, M., Fukasawa, M. (2011). Impacts of the Fukushima nuclear power plants on marine radioactivity. *Environmental science and technology,* 45(23): 9931-9935.

Bănică, A., Muntele, I., Grozavu, A. (2017). Assessing seismic risk in the urban areas of Romania using GIS-based multi-criteria analysis. *Natural Hazards,* 89(3): 1139-1165.

Bıçakcı, A. S. and Evren, A. G. (2022). Thinking multiculturality in the age of hybrid threats: Converging cyber and physical security in Akkuyu nuclear power plant. *Nuclear Engineering and Technology,* 54(7): 2467-2474.

Cai, H.; Jia, X.; Feng, J.; Yang, Q.; Hsu, Y. M.; Chen, Y.; Lee, J. (2019). A combined filtering strategy for short term and long-term wind speed prediction with improved accuracy. *Renewable energy,* 136: 1082-1090.

Cao, B., Cui, W., Chen, C., Chen, Y. (2020). Development and uncertainty analysis of radionuclide atmospheric dispersion modeling codes based on Gaussian plume model. *Energy,* 194: 116925.

Carrassi, A., Bocquet, M., Bertino, L., Evensen, G. (2018). Data assimilation in the geosciences: An overview of methods, issues, and perspectives. *Wiley Interdisciplinary Reviews: Climate Change,* 9(5): e535.

Celik, M. A. and Gülersoy, A. E. (2018). Climate classification and drought analysis of Mersin. *Manisa Celal Bayar Üniversitesi Sosyal Bilimler Dergisi,* 16(1): 1-26.

Cetin, M. (2020). The changing of important factors in the landscape planning occur due to global climate change in temperature, Rain and climate types: A case study of Mersin City. *Turkish Journal of Agriculture-Food Science and Technology,* 8(12): 2695-2701.

Chadly, A., Aldayyani, H. Y., Hamasha, M. M., Amer, S. E., Maalouf, M., Mayyas, A. (2024). Selection of optimal strategy for managing decentralized solar PV systems considering uncertain weather conditions. *Scientific Reports,* 14(1): 12269.

Chaisan, K., Smith, J. T., Bossew, P., Kirchner, G., Laptev, G. V. (2013). Worldwide isotope ratios of the Fukushima release and early-phase external dose reconstruction. *Scientific Reports,* 3(1): 2520.

Chakraborty, L., Thistlethwaite, J., Scott, D., Henstra, D., Minano, A., Rus, H. (2023). Assessing social vulnerability and identifying spatial hotspots of flood risk to inform socially just flood management policy. *Risk Analysis,* 43(5): 1058-1078.

Chelariu, O. E., Minea, I., Iațu, C. (2024). Integrated assessment of geophysical and social vulnerability to natural hazards in North-East Region, Romania. *Geomatics, Natural Hazards and Risk,* 15(1): 2384607.

Chen, Z. (2003). Bayesian filtering: From Kalman filters to particle filters, and beyond. *Statistics,* 182(1): 1-69.

Chino, M., Nakayama, H., Nagai, H., Terada, H., Katata, G., Yamazawa, H. (2011). Preliminary estimation of release amounts of 131I and 137Cs accidentally discharged from the Fukushima Daiichi nuclear power plant into the atmosphere. *Journal of nuclear science and technology,* 48(7): 1129-1134.

Chiu, Y. C. and Zheng, H. (2007). Real-time mobilization decisions for multi-priority emergency response resources and evacuation groups: model formulation and solution. *Transportation Research Part E: Logistics and Transportation Review,* 43(6): 710-736.

Choi, T.A., Costes, S.V., Abergel, R.J. (2015). Understanding the Health Impacts and Risks of Exposure to Radiation. In Ahn, J., Carson, C., Jensen, M., Juraku, K., Nagasaki, S., Tanaka, S. (Eds.), *Reflections on the Fukushima Daiichi Nuclear Accident* (pp 259-281). Springer, Cham.

Chowdhuri, I., Pal, S. C., Saha, A., Chakrabortty, R., Roy, P. (2022). Mapping of earthquake hotspot and coldspot zones for identifying potential landslide hotspot areas in the Himalayan region. *Bulletin of Engineering Geology and the Environment,* 81(7): 257.

City Population: Japan. (2020). Accessed 2020, http://www.citypopulation.de/Japan-Fukushima.html

Cooke, M. W., Trudel, M., Gurney-Smith, H. J., Kellogg, J. P., Cullen, J. T., Francisco, B. B. A., ... (2022). Radioactivity concentration measurements in fish and shellfish samples from the west coast of Canada after the Fukushima nuclear accident (2011–2018). *Journal of Environmental Radioactivity,* 251: 106934.

Cope, M. R. and Slack, T. (2017). Emplaced social vulnerability to technological disasters: Southeast Louisiana and the BP Deepwater Horizon oil spill. *Population and Environment,* 38: 217-241.

Cousins, C., Miller, D. L., Bernardi, G., … (2011). International commission on radiological protection. *ICRP Publication,* 120: 1-125.

Csereklyei, Z. (2014). Measuring the impact of nuclear accidents on energy policy. *Ecological economics,* 99: 121-129.

Cutter, S. L., Boruff, B. J., Shirley, W. L. (2003). Social Vulnerability to Environmental Hazards. *Social Science Quarterly,* 84(2): 242–261.

Cutter, S. L., Mitchell, J. T., Scott, M. S. (2000). Revealing the vulnerability of people and places: A case study of Georgetown County, South Carolina. *Annals of the association of American Geographers,* 90(4): 713-737.

D'Auria, F., Debrecin, N., Glaeser, H. (2017). Strengthening nuclear reactor safety and analysis. *Nuclear Engineering and Design,* 324: 209-219.

Dalnoki-Veress, F., McKallagat, C., Klebesadal, A. (2014). Local Health Department Planning for a Radiological Emergency: An Application of the AHP Tool to Emergency Preparedness Prioritization. *Public Health Reports,* 129(4): 136–144.

Debnath, B., Bari, A. M., de Jesus Pacheco, D. A., Karmaker, C. L. (2023). An integrated Best–Worst Method and Interpretive Structural Modeling approach for assessing the barriers to circular economy implementation. *Decision Analytics Journal,* 7: 100250.

Demir, G., Chatterjee, P., Pamucar, D. (2024). Sensitivity analysis in multi-criteria decision making: A state-of-the-art research perspective using bibliometric analysis. *Expert Systems with Applications,* 237: 121660.

Demirbaş, A. (2001). Energy balance, energy sources, energy policy, future developments and energy investments in Türkiye. *Energy conversion and Management,* 42(10): 1239-1258.

Demiryay, B. (2022). *Identification of Evacuation Zones by Superposed Hazard Mapping Method in Case of a Hypothetical Nuclear Power Plant Accident: The Case of Akkuyu Nuclear Power Plant* (Master's thesis). Middle East Technical University,Türkiye.

Deng, Q., Zhang, B., Zhou, Z., Deng, H., Zhou, L., Zhou, Z., Jiang, H. (2022). Evacuation time estimation model in large buildings based on individual characteristics and real-time congestion situation of evacuation exit. *Fire,* 5(6): 204.

Di Nicola, F., Brattich, E., Di Sabatino, S. (2022). A new approach for roughness representation within urban dispersion models. *Atmospheric Environment,* 283: 119181.

Di Ronco, A.; Giacobbo, F.; Cammi, A. (2020). A Kalman filter-based approach for online source-term estimation in accidental radioactive dispersion events. *Sustainability,* 12(23): 10003.

Dolan, G. and Messen, D. (2012). Social vulnerability: An emergency managers' planning tool. *Journal of Emergency Management,* 10(3): 161-169.

Donthu, N., Kumar, S., Mukherjee, D., Pandey, N., Lim, W. M. (2021). How to conduct a bibliometric analysis: An overview and guidelines. *Journal of business research,* 133: 285-296.

Drace, Z., Ojovan, M. I., Samanta, S. K. (2022). Challenges in planning of integrated nuclear waste management. *Sustainability,* 14(21): 14204.

Drozdovitch, V., Bouville, A., Chobanova, N., Filistovic, V., Ilus, T., Kovacic, M., ... (2007). Radiation exposure to the population of Europe following the Chernobyl accident. *Radiation Protection Dosimetry,* 123(4): 515-528.

Dubrova, Y. E., Nesterov, V. N., Krouchinsky, N. G., Ostapenko, V. A., Neumann, R., Neil, D. L., Jeffreys, A. J. (1996). Human minisatellite mutation rate after the Chernobyl accident. *Nature,* 380(6576): 683-686.

Duffield, J. S. (2016). Japanese energy policy after Fukushima daiichi: nuclear ambivalence. *Political Science Quarterly,* 131(1): 133-162.

Dulebenets, M. A., Pasha, J., Abioye, O. F., Kavoosi, M., Ozguven, E. E., Moses, R., ... (2019). Exact and heuristic solution algorithms for efficient emergency evacuation in areas with vulnerable populations. *International journal of disaster risk reduction,* 39: 101114.

Dumitrescu, C., Radu, V., Gheorghe, R., Tăbîrcă, A. I., Ștefan, M. C., Manea, L. (2024). Crowd Panic Behavior Simulation Using Multi-Agent Modeling. *Electronics,* 13(18): 3622.

Eeckhoudt, L., Schieber, C., Schneider, T. (2000). Risk aversion and the external cost of a nuclear accident. *Journal of environmental Management,* 58(2): 109-117.

Ehlken, S. and Kirchner, G. (2002). Environmental processes affecting plant root uptake of radioactive trace elements and variability of transfer factor data: a review. *Journal of environmental radioactivity,* 58(2-3): 97-112.

Eicher, C. L., Brewer, C. A. (2001). Dasymetric mapping and areal interpolation: Implementation and evaluation. *Cartography and Geographic Information Science,* 28(2): 125-138.

Eidemüller, D. (2021). Reactors, Bombs and Visions: A Brief History of the Nuclear Age. In *Nuclear Power Explained*. Springer Praxis Books (pp 1-26). Springer, Cham.

Eiser, J. R., Hannover, B., Mann, L., Morin, M., van Der Pligt, J., Webley, P. (1990). Nuclear attitudes after Chernobyl: A cross-national study. *Journal of Environmental Psychology,* 10(2): 101-110.

Eleveld, H., Twenhoefel, C. J. W., Bader, S. (2006). Evaluations of a data assimilation methodology in a nuclear emergency response system. *Geophysical Research Abstracts,* 8: 2.

EPA. (2017). U.S. Environmental Protection Agency Protective Action Guides (PAGs) Manual, Washington, D.C., January 2017.

Escobar, M. T., Aguarón, J., Moreno-Jiménez, J. M. (2004). A note on AHP group consistency for the row geometric mean priorization procedure. *European Journal of Operational Research,* 153(2): 318-322.

Espinosa-Paredes, G., Nuñez-Carrera, A., Laureano-Cruces, A. L., Vázquez-Rodríguez, A., Espinosa-Martinez, E. G. (2008). Emergency management for a nuclear power plant using fuzzy cognitive maps. *Annals of Nuclear Energy,* 35(12): 2387-2396.

Essa, K. S. and El Saied, S. I. (2023). Maximum ground level concentration for Gaussian plume formula using standard and Briggs methods. *Environmental Quality Management,* 32(4): 73-81.

Evangeliou, N., Hamburger, T., Talerko, N., Zibtsev, S., Bondar, Y., Stohl, A., ... (2016). Reconstructing the Chernobyl Nuclear Power Plant (CNPP) accident 30 years after. A unique database of air concentration and deposition measurements over Europe. *Environmental pollution,* 216: 408-418.

Fan, T., Wong, S. C., Zhang, Z., Du, J. (2024). Stochastic Lighthill-Whitham-Richards traffic flow model for nonlinear speed-density relationships. *Transportmetrica B: Transport Dynamics,* 12(1): 2419402.

Farhat, H., Alinier, G., Chaabna, K., El Aifa, K., Abougalala, W., Laughton, J., Ben Dhiab, M. (2024). Preparedness and emergency response strategies for chemical, biological, radiological and nuclear emergencies in disaster management: a qualitative systematic review. *Journal of Contingencies and Crisis Management,* 32(3): e12592.

Fatemi, F., Ardalan, A., Aguirre, B., Mansouri, N., Mohammadfam, I. (2017). Social vulnerability indicators in disasters: Findings from a systematic review. *International journal of disaster risk reduction,* 22: 219-227.

Fekete, A. (2019). Social vulnerability change assessment: monitoring longitudinal demographic indicators of disaster risk in Germany from 2005 to 2015. *Natural Hazards,* 95(3): 585-614.

Fekete, A. (2022). Phasing out of nuclear-phasing out of risk? Spatial assessment of social vulnerability and exposure to nuclear power plants in Germany. *Progress in disaster science,* 15: 100242.

Fekete, A. and Neuner, S. (2023). Spatial industrial accident exposure and social vulnerability assessment of hazardous material sites, chemical parks, and nuclear power plants in Germany. *International Journal of Disaster Risk Science,* 14(2): 223-236.

Feldhoff, T. (2018). Visual representations of radiation risk and the question of public (mis-) trust in post-Fukushima Japan. *Societies,* 8(2):32.

Feldman, E. A. (2015). Compensating the victims of Japan's 3-11 Fukushima disaster. *Asian-Pacific Law and Policy Journal,* 127: 1632.

Feng, T., Liu, K., Liang, C. (2023). An improved cellular automata traffic flow model considering driving styles. *Sustainability,* 15(2): 952.

Fentiman, A. W. (2009). Transportation of Radioactive Materials. *Environmentally Conscious Materials Handling,* 217-237.

Figueiredo, C. J. J. D., de Miranda Mota, C. M., de Araujo, K. G. D., Rosa, A. G. F., de Souza, A. P. G. (2022). Measuring COVID-19 Vulnerability for Northeast Brazilian Municipalities: Social, Economic, and Demographic Factors Based on Multiple Criteria and Spatial Analysis. *ISPRS International Journal of Geo-Information,* 11(8): 449.

Filburn, T. and Bullard, S., (2016). *Chernobyl Accident. Three Mile Island, Chernobyl and Fukushima: Curse of the Nuclear Genie.* Springer Charm.

Fisher, N. S., Beaugelin-Seiller, K., Hinton, T. G., Baumann, Z., Madigan, D. J., Garnier-Laplace, J. (2013). Evaluation of radiation doses and associated risk from the Fukushima nuclear accident to marine biota and human consumers of seafood. *Proceedings of the National Academy of Sciences,* 110(26): 10670-10675.

Flanagan, B. E., Gregory, E. W., Hallisey, E. J., Heitgerd, J. L., Lewis, B. (2011). A social vulnerability index for disaster management. *Journal of homeland security and emergency management,* 8(1): 1-22.

Fox, S., Agyemang, F., Hawker, L., Neal, J. (2024). Integrating social vulnerability into high-resolution global flood risk mapping. *Nature communications,* 15(1): 3155.

Frazier, T. G., Thompson, C. M., Dezzani, R. J. (2014). A framework for the development of the SERV model: A Spatially Explicit Resilience-Vulnerability model. *Applied Geography,* 51: 158-172.

Frigerio, I., Ventura, S., Strigaro, D., Mattavelli, M., De Amicis, M., Mugnano, S., Boffi, M. (2016). A GIS-based approach to identify the spatial variability of social vulnerability to seismic hazard in Italy. *Applied geography,* 74: 12-22.

Funabashi, Y. and Kitazawa, K. (2012). Fukushima in review: A complex disaster, a disastrous response. *Bulletin of the Atomic Scientists,* 68(2): 9-21.

Furlan, E., Dalla Pozza, P., Michetti, M., Torresan, S., Critto, A., Marcomini, A. (2021). Development of a Multi-Dimensional Coastal Vulnerability Index: Assessing vulnerability to inundation scenarios in the Italian coast. *Science of the Total Environment,* 772: 144650.

Gayen, S., Villalta, L. I. V., Haque, S. M. (2020). Comparative social vulnerability assessment in Purba Medinipur district, West Bengal, India. *European Journal of Geography,* 11(1): 93-107.

Geist, E. (2015). Political Fallout: The Failure of Emergency Management at Chernobyl. *Slavic Review,* 74(1): 104-126.

Gill, J. C. and Malamud, B. D. (2014). Reviewing and visualizing the interactions of natural hazards. *Reviews of geophysics,* 52(4): 680-722.

Giovannini, L., Ferrero, E.; Karl, T., Rotach, M. W., Staquet, C., Trini Castelli, S., Zardi, D. (2020). Atmospheric pollutant dispersion over complex terrain: Challenges and needs for improving air quality measurements and modeling. *Atmosphere,* 11(6): 646.

Grave, I., Bojórquez-Tapia, L. A., Estrada-Barón, A., Nelson, D. R., Eakin, H. (2022). Analytic hierarchy process and sensitivity analysis implementation for social vulnerability assessment: A case study from Brazil. *Journal of Multi-Criteria Decision Analysis,* 29(5-6): 381-392.

Gu, Z. (2018). History review of nuclear reactor safety. *Annals of Nuclear Energy,* 120: 682-690.

Guillard-Gonçalves, C. and Zêzere, J. L. (2018). Combining social vulnerability and physical vulnerability to analyse landslide risk at the municipal scale. *Geosciences,* 8(8): 294.

Güler M. Ç. (2018). *Dynamics of the Russian foreign policy between 2000-2019: nuclear energy as a foreign policy tool in the case of Türkiye* (Master thesis). Middle East Technical University, Graduate School of Social Sciences, Eurasian Studies, Turkiye.

Hammer, C. C., Brainard, J., Innes, A., Hunter, P. R. (2019). (Re-) conceptualising vulnerability as a part of risk in global health emergency response: updating the pressure and release model for global health emergencies. *Emerging Themes in Epidemiology,* 16: 1-8.

Han, G., Li, W., Fu, H., … (2013). An ensemble estimation of impact times and strength of Fukushima nuclear pollution to the east coast of China and the west coast of America. *Science China Earth Sciences,* 56: 1447-1451.

Hancerlioglu, A., Turhan, Ş., Kurnaz, A. (2019). Evaluation of the Excess Lifetime Cancer Risk Due to Natural Radioactivity in Tap Water Consumed in Nevşehir Province, Türkiye. *Bitlis Eren Üniversitesi Fen Bilimleri Dergisi,* 8: 46-48.

Handler, I. (2016). The impact of the Fukushima disaster on Japan's travel image: An exploratory study on Taiwanese travellers. *Journal of Hospitality and Tourism Management,* 27: 12-17.

Harada, K. H., Niisoe, T., Imanaka, M., … (2014). Radiation dose rates now and in the future for residents neighboring restricted areas of the Fukushima Daiichi Nuclear Power Plant. *Proceedings of the National Academy of Sciences,* 111(10): E914-E923.

Hardie, S. M. L. and McKinley, I. G. (2014). Fukushima remediation: status and overview of future plans. *Journal of environmental radioactivity,* 133: 75-85.

Hasegawa, A., Ohira, T., Maeda, M., Yasumura, S., Tanigawa, K. (2016). Emergency responses and health consequences after the Fukushima accident; evacuation and relocation. *Clinical Oncology,* 28(4): 237-244.

Hashimoto, S. (2023). Overview of radiocesium dynamics in forests: first decade and future perspectives. In Nakanishi, T. M., Tanoi, k. (Eds.), *Agricultural Implications of Fukushima Nuclear Accident (IV) After 10 Years* (pp. 133-147). Springer, Singapore.

Hatch, M., Ron, E., Bouville, A., Zablotska, L., Howe, G. (2005). The Chernobyl disaster: cancer following the accident at the Chernobyl nuclear power plant. *Epidemiologic reviews,* 27(1): 56-66.

Hayashi, M. and Hughes, L. (2013). The Fukushima nuclear accident and its effect on global energy security. *Energy policy,* 59: 102-111.

He, B. and Guan, Q. (2024). Investigating the effects of spatial scales on social vulnerability index: a hybrid uncertainty and sensitivity analysis approach combined with remote sensing land cover data. *Risk Analysis,* 44(11): 2723-2739.

He, B. and Guan, Q. (2022). The statistical analysis and prediction associated with nuclear meltdown accidents risk evaluation. *International Journal of Nuclear Safety and Security,* 1(2): 104-123.

He, Z., Shen, K., Lan, M., Weng, W. (2024). An evacuation path planning method for multi-hazard accidents in chemical industries based on risk perception. **Reliability Engineering and System Safety,** 244: 109912.

Hirose, K. (2016). Fukushima Daiichi Nuclear Plant accident: Atmospheric and oceanic impacts over the five years. *Journal of Environmental Radioactivity,* 157: 113-130.

Howe, G. R. (2007). Leukemia following the Chernobyl accident. *Health Physics,* 93(5): 512-515.

Hsu, Y. T. and Peeta, S. (2014). Risk-based spatial zone determination problem for stage-based evacuation operations. *Transportation research part C: Emerging Technologies,* 41: 73-89.

Huhtala, A. and Remes, P. (2017). Quantifying the social costs of nuclear energy: Perceived risk of accident at nuclear power plants. *Energy Policy,* 105: 320-331.

IAEA. (2015). *The Fukushima Daiichi Accident Report by the Director General.* Vienna: International Atomic Energy Agency.

IAEA. (2011). *Actions to Protect the Public in an Emergency due to Severe Conditions at a Light Water Reactor*. IAEA General Safety Guide No. GSG-2, Vienna.

Iban, M. C. and Sahin, E. (2022). Monitoring land use and land cover change near a nuclear power plant construction site: Akkuyu case, Türkiye. *Environmental Monitoring and Assessment,* 194(10): 724.

Igarashi, Y., Nanba, K., Wada, T., Wakiyama, Y., Onda, Y., Moritaka, S., Konoplev, A. (2022). Factors controlling the dissolved 137Cs seasonal fluctuations in the Abukuma River under the influence of the Fukushima Nuclear Power Plant accident. *Journal of Geophysical Research: Biogeosciences,* 127(1): e2021JG006591.

Igbokwe, J. I. and Ajie, U. E. (2023). Implementation of origin-destination cost matrix intelligent transport system for port Harcourt metropolitan city of rivers state, Nigeria. *Environmental Review,* 9(2): 34-44.

Isazade, V., Qasimi, A. B., Dong, P., Kaplan, G., Isazade, E. (2023). Integration of Moran's I, geographically weighted regression (GWR), and ordinary least square (OLS) models in spatiotemporal modeling of COVID-19 outbreak in Qom and Mazandaran provinces, Iran. *Modeling Earth Systems and Environment,* 9(4): 3923-3937.

Ishikawa, T. (2017). Radiation doses and associated risk from the Fukushima nuclear accident: a review of recent publications. *Asia Pacific Journal of Public Health,* 29(2): 18S-28S.

Ishikawa, T., Yasumura, S., Ozasa, K., Kobashi, G., Yasuda, H., Miyazaki, M., ... (2015). The Fukushima Health Management Survey: estimation of external doses to residents in Fukushima Prefecture. *Scientific reports,* 5(1): 12712.

Isia, I., Hadibarata, T., Hapsari, R. I., Jusoh, M. N. H., Bhattacharjya, R. K., Shahedan, N. F. (2023). Assessing social vulnerability to flood hazards: a case study of Sarawak's divisions. *International journal of disaster risk reduction,* 97: 104052.

Islam, M. S., Swapan, M. S. H., Haque, S. M. (2013). Disaster risk index: How far should it take account of local attributes?. *International Journal of Disaster Risk Reduction,* 3: 76-87.

Ivanov, M. M., Ivanova, N. N., Golosov, V. N., Shamshurina, E. N. (2016). Assessing the accumulation of sorbed isotope 137 Cs within the upper components of the fluvial network in the zone of Chernobyl contamination. *Geography and Natural Resources,* 37: 355-361.

Jafer, S. and Lawler, R. (2016). Emergency crowd evacuation modeling and simulation framework with cellular discrete event systems. *Simulation,* 92(8): 795-817.

Jahan, I., Ansary, M. A., Ara, S., Islam, I. (2011). Assessing social vulnerability to earthquake hazard in Old Dhaka, Bangladesh. *Asian Journal of Environment and Disaster Management,* 3(3): 285-300.

Jeong, H. J., Han, M. H., Hwang, W. T., Kim, E. H. (2008). Application of data assimilation to improve the forecasting capability of an atmospheric dispersion model for a radioactive plume. *Annals of Nuclear Energy,* 35(5): 838-844.

Jewell, J. and Ates, S. A. (2015). Introducing nuclear power in Türkiye: A historic state strategy and future prospects. *Energy Research and Social Science,* 10: 273-282.

Johnson, J. B. (2022). An introduction to atmospheric pollutant dispersion modelling. *Environmental Sciences Proceedings,* 19(1): 18.

Jouin, M., Gouriveau, R., Hissel, D., Péra, M. C., Zerhouni, N. (2016). Particle filter-based prognostics: Review, discussion and perspectives. *Mechanical Systems and Signal Processing,* 72: 2-31.

Kabatchenko, I.M., Kulikov, E.A., Litvinenko, G.I. … (2020). Estimation of Extreme Sea Level in the Akkuyu Nuclear Power Plant Area. *Russ. Meteorol. Hydrol.,* 45: 39-44.

Kahle, W. J. (2022). *Human Conflict and Nuclear Weapons* (Doctoral dissertation). Johns Hopkins University.

Kalkan, S. K., Forkapić, S., Marković, B. S., … (2021). Deposition of 137Cs and precipitation distribution in Vojvodina, Northern Serbia after the Chernobyl accident. *Chemosphere,* 264: 128471.

Kanda, R., Minamihisamatsu, M., Hayata, I. (2002). Dynamic analysis of chromosome aberrations in three victims of the Tokai-mura criticality accident. *International journal of radiation biology,* 78(9): 857-862.

Kantarcioglu, V.D. (2018). *Development of 3+ level probabilistic safety assessment method for severe accidents in nuclear power plants and application for Akkuyu Nuclear Power Plant.* (Doctoral dissertation). Hacettepe University, Turkiye.

Karanci, A. N., Aksit, B., Dirik, G. (2005). Impact of a community disaster awareness training program in Türkiye: Does it influence hazard-related cognitions and preparedness behaviors. *Social Behavior and Personality: an international journal,* 33(3): 243-258.

Karar, M. E., Abdel-Aty, A. H., Owyed, S., Reyad, O. (2024). A New Gated Recurrent Unit Network-Based Wind Turbine Power Prediction. *Arabian Journal for Science and Engineering,* 50: 7017-7026.

Kartal, R. F., Beyhan, G., Keskinsezer, A., Kadirioğlu, F. T. (2014). Seismic hazard analysis of Mersin Province, Türkiye using probabilistic and statistical methods. *Arabian Journal of Geosciences,* 7, 4443-4459.

Kashinath, S. A., Mostafa, S. A., Mustapha, A., Mahdin, H., Lim, D., Mahmoud, M. A., ... (2021). Review of data fusion methods for real-time and multi-sensor traffic flow analysis. *IEEE Access,* 9: 51258-51276.

Kaur, N. and Kaur, H. (2022). A multi-agent-based evacuation planning for disaster management: a narrative review. *Archives of Computational Methods in Engineering,* 29(6): 4085-4113.

Kaygusuz, K. and Avci, A. C. (2021). Nuclear power in Türkiye for low carbon economy and energy security: a socioeconomic analysis. *Journal of Engineering Research and Applied Science,* 10(2): 1881-1889.

Kazakov, V.S., Demidchik, E.P., Astakhova, L.N., … (1992). Thyroid cancer after Chernobyl. *Nature,* 359 (3): 21-22.

Kazibudzki, P. T. (2021). On the statistical discrepancy and affinity of priority vector heuristics in pairwise-comparison-based methods. *Entropy,* 23(9): 1150.

Khalilpourazari, S. and Pasandideh, S. H. R. (2021). Designing emergency flood evacuation plans using robust optimization and artificial intelligence. *Journal of Combinatorial Optimization,* 41: 640-677.

Kharecha, P. A. and Sato, M. (2019). Implications of energy and CO2 emission changes in Japan and Germany after the Fukushima accident. *Energy Policy,* 132: 647-653.

Kim, S. and Kim, S. (2017). Impact of the Fukushima nuclear accident on belief in rumors: The role of risk perception and communication. **Sustainability,** 9(12): 2188.

Kim, C. H., Song, C. K., Lee, S. H., Song, S. K. (2008). Simulating mesoscale transport and diffusion of radioactive noble gases using the Lagrangian particle dispersion model. *Journal of Environmental Radioactivity,* 99(10): 1644-1652.

Kim, J. S. and Park, S. H. (2016). A study of the negotiation factors for Korean tourists visiting Japan since the Fukushima nuclear accident using Q-methodology. *Journal of Travel and Tourism Marketing,* 33(5): 770-782.

Kim, K., Jeon-Young, K., Hwang, C. (2025). Identifying Indicators Contributing to the Social Vulnerability Index via a Scoping Review. *Land,* 14(2): 263.

Kinoshita, N., Sueki, K., Sasa, K. (2011). Assessment of individual radionuclide distributions from the Fukushima nuclear accident covering central-east Japan. *Proceedings of the National Academy of Sciences,* 108(49): 19526-19529.

Kitani, M. and Murakami, H. (2022). One-sample location test based on the sign and Wilcoxon signed-rank tests. *Journal of Statistical Computation and Simulation,* 92(3): 610-622.

Klampanos, I. A., Davvetas, A., Andronopoulos, S., Pappas, C., Ikonomopoulos, A., Karkaletsis, V. (2018). Autoencoder-driven weather clustering for source estimation during nuclear events. *Environmental Modelling and Software,* 102: 84-93.

Korsakov, A. V., Geger, E. V., Lagerev, D. G., Pugach, L. I., Mousseau, T. A. (2020). De novo congenital malformation frequencies in children from the Bryansk region following the Chernobyl disaster (2000-2017). *Heliyon,* 6(8): e04616.

Kortov, V. and Ustyantsev, Y. (2013). Chernobyl accident: causes, consequences and problems of radiation measurements. *Radiation Measurements,* 55: 12-16.

Kulikov, V. I., Zhylmaganbetov, N. M., Kavun, O. Y., Popykin, A. I., Smirnova, A. A., Starova, N. A., ... (2022). Computer Simulation of Measurements of VVER-1200 Emergency Protection Efficacy. *Atomic Energy,* 132(5): 263-271.

Kumar, D. and Bhattacharjya, R. K. (2020). Study of integrated social vulnerability index SoVI of hilly region of Uttarakhand, India. *Environmental and Climate Technologies,* 24(1): 105-122.

Kundu, D., Karmakar, S., Srinivas, C. V., Gopalakrishnan, V., Venkatraman, B. (2025). Development of source term estimation model using Kalman filter technique and its evaluation against reversal method. *Progress in Nuclear Energy,* 180: 105618.

Kundu, D., Srinivas, C. V., Chandrasekaran, S., Venkatraman, B. (2022). Radiological consequence assessment for hypothetical nuclear explosion scenario using HotSpot. *Progress in Nuclear Energy,* 147: 104192.

Kurokawa, K. (2013). Fukushima nuclear accident independent investigation commission by the National Diet of Japan. *Nippon Genshiryoku Gakkai-Shi,* 55(3): 146-151.

Kyriakides, K. A. (2023). The Akkuyu nuclear power plant in Türkiye: Some causes for concern. *Journal of Balkan and Near Eastern Studies*, 25(3): 340-377.

Lapietra, I., Colacicco, R., Capolongo, D., La Salandra, M., Rinaldi, A., Dellino, P. (2024). Unveiling social vulnerability to natural hazards in the EEA and UK: A systematic review with insights for enhanced emergency planning and risk reduction. *International Journal of Disaster Risk Reduction,* 108: 104507.

Lean, P., Hólm, E. V., Bonavita, M., Bormann, N., McNally, A. P., Järvinen, H. (2021). Continuous data assimilation for global numerical weather prediction. *Quarterly Journal of the Royal Meteorological Society,* 147(734), 273-288.

Ledford Christopher, B. (2009). *Dynamic Modeling of the Economic Impacts of a Terrorist Attack Using a Radiological Dispersion Device* (Master thesis). Air Force Institute of Technology, USA.

Lee, C., Chae, Y. H., Seong, P. H. (2021). Development of a method for estimating security state: Supporting integrated response to cyber-attacks in NPPs. *Annals of Nuclear Energy,* 158: 108287.

Leenhardt, L. and Aurengo, A. (2000). Post-Chernobyl thyroid carcinoma in children. *Best Practice and Research Clinical Endocrinology and Metabolism,* 14(4): 667-677.

Lehmann, H. and Wadsworth, J. (2011). The impact of Chernobyl on health and labour market performance. *Journal of health economics,* 30(5): 843-857.

Leng, Q., Mohamat-Yusuff, F., Mohamed, K. N., Zainordin, N. S., Hassan, M. Z. (2024). Impacts of thermal and cold discharge from power plants on marine benthos and its mitigation measures: a systematic review. *Frontiers in Marine Science,* 11: 1465289.

Li, C., Dos Reis, A. A., Ansari, A., Bertelli, L., Carr, Z., Dainiak, N., ... (2022). Public health response and medical management of internal contamination in past radiological or nuclear incidents: A narrative review. *Environment international,* 163: 107222.

Li, H. and Zou, H. (2022). Short-term wind power prediction based on data reconstruction and improved extreme learning machine. *Arabian Journal for Science and Engineering,* 47(3): 3669-3682.

Li, T., Sun, J., Fei, L. (2025). Application of Multiple-Criteria Decision-Making Technology in Emergency Decision-Making: Uncertainty, Heterogeneity, Dynamicity, and Interaction. *Mathematics,* 13(5): 731.

Liao, J., Wang, X., Wang, H., … (2025). Geographical impact on the distribution of polycyclic aromatic hydrocarbons (PAHs) in hilly terrain topsoil: A case study at Chongqing, SW, China. *Journal of Hazardous Materials,* 487: 137085.

Liland, A., Lochard, J., Skuterud, L. (2009). How long is long-term? Reflections based on over 20 years of post-Chernobyl management in Norway. *Journal of environmental radioactivity,* 100(7): 581-584.

Liu, Y., Li, H., Sun, S., Fang, S. (2017). Enhanced air dispersion modelling at a typical Chinese nuclear power plant site: Coupling RIMPUFF with two advanced diagnostic wind models. *Journal of Environmental Radioactivity,* 175: 94-104.

Lixin, Y., Ke, C., Xiaoying, C., Yueling, S., Xiaoqing, C., Ye, H. (2017). Analysis of social vulnerability of residential community to hazards in Tianjin, China. *Natural Hazards,* 87: 1223-1243.

Locatelli, G., Mancini, M., Todeschini, N. (2013). Generation IV nuclear reactors: Current status and future prospects. *Energy Policy,* 61: 1503-1520.

Lu, W., Han, L. D., Liu, C., Long, K. (2014). A multiple-source, nearest destination, shortest path problem in evacuation assignments. *CICTP 2014: Safe, Smart, and Sustainable Multimodal Transportation Systems,* (1): 3691-3702.

Lyman, E., Schoeppner, M., von Hippel, F. (2017). Nuclear safety regulation in the post-Fukushima era. *Science,* 356(6340): 808-809.

Lyu, H.-M., Zhou, W.-H., Shen, S.-L., Zhou, A.-N. (2020). Inundation risk assessment of metro system using AHP and TFN-AHP in Shenzhen. *Sustainable Cities and Society,* 56: 102103.

Ma, Y., Xu, W., Qin, L., Zhao, X., Du, J. (2019). Emergency shelters location-allocation problem concerning uncertainty and limited resources: a multi-objective optimization with a case study in the Central area of Beijing, China. Geomatics, *Natural Hazards and Risk,* 10(1): 1242-1266.

Maeda, M. and Oe, M. (2017). Mental health consequences and social issues after the Fukushima disaster. *Asia Pacific Journal of Public Health,* 29(2): 36S-46S.

Maletic, D., Maletic, M., Lovrencic, V., Al-Najjar, B., Gomiscek, B. (2014). An application of analytic hierarchy process (AHP) and sensitivity analysis for maintenance policy selection. *Organizacija,* 47(3): 177.

Mamikhin, S. V., Golosov, V. N., Paramonova, T. A., Shamshurina, E. N., Ivanov, M. M. (2016). Vertical distribution of 137 Cs in alluvial soils of the Lokna River floodplain (Tula oblast) long after the Chernobyl accident and its simulation. *Eurasian Soil Science,* 49: 1432-1442.

Manap, N., Borhan, M. N., Yazid, M. R. M., Hambali, M. K. A., Rohan, A. (2019). Determining spatial patterns of road accidents at expressway by applying Getis-Ord Gi* spatial statistic. *Int. J. Recent Technol. Eng,* 8(3S3): 345-350.

Marler, R. T. and Arora, J. S. (2010). The weighted sum method for multi-objective optimization: new insights. *Structural and multidisciplinary optimization,* 41: 853-862.

Mathew, M. D. (2022). Nuclear energy: A pathway towards mitigation of global warming. *Progress in Nuclear Energy,* 143: 104080.

Matsunaga, H., Orita, M., Taira, Y., Takamura, N. (2021). Awareness of the implementation of stable iodine prophylaxis by parental guardians living in the urgent protective action planning zone of an operating nuclear power plant in Japan. *BMC Public Health*, 21: 1-9.

Mazur, A. (2019). Hypothetical Accident In Polish Nuclear Power Plant. Worst Case Scenario for Main Polish Cities. *Ecological Chemistry and Engineering,* 26(1): 9-28.

McLellan, B. C., Zhang, Q., Utama, N. A., Farzaneh, H., Ishihara, K. N. (2013). Analysis of Japan's post-Fukushima energy strategy. *Energy Strategy Reviews,* 2(2): 190-198.

Mennis, J. (2009). Dasymetric mapping for estimating population in small areas. *Geography Compass,* 3(2): 727-745.

Mettler Jr, F. A., Gus'kova, A. K., Gusev, I. (2007). Health effects in those with acute radiation sickness from the Chernobyl accident. *Health physics,* 93(5): 462-469.

Mohamed, A. M. I., AlamEldien, A., Saif, A. (2013). Air Quality Assessment of West Port-Said Industrial Region, Egypt. *ICFD11: Eleventh International Conference of Fluid Dynamics,* Alexandria, Egypt, December 19-21.

Mohammed Saeed, I. M., Saleh, M. A. M., Hashim, S., Hama, Y. M. S., Hamza, K., Al-Shatri, S. H. (2020). The radiological assessment, hazard evaluation, and spatial distribution for a hypothetical nuclear power plant accident at Baiji potential site. *Environmental Sciences Europe,* 32: 1-12.

Morita, T., Ambe, D., Miki, S., Kaeriyama, H., Shigenobu, Y. (2020). Impacts of the Fukushima nuclear accident on fishery products and fishing industry. In Fukumoto, M. (Eds.). *Low-Dose Radiation Effects on Animals and Ecosystems: Long-Term Study on the Fukushima Nuclear Accident* (pp.31-41). Springer, Singapore.

Mousseau, T. A. (2021). The biology of Chernobyl. *Annual Review of Ecology, Evolution, and Systematics,* 52(1): 87-109.

Mullner, N. (2019). Three Decades after Chernobyl: Technical or Human Causes?. In Haas, R., Mez, L., Ajanovic, A. (Eds.). *The Technological and Economic Future of Nuclear Power* (pp.323-340). Wiesbaden: Springer Fachmedien Wiesbaden.

Murakami, M., Takebayashi, Y., Ono, K., Kubota, A., Tsubokura, M. (2020). The decision to return home and wellbeing after the Fukushima disaster. *International Journal of Disaster Risk Reduction,* 47: 101538.

Muramatsu, H., Kawasumi, K., Kondo, T. (2015). Size-distribution of airborne radioactive particles from the Fukushima accident. *J Radioanal Nucl Chem.,* 303: 1459-1463.

Musolino, G., Polimeni, A., Rindone, C., Vitetta, A. (2013). Travel time forecasting and dynamic routes design for emergency vehicles. *Procedia-Social and Behavioral Sciences,* 87: 193-202.

Mérigoux, N. (2022). Multiphase Eulerian-Eulerian CFD supporting the nuclear safety demonstration. *Nuclear Engineering and Design,* 397: 111914.

Møller, A. . and Mousseau, T. A. (2006). Biological consequences of Chernobyl: 20 years on. *Trends in Ecology and Evolution,* 21(4): 200-207.

Møller, A. P. and Mousseau, T. A. (2011). Conservation consequences of Chernobyl and other nuclear accidents. *Biological Conservation,* 144(12): 2787-2798.

Müller, A., Reiter, J., Weiland, U. (2011). Assessment of urban vulnerability towards floods using an criteria-based approach – a case study for Santiago de Chile. *Natural Hazards and Earth System Sciences,* 11(8): 2107-2123.

Nakajima, K., Yamanaka, T., Ooka, R., Kikumoto, H., Sugawara, H. (2020). Observational assessment of applicability of Pasquill stability class in urban areas for detection of neutrally stratified wind profiles. *Journal of Wind Engineering and Industrial Aerodynamics,* 206: 104337.

Naoum, S. and Spyropoulos, V. (2021). The nuclear accident at Chernobyl: Immediate and further consequences. *Romanian Journal of Military Medicine,* 124(2): 184.

Nasstrom, J. S., Sugiyama, G., Baskett, R. L., Larsen, S. C., Bradley, M. M. (2007). The National Atmospheric Release Advisory Center modelling and decision-support system for radiological and nuclear emergency preparedness and response. *International Journal of Emergency Management,* 4(3): 524-550.

Nazeer, M. and Bork, H. R. (2019). Flood vulnerability assessment through different methodological approaches in the context of North-West Khyber Pakhtunkhwa, Pakistan. *Sustainability,* 11(23): 6695.

Nesheiwat, J. and Cross, J. S. (2013). Japan's post-Fukushima reconstruction: A case study for implementation of sustainable energy technologies. *Energy Policy,* 60: 509-519.

Neureiter, N. P., Garrick, B. J., Bari, R. A., Beard, J., Percy, M., Brewster, M. Q., Corradini, M. L. (2014). *Lessons learned from the Fukushima nuclear accident for improving safety of US nuclear plants.* Washington, DC: The National Academies Press.

NEA. (2000). *Methodologies for assessing the economic consequences of nuclear reactor accidents.* OECD Publishing, Paris.

NEA. (2012). *Japan's compensation system for nuclear damage: As Related to the TEPCO Fukushima Daiichi Nuclear Accident,* Legal Affairs, OECD Publishing, Paris.

NEA. (2021). *Fukushima Daiichi nuclear power plant accident, ten years on: Progress, lessons and challenges.* OECD Publishing, Paris.

Nihei, N. (2023). Recovery of food production from radioactive contamination caused by the Fukushima nuclear accident. In Nakanishi, T. M., Tanoi, K. (Eds.), *Agricultural Implications of Fukushima Nuclear Accident* (Vol. IV, pp. 9-15). Springer, Singapore.

Nikiforov, Y. and Gnepp, D. R. (1994). Pediatric thyroid cancer after the Chernobyl disaster. Pathomorphologic study of 84 cases (1991-1992) from the Republic of Belarus. *Cancer,* 74(2): 748-766.

Noaeen, M., Naik, A., Goodman, L., Crebo, J., Abrar, T., Abad, Z. S. H., ... (2022). Reinforcement learning in urban network traffic signal control: A systematic literature review. *Expert Systems with Applications*, 199: 116830.

NRA. (2013). Nuclear Regulation Authority (Japan), Guidelines on Nuclear Emergency Preparedness, Tokyo, July 2009.

NRB-99. (2009). Russian Radiation Safety Standards (NRB-99/2009), Federal Standards for Radiation Protection, Moscow. January 2015.

Nurliati, G., Romli, M., Hikmat, M. C. C., Sriwahyuni, H., TH, N. H., Suryantoro, S., ... (2024). Literature survey and analysis of phytoremediation strategies for Cs-137 decontamination. *Nuclear Engineering and Design,* 427: 113414.

Obaid, H. B., Trafalis, T. B., Abushaega, M. M., Altherwi, A., Hamzi, A. (2024). Optimizing Dynamic Evacuation Using Mixed-Integer Linear Programming. *Mathematics,* 13(1): 12.

Oe, M., Takebayashi, Y., Sato, H., Maeda, M. (2021). Mental health consequences of the Three Mile Island, Chernobyl, and Fukushima nuclear disasters: a scoping review. *International Journal of Environmental Research and Public Health,* 18(14): 7478.

Ogie, R. and Pradhan, B. (2020). Social vulnerability to natural hazards in Wollongong: comparing strength-based and traditional methods. *Australian Journal of Emergency Management,* 35(1): 60-68.

Ogorodnikov, B. I., Skitovich, V. I., Budyka, A. K. (1998). Size distribution of artificial and natural radioactive aerosols in the 30-kilometer zone of the Chernobyl AES in 1986-1996. *Radiatsionnaia Biologiia, Radioecologiia,* 38(6): 889-892.

Oğul, H. and Karaağaç, M. O. (2019). Public attitudes toward nuclear power plants in Türkiye. *Pamukkale Üniversitesi Mühendislik Bilimleri Dergisi,* 25(4): 423-429.

Ohba, T., Tanigawa, K., Liutsko, L. (2021). Evacuation after a nuclear accident: Critical reviews of past nuclear accidents and proposal for future planning. *Environment International,* 148: 106379.

Ohtsuru, A., Tanigawa, K., Kumagai, A., … (2015). Nuclear disasters and health: lessons learned, challenges, and proposals. *The Lancet,* 386(9992):489-497.

Oktari, R. S., Munadi, K., Idroes, R., Sofyan, H. (2020). Knowledge management practices in disaster management: Systematic review. *International Journal of Disaster Risk Reduction,* 51: 101881.

Oloruntoba, R., Sridharan, R., Davison, G. (2018). A proposed framework of key activities and processes in the preparedness and recovery phases of disaster management. *Disasters,* 42(3): 541-570.

Omoto, A. (2005). Nuclear power for sustainable development and relevant IAEA activities for the future. *Progress in Nuclear Energy,* 47(1-4): 16-26.

Onopriyenko, O. P., Trishchynska, M. A., Kolosova, T. V. (2024). Hospital assessment of the dynamics of mortality and primary disability after a stroke among Chernobyl liquidators in the Left-bank Ukraine (modern view of the problem and own research). *International Neurological Journal,* 20(6): 305-315.

Orhan, O. (2021). Land suitability determination for citrus cultivation using a GIS-based multi-criteria analysis in Mersin, Türkiye. *Computers and Electronics in Agriculture,* 190: 106433.

Ortega, J., Moslem, S., Palaguachi, J., Ortega, M., Campisi, T., Torrisi, V. (2021). An integrated multi criteria decision making model for evaluating park-and-ride facility location issue: A case study for cuenca city in Ecuador. *Sustainability,* 13(13): 7461.

Orui, M., Nakayama, C., Moriyama, N., Tsubokura, M., Watanabe, K., Nakayama, T., ... (2021). Those who have continuing radiation anxiety show high psychological distress in cases of high post-traumatic stress: the Fukushima nuclear disaster. *International Journal of Environmental Research and Public Health,* 18(22): 12048.

Ozay, B. and Orhan, O. (2023). Flood susceptibility mapping by best–worst and logistic regression methods in Mersin, Türkiye. *Environmental Science and Pollution Research,* 30(15): 45151-45170.

Ozmen, M. (2023). Evaluating earthquake vulnerability of 2023 Kayseri, Türkiye via BWM-ABAC method. *Sādhanā,* 48(3): 179.

Pacini, F., Vorontsova, T., Demidchik, E. P., Molinaro, E., Agate, L., Romei, C., … (1997). Post-Chernobyl thyroid carcinoma in Belarus children and adolescents: comparison with naturally occurring thyroid carcinoma in Italy and France. *The Journal of Clinical Endocrinology and Metabolism,* 82(11): 3563-3569.

Panov, A. V., Komarova, L. N., Lyapunova, E. R., Mel'nikova, A. A. (2024). Peculiarities of the exposure dose formation on the population in the most affected regions of Russia after the Chernobyl NPP accident. *Nuclear Energy and Technology,* 10(1): 41-46.

Park, S., Sohn, S., Jae, M. (2021). Cohort-based evacuation time estimation using TSIS-CORSIM. *Nuclear Engineering and Technology,* 53(6): 1979-1990.

Pence, J., Miller, I., Sakurahara, T., Whitacre, J., Reihani, S., Kee, E., Mohaghegh, Z. (2019). GIS-based integration of social vulnerability and level 3 probabilistic risk assessment to advance emergency preparedness, planning, and response for severe nuclear power plant accidents. *Risk Analysis,* 39(6): 1262-1280.

Petryna, A. (2013). *Life exposed: biological citizens after Chernobyl.* Princeton University Press.

PHE. (2019). Public Health England (PHE), Guidance on Radiation Protection in Emergency Response, London.

Pianosi, F., Beven, K., Freer, J., Hall, J. W., Rougier, J., Stephenson, D. B., Wagener, T. (2016). Sensitivity analysis of environmental models: A systematic review with practical workflow. *Environmental Modelling and Software,* 79: 214-232.

Polleri, M. (2020). Post-political uncertainties: Governing nuclear controversies in post-Fukushima Japan. *Social Studies of Science,* 50(4): 567-588.

Rabes, H. M., Demidchik, E. P., Sidorow, J. D., Lengfelder, E., Beimfohr, C., Hoelzel, D., Klugbauer, S. (2000). Pattern of radiation-induced RET and NTRK1 rearrangements in 191 post-chernobyl papillary thyroid carcinomas: biological, phenotypic, and clinical implications. *Clinical Cancer Research,* 6(3): 1093-1103.

Raisali, G., Davilu, H., Haghighishad, A., Khodadadi, R., Sabet, M. (2006). Calculation of total effective dose equivalent and collective dose in the event of a LOCA in Bushehr nuclear power plant. *Radiation Protection Dosimetry,* 121(4): 382-390.

Ramana, M. V. (2018). Technical and social problems of nuclear waste. *Wiley Interdisciplinary Reviews: Energy and Environment,* 7(4): e289.

Reed, B. C. (2014). *The history and science of the Manhattan Project.* Heidelberg: Springer.

Rey, D. and Neuhäuser, M. (2011). Wilcoxon-Signed-Rank Test. In Lovric, M. (Eds.). *International Encyclopedia of Statistical Science* (pp. 1658-1659). Springer, Berlin, Heidelberg.

Rezaei, J. (2015). Best-worst multi-criteria decision-making method. *Omega,* 53: 49-57.

Romanowska, A. and Jamroz, K. (2021). Comparison of traffic flow models with real traffic data based on a quantitative assessment. *Applied Sciences,* 11(21): 9914.

Rosner, B., Glynn, R. J., Lee, M. L. T. (2006). The Wilcoxon signed rank test for paired comparisons of clustered data. *Biometrics,* 62(1): 185-192.

Rufat, S., Tate, E., Emrich, C.T., Antolini, F. (2019). How valid are social vulnerability models?. *Annals of the American Association of Geographers,* 109(4): 1131-1153.

Rzeszutek, M. (2019). Parameterization and evaluation of the CALMET/CALPUFF model system in near-field and complex terrain-Terrain data, grid resolution and terrain adjustment method. *Science of the Total Environment,* 689: 31-46.

Saaty, T. L. (1980). The analytic hierarchy process (AHP). *The Journal of the Operational Research Society,* 41(11): 1073-1076

Saaty, T. L. (2004). Decision making – the analytic hierarchy and network processes (AHP/ANP). *Journal of systems science and systems engineering*, 13: 1-35.

Sadekin, S., Zaman, S., Mahfuz, M., Sarkar, R. (2019). Nuclear power as foundation of a clean energy future: A review. *Energy Procedia,* 160: 513-518.

Sadri, A. M., Ukkusuri, S. V., Murray-Tuite, P., Gladwin, H. (2014). How to evacuate: model for understanding the routing strategies during hurricane evacuation. *Journal of Transportation Engineering,* 140(1): 61-69.

Saegusa, T., Shirai, K., Arai, T., Tani, J., Takeda, H., Wataru, M., ... (2010). Review and future issues on spent nuclear fuel storage. *Nuclear Engineering and Technology,* 42(3): 237-248.

Saenko, V., Ivanov, V., Tsyb, A., Bogdanova, T., Tronko, M., Demidchik, Y., … (2011). The Chernobyl accident and its consequences. *Clinical Oncology,* 23(4): 234-243.

Safaei, A. S., Farsad, S., Paydar, M. M. (2020). Emergency logistics planning under supply risk and demand uncertainty. *Operational Research,* 20: 1437-1460.

Sagara, A., Fujimoto, N., Morita, K., Fukuda, K. (2000). Study on the social economic estimation of Chernobyl accident. *Kyushu Diagaku Kogaku Shuho,* 73.

Sahu, N. and Mishra, M. M. (2021). Assessing the vulnerability index of COVID-19 pandemic in India. *Geography, Environment, Sustainability,* 14(4): 131-139.

Sakai, M., Tsuji, H., Ishii, Y., Ozaki, H., Takechi, S., Jo, J., ... (2021). Untangling radiocesium dynamics of forest-stream ecosystems: A review of Fukushima studies in the decade after the accident. *Environmental Pollution,* 288: 117744

Sakauchi, K. and Otaki, J. M. (2023). Imaging Plate Autoradiography for Ingested Anthropogenic CS-137 in Butterfly Bodies: Implications for the Biological Impacts of the Fukushima Nuclear Accident. *Life,* 13(5): 1211.

Samet, J. M. (2016). *The financial costs of the Chernobyl nuclear power plant disaster* (Doctoral dissertation). Keck School of Medicine, USA.

Sandal, E. K., Adıgüzel, F., Karademir, N. (2020). Changes in land use between the years of 1990-2018 in Mersin province based on CORINE (Coordination of Information on The Environment) System. *Kastamonu University Journal of Engineering and Sciences,* 6(1): 8-18.

Santana, L. P. (2016). Management of radioactive waste: A review. *Proceedings of the International Academy of Ecology and Environmental Sciences,* 6(2): 38.

Saylan, E. and Aygün, C. (2024). Thermoeconomic analysis and environmental impact assessment of the Akkuyu nuclear power plant. *Journal of Thermal Analysis and Calorimetry,* 149(12): 6531-6550.

Schwaiger, M., Mück, K., Benesch, T., Feichtinger, J., Hrnecek, E., Lovranich, E. (2004). Investigation of food contamination since the Chernobyl fallout in Austria. *Applied radiation and isotopes,* 61(2-3): 357-360.

Schwarz, A. (2025). Crisis and Risk Communication Research in Germany. In A. Schwarz, M. W. Seeger, S. Kim (Eds.), *The Handbook of International Crisis and Risk Communication Research* (2nd ed., Vol 32, pp. 417-434). Wiley.

Serim, A. T., Özkil, M., Üremiş, İ., Uludag, A. (2023). Changes in the weed flora of cotton fields in the Eastern Mediterranean region of Turkiye. *Mustafa Kemal Üniversitesi Tarım Bilimleri Dergisi,* 28(3): 633-648.

Shafapourtehrany, M., Yariyan, P., Ozener, H., Pradhan, B., Shabani, F. (2022). Evaluating the application of K-mean clustering in Earthquake vulnerability mapping of Istanbul, Türkiye. *International Journal of Disaster Risk Reduction,* 79: 103154.

Sharifi, A. and Yamagata, Y. (2016). Principles and criteria for assessing urban energy resilience: A literature review. *Renewable and Sustainable Energy Reviews,* 60: 1654-1677.

Sime, R.L. (2012). The Politics of Forgetting: Otto Hahn and the German Nuclear-Fission Project in World War II. *Phys. Perspect.,* 14: 59-94.

Singh, M. and Pant, M. (2021). A review of selected weighing methods in MCDM with a case study. *International Journal of System Assurance Engineering and Management,* 12: 126-144.

Singh, S. R., Eghdami, M. R., Singh, S. (2014). The concept of social vulnerability: A review from disasters perspectives. *International Journal of Interdisciplinary and Multidisciplinary Studies,* 1(6): 71-82.

Siracusa, J. M. and Warren, A. (2018). The nuclear non-proliferation regime: an historical perspective. *Diplomacy and Statecraft,* 29(1): 3-28.

Sisman, S. and Aydinoglu, A. C. (2022). A modelling approach with geographically weighted regression methods for determining geographic variation and influencing factors in housing price: A case in Istanbul. *Land use policy,* 119: 106183.

Skrynyk, O. Y., Chernysh, R. I., Hrytsyuk, Y. Y. (2010). Formation of a large scale spot-like structure of the total deposition due to a powerful elevated finite source. *Advances in Science and Research,* 4(1): 37-41.

Slovic, P., Flynn, J., Mertz, C. K., Poumadere, M., Mays, C. (2000). Nuclear power and the public: A comparative study of risk perception in France and the United States.In Renn, O. and Rohrmann, B. (Eds.). *Cross-cultural risk perception: A survey of empirical studies* (pp.55-102). Dordrecht, The Netherlands: Kluwer Academic.

Smith, J. N., Brown, R. M., Williams, W. J., Robert, M., Nelson, R., Moran, S. B. (2015). Arrival of the Fukushima radioactivity plume in North American continental waters. *Proceedings of the National Academy of Sciences,* 112(5): 1310-1315.

Song, W., Zhu, L., Li, Q., Wang, X. D., Liu, Y., Dong, Y. C. (2009). Evacuation model and application for emergency events. *The Fourth International Conference on Computer Sciences and Convergence Information Technology,* Seoul, Korea, April 24-26.

Sotelo-Salas, C., Monardes-Concha, C. A., Pérez-Galarce, F., Santa González, R. (2024). A multi-objective optimization model for planning emergency shelters after a tsunami. *Socio-Economic Planning Sciences,* 93: 101909.

Speekenbrink, M. (2016). A tutorial on particle filters. *Journal of Mathematical Psychology,* 73: 140-152.

Sportisse, B. (2007). A review of parameterizations for modelling dry deposition and scavenging of radionuclides. *Atmospheric Environment,* 41(13): 2683-2698.

Srinivasan, T. N. and Rethinaraj, T. G. (2013). Fukushima and thereafter: Reassessment of risks of nuclear power. *Energy policy,* 52: 726-736.

SSK. (2014). German Radiation Protection Commission Guidelines for Nuclear Emergency Management, Berlin, 2014.

Starczewski, T. (2023). Simulation research on the relationship between selected inconsistency indices used in AHP. *Entropy,* 25(10): 1464.

State Statistics Service of Ukraine. (2023). Retrieved March 20, 2023, from https://stat.gov.ua/en/topics/population-and-social-statistics

Steinhauser, G., Brandl, A., Johnson, T. E. (2014). Comparison of the Chernobyl and Fukushima nuclear accidents: a review of the environmental impacts. *Science of the total environment,* 470: 800-817.

Stepanenko, V. F., Gavrilin, Y. I., Snykov, V. P., Shevchuk, V. E., Göksu, H. Y., Voilleque, P. G., Orlov, M. Y. (2002). Elevated exposure rates under inclined birch trees indicate the occurrence of rainfall during radioactive fallout from Chernobyl. *Health physics,* 82(2): 240-243.

Stohl, A., Seibert, P., Wotawa, G., Arnold, D., Burkhart, J. F., Eckhardt, S., ... (2012). Xenon-133 and caesium-137 releases into the atmosphere from the Fukushima Dai-ichi nuclear power plant: determination of the source term, atmospheric dispersion, and deposition. *Atmospheric Chemistry and Physics,* 12(5): 2313-2343.

Stoia, N. L., Niţă, M. R., Popa, A. M., Iojă, I. C. (2022). The green walk – an analysis for evaluating the accessibility of urban green spaces. *Urban forestry and urban greening,* 75: 127685.

Straub, J. (2019). Mutual assured destruction in information, influence and cyber warfare: Comparing, contrasting and combining relevant scenarios. *Technology in Society,* 59: 101177.

Sugiyama, G. and Chan, S. T. (1997). New meteorological data assimilation model for real-time emergency response. *The 10th Joint Conference on the Applications of Air Pollution Meteorology with the Air and Waste Management Association Phoenix,* AZ, January 11-16.

Sun Z, Imano H, Eguchi E, … (2022). The associations between evacuation status and lifestyle-related diseases in Fukushima after the Great East Japan Earthquake: the Fukushima Health Management Survey. *International Journal of Environmental Research and Public Health,* 19(9): 5661.

Sun, Y., Fang, M., Su, Y. (2021). AGV path planning based on improved Dijkstra algorithm. *Journal of Physics: Conference Series,* 1746(1): 012052.

Svendsen, E. R., Yamaguchi, I., Tsuda, T., Guimaraes, J. R. D., Tondel, M. (2016). Risk communication strategies: lessons learned from previous disasters with a focus on the Fukushima radiation accident. *Current environmental health reports,* 3: 348-359.

T.C. Çevre, Şehircilik ve İklim Değişikliği Bakanlığı. (2021). Mersin İli 2021 yılı çevre durum raporu. Retrieved from https://webdosya.csb.gov.tr/db/ced/icerikler/mers-n_-cdr2021-20221227141341.pdf

TAEA. (2019). Turkish Atomic Energy Authority (TAEA), Nuclear Emergency Preparedness Regulations, Ankara.

Taghizadeh-Hesary, F., Yoshino, N., Rasoulinezhad, E. (2017). Impact of the Fukushima nuclear disaster on the oil-consuming sectors of Japan. *Journal of Comparative Asian Development,* 16(2): 113-134.

Tate, E. (2012). Social vulnerability indices: a comparative assessment using uncertainty and sensitivity analysis. *Natural Hazards,* 63: 325-347.

The Japan Times. (2023) *Evacuation order lifted for part of Fukushima town. Retrieved 02 April 2023, from* https://www.neimagazine.com/news/evacuation-order-lifted-for-part-of-fukushima-town-10731131/#:~:text=The%20nuclear%20evacuation%20order%20has,first%20time%20in%2012%20years.

The National Diet of Japan. (2012) The official report of the Fukushima nuclear accident independent Investigation Commission. Tokyo.

Thielen, H. (2012). The Fukushima Daiichi nuclear accident – an overview. *Health Physics,* 103(2): 169-174.

Thiry, Y., Colle, C., Yoschenko, V., Levchuk, S., Van Hees, M., Hurtevent, P., Kashparov, V. (2009). Impact of Scots pine (Pinus sylvestris L.) plantings on long term 137Cs and 90Sr recycling from a waste burial site in the Chernobyl Red Forest. *Journal of Environmental Radioactivity,* 100(12): 1062-1068.

Tronko, M., Bogdanova, T., Voskoboynyk, L., Zurnadzhy, L., Shpak, V., Gulak, L. (2010). Radiation induced thyroid cancer: fundamental and applied aspects. *Experimental oncology,* 32(3): 200-204.

Tsujiuchi, T., Yamaguchi, M., Masuda, K., Tsuchida, M., Inomata, T., Kumano, H., ... (2016). High prevalence of post-traumatic stress symptoms in relation to social factors in affected population one year after the Fukushima nuclear disaster. *PloS one,* 11(3): e0151807.

EPA. (2004). User's guide for the AMS/EPA regulatory model (AERMOD).

EPA. (2017). Protective action guides and planning guidance for radiological incidents. Radiation Protection Division.

EPA. (2011). Exposure Factors Handbook: 2011 Edition (Final Report). U. S. Environmental Protection Agency, Washington, DC, EPA/600/R-09/052F, 2011.

Uluer, G. S. and Çağlayan, Ç. (2021). The economic and environmental importance of Akkuyu nuclear power plant in Türkiye. *Handbook of Research on Strategic Management for Current Energy Investments,* 1: 300-319.

Unver, L. Ö. (2014). *Development of a radioecological model for accidental release of radionuclides: Akkuyu and Sinop Nuclear Power Plants* (Doctoral dissertation). Middle East Technical University, Ankara.

Urbanik II, T. (2000). Evacuation time estimates for nuclear power plants. *Journal of Hazardous Materials,* 75(2-3): 165-180.

Uysal, O., Aydın, B., Subaşı, O. S., Aktaş, E. (2021). Effect of good agricultural practices on energy use in citrus farming in Türkiye: case of Mersin province. *Horticultural Studies,* 38(2): 125-133.

Vaidya, O. S. and Kumar, S. (2006). Analytic hierarchy process: An overview of applications. *European Journal of Operational Research,* 169(1): 1-29.

Wachtel, G., Schmöcker, J. D., Hadas, Y., Gao, Y., Nahum, O. E., Ben-Moshe, B. (2021). Planning for tourist urban evacuation routes: A framework for improving the data collection and evacuation processes. *Environment and Planning B: Urban Analytics and City Science,* 48(5): 1108-1125.

Waddington, I., Thomas, P. J., Taylor, R. H., Vaughan, G. J. (2017). J-value assessment of relocation measures following the nuclear power plant accidents at Chernobyl and Fukushima Daiichi. *Process Safety and Environmental Protection,* 112: 16-49.

Wakamatsu, H. and Miyata, T. (2021). Effects of radioactive safety information on consumer fears of radioactive contamination from oyster products in Japan. *Marine Policy,* 126: 104401.

Wang, P., Yan, X., Zhao, F. (2019). Multi-objective optimization of control parameters for a pressurized water reactor pressurizer using a genetic algorithm. *Annals of Nuclear Energy,* 124: 9-20.

Wang, R.; Chen, B.; Qiu, S.; Zhu, Z.; Qiu, X. (2017). Data assimilation in air contaminant dispersion using a particle filter and expectation-maximization algorithm. *Atmosphere,* 8(9): 170.

Wang, X., Guan, M., Dong, C., Wang, J., Fan, Y., Xin, F., Lian, G. (2022). A multi-indicator evaluation method for spatial distribution of urban emergency shelters. *Remote Sensing,* 14(18): 4649.

Wheeler, D. C. (2021). Geographically weighted regression. In Fischer, M. and Nijkamp, P. (Eds.). *Handbook of Regional Science* (pp. 1435-11459). Berlin, Heidelberg: Springer Berlin Heidelberg.

Wittneben, B. B. (2012). The impact of the Fukushima nuclear accident on European energy policy. *Environmental Science and Policy,* 15(1): 1-3.

Wooten, W. W. (2002). External and Internal Dose to Individuals After 131I Outpatient Therapy. *Journal of Nuclear Medicine,* 43(4): 575-575.

Worgul, B. V., Kundiyev, Y. I., Sergiyenko, N. M., Chumak, V. V., Vitte, P. M., Medvedovsky, C., ... (2007). Cataracts among Chernobyl clean-up workers: implications regarding permissible eye exposures. *Radiation Research,* 167(2): 233-243.

World Health Organization. (2021) *Fukushima: radiation exposure.* Retrieved February 2005. https://world-nuclear.org/information-library/safety-and-security/safety-of-plants/appendices/fukushima-radiation-exposure.aspx.

World Health Organization. (2006). *Health effects of the Chernobyl accident and special health care programs.* Retrieved 01 May, 2006. https://www.who.int/publications/i/item/9241594179

World Health Organization. (2012). *Preliminary dose estimation from the nuclear accident after the 2011 Great East Japan earthquake and tsunami.* Retrieved 06 May, 2012. https://www.who.int/publications/i/item/9789241503662

World Health Organization. (2013). *Health risk assessment from the nuclear accident after the 2011 Great East Japan earthquake and tsunami, based on a preliminary dose estimation.* Retrieved 11 August, 2017. https://www.who.int/publications/i/item/9789241505130

Xiao, D., Li, J., Zhang, Z., Gu, Z., Fu, Y., Niu, J. (2025). Optimization of personnel evacuation routes for sudden nuclear accidents based on hybrid genetic-grey wolf optimizer algorithm. *Nuclear Engineering and Technology,* 57(3): 103223.

Xiao, X., Liang, J., Tong, J., Wang, H. (2024). Emergency decision support techniques for nuclear power plants: Current state, challenges, and future trends. *Energies,* 17(10): 2439.

Xie, W., and Meng, Q. (2023). An Integrated PCA-AHP Method to Assess Urban Social Vulnerability to Sea Level Rise Risks in Tampa, Florida. *Sustainability,* 15(3): 2400.

Xu, H., Zhang, B., Liu, Y. (2021). New safety strategies for nuclear power plants: A review. *International Journal of Energy Research,* 45(8): 11564-11588.

Xu, Z., Chen, X., Wu, S. R., Gong, M., Du, Y., Wang, J., ... (2019). Spatial-temporal assessment of water footprint, water scarcity and crop water productivity in a major crop production region. *Journal of Cleaner Production,* 224: 375-383.

Yaagoubi, R., Miky, Y., Faisal, K., Al Shouny, A. (2023). A combined agent-based modeling and GIS approach for HAJJ crowd simulation. *Journal of Engineering Research,* 11(1): 100014.

Yabe, H., Suzuki, Y., Mashiko, H., Nakayama, Y., Hisata, M., Niwa, S. I., ... (2014). Psychological distress after the Great East Japan Earthquake and Fukushima Daiichi Nuclear Power Plant accident: results of a mental health and lifestyle survey through the Fukushima Health Management Survey in FY2011 and FY2012. *Fukushima Journal of Medical Science,* 60(1): 57-67.

Yamane, F., Ohgaki, H., Asano, K. (2013). The immediate impact of the Fukushima Daiichi accident on local property values. *Risk Analysis,* 33(11): 2023-2040.

Yang, Y., Cao, B., Chen, Y. (2013). Simulation of the atmospheric dispersion of radionuclides using gaussian plume model. *International Conference on Nuclear Engineering,* Chengdu, China, July 29 – August 02.

Yanovskiy, M., Levi, O. N., Shaki, Y. Y., Socol, Y. (2020). Consequences of a large-scale nuclear accident and guidelines for evacuation: a cost-effectiveness analysis. *International Journal of Radiation Biology,* 96(11): 1382-1389.

Yasunari, T. J., Stohl, A., Hayano, R. S., Burkhart, J. F., Eckhardt, S., Yasunari, T. (2011). CS-137 deposition and contamination of Japanese soils due to the Fukushima nuclear accident. *Proceedings of the National Academy of Sciences,* 108(49): 19530-19534.

Yasutaka, T. and Naito, W. (2016). Assessing cost and effectiveness of radiation decontamination in Fukushima Prefecture, Japan. *Journal of Environmental Radioactivity,* 151: 512-520.

Yavuz, C. (2023). Distinctive stochastic tsunami hazard and environmental risk assessment of Akkuyu nuclear power plant by Monte Carlo simulations. *Arabian Journal for Science and Engineering,* 48(1): 573-582.

Yorucu, V. and Katircioğlu, S. T. (2014). Radioactive convergence of nuclear leakage in Fukushima: economic impact analysis of triple tragic events. *Renewable and Sustainable Energy Reviews,* 35: 400-409.

Yoschenko, V., Ohkubo, T., Kashparov, V. (2018). Radioactive contaminated forests in Fukushima and Chernobyl. *Journal of Forest Research,* 23(1): 3-14.

Yuan, F. and Han, L. D. (2010). A multi-objective optimization approach for evacuation planning. *Procedia Engineering,* 3: 217-227.

Zhang, Q., Xue, Y., Wang, D., Niu, M. (2019). Asymptotic formula on average path length in a hierarchical scale-free network with fractal structure. *Chaos, Solitons and Fractals,* 122: 196-201.

Zhang, S., Han, G., Xie, Y., Ruiz, J. J. (2015). Data assimilation in numerical weather and climate models. *Advances in Meteorology,* 2015: 1-2.

Zhang, T., Wang, D., Lu, Y. (2023). Machine learning-enabled regional multi-hazards risk assessment considering social vulnerability. *Scientific reports,* 13(1): 13405.

Zhang, X. L., Su, G. F., Yuan, H. Y., Chen, J. G., Huang, Q. Y. (2014). Modified ensemble Kalman filter for nuclear accident atmospheric dispersion: Prediction improved and source estimated. *Journal of Hazardous Materials,* 280: 143-155.

Zhang, X. and Liu, C. A. (2023). Model averaging prediction by K-fold cross-validation. *Journal of Econometrics,* 235(1): 280-301.

Zhang, X., Wang, C., Li, E., Xu, C. (2014). Assessment model of ecoenvironmental vulnerability based on improved entropy weight method. *The Scientific World Journal,* 2014(1): 797814.

Zhao, D., Mihăiţă, A. S., Ou, Y., Grzybowska, H., Li, M. (2024). Origin–destination matrix estimation for public transport: A multi-modal weighted graph approach. *Transportation Research Part C: Emerging Technologies,* 165: 104694.

Zhong, G., Lu, Y., Chen, W., Zhai, G. (2023). Multi-objective optimization approach of shelter location with maximum equity: an empirical study in Xin Jiekou district of Nanjing, China. *Geomatics, Natural Hazards and Risk,* 14(1): 2165973.

Zhu, Y. G. and Smolders, E. (2000). Plant uptake of radiocaesium: a review of mechanisms, regulation and application. *Journal of Experimental Botany,* 51(351): 1635-1645.

Zhuang, S., Fang, S., Dong, X. (2022). Local-Scale Atmospheric Dispersion Modelling of Radionuclides Following the Fukushima Daiichi Nuclear Accident Using SWIFT-RIMPUFF. *The International Conference on Nuclear Engineering,* Shenzhen, China, August 08-12.

Zou, Y., Zou, S., Niu, C. (2018). The optimization of emergency evacuation from nuclear accidents in China. *Sustainability,* 10(8): 2737.

Zubair, M., Ahmed, E., Hartanto, D. (2022). Estimation of public exposure during normal operation of unit-1 Barakah Nuclear Power Plant using GALE and HOTSPOT. *South African Journal of Chemical Engineering,* 41: 235-243.

Žurovec, O., Čadro, S., Sitaula, B. K. (2017). Quantitative assessment of vulnerability to climate change in rural municipalities of Bosnia and Herzegovina. *Sustainability,* 9(7): 1208.

CURRICULUM VITAE

Name Surname **:** Maryna BATUR

EDUCATION **:**

- **B.Sc.** **:** 2008, Dnipro University of Technology, Faculty of Architecture, Civil Engineering and Land Management, Department of Mine Surveying
- **M.Sc.** **:** 2020, Boğaziçi University, Kandilli Observatory and Earthquake Research Institute, Department of Geodesy

PUBLICATIONS, PRESENTATIONS AND PATENTS ON THE THESIS:

Articles

- **Batur M.,** Karaman H., Alkan R. M., Ozener H. 2025. Mapping social vulnerability to nuclear accidents: a comprehensive framework using BWM and AHP methods. *Applied Spatial Analysis and Policy*, 18, 45.
- **Batur M.,** Alkan R. M., Karaman H., Ozener H. 2025. Multi-dimensional optimization of nuclear emergency shelters: balancing capacity, evacuation efficiency, and supply accessibility. *International Journal of Engineering and Geosciences*, 10(2), 244-261.
- **Batur M.,** Alkan R. M., Karaman H., Ozener H. 2024. Recommendations for protective actions based on projected public health risks following a postulated nuclear power plant accident. *Malaysian Journal of Fundamental and Applied Sciences*, 20, 923-938.
- **Batur M.,** Alkan R. M. 2024. Bibliometric analysis of the greatest nuclear disasters: what is known so far and what are the prospects?. *The International Archive of the Photogrammetry, Remote Sensing and Spatial Information Sciences*, XLVIII-4/W9-2024, 61-68.
- **Batur M.,** Alkan R. M. 2023. What can we learn from past nuclear accidents? A comparative assessment of emergency response to accidents at the Three Mile Island, Chernobyl, and Fukushima Nuclear Power Plants. *Advanced Land Management*, 3(2), 23-36.

Presentations

- **Batur M.,** Alkan R. M. 2024. Seasonal effect on the spatiotemporal dispersion of radionuclides during a postulated accident at a nuclear power plant. International Congress on Information Technologies in Medicine, Pharmasy, Agriculture, Food, Forestry, Environment, and Engineering, May 08-10, 2024, Tokat/Turkiye.
- **Batur M.,** Alkan R. M. 2024. Bibliometric analysis of the greatest nuclear disasters: what is known so far and what are the prospects?. The 8th International Conference on Geoinformation Advances, January 11-13, 2024, Istanbul/Turkiye.
- **Batur M.,** Alkan R. M. 2023. Critical issues in emergency planning for nuclear power plant accidents. The 6th Intercontinental Geoinformation Days, June 13-14, 2023, Baku/Azerbaijan.